AD

AD 685861

USAAVLABS TECHNICAL REPORT 68-18B

PREDICTION OF ROTOR INSTABILITY AT HIGH FORWARD SPEEDS

VOLUME II

CLASSICAL FLUTTER

By

Clifford J. Astill

Charles F. Niebanck

February 1969

U. S. ARMY AVIATION MATERIEL LABORATORIES
FORT EUSTIS, VIRGINIA

CONTRACT DA 44-177-AMC-332(T)

UNITED AIRCRAFT CORPORATION
SIKORSKY AIRCRAFT DIVISION
STRATFORD, CONNECTICUT

This document has been approved for public release and sale; its distribution is unlimited.

U S ARMY MATERIEL COMMAND

D D C
RECEIVED
APR 16 1969
C

Reproduced by the
CLEARINGHOUSE
for Federal Scientific & Technical
Information Springfield Va 22151

217

DEPARTMENT OF THE ARMY
U. S. ARMY AVIATION MATERIEL LABORATORIES
FORT EUSTIS, VIRGINIA 23604

This contract was initiated to determine the aeroelastic stability limits of articulated and unarticulated helicopter rotor systems at high forward speeds. The four primary modes of aeroelastic instability (classical flutter, stall flutter, torsional divergence, and flapping or flatwise bending instability) were investigated. The possibility of a flap-lag instability suggested by Dr. Maurice I. Young of the Vertol Division, The Boeing Company, was investigated as a special case of flapping instability.

The results are published as a five-volume set; the subject of each volume is as follows:

Volume I	Equations of Motion
Volume II	Classical Flutter
Volume III	Stall Flutter
Volume IV	Torsional Divergence
Volume V	Flapping Instability

These reports have been reviewed by the U. S. Army Aviation Materiel Laboratories. These reports, which are published for the exchange of information and the stimulation of ideas, are considered to be technically sound with regard to technical approach, results, conclusions, and recommended parameter ranges for accurate usage.

Task 1F125901A13904
Contract DA 44-177-AMC-332(T)
USAAVLABS Technical Report 68-18B
February 1969

PREDICTION OF ROTOR INSTABILITY AT HIGH FORWARD SPEEDS

SER-50469

Volume II

Classical Flutter

By

Clifford J. Astill
and
Charles F. Niebanck

Prepared by

United Aircraft Corporation
Sikorsky Aircraft Division
Stratford, Connecticut

for

U. S. ARMY AVIATION MATERIEL LABORATORIES
FORT EUSTIS, VIRGINIA

This document has been approved for public release and sale; its distribution is unlimited.

SUMMARY

The purposes of this research program were to extend or develop analytical methods for determining rotor blade aeroelastic stability limits and to perform stability calculations over a range of design and operating variables for articulated and nonarticulated configurations. The usefulness of simpler analytical methods is investigated by comparing results with operating boundaries from the more elaborate analysis.

In the part of the investigation presented in this volume, analytical study was made of the effects of high forward speed on the flutter characteristics of helicopter rotor blades.

Linearized equations of motion were used to represent the dynamics of the rotor blades. The aerodynamic forces were obtained by using a fixed azimuth approach with fixed-wing two-dimensional compressible flow aerodynamic coefficients.

Flutter speeds and flutter frequencies were calculated for two model helicopter blades for which experimental data were available. One blade had been tested in hover at high tip Mach numbers; the other, at high advance ratios with low tip Mach numbers. Agreement between theoretical and experimental data was qualitative.

A parametric study was made of the effect on flutter speed of varying blade chordwise elastic axis and center-of-gravity position, torsional and flatwise bending stiffness, and blade mass ratio and feathering mass moment of inertia.

The extended Normal Mode Transient Analysis was used to perform blade response calculations corresponding to blade configurations and flight conditions for which classical flutter was calculated.

FOREWORD

The investigation presented in this volume is part of a more general study of rotor blade aeroelastic instabilities, which is contained in five volumes. The work was performed under Contract DA 44-177-AMC-332(T) with the U. S. Army Aviation Materiel Laboratories, Fort Eustis, Virginia. Mr. Joseph McGarvey monitored the program for USAAVLABS.

The rotor blade classical flutter analysis presented in this volume was developed at Sikorsky Aircraft by Mr. Clifford J. Astill, who also conducted the study of parameter variations and the comparison with available test data. Mr. Charles F. Niebanck, also of Sikorsky Aircraft, conducted calculations with the method presented in Volume I, and compared the results with corresponding flutter calculations, which were carried out with the method presented in this volume.

Volume I of this report contains the development of the differential equations of motion of an elastic rotor blade with chordwise mass unbalance.

Volume III describes a stall flutter analysis based on the calculation of aerodynamic work for a cycle of blade torsional vibration. Two-dimensional unsteady airfoil test data were used in the evaluation of the aerodynamic work. The analysis was used to generate stall flutter boundaries.

Volume IV contains the results of a study of static torsional divergence. A set of design charts and the effects of a range of parameter variations are presented. The results of the static divergence calculation are compared with results calculated by using the method developed in Volume I.

Volume V presents the results of a study of flapping and coupled flap-lag instability. The results of a parametric study based on a single-degree-of-freedom flapping or flatwise bending analysis are presented. Comparisons are made with results from the more elaborate analysis developed in Volume I. The analysis developed in Volume I was used to determine the coupled flap-lag response of a rotor to a number of sudden control changes. The results of these calculations are also presented in Volume V.

TABLE OF CONTENTS

	Page
SUMMARY	iii
FOREWORD	v
LIST OF ILLUSTRATIONS	viii
LIST OF TABLES	xiii
LIST OF SYMBOLS	xiv
INTRODUCTION	1
ASSUMPTIONS	4
EQUATIONS OF MOTION	5
AERODYNAMIC COEFFICIENTS	53
GENERAL PROCEDURES FOR OBTAINING FLUTTER SOLUTIONS	73
DOCUMENTATION OF COMPUTER PROGRAM	76
COMPUTER SOLUTION TEST CASE	78
CORRELATION OF CLASSICAL FLUTTER CALCULATIONS WITH AVAILABLE EXPERIMENTAL DATA	80
EFFECTS OF VARIATIONS IN PARAMETERS	94
SIGNIFICANCE OF CLASSICAL FLUTTER ANALYSIS AND RESULTS	100
EXTENDED NORMAL MODE TRANSIENT ANALYSIS CALCULATIONS CORRESPONDING TO CLASSICAL FLUTTER INVESTIGATIONS	102
CONCLUSIONS	189
RECOMMENDATIONS	190
REFERENCES CITED	191
DISTRIBUTION	193

LIST OF ILLUSTRATIONS

Figure		Page
1	Notation for Forces and Displacements	102
2	A Complex Polar Plot of $C(k) = F(k) + iG(k)$	102
3	A Typical V-g Plot	103
4	A Typical Variation of Decay Rate C/C_c	103
5	Notation for the Blade Axes	104
6	Notation for Blade Displacements	105
7	Radial Displacements Resulting From Edgewise Bending	106
8	Radial Displacements Resulting from Flatwise Bending	106
9	Air Velocity Relative to the Blade	107
10	Relation Between the Displacement at 25% Chord and at the Elastic Axis	107
11	Arbitrary Chordwise Displacement of the Mass Balance Center of Gravity and the Elastic Axis	108
12	Arbitrary Chordwise Displacement of the Aerodynamic Center	108
13	Geometric and Kinematic Relationship Between an Airfoil in Forward and Reverse Flow	109
14	Notation Used for an Airfoil in Either Direct Flow or Reverse Flow	110
15	Notation Used for a Two-Dimensional Chordwise Rigid Airfoil in Direct Flow and Reverse Flow	111
16	Example of the Use of the Frequency Versus Decay-Rate Digital Plot	112
17	Example of the Digital Plot of Decay Rate and Frequency Versus Forward Velocity	112
18	Position of the Aerodynamic Center, Elastic Axis and Center of Gravity for the Computer Solution Test Case	113

Figure		Page
19	Comparison of Sikorsky Flutter Analysis Results for Flutter Frequency with the Solution of Reference 12 . . .	114
20	Comparison of Sikorsky Flutter Analysis Results for Decay Rate With the Solution of Reference 12	115
21	Comparison of the Sikorsky Flutter Analysis Results for Flutter Frequency with the Solution of Reference 12 Using Simplified Aerodynamics	116
22	Comparison of the Sikorsky Flutter Analysis Results for Decay Rate with the Solution of Reference 12 Using Simplified Aerodynamics	117
23	Comparison of Calculated and Measured Flutter Speeds for the Model Helicopter Blade NACA 23012 1(R)	118
24	Comparison of Calculated and Measured Flutter Speeds for the Model Blade NACA 23012 2(R)	119
25	Variation of Solution Frequency With Change in Rotor Speed for the Model Blade NACA 23012 2(R); Tip Mach Number $<$ 0.2	120
26	Variation of Solution Decay Rate With Change in Rotor Speed for the Model Blade NACA 23012 2(R); Tip Mach Number $<$ 0.2	121
27	Comparison of Calculated and Measured Flutter Speeds for the Model Blade NACA 23012 2(F)	122
28	Comparison of Calculated and Measured Flutter Speeds for the CAL Blade Model 4; $\bar{x}_E/C = .139$, $\bar{\omega}_{\phi_1}/\bar{\omega}_{\theta_0} = .63$	124
29	Variation of Solution Frequency With Change in Rotor Speed for the CAL Blade Model 4; $\bar{x}_E/C = .139$, $\bar{\omega}_{\phi_1}/\bar{\omega}_{\theta_0} = .63$, $\mu = 0$	125
30	Variation of Solution Decay Rate With Change in Rotor Speed for the CAL Blade Model 4; $\bar{x}_E/C = .139$, $\bar{\omega}_{\phi_1}/\bar{\omega}_{\theta_0} = .63$, $\mu = 0$	126
31	Comparison of Calculated and Measured Flutter Speeds for the CAL Blade Model 4; $\bar{x}_E/C = .139$, $\bar{\omega}_{\phi_1}/\bar{\omega}_{\theta_0} = 1.31$	127

Figure		Page
32	Variation of Solution Frequency With Change in Rotor Speed for the CAL Blade Model 4; $\bar{x}_E/C = .139$, $\bar{\omega}_{\phi_1}/\bar{\omega}_{\theta_0} = .63$, $\mu = .5$	128
33	Variation of Solution Decay Rate With Change in Rotor Speed for the CAL Blade Model 4; $\bar{x}_E/C = .139$, $\bar{\omega}_{\phi_1}/\bar{\omega}_{\theta_0} = .63$, $\mu = .5$	129
34	Comparison of Calculated and Measured Flutter Speeds for the CAL Blade Model 4; $\bar{x}_E/C = .044$, $\bar{\omega}_{\phi_1}/\bar{\omega}_{\theta_0} = 1.05$	130
35	Comparison of Calculated and Measured Flutter Speeds for the CAL Blade Model 4; $\bar{x}_E/C = .0036$, $\bar{\omega}_{\phi_1}/\bar{\omega}_{\theta_0} = 1.03$	131
36	Comparison of Calculated and Measured Flutter Speeds for the CAL Blade Model 4; $\bar{x}_E/C = .0036$, $\bar{\omega}_{\phi_1}/\bar{\omega}_{\theta_0} = 1.44$	132
37	Variation of Solution Frequency With Change in Rotor Speed for the Nominal Articulated Blade; $\mu = 0$	133
38	Variation of Solution Decay Rate With Change in Rotor Speed for the Nominal Articulated Blade; $\mu = 0$	134
39	Varying the Chordwise Position of the Elastic Axis for an Articulated Blade	135
40	Variation of Modal Amplitude Ratio and Phase Angle With Change in Advance Ratio for the Nominal Articulated Blade	136
41	Variation of Modal Amplitude Ratio and Phase Angle With Change in Advance Ratio for the Articulated Blade, Case 1.A2	137
42	Varying the Chordwise Position of the Center of Gravity for an Articulated Blade	138
43	Varying the Blade Torsional Stiffness for an Articulated Blade; GJ_{NOM}=12,436 Lb-In^2	139
44	Typical Variation of Torsion Frequency With Change in Advance Ratio for Large Center-of-Gravity Offset	140

Figure		Page
45	Varying the Blade Flatwise Bending Stiffness for an Articulated Blade; $EI_{z_{NOM}}$ = 29,500 Lb-In^2	140
46	Varying the Blade Mass for an Articulated Blade; m_{NOM} = .0162 Slug/Ft	141
47	Varying the Blade Pitching Inertia for an Articulated Blade; $I_{\alpha_{NOM}}$ = .742 x 10^{-4} Slug-Ft^2/Ft . . .	142
48	Variation of Solution Frequency With Change in Rotor Speed for the Nominal Nonarticulated Blade; μ = 0	143
49	Variation of Solution Decay Rate With Change in Rotor Speed for the Nominal Nonarticulated Blade; μ = 0	144
50	Variation of Critical Advance Ratio With Change in Rotor Speed for the Nominal Nonarticulated Blade	145
51	Varying the Chordwise Position of the Elastic Axis for a Nonarticulated Blade	146
52	Varying the Chordwise Position of the Center of Gravity for a Nonarticulated Blade	147
53	Varying the Blade Torsional Stiffness for a Nonarticulated Blade; GJ_{NOM} = 12,436 Lb-In^2	148
54	Varying the Blade Flatwise Bending Stiffness for a Nonarticulated Blade; $EI_{z_{NOM}}$ = 29,500 Lb-In^2	149
55	Varying the Blade Mass for a Nonarticulated Blade; m_{NOM} = .0162 Slug/Ft	150
56	Varying the Blade Pitching Inertia for a Nonarticulated Blade; $I_{\alpha_{NOM}}$ = .742 x 10^{-4} Slug-Ft^2/Ft. .	151
57	Articulated Blade Flapping and Torsion Modal Time History; μ = .30 , A_{1s} = 0° , B_{1s} = 0° , $\theta_{.75R}$ = 1.0° , $\alpha_s \cong$ 0°	152
58	Articulated Blade Flapping and Torsion Modal Time History; μ = .15 , A_{1s} = 0° , B_{1s} = 0° , $\theta_{.75R}$ = 1.0° , $\alpha_s \cong$ 0°	154

Figure		Page

59 Effect of Aft Center-of-Gravity Position on Articulated Blade Tip Motions Versus Azimuth Angle; $\mu = .30$, $A_{1S} = 0°$, $B_{1S} = 0°$, $\theta_{.75R} = 1.0°$, $\alpha_S \cong 0°$ 157

60 Articulated Blade Elastic Deformations Versus Azimuth Angle With Aft Center-of-Gravity Position; $\mu = .30$, $A_{1S} = 0°$, $B_{1S} = 0°$, $\theta_{.75R} = 1.0°$, $\alpha_S \cong 0°$ 158

61 Articulated Blade Elastic Deformations Versus Azimuth Angle With Aft Center-of-Gravity Position; $\mu = .15$, $A_{1S} = 0°$, $B_{1S} = 0°$, $\theta_{.75R} = 1.0°$, $\alpha_S \cong 0°$ 160

62 Nonarticulated Blade Deformation Versus Azimuth Angle With Aft Center-of-Gravity Position; $\mu = .30$, $A_{1S} = 0°$, $B_{1S} = 0°$, $\theta_{.75R} = 1.0°$, $\alpha_S \cong 0°$, $\bar{X}/C_b = -.20$ 163

63 One-Half Peak-to-Peak Articulated Blade Deformations Versus Aft Center-of-Gravity Position; $\mu = .30$, $A_{1S} = 0°$, $B_{1S} = 0°$, $\theta_{.75R} = 1.0°$, $\alpha_S \cong 0°$ 164

64 One-Half Peak-to-Peak Articulated Blade Deformations Versus Aft Center-of-Gravity Position; $\mu = .15$, $A_{1S} = 0°$, $B_{1S} = 0°$, $\theta_{.75R} = 1.0°$, $\alpha_S \cong 0°$ 165

65 One-Half Peak-to-Peak Nonarticulated Blade Deformations Versus Aft Center-of-Gravity Position; $\mu = .30$, $A_{1S} = 0°$, $B_{1S} = 0°$, $\theta_{.75R} = 1.0°$, $\alpha_S \cong 0°$ 166

LIST OF TABLES

Table		Page
I	Example of the Application of Reverse-Flow Relations	167
II	Example of Errors in the Tabulated Coefficients	167
III	Airfoil Data Used for the Test Case	168
IV	Comparison of Flutter Speeds	169
V	Aerodynamic Coefficients Used for the Test Case	169
VI	NACA Model Blade Properties	170
VII	Cornell Aeronautical Laboratory Model Blade Properties	172
VIII	Cases Used for Correlation With Cornell Data	174
IX	Effect on Flutter Speed of Varying Mass Balance	174
X	Basic Properties of the Blade Used for the Parameter Variation Study	175
XI	Cases Considered in the Variation of Parameters	176
XII	Compressible Flow Flutter Coefficients	178
XIII	Blade Configurations and Flight Conditions for Extended Normal Mode Analysis Calculations Corresponding to Classical Flutter Investigations	188

LIST OF SYMBOLS

a_{EA}	distance of the elastic axis aft of the blade mid-chord divided by the blade semichord
a'_{EA}	distance of the elastic axis aft of the blade mid-chord divided by the blade semichord, prior to an arbitrary variation in elastic axis position
$\Delta\left[a\right]$	a matrix of structural coefficients expressed in terms of a unit span increment
$\Delta\left[\bar{a}\right]_k$	a matrix of structural coefficients expressed in terms of the kth finite span increment
$a_{\beta\theta_o}$	product of inertia defined in Reference 14
$a_{\beta\beta}$	flapping moment of inertia defined in Reference 14
$a_{\theta_o\theta_o}$	pitching moment of inertia defined in Reference 14
A^*	speed of sound, ft/sec
AC	aerodynamic center chordwise position aft of leading edge, percent of chord
A_{1S}	lateral cyclic pitch, deg
$\left[A_s\right]$	structural generalized mass matrix, slug-ft^2
$\left[A\right]_T$	total generalized mass matrix
$\left[A_U\right]$	complex aerodynamic coefficient matrix
b	blade semichord, ft
b_R	arbitrary blade reference semichord, ft
B_{1S}	longitudinal cyclic pitch, deg
$\left[B\right]_{AERO}$	aerodynamic generalized damping matrix, ft-lb-sec
$\left[B_s\right]$	structural generalized damping and gyroscopic matrix, ft-lb-sec
$\left[B\right]_T$	total generalized damping and gyroscopic matrix
$\left[B_D\right]_T$	structural generalized damping matrix
$\left[B_C\right]$	chord variation matrix

$[B_U]$	structural coefficient matrix
C_b	blade chord, ft
C/C_c	solution decay rate divided by critical decay rate
$C(k)$	Theodorsen function, Reference 17
C_{L_α}	rate of change of lift coefficient with angle of attack
CG	center of gravity chordwise position aft of leading edge, percent of chord
$[C]_{AERO}$	aerodynamic generalized stiffness matrix, ft-lb
$[C_s]$	structural generalized stiffness matrix, ft-lb
${}^{Q}[C_s]$	structural generalized stiffness matrix for final form of equations
$[C]_T$	total generalized stiffness matrix
ds	infinitesmal element of surface area
$D_{\ddot{q}}$	general aerodynamic inertia term
$D_{g_{ii}}$	viscous structural damping generalized force coefficient, ft-lb-sec
$[\dot{D}]$	aerodynamic damping matrix
$[D]$	aerodynamic stiffness matrix
$[D_g]$	structural damping matrix
e	flapping hinge offset, ft
$\vec{e}_1, \vec{e}_2, \vec{e}_3$	triad of unit vectors fixed in the blade
EA	elastic axis position aft of leading edge, percent of chord
EI_x	edgewise bending stiffness, lb-in.^{2}
EI_z	flatwise bending stiffness, lb-in.^{2}
$[E]$	elastic stiffness matrix
f_i	nondimensional flatwise displacement of the ith mode, $f_i = -g_i^z/b_R$
$f(x_1, z_1, r)$	a function of x_1, z_1, and r

F_i	torsional displacement of the ith mode, rad
$F(k)$	real part of Theodorsen function, Reference 17
g	structural damping coefficient
g_i^x	edgewise displacement of the ith mode, ft
g_i^z	flatwise displacement of the ith mode, ft
$G(k)$	imaginary part of Theodorsen function, Reference 17
GJ	torsional stiffness, lb-in^2
$[G]$	gyroscopic generalized inertia matrix, slug-ft^2
$\Omega[G]$	gyroscopic generalized inertia matrix for final form of equations, sec
$[G_M]$	mode shape matrix used in calculating the aerodynamic matrices
h_{EA}	vertical displacement (positive down) of the elastic axis, ft
$h_{c/4}$	vertical displacement (positive down) of the 25% chord, ft
h_x	edgewise displacement (positive aft) of the elastic axis, ft
h_z	flatwise displacement (positive up) of the elastic axis, ft
h_z''	bending curvature in flatwise dimension, $h_z'' = d^2(h_z/R)/d(r/R)^2$
h_{zp}''	one-half peak-to-peak value of h_z''
$[H]$	elastic axis position variation matrix
I_β	mass moment of inertia about flapping hinge, slug-ft^2
I_{xx}	flatwise moment of inertia per unit span, slug-ft^2/ft
I_{xy}	product of inertia per unit span, slug-ft^2/ft
I_{xz}	product of inertia per unit span, slug-ft^2/ft
I_{xz}'	product of inertia per unit span prior to a variation in mass balance or elastic axis position, slug-ft^2/ft

I_{zz}	edgewise moment of inertia per unit span, slug-ft^2/ft
I'_{zz}	edgewise moment of inertia per unit span prior to a variation in mass balance or elastic axis position, slug-ft^2/ft
I_α	blade pitching mass moment of inertia per unit span, slug-ft^2/ft
I_θ	mass moment of inertia per unit span about lagging hinge, slug-ft^2/ft
J_{xx}	integral along blade of I_{xx} with respect to r from root to tip, slug-ft^2
J_{zz}	integral along blade of I_{zz} with respect to r from root to tip, slug-ft^2
k	reduced frequency parameter
$\bar{k}$	reduced frequency parameter normalized to facilitate interpolation
k_a	polar radius of gyration of the tensile cross section, ft
$[K]$	generalized elastic stiffness matrix, lb-ft
l	arbitrary reference length, ft
l_h	aerodynamic coefficient, Eq. (16)
$l_{\dot{h}}$	aerodynamic coefficient, Eq. (16)
l_α	aerodynamic coefficient, Eq. (16)
$l_{\dot{\alpha}}$	aerodynamic coefficient, Eq. (16)
L	lift (positive up) acting on a strip of width Δr and chord, 2b, lb
$\bar{L}$	value of L in reverse flow, lb
$\tilde{L}$	lift (positive up) acting on a strip of width Δr and chord 2b, after an arbitrary change in the aerodynamic center, lb
$[L]$	generalized elastic tension stiffness coefficient matrix, slug-ft^2
${}^{Q}[L]$	generalized elastic tension stiffness coefficient matrix for the final form of the equations, sec^2

m	mass per unit span, slugs/ft
m_h	aerodynamic coefficient, Eq. (16)
$m_{\dot{h}}$	aerodynamic coefficient, Eq. (16)
$m\bar{x}$	edgewise mass moment about the elastic axis per unit span, slug-ft/ft
$m\bar{z}$	flatwise mass moment about the chord line per unit span, slug-ft/ft
m_α	aerodynamic coefficient, Eq. (16)
$m_{\dot{\alpha}}$	aerodynamic coefficient, Eq. (16)
M	pitching moment (positive nose up) acting on a strip of width Δr and chord 2b, lb-ft
$\tilde{M}$	pitching moment (positive nose up) acting on a strip of width Δr and chord 2b, after an arbitrary change of the aerodynamic center, lb-ft
M_N	Mach number
M_t	advancing blade tip Mach number
${}^{G}M_{ij}$	generalized inertia, slug-ft^2
$\left[{}^{G}M\right]$	generalized inertia matrix, slug-ft^2
$\mathcal{M}$	integral of mass moment increments about an arbitrary blade spanwise station, slug-ft
p	arbitrary constant used to normalize the reduced frequency parameter
P	pressure difference across the airfoil in direct flow, lb/ft^2
$\bar{P}$	pressure difference across the airfoil in reverse flow, lb/ft^2
q	generalized displacement
q_{θ_1}	first torsion modal displacement
Q	generalized force, ft-lb
r	spanwise distance from the rotation axis, ft

$\bar{r}$	spanwise distance from the flapping hinge, ft
r_m	ratio of flapping to torsion displacements
$\bar{r}_m$	normalized value of r_m ; $\bar{r}_m = r_m/(r_m+10)$
r_α	radius of gyration about the pitch axis
R	blade radius, ft
s	arc length, ft
S_β	mass moment about flapping hinge, slug-ft
S_θ	mass moment about lagging hinge, slug-ft
t_a	aerodynamic center position variation coefficient
$t_a b\delta_{AC}$	distance the aerodynamic center is shifted aft because of an arbitrary variation, ft
t_b	mass balance position variation coefficient
$t_b\Delta\bar{x}$	distance the center of gravity of the mass balance weight is shifted aft because of an arbitrary variation, ft
t_e	elastic axis position variation coefficient
$t_e b\Delta\alpha_{EA}$	distance the elastic axis is shifted aft because of an arbitrary variation, ft
t_n	mass balance weight variation coefficient
T	kinetic energy, ft-lb
$[T]$	centrifugal generalized inertia matrix, slug-ft^2
${}^a[T]$	centrifugal generalized inertia matrix for final form of the equations, sec^2
U	potential energy, ft-lb
$\vec{V}$	velocity vector, ft/sec
V_D	disc inflow velocity, ft/sec
V_H	helicopter forward velocity, ft/sec
V_x	blade relative velocity component normal to the blade radius parallel to the plane of rotation

V	velocity of the air normal to the blade radius, ft/sec
V	arbitrary reference velocity, ft/sec
$V_{0.8R}$	velocity of the air normal to the blade radius at the 80% radius, ft/sec
w	vertical velocity in direct flow of air in contact with the airfoil, ft/sec
w_a	amplitude of sinusoidal variation in w
$\bar{w}$	vertical velocity in reverse flow of air in contact with the airfoil, ft/sec
$\bar{w}_a$	amplitude of sinusoidal variation in $\bar{w}$
x, y, z	coordinates of a point on a blade in the rotating coordinate system, ft
x_o, y_o, z_o	coordinates of a point on the blade in the x, y, z system when blade deflections are zero, ft
x_B, y_B	coordinates of a point on a blade in the fixed coordinate system, ft
${}^{o}\left(\frac{\partial x, y, z}{\partial q_i}\right)$	derivatives of x, y, z evaluated when blade deflections are zero, ft
${}^{o}\left(\frac{\partial^2 x, y, z}{\partial q_i \partial q_j}\right)$	derivatives of x, y, z evaluated when blade deflections are zero, ft
x_l, y_l, z_l	coordinates of a point with respect to an axis system fixed at the intersection of the elastic axis and a blade section, ft
x_{EA}, z_{EA}	coordinates of a point on the elastic axis in the x, y, z coordinate system, ft
x_P, y_P, z_P	coordinates of a generic point in the x, y, z coordinate system, ft
$\bar{x}$	distance of the center-of-gravity aft of the elastic axis, ft
$\bar{x}_b^*$	distance of the balance weights ahead of the 25% chord, ft
$\bar{x}_E$	equivalent center-of-gravity location, defined on p. 85 and in Reference 14, ft
$\bar{x}_S$	distance of the center-of-gravity aft of the elastic axis, ft

$\bar{x}'$	distance of the center-of-gravity aft of the elastic axis prior to a variation in mass balance or elastic axis position, ft.
$[x_1]$	transformed aerodynamic damping matrix
$[x_2]$	transformed aerodynamic stiffness matrix
y_v	natural frequency variation coefficient
$y_v \omega_{vi}$	variation of the natural frequency of the ith mode, rad/sec
z_1	vertical deflection of blade tip due to blade flapping and bending
$\bar{z}$	distance of the center of gravity above the elastic axis, ft.
z_s	displacement of a generic point on the chord line in direct flow, ft.
z_{sa}	amplitude of a sinusoidal variation in z_s
$\bar{z}_s$	displacement of a generic point on the chord line in reverse flow, ft.
$\bar{z}_{sa}$	amplitude of a sinusoidal variation in $\bar{z}_s$
α	pitch displacement, rad
α_s	shaft angle of attack, deg
β	blade flapping angle, rad
β_s	blade coning angle, rad
γ_1	bending slope in the x-y plane
γ_2	bending slope in the y-z plane
γ	distance of the elastic axis aft of the aerodynamic center divided by the radius of gyration about the pitch axis
$\{\delta\}$	plunging and pitching deflection column matrix at the 25% chord
Δb	distance of aerodynamic center aft of the 25% chord position prior to an arbitrary variation, ft

Δr	spanwise width of a blade segment
Δ_1	change in radial position of points off the elastic axis due to edgewise bending slope, ft.
Δ_2	change in radial position of points off the elastic axis due to flatwise bending slope, ft.
Δ_3	change in radial position due to curvature of the elastic axis, ft.
$[\Delta]$	aerodynamic center variation matrix
ϵ	distance of the blade mid-chord aft of the axis at a blade section under consideration
η	distance along the radius, nondimensionalized by reference length
η_I	innermost nondimensional radius at which aerodynamic forces are effective
η_P	outermost nondimensional radius at which aerodynamic forces are effective
θ	phase angle between bending and torsion displacements, deg
θ_e	blade local elastic twist, rad
θ_e'	nondimensional rate of blade local elastic twist, $\theta_e' = d(\theta_e)/d(r/R)$
θ_{ep}'	one-half peak-to-peak value of θ_e'
$(\theta_{0.75R})_S$	collective pitch measured at 75% rotor radius, deg
$(\theta_{0.8R})_S$	collective pitch measured at 80% rotor radius, deg
$\theta_{e_{1.0}}$	elastic twist at blade tip, deg
μ	advance ratio, $\mu = V/\Omega R$
μ_M	blade mass density ratio, $\mu_M = m/\rho\pi b^2$
ρ	density of the air at the desired altitude, slugs/ft^3
ρ_b	blade structural density, slugs/ft^3
ρ_{SL}	density of the air at sea level, slugs/ft^3

σ_D	air density ratio $\sigma_D = \rho/\rho_{SL}$
τ	nondimensional time
$[\Phi]$	mode shape matrix used in calculating the generalized inertia matrix, ft.
ψ	azimuthal angle of blade in rotor disc, zero downwind, rad.
ω	solution frequency, rad/sec
ω_R	reference frequency, rad/sec
ω_f	flutter frequency, rad/sec
ω_a	solution frequency used when calculating $\ell_{\dot{\alpha}}$, rad/sec
ω_i	ith mode natural frequency at a rotor speed ΩR rad/sec
ω_{h_i}	ith flatwise bending natural frequency, rad/sec
ω_{α_i}	ith torsional natural frequency, rad/sec
$\overline{\omega_{\theta_0}}$	nonrotating rigid-body pitch frequency, rad/sec
$\overline{\omega_{\phi_1}}$	nonrotating first flatwise bending frequency, rad/sec
Ω	rotor rotational speed, rad/sec
Ω_R	rotational speed at which the input modes are determined, rad/sec

SUBSCRIPTS

b	refers to a balance weight whose mass and position are variable
CG	refers to the center-of-gravity position
EA	refers to the elastic axis position
h	refers to vertical translation
i	refers to the ith degree of freedom (mode or generalized coordinate)
ij	refers to the element in the ith row and jth column of a matrix

j	refers to the jth degree of freedom (mode or generalized coordinate)
k	refers to the kth blade segment or the corresponding blade station which is situated on that segment. When applied to a structural parameter, it implies that the quantity is the contribution for that segment, instead of the contribution per unit span
LE	refers to the leading edge
ND	refers to the last of a number of degrees of freedom considered
NOM	refers to a nominal value
NS	refers to the outermost blade segment
r	refers to the r th degree of freedom (mode or generalized coordinate)
R	refers to a reference value
α	refers to a rotation in pitch
ϕ	refers to a mass property of the blade itself, exclusive of a balance weight whose mass and position are variable
0	refers to an undeflected blade position
C/4	refers to the 25% chord station
C/2	refers to the 50% chord station
3C/4	refers to the 75% chord station

SUPERSCRIPTS

F	refers to forward flow
h	refers to vertical translation
R	refers to reverse flow
$\alpha_{(3/4)}$	refers to rotation about the 75% chord
0	refers to an aerodynamic center position prior to an arbitrary variation
N	refers to an aerodynamic center position after an arbitrary variation

δ	refers to a matrix of blade inertial properties appropriate to either a local blade station or a local blade segment. Units of the matrix elements are then per unit length or per segment respectively
Δ	refers to a matrix of generalized structural coefficients appropriate to either a local blade station or a local blade segment. Units of the matrix elements are per unit length or per segment respectively

DERIVATIVE NOTATION

$\dot{f}(t)$	first derivative of a function with respect to real time, $\dot{f}(t) = df(t)/dt$
$\ddot{f}(t)$	second derivative of a function of time with respect to real time, $\ddot{f}(t) = d^2 f(t)/dt^2$

MISCELLANEOUS

$[P]'$	denotes the transpose of any matrix $[P]$
$\vec{n}$	denotes that a function n is a vector
δn	denotes a virtual change in any function n

BLANK PAGE

INTRODUCTION

In the past, classical flutter of helicopter rotor blades has not been a serious problem because it has been customary to place the blade elastic axis and the center of gravity on or near the 25% chord point. This means that the elastic axis, the axis of aerodynamic centers, and the center-of-gravity axis are effectively coincident, thus eliminating coupled bending-torsion flutter and also single-degree-of-freedom flutter. Of course, the axes are never exactly coincident; but for small deviations from coincidence, the application of suitable flutter criteria is sufficient to guard against the possibility of the occurrence of classical flutter.

Placing the three axes in coincidence involves some penalty in weight and increased complexity. To provide improved structural efficiency, consideration is being given to moving the axes apart, such as occurs with fixed wings. Once the axes are no longer in approximate coincidence, the blade becomes very susceptible to classical flutter and at the same time not very amenable to a flutter clearance based on the application of flutter criteria. Therefore, flutter calculations have to be undertaken; this requires the use of an aerodynamic theory. The blade tip Mach number of some current helicopters approaches unity for certain flight conditions so that compressibility effects are very important. As yet, no general unsteady aerodynamic theory exists for helicopter rotor blades operating at high tip Mach numbers and high advance ratios. Therefore, when flutter calculations are made for these flight conditions, some approximate aerodynamic theory has to be employed.

In addition to the tendency for modern helicopter rotor blades to operate at high tip Mach numbers and high advance ratios, some current designs call for the rotor to operate in unusual flight conditions. For example, the stopped rotor compound helicopter requires that the rotor be stopped at the transition speed, at which time the lift is transferred to a pair of fixed wings. During the last few revolutions before the rotor stops, each blade as it passes through $\psi = 270^{\circ}$ becomes effectively a fixed wing traveling in reverse flow at the helicopter transition speed, with the elastic axis at 75% chord. This immediately raises the possibility of low-speed flutter. This term is applied to the single degree of freedom classical torsional flutter that occurs when the still air nodal line of a fundamental mode lies on or near the 75% chord point. With the nodal line in this position, it is possible for flutter to occur at very low airspeeds. In the past, this type of flutter was mainly of academic interest and consequently theoretical and experimental studies of this phenomenon are noticeably absent from the literature. However, with the advent of stopped-rotor helicopters, low-speed flutter will have to be given serious consideration. The methods developed in this study are directly applicable for this condition.

Thus, for current and future helicopter rotor blades, classical flutter calculations begin to acquire the same importance as they have in the past for fixed wings. The present study is part of the current effort that is being made in this direction. The study is strongly oriented toward pro-

viding a method for rapidly obtaining estimates of rotating blade classical flutter speed and the effect on the flutter speed of varying parameters such as blade chordwise elastic axis position. Such a method is mandatory for design use, where introduction of new blade concepts requires that the classical flutter solutions be attempted with the best available method of analysis. Consistent with the approach, the fixed azimuth method was chosen in conjunction with the use of a digital computer to obtain solutions to the equations of motion. This is in contrast to some recent studies which have used an analogue computer to integrate the equations of motion with time varying coefficients. The fixed azimuth approach is an expedient way of converting the time varying coefficients to fixed coefficients which are more convenient for digital computation. It is probably the major assumption made in deriving the equations of motion. With a rotating blade, the first two aerodynamic effects listed below result in time varying coefficients in the equations of motion.

1. The dynamic pressure varying azimuthally for $\mu > 0$.

2. The indicial aerodynamic response due to the varying of the velocity field azimuthally for $\mu > 0$.

3. There is a phase lag between the occurrence of maximum angle of incidence and the resulting development of maximum lift when the blade executes simple harmonic oscillations. This phase lag is the result of indicial aerodynamic response to the varying geometric angle of attack; for simple harmonic oscillations, it is integrated to give an in-phase and quadrature response.

4. The aerodynamic forces are determined by multiple nonplanar shed wakes.

The fixed azimuth approach considers a particular azimuth angle only. The instantaneous velocity of the blade at this azimuth angle is considered to apply for all time, that is, $-\infty < t < \infty$, and the aerodynamic forces are calculated in accordance with the assumption. Hence, only the third effect is taken into account, the lag effects being derived from fixed-wing theory. The neglect of the first two effects causes the coefficients in the equations of motion to be time invariant. The analogue computer studies referred to above considered only the first effect, so that steady-state aerodynamics were used. So while the coefficients in the equations of motion were time varying, all but the first effect was neglected. In this respect it should be noted that when steady-state aerodynamic coefficients are used, it is not possible to predict single-degree-of-freedom classical flutter which depends on unsteady aerodynamic lag effects.

The fixed azimuth classical flutter study begins with the derivation of the equations of motion, and the presentation of the set of assumptions and approximations upon which the equations are based. These equations of motion are used to calculate the flutter speeds of sets of model rotor blades for which experimental results are available for correlation. Then

the method described in this volume is applied to the investigation of the change in flutter speed due to a change in various parameters. Finally, the results of a number of calculations made with the more elaborate Extended Normal Mode Transient Analysis described in Volume I are presented and compared with the corresponding fixed azimuth classical flutter calculations.

ASSUMPTIONS

1. The equations of motion are linearized by assuming that the linear and angular displacements of a blade element are small.

2. Strip theory is used to compute the aerodynamic forces. This implies that the pressure distribution on any chordwise strip of a blade is the same as if that strip were part of a two-dimensional blade which performed the same motion everywhere as the strip under consideration. Thus, the interaction between strips is not accounted for.

3. The aerodynamic forces are calculated using a fixed azimuth approach. This method considers a particular azimuth angle only. The instantaneous velocity of the blade at this azimuth angle is considered to apply for all time, that is, $-\infty < t < \infty$ The aerodynamic forces are calculated in accordance with this assumption; as a result, the coefficients in the equations of motion become time invariant. Also, the indicial aerodynamic response associated with the changing velocity field is neglected.

4. The assumed two-dimensional oscillatory aerodynamic forces acting on a strip are approximated by two-dimensional fixed-wing theory. This means that the following assumptions are made:

    a. The steady angle of incidence is small and, hence, well below the stall region.

    b. Effects due to a nonplanar wake and interaction between shed wakes are neglected.

5. The contribution to the generalized stiffness of bending modes due to radial flow is neglected. This means that the solutions in the region of $\psi = 0^{\circ}$ and 180° become increasingly less accurate as advance ratio increases.

6. Zero steady state:

    a. Blade twist.

    b. Blade pitch angle.

    c. Blade lag angle.

EQUATIONS OF MOTION

GENERAL DISCUSSION

The form in which the equations are cast for eigenvalue solution is intimately tied up with the notation used to represent the aerodynamic forces. Measuring the blade displacements and the aerodynamic forces at the 25% chord, then for simple harmonic motion, the lift L and moment M acting on a blade segment of width Δr of a nonrotating blade in incompressible two dimensional flow, are given, as shown in Figure 1, by the following equation:

$$\frac{1}{\pi\rho b^3 \Delta r}\begin{bmatrix} L \\ -\frac{M}{b} \end{bmatrix}_{C/4} = \begin{bmatrix} 1 & \frac{1}{2} \\ \frac{1}{2} & \frac{3}{8} \end{bmatrix}\begin{bmatrix} \frac{\ddot{h}}{b} \\ \ddot{\alpha} \end{bmatrix}_{C/4} + \left(\frac{V}{b}\right)\begin{bmatrix} 2C(k) & 1+2C(k) \\ 0 & 1 \end{bmatrix}\begin{bmatrix} \frac{\dot{h}}{b} \\ \dot{\alpha} \end{bmatrix}_{C/4} + \left(\frac{V}{b}\right)^2\begin{bmatrix} 0 & 2C(k) \\ 0 & 0 \end{bmatrix}\begin{bmatrix} \frac{h}{b} \\ \alpha \end{bmatrix}_{C/4} \tag{1}$$

where

$C(k) = F(k) + iG(k)$ is the Theodorsen circulation function

$k = \omega b/V$ is the reduced frequency parameter

A complex polar plot of $C(k)$ is shown in Figure 2. The following points should be noted:

1. The acceleration (inertia) coefficients are constant; thus, the aerodynamic inertias are indistinguishable from structural inertias.

2. The velocity (damping) and displacement (stiffness) coefficients are functions of the complex circulation function $C(k)$. They vary with reduced frequency k, but remain finite as k ranges from zero (steady flow) to infinity (zero forward velocity).

When these coefficients are incorporated into the flutter equations, it is customary to modify them with the relations for simple harmonic motion; namely,

$$\dot{q} = i\omega q$$

$$\ddot{q} = -\omega^2 q$$

$$i = \sqrt{-1} \tag{2}$$

where q is any displacement, such as α or h .

Two methods are widely used and result in different methods of presenting the equations of motion. They are the "V-g method" and the "decay-rate method".

The V-g method is used in the United States. A discussion of this method appears for example, on page 241 of Reference 1. The aerodynamic inertia, damping and displacement coefficient matrices are combined to form a single aerodynamic complex stiffness matrix. The above equation (1) becomes

$$\frac{1}{\pi\rho b^3\omega^2\Delta r}\begin{bmatrix} -L \\ \frac{M}{b} \end{bmatrix}_{C/4} = \begin{bmatrix} 1-\frac{2i}{k}C(k) & \frac{1}{2}-\frac{i}{k}\left[1+2C(k)\right]-\frac{2}{k^2}C(k) \\ \frac{1}{2} & \frac{3}{8}-\frac{i}{k} \end{bmatrix}\begin{bmatrix} \frac{h}{b} \\ \alpha \end{bmatrix}_{C/4} \tag{3}$$

The terms involving $i = \sqrt{-1}$ were formerly damping coefficients. It should be noted that

$$\lim_{k \to 0} \frac{C(k)}{k} = \infty - i\infty \tag{4}$$

so that the aerodynamic coefficients become infinite for the case of steady flow. This is due to the algebraic rearranging of the terms and does not imply that the total aerodynamic forces become infinite. The coefficients remain finite for the case of zero forward speed $(k = \infty)$.

With the aerodynamic forces expressed in the above manner, the equations of motion can be put into the following form

$$\left\{\left[A\right] - \left(\frac{\omega_R}{\omega}\right)^2 (1+ig)\left[B_U\right]\right\}\left\{q\right\} = \left\{0\right\} \tag{5}$$

For a particular value of the reduced frequency k, the coefficient matrix $[A_U]$ can be evaluated, and the eigenvalue yields the flutter frequency ω and the value of the structural damping coefficient g (assumed here to be the same for each mode) required to keep the system oscillating with simple harmonic motion. The forward speed V is found using ω and the value of k assumed when calculating the coefficient matrix $[A_U]$.

That is,

$$V = \left(\frac{V}{\omega b}\right)\omega b = \omega\left(\frac{b}{k}\right) \tag{6}$$

The forward speed will be different for each mode. When the process is repeated, assuming different values for k gives the familiar V-g plot, as in Figure 3.

The decay-rate method is used in Great Britain. The complex aerodynamic forces are rearranged into real coefficient matrices, with the relations for simple harmonic motion being used, so that the equations become, with forces and displacements referred to the leading edge,

$$\frac{-1}{\rho b^3 \Delta r}\begin{bmatrix} -L \\ \frac{M}{b} \end{bmatrix} = \begin{bmatrix} \pi & \pi \\ \pi & \frac{9\pi}{8} \end{bmatrix}\begin{bmatrix} \frac{\ddot{h}}{b} \\ \ddot{\alpha} \end{bmatrix} + \left(\frac{V}{b}\right)\begin{bmatrix} 2\pi F & \pi\left[1+3F+\frac{2G}{k}\right] \\ \pi F & \pi\left[\frac{3}{2}+\frac{3}{2}F+\frac{G}{k}\right] \end{bmatrix}\begin{bmatrix} \frac{\dot{h}}{b} \\ \dot{\alpha} \end{bmatrix}$$

$$+\left(\frac{V}{b}\right)^2\begin{bmatrix} -2\pi kG & \pi\left[2F-3kG\right] \\ -\pi kG & \frac{\pi}{2}\left[2F-3kG\right] \end{bmatrix}\begin{bmatrix} \frac{h}{b} \\ \alpha \end{bmatrix} \tag{7}$$

again it should be noted that

$$\lim_{k \to 0} \frac{G(k)}{k} = -\infty \tag{8}$$

Some of the coefficients become infinite for both steady flow $(k = 0)$ and zero forward speed $(k = \infty)$.

With the aerodynamic coefficients expressed in the above manner, the equations of motion can be put into the following form:

$$[A]_T\{\ddot{q}\} + \left(V[B]_{AERO} + [B_R]\right)\{\dot{q}\} + \left(V^2[C]_{AERO} + [E]\right)\{q\} = \{0\} \tag{9}$$

V and V^2 give the effect of dynamic pressure so that the variation of the aerodynamic matrices $[B]_{AERO}$ and $[C]_{AERO}$ with k is due only to the unsteadiness of the flow. This is in contrast to the V-g method where the variation of the complex matrix $[A_U]$ with k includes the effect of dynamic pressure. This occurs because the dynamic pressure is expressed in terms of the reduced frequency k according to

$$\tfrac{1}{2}\rho V^2 = \omega^2\left(\tfrac{1}{2}\rho\frac{b^2}{k^2}\right) \tag{10}$$

In the V-g method, the ω^2 is divided out and appears only in the complex eigenvalue

$$\left(\frac{\omega_R}{\omega}\right)^2 (1 + ig) \tag{11}$$

In the decay-rate method, the equations are solved by assuming a value for k which allows all the matrices to be computed. That is, the degree of unsteadiness of the flow at the flutter condition is assumed in advance. Then for a particular forward speed V, the total damping matrix $V[B]_{AERO} + [B_R]$ and the total stiffness matrix $V^2[C]_{AERO} + [E]$ are formed, and the eigenvalue solution is obtained. This process is repeated for a number of values for V and V^2 but using always the same matrices $[B]_{AERO}$ and $[C]_{AERO}$ and, hence, the same assumed value for k. This gives a plot of the exponential decay rate C/C_c for each of the modes, as in Figure 4. The decay rate is nondimensionalized with respect to the critical damping rate in the usual manner.

When using the decay-rate method, the convention of plotting C/C_c with the stable region above the abscissa is usually followed. It is of interest to examine the relationship between the two methods. The two methods will yield the same flutter speed and frequency. However, the variation of g versus V will be different from the variation of C/C_c versus V even though they cross the abscissa at the same point. Sometimes an attempt is made to convert C/C_c to ζ using the relation

$$g = 2\left(\frac{C}{C_c}\right) \tag{12}$$

This is actually a contraction of the equation

$$g = 2\left(\frac{C}{C_c}\right)\left(\frac{\omega_h}{\omega}\right) \tag{13}$$

which is exact for a single-degree-of-freedom system. However, the above conversion has no justification for multi-degree-of-freedom systems.

The question arose as to which of the above methods to use in the present study. The velocity distribution across the blade varies with forward speed for a constant rotor speed. If the helicopter forward velocity V_H is used in place of V, the above methods may be applied to the rotating blade in the same way that they are applied to calculating fixed-wing flutter speeds. However, the aerodynamic matrices are now a function of the advance ratio μ, which has to be known in advance in order to be able to calculate the matrices.

If the V-ζ method is used, it is necessary to assume a value for $\mu = V_H/\Omega R$; and corresponding to the value of $k = \omega b/V_H$ chosen, the flutter solution gives a value of V_H for each mode. The corresponding value of rotor speed is found from the equation

$$\Omega = \frac{V_H}{\mu R} \tag{14}$$

Thus, the rotor speed Ω will be different for each mode. In obtaining a V_H-g plot, it is required either that the rotor speed be constant or that it vary in some prescribed manner with V_H . In either case, it is most unlikely that Ω for the mode of interest, calculated using the above relationship, will follow the required variation. As it is necessary to have Ω very close to its correct value, an iteration procedure is required.

When applying the decay-rate method, the forward velocity is stated; with Ω known, then μ is known in advance. Only k has to be assumed, so that the method of solution is basically the same for both fixed wings and rotating blades. Because the solutions are obtained for specified values of V and k, then from the relation

$$\omega = \left(\frac{V}{b}\right)k \tag{15}$$

this, in effect, means that the solution frequency ω has been assumed in order to obtain a solution. It must be clearly understood that this implies only that the degree of unsteadiness of the flow is assumed in advance. For flutter not involving aerodynamic control surfaces, as is the case with the present study, fixed-wing flutter solutions indicate that the solution frequency and decay rate is relatively insensitive to the assumed degree of unsteadiness of the flow. Hence, a reasonable guess at the flutter frequency gives solutions sufficiently accurate for most flutter investigations, especially when the approximate location only of stability boundaries is required, and this comprises by far the major part of most flutter investigations. Should a very accurate value of flutter speed be required, or, alternatively, if the assumed flutter frequency turns out to be very inaccurate, then one iteration using the calculated flutter frequency is all that is needed to obtain satisfactory correspondence between the calculated and the assumed flutter frequency.

It was decided that the decay-rate method of solution was more direct than the V-g method for analyzing rotor blade flutter, and so this method was adopted. One modification to the decay-rate method is necessary when it is applied to rotating blades, and that is to recalculate the aerodynamic matrices for each forward velocity, as they are now a function of advance ratio.

Having chosen to use the decay-rate method, it was then necessary to choose a definition of the aerodynamic coefficients. Various notations are used in presenting the aerodynamic forces, but none of these is entirely suitable for the present study. Some take the factor π outside the equation so that the steady-flow rate of change of lift coefficient with angle of attack becomes equal to 2. Others take out the factor 2 so that $C_{L\alpha} = \pi$ at $k = 0$. For convenience, it was decided to take out a factor of 2π, giving $C_{L\alpha} = 1.0$ at $k = 0$ so that this term then becomes a measure of the aerodynamic efficiency. The aerodynamic coefficients are defined as follows again with reference to Figure 1:

$$\frac{-1}{2\pi\rho b^3 \Delta r}\begin{bmatrix} -L \\ \frac{M}{b} \end{bmatrix}_{c/4} = \left(\frac{V}{b}\right)\begin{bmatrix} l_{\dot{h}} & l_{\dot{\alpha}} \\ -m_{\dot{h}} & -m_{\dot{\alpha}} \end{bmatrix}\begin{bmatrix} \frac{\dot{h}}{b} \\ \dot{\alpha} \end{bmatrix}_{c/4} + \left(\frac{V}{b}\right)^2\begin{bmatrix} l_h & l_\alpha \\ -m_h & -m_\alpha \end{bmatrix}\begin{bmatrix} \frac{h}{b} \\ \alpha \end{bmatrix}_{c/4} \tag{16}$$

Here, the aerodynamic acceleration (inertia) terms have been combined with the displacement of coefficients with the following relation being used:

$$D_{\ddot{q}}\,\ddot{q} = -\omega^2 D_{\ddot{q}}\,q = -\left(\frac{V}{b}\right)^2 \left[k^2 D_{\ddot{q}}\right] q \tag{17}$$

Although for incompressible flow any acceleration coefficient $D_{\ddot{q}}$ is a constant, the equivalent displacement coefficient $k^2 D_{\ddot{q}}$ varies with k and becomes infinite for zero forward speed $(k = \infty)$. When the decay-rate method is used, it is desirable that the variation of the coefficient with change in k be a minimum in order to keep the calculated flutter speed relatively insensitive to the value of k assumed in obtaining the solution. Hence, it would be desirable to keep the acceleration coefficients separate, but the following two factors weighed against this:

1. In compressible flow, the acceleration coefficients become complex functions of the reduced frequency k.

2. Most tables of compressible coefficients have already lumped the acceleration coefficients in with the displacement coefficients.

For incompressible flow, the above coefficients have the following form:

$$\ell_{\dot{h}} = F(k) \tag{18}$$

$$\ell_{\dot{\alpha}} = \frac{1}{2} + F(k) + \frac{G(k)}{k} \tag{19}$$

$$\ell_{h} = -k\left(G(k) + \frac{k}{2}\right) \tag{20}$$

$$\ell_{\alpha} = F(k) - k\left(G(k) + \frac{k}{4}\right) \tag{21}$$

$$-m_{\ddot{h}} = 0 \tag{22}$$

$$-m_{\ddot{\alpha}} = \frac{1}{2} \tag{23}$$

$$-m_{h} = -\frac{k^2}{4} \tag{24}$$

$$-m_{\alpha} = -\frac{3}{16}k^2 \tag{25}$$

It should be noted that

$$\lim_{k \to 0} \ell_{\dot{\alpha}} = -\infty \tag{26}$$

and that

$$\lim_{k \to \infty} \ell_h = -\infty \tag{27}$$

$$\lim_{k \to \infty} \ell_\alpha = -\infty \tag{28}$$

$$\lim_{k \to \infty} (-m_h) = -\infty \tag{29}$$

$$\lim_{k \to \infty} (-m_\alpha) = -\infty \tag{30}$$

KINETIC ENERGY

Consider a set of axes ($\bar{X}$, $\bar{Y}$, Z) fixed in the helicopter with the Z axis coinciding with the rotor shaft axis and the $\bar{X}$ axis pointing aft, as shown in Figure 5. Then consider another set of axes (X , Y , Z) rotating with the Y axis coincident with the blade under consideration. The blade is assumed to have zero twist, zero steady pitch angle with the tip path plane lying in the $\overline{XY}$ plane.

The coordinates of any point $(\bar{x},\bar{y})$ on the blade are given by

$$\begin{bmatrix} \bar{x} \\ \bar{y} \end{bmatrix} = \begin{bmatrix} \cos\Omega t & -\sin\Omega t \\ \sin\Omega t & \cos\Omega t \end{bmatrix} \begin{bmatrix} x \\ y \end{bmatrix} \tag{31}$$

The kinetic energy T of the blade is given by

$$T = \frac{1}{2} \int_{\text{BLADE}} \left(\dot{\bar{x}}^2 + \dot{\bar{y}}^2 + \dot{z}^2 \right) dm \tag{32}$$

where dm is an elementary mass point at $(\bar{x}, \bar{y}, z)$ on the blade.

$$T = \frac{1}{2} \int_{\text{BLADE}} \left[\dot{x}^2 + \dot{y}^2 + \dot{z}^2 + 2\Omega(x\dot{y} - y\dot{x}) + \Omega^2(x^2+y^2) \right] dm \tag{33}$$

Generalized coordinates $q_1 \ldots q_n$ may be used to describe the displacement of the blade relative to the rotating axes. That is,

$$x = x(q_1, ---, q_n) \tag{34}$$

$$y = y(q_1 ---, q_n) \tag{35}$$

$$z = z(q_1, ---, q_n) \tag{36}$$

If the above terms are expanded in terms of a set of Maclaurin's series, the following result is obtained.

$$x = x_o + \sum_i \left(\frac{\partial x}{\partial q_i}\right)_o q_i + \frac{1}{2} \sum_i \sum_j \left(\frac{\partial^2 x}{\partial q_i \partial q_j}\right) q_i q_j + \cdots \tag{37}$$

$$y = y_o + \sum_i \left(\frac{\partial y}{\partial q_i}\right)_o q_i + \frac{1}{2} \sum_i \sum_j \left(\frac{\partial^2 y}{\partial q_i \partial q_j}\right) q_i q_j + \cdots \tag{38}$$

$$z = z_o + \sum_i \left(\frac{\partial z}{\partial q_i}\right)_o q_i + \frac{1}{2} \sum_i \sum_j \left(\frac{\partial^2 z}{\partial q_i \partial q_j}\right) q_i q_j + \cdots \tag{39}$$

where x_o, y_o and z_o are the values of x, y and z when each q_i is equal to zero. The derivatives are also evaluated when q_i equals zero.

Substituting into the expression for the kinetic energy and neglecting higher order terms gives

$$\begin{aligned} T = \frac{1}{2} \int_{\text{BLADE}} \Bigg\{ & \sum_i \sum_j \dot{q}_i \dot{q}_j \left[\left(\frac{\partial x}{\partial q_i}\right)_o \left(\frac{\partial x}{\partial q_j}\right)_o + \left(\frac{\partial y}{\partial q_i}\right)_o \left(\frac{\partial y}{\partial q_j}\right)_o + \left(\frac{\partial z}{\partial q_i}\right)_o \left(\frac{\partial z}{\partial q_j}\right)_o \right] \\ & + 2\Omega \sum_i \sum_j q_i \dot{q}_j \left[\left(\frac{\partial x}{\partial q_i}\right)_o \left(\frac{\partial y}{\partial q_j}\right)_o - \left(\frac{\partial y}{\partial q_i}\right)_o \left(\frac{\partial y}{\partial q_j}\right)_o \right] \\ & + \Omega^2 \sum_i \sum_j q_i q_j \left[\left(\frac{\partial x}{\partial q_i}\right)_o \left(\frac{\partial x}{\partial q_j}\right)_o + \left(\frac{\partial y}{\partial q_i}\right)_o \left(\frac{\partial y}{\partial q_j}\right)_o + x_o \left(\frac{\partial^2 x}{\partial q_i \partial q_j}\right)_o + y_o \left(\frac{\partial^2 y}{\partial q_i \partial q_j}\right)_o \right] \\ & + 2\Omega^2 \sum_i q_i \left[x_o \left(\frac{\partial x}{\partial q_i}\right)_o + y_o \left(\frac{\partial y}{\partial q_i}\right)_o \right] \Bigg\} dm \end{aligned} \tag{40}$$

This is

$$T = \frac{1}{2}\sum_i\sum_j {}^{G}M_{ij}\,\dot{q}_i\,\dot{q}_j + \Omega\sum_i\sum_j G_{ij}\,q_i\,\dot{q}_j + \frac{\Omega^2}{2}\sum_i\sum_j T_{ij}\,q_i\,q_j + \Omega^2\sum_i q_i\int_{BLADE}\left[x_o\left(\frac{\partial x}{\partial q_i}\right)_o + y_o\left(\frac{\partial y}{\partial q_i}\right)_o\right]dm \tag{41}$$

where

$${}^{G}M_{ij} = \int_{BLADE}\left[\left(\frac{\partial x}{\partial q_i}\right)_o\left(\frac{\partial x}{\partial q_j}\right)_o + \left(\frac{\partial y}{\partial q_i}\right)_o\left(\frac{\partial y}{\partial q_j}\right)_o + \left(\frac{\partial z}{\partial q_i}\right)_o\left(\frac{\partial z}{\partial q_j}\right)_o\right]dm \tag{42}$$

$$G_{ij} = \int_{BLADE}\left[\left(\frac{\partial x}{\partial q_i}\right)_o\left(\frac{\partial y}{\partial q_j}\right)_o - \left(\frac{\partial y}{\partial q_i}\right)_o\left(\frac{\partial x}{\partial q_j}\right)_o\right]dm \tag{43}$$

$$T_{ij} = \int_{BLADE}\left[\left(\frac{\partial x}{\partial q_i}\right)_o\left(\frac{\partial x}{\partial q_j}\right)_o + \left(\frac{\partial y}{\partial q_i}\right)_o\left(\frac{\partial y}{\partial q_j}\right)_o + x_o\left(\frac{\partial^2 x}{\partial q_i\,\partial q_j}\right)_o + y_o\left(\frac{\partial^2 y}{\partial q_i\,\partial q_j}\right)_o\right]dm \tag{44}$$

Note that

$${}^{G}M_{ij} = {}^{G}M_{ji} \tag{45}$$

$$G_{ij} = -G_{ji} \tag{46}$$

$$T_{ij} = T_{ji} \tag{47}$$

POTENTIAL ENERGY

The potential energy arises from the elastic deflection of the blade and control system and from the motion of the blade in a gravitational field. It is a function of the generalized coordinates q_i and is shown as follows:

$$U = U(q_1, ---, q_n) \tag{48}$$

If Maclaurin's expansion is used, Eq. (48) may be expanded to give

$$U = U_o + \sum_i\left(\frac{\partial U}{\partial q_i}\right)_o q_i + \frac{1}{2}\sum_i\sum_j\left(\frac{\partial^2 U}{\partial q_i\,\partial q_j}\right)_o q_i\,q_j \tag{49}$$

where

$$U_o = U(0, - - - , 0) \tag{50}$$

$$\left(\frac{\partial U}{\partial q_i}\right)_o = \frac{\partial U}{\partial q_i}(0, - - - , 0) \tag{51}$$

and where higher order terms have been neglected. The gravitational forces have a negligible influence on the perturbation deflections q_i, and so it is assumed that the generalized spring forces

$$\bar{K}_{ij} = \left(\frac{\partial^2 U}{\partial q_i \partial q_j}\right)_o \tag{52}$$

do not depend on gravitational forces.

Hence,

$$U = U_o + \sum_i \left(\frac{\partial U}{\partial q_i}\right)_o q_i + \frac{1}{2} \sum_i \sum_j \bar{K}_{ij} q_i q_j \tag{53}$$

LAGRANGE'S EQUATION OF MOTION

The equations of motion in the form of Lagrange's Equation will be used which, for the r th generalized coordinate q_r, may be written

$$\frac{d}{dt}\left(\frac{\partial T}{\partial \dot{q}_r}\right) - \frac{\partial T}{\partial q_r} + \frac{\partial U}{\partial q_r} = Q_r \qquad r = 1, - - -, n \tag{54}$$

where Q_r accounts for all forces not included in T and U. It may be separated into an initial steady component $(Q_r)_o$ and a perturbation component ΔQ_r. Substituting the expressions for T and U into the above equation gives

$$\sum_j \left[{}^G M_{rj} \ddot{q}_j + \Omega(G_{jr} - G_{rj}) \dot{q}_j + (\bar{K}_{rj} - \Omega^2 T_{rj}) q_j\right] + \left(\frac{\partial U}{\partial q_r}\right)_o - \Omega^2 \int_{BLADE} \left[x_o \left(\frac{\partial x}{\partial q_r}\right)_o + y_o \left(\frac{\partial y}{\partial q_r}\right)_o\right] dm = (Q_r)_o + \Delta Q_r \tag{55}$$

The steady generalized force $(Q_r)_o$ must be in equilibrium with the initial elastic, gravitational, and centrifugal forces; that is,

$$\left(\frac{\partial U}{\partial q_r}\right)_o - \Omega^2 \int_{BLADE} \left[x_o \left(\frac{\partial x}{\partial q_r}\right)_o + y_o \left(\frac{\partial y}{\partial q_r}\right)_o \right] dm = (Q_r)_o \tag{56}$$

Hence, the equation of motion reduces to

$$\sum_j \left[{}^G M_{rj} \ddot{q}_j - 2\Omega G_{rj} \dot{q}_j + \left(\overline{K}_{rj} - \Omega^2 T_{rj}\right) q_j \right] = \Delta Q_r \qquad r = 1, - - -, n \tag{57}$$

The generalized force ΔQ_r is due to

1. Aerodynamic forces acting on the blade
2. Mechanical damping forces

They can be determined from the work done by these forces in a virtual displacement using the relationship

$$\Delta Q_r = \frac{\partial W}{\partial q_r} \tag{58}$$

The general form of the equations of motion having been obtained, a set of generalized coordinates can be chosen and the general expressions can be evaluated.

A new set of axis (X_1 , Y_1 , Z_1) are introduced, which are fixed in the blade as shown in Figure 6. The origin O_1 coincides with the blade elastic axis at the section under consideration. With each q_i equal to zero,

O_1X_1 coincides with OX

O_1Y_1 is parallel to OY

O_1Z_1 is parallel OZ

h_z is the flatwise displacement of the elastic axis

h_x is the edgewise displacement of the elastic axis

α is the blade pitch displacement

ϵ is the distance of the blade mid-chord aft of the axis at the section under consideration

$a_{EA}b$ is the distance of the elastic axis aft of the mid-chord

Consider a generic point $P(x_1, y_1, z_1)$ of the blade. Then the x and z coordinates of P referred to the XZ axes are given by

$$x_P = \epsilon + a_{EA}b + h_x + x_1 \cos\alpha + z_1 \sin\alpha \tag{59}$$

$$z_P = h_z - x_1 \sin\alpha + z_1 \cos\alpha \tag{60}$$

For small angles,

$$\cos\alpha \simeq 1 - \frac{\alpha^2}{2} \tag{61}$$

$$\sin\alpha \simeq \alpha \tag{62}$$

Then,

$$x_P = (\epsilon + a_{EA}b + x_1) + h_x + z_1\alpha - x_1\frac{\alpha^2}{2} \tag{63}$$

$$z_P = z_1 + h_z - x_1\alpha - z_1\frac{\alpha^2}{2} \tag{64}$$

where third order terms in the deflection h_x, h_y, h_z and α have been neglected. Finding an expression for y_p will be accomplished in three steps. The first of these is depicted in Figure 7.

For this derivation, the effect of having $(\epsilon + a_{EA}b)$ variable is neglected, so that the undeflected elastic axis is taken as being parallel to the OY axis

$$\tan\gamma_1 = \frac{dh_x}{dy} = \frac{\Delta_1}{x_p - x_{EA}} \tag{65}$$

Substituting for x_p and x_{EA} and neglecting third order terms in the modal deflections gives

$$\Delta_1 = \left[x_1 + z_1\alpha\right]\left(\frac{dh_x}{dy}\right) \tag{66}$$

The second of the three steps is shown in Figure 8, where

$$\tan\gamma_2 = \frac{dh_z}{dy} = \frac{\Delta_2}{z_P - z_{EA}} \tag{67}$$

Substituting for z_p and z_{EA} and neglecting third-order terms in the modal deflections gives

$$\Delta_2 = \left[z_1 - x_1\alpha \right] \left(\frac{dh_z}{dy}\right) \tag{68}$$

The third step considers apparent blade shortening, Δ_3 .
Let s be the arc length measured along the elastic axis

Then

$$ds = dy\sqrt{1+\left(\frac{dx}{dy}\right)^2+\left(\frac{dz}{dy}\right)^2} \tag{69}$$

With expansion by the binomial theorem and with higher order terms being neglected, the total blade shortening at station y is given by

$$\Delta_3 = \int_0^y (ds - dy) \tag{70}$$

$$\Delta_3 = \frac{1}{2}\int_0^y \left[\left(\frac{dx}{dy}\right)^2 + \left(\frac{dz}{dy}\right)^2 \right] dy \tag{71}$$

$$\Delta_3 = \frac{1}{2}\int_0^y \left[\left(\frac{dh_x}{dy}\right)^2 + \left(\frac{dh_z}{dy}\right)^2 \right] dy \tag{72}$$

Hence, the y coordinate of P referred to the XYZ axes is given by

$$y_P = r - (\Delta_1 + \Delta_2 + \Delta_3) \tag{73}$$

$$y_P = r - \left[x_1 + z_1\alpha\right]\left(\frac{dh_x}{dy}\right) - \left[z_1 - x_1\alpha\right]\left(\frac{dh_z}{dy}\right) - \frac{1}{2}\int_0^y \left[\left(\frac{dh_x}{dy}\right)^2 + \left(\frac{dh_z}{dy}\right)^2 \right] dy \tag{74}$$

That is, the coordinates of P referred to XYZ axes are given by

$$x_P = (\epsilon + a_{EA}b + x_1) + h_z + z_1\alpha - x_1\frac{\alpha^2}{2} \tag{75}$$

$$y_P = r - \left[x_1 + z_1\alpha\right]\left(\frac{dh_x}{dy}\right) - \left[z_1 - x_1\alpha\right]\left(\frac{dh_z}{dy}\right) - \frac{1}{2}\int_0^y \left[\left(\frac{dh_x}{dy}\right)^2 + \left(\frac{dh_z}{dy}\right)^2 \right] dy \tag{76}$$

$$z_P = z_1 + h_z - x_1\alpha - z_1\frac{\alpha^2}{2} \tag{77}$$

The displacements of the point P can now be expressed as being due to two generalized coordinates q_1 and q_2. This will give the form of the coupling terms between the two generalized coordinates and will allow the final equations of motion to be generalized by inspection to include any number of generalized coordinates.

Put

$$h_x(y,t) = g_1^x(y)\, q_1(t) + g_2^x y \; q_2(t) \tag{78}$$

$$h_z(y,t) = g_1^z(y)\, q_1(t) + g_2^z(y)\, q_2(t) \tag{79}$$

$$\alpha(y,t) = F_1(y)\, q_1(t) + F_2(y)\, q_2(t) \tag{80}$$

where $q_i^x(y)$, $q_i^z(y)$ and $F_i(y)$ are respectively the edgewise, flatwise, and torsional mode shapes of the ith generalized coordinate. Substituting into the expressions for x_p, y_p and z_p and neglecting third and higher order products of the generalized coordinates gives

$$x_p = (\epsilon + a_{EA} b + x_1) + (g_1^x + z_1 F_1) q_1 + (g_2^x + z_1 F_2) q_2 - \tfrac{1}{2} x_1 F_1^2 q_1^2 - x_1 F_1 F_2 q_1 q_2 - \tfrac{1}{2} x_1 F_2^2 q_2^2 \tag{81}$$

$$\begin{aligned} y_p = r &- \left[x_1 \left(\frac{dg_1^x}{dy}\right) + z_1 \left(\frac{dg_1^z}{dy}\right) \right] q_1 - \left[x_1 \left(\frac{dg_2^x}{dy}\right) + z_1 \left(\frac{dg_2^z}{dy}\right) \right] q_2 \\ &- \left[z_1 F_1 \left(\frac{dg_1^x}{dy}\right) - x_1 F_1 \left(\frac{dg_1^z}{dy}\right) + \frac{1}{2} \int_0^y \left\{ \left(\frac{dg_1^x}{dy}\right)^2 + \left(\frac{dg_1^z}{dy}\right)^2 \right\} dy \right] q_1^2 \\ &- \left[z_1 \left\{ F_1 \left(\frac{dg_2^x}{dy}\right) + F_2 \left(\frac{dg_1^x}{dy}\right) \right\} - x_1 \left\{ F_1 \left(\frac{dg_2^z}{dy}\right) + F_2 \left(\frac{dg_2^z}{dy}\right) \right\} \right. \\ &\qquad \left. + \int_0^y \left\{ \left(\frac{dg_1^x}{dy}\right)\left(\frac{dg_2^x}{dy}\right) + \left(\frac{dg_2^z}{dy}\right)\left(\frac{dg_1^z}{dy}\right) \right\} dy \right] q_1 q_2 \\ &- \left[z_1 F_2 \left(\frac{dg_2^x}{dy}\right) - x_1 F_2 \left(\frac{dg_2^z}{dy}\right) + \frac{1}{2} \int_0^y \left\{ \left(\frac{dg_2^x}{dy}\right)^2 + \left(\frac{dg_2^z}{dy}\right)^2 \right\} dy \right] q_2^2 \end{aligned} \tag{82}$$

$$z_p = z_1 - (g_1^z - x_1 F_1)\, q_1 + (g_2^z - x_1 F_2)\, q_2 - \frac{1}{2} z_1 F_1^2 q_1^2 - z_1 F_1 F_2 q_1 q_2 - \frac{1}{2} z_1 F_2^2 q_2^2 \tag{83}$$

Differentiating the above expressions with respect to q_1 and q_2 and evaluating the terms at $q_1 = q_2 = 0$ gives the following results:

$$(x_p)_0 = \epsilon + a_{EA} b + x_1 \tag{84}$$

$$\left(\frac{\partial x_p}{\partial q_1}\right)_0 = g_1^x + z_1 F_1 \tag{85}$$

$$\left(\frac{\partial x_p}{\partial q_2}\right)_0 = g_2^x + z_1 F_2 \tag{86}$$

$$\left(\frac{\partial^2 x_p}{\partial q_1^2}\right)_0 = -x_1 F_1^2 \tag{87}$$

$$\left(\frac{\partial^2 x_p}{\partial q_1 \partial q_2}\right)_0 = -x_1 F_1 F_2 \tag{88}$$

$$\left(\frac{\partial^2 x_p}{\partial q_2^2}\right)_0 = -x_1 F_2^2 \tag{89}$$

$$(y_p)_0 = r \tag{90}$$

$$\left(\frac{\partial y_p}{\partial q_1}\right)_0 = -\left[x_1\left(\frac{dg_1^x}{dy}\right) + z_1\left(\frac{dg_1^z}{dy}\right)\right] \tag{91}$$

$$\left(\frac{\partial y_p}{\partial q_2}\right)_0 = -\left[x_1\left(\frac{dg_2^x}{dy}\right) + z_1\left(\frac{dg_2^z}{dy}\right)\right] \tag{92}$$

$$\left(\frac{\partial^2 y_p}{\partial q_1^2}\right)_0 = -2\left\{z_1 F_1\left(\frac{dg_1^x}{dy}\right) - x_1 F_1\left(\frac{dg_1^z}{dy}\right) + \frac{1}{2}\int_0^y \left[\left(\frac{dg_1^x}{dy}\right)^2 + \left(\frac{dg_1^z}{dy}\right)^2\right] dy\right\} \tag{93}$$

$$\left(\frac{\partial^2 y_p}{\partial q_1 \partial q_2}\right)_0 = -\left\{ z_1\left[F_1\left(\frac{dg_2^x}{dy}\right) + F_2\left(\frac{dg_1^x}{dy}\right)\right] - x_1\left[F_1\left(\frac{dg_2^z}{dy}\right) + F_2\left(\frac{dg_1^z}{dy}\right)\right] + \int_0^y \left[\left(\frac{dg_1^x}{dy}\right)\left(\frac{dg_2^x}{dy}\right) + \left(\frac{dg_2^z}{dy}\right)\left(\frac{dg_1^z}{dy}\right)\right] dy \right\} \tag{94}$$

$$\left(\frac{\partial^2 y_p}{\partial q_2^2}\right)_0 = -2\left\{ z_1 F_2\left(\frac{dg_2^x}{dy}\right) - x_1 F_2\left(\frac{dg_2^z}{dy}\right) + \frac{1}{2}\int_0^y \left[\left(\frac{dg_2^x}{dy}\right)^2 + \left(\frac{dg_2^z}{dy}\right)^2\right] dy \right\} \tag{95}$$

$$(z_p)_0 = z_1 \tag{96}$$

$$\left(\frac{\partial z_p}{\partial q_1}\right)_0 = g_1^z - x_1 F_1 \tag{97}$$

$$\left(\frac{\partial z_p}{\partial q_2}\right)_0 = g_2^z - x_1 F_2 \tag{98}$$

$$\left(\frac{\partial^2 z_p}{\partial q_1^2}\right)_0 = -z_1 F_1^2 \tag{99}$$

$$\left(\frac{\partial^2 z_p}{\partial q_1 \partial q_2}\right)_0 = -z_1 F_1 F_2 \tag{100}$$

$$\left(\frac{\partial^2 z_p}{\partial q_2^2}\right)_0 = -z_1 F_2^2 \tag{101}$$

These derivatives are now substituted into the generalized coefficients ${}^{G}M_{ij}$, G_{ij} , and T_{ij} . Before this is done, it is convenient to define the following mass terms:

$$m = \iint \rho_b \, dx_1 \, dz_1 \tag{102}$$

$$m\bar{x} = \iint \rho_b x_1 \, dx_1 \, dz_1 \tag{103}$$

$$m\bar{x}_s = m\bar{x} + m(\epsilon_s + a_{EA}b) \tag{104}$$

$$m\bar{z} = \iint \rho_b z_1 \, dx_1 dz_1 \tag{105}$$

$$I_{xx} = \iint \rho_b z_1^2 \, dx_1 \, dz_1 \tag{106}$$

$$I_{xz} = \iint \rho_b x_1 z_1 \, dx_1 \, dz_1 \tag{107}$$

$$I_{zz} = \iint \rho_b x^2 \, dx_1 \, dz_1 \tag{108}$$

$$I_{yy} = \iint \rho_b (z_1^2 + x_1^2) dx_1 \, dz_1 \tag{109}$$

$$= I_{xx} + I_{zz}$$

where ρ_b = blade structural density and the integration $\iint$ is over the blade cross section .

The following relation will also be used:

$$\int_0^R f(x_1, z_1, r) dm = \iiint f(x_1, z_1, r) \rho_b \, dx_1 \, dz_1 \, dr \tag{110}$$

$$\int_0^R f(x_1, z_1, r) dm = \int_0^R \left[\iint \rho_b f(x_1, z_1, r) dx_1 \, dz_1 \right] dr \tag{111}$$

where r is now used instead of y to refer to the blade spanwise coordinate.

GENERALIZED INERTIAS

Since the generalized inertia is being developed with respect to q_1 and q_2 , $i = 1$ and $j = 2$ in this case.

$$
{}^{G}M_{ij} = {}^{G}M_{12} = \int_0^R \left[\left(\frac{\partial x_p}{\partial q_1}\right)_0 \left(\frac{\partial x_p}{\partial q_2}\right)_0 + \left(\frac{\partial y_p}{\partial q_1}\right)_0 \left(\frac{\partial y_p}{\partial q_2}\right)_0 + \left(\frac{\partial z_p}{\partial q_1}\right)_0 \left(\frac{\partial z_p}{\partial q_2}\right)_0 \right] dm \tag{112}
$$

$$
= \int_0^R \Big\{ (g_1^x g_2^x + g_1^z g_2^z) m - (g_1^z F_2 + g_2^z F_1) m\bar{x} + (g_1^x F_2 + g_2^x F_1) m\bar{z}
$$

$$
+ \left(\frac{dg_1^z}{dr}\right)\left(\frac{dg_2^z}{dr}\right) I_{xx} + \left[\left(\frac{dg_1^x}{dr}\right)\left(\frac{dg_2^z}{dr}\right) + \left(\frac{dg_2^x}{dr}\right)\left(\frac{dg_1^z}{dr}\right) \right] I_{xz}
$$

$$
+ \left(\frac{dg_1^x}{dr}\right)\left(\frac{dg_2^x}{dr}\right) I_{zz} + F_1 F_2 I_{yy} \Big\} dr \tag{113}
$$

$$
= \int_0^R \left[g_1^z \; g_1^x \; \frac{dg_1^z}{dr} \; \frac{dg_1^x}{dr} \; F_1 \; \frac{dF_1}{dr} \right] \begin{bmatrix} m & 0 & 0 & 0 & -m\bar{x} & 0 \\ 0 & m & 0 & 0 & m\bar{z} & 0 \\ 0 & 0 & I_{xx} & I_{xz} & 0 & 0 \\ 0 & 0 & I_{xz} & I_{zz} & 0 & 0 \\ -m\bar{x} & m\bar{z} & 0 & 0 & I_{yy} & 0 \\ 0 & 0 & 0 & 0 & 0 & 0 \end{bmatrix} \begin{bmatrix} g_2^z \\ g_2^x \\ \frac{d}{dr}(g_2^z) \\ \frac{d}{dr}(g_2^x) \\ F_2 \\ \frac{d}{dr}(F_2) \end{bmatrix} dr \tag{114}
$$

GENERALIZED GYROSCOPIC INERTIAS

The subscripts of G_{ij} are again $i = 1$ and $j = 2$, as for the ${}^{G}M_{12}$ mass property developed above in Eq. (112) through (114).

$$
G_{ij} = G_{12} = \int_0^R \left[\left(\frac{\partial x_p}{\partial q_1}\right)_0 \left(\frac{\partial y_p}{\partial q_2}\right)_0 - \left(\frac{\partial y_p}{\partial q_1}\right)_0 \left(\frac{\partial x_p}{\partial q_2}\right)_0 \right] dm \tag{115}
$$

$$
= \int_0^R \Big\{ -\left[g_1^x \left(\frac{dg_2^x}{dr}\right) - g_2^x \left(\frac{dg_1^x}{dr}\right) \right] m\bar{x} - \left[g_1^x \left(\frac{dg_2^z}{dr}\right) - g_2^x \left(\frac{dg_1^z}{dr}\right) \right] m\bar{z}
$$

$$
+ \left[\left(\frac{dg_1^x}{dr}\right) F_2 - \left(\frac{dg_2^x}{dr}\right) F_1 \right] I_{xz} + \left[\left(\frac{dg_1^z}{dr}\right) F_2 - \left(\frac{dg_2^z}{dr}\right) F_1 \right] I_{xx} \Big\} dr \tag{116}
$$

$$G_{12} = \int_0^R \left[g_1^z \; g_1^x \; \frac{dg_1^z}{dr} \; \frac{dg_1^x}{dr} \; F_1 \; \frac{dF_1}{dr} \right] \begin{bmatrix} 0 & 0 & 0 & 0 & 0 & 0 \\ 0 & 0 & -m\bar{z} & -m\bar{x} & 0 & 0 \\ 0 & m\bar{z} & 0 & 0 & I_{xx} & 0 \\ 0 & m\bar{x} & 0 & 0 & I_{xz} & 0 \\ 0 & 0 & -I_{xx} & -I_{xz} & 0 & 0 \\ 0 & 0 & 0 & 0 & 0 & 0 \end{bmatrix} \begin{bmatrix} g_2^z \\ g_2^x \\ \frac{d}{dr}(g_2^z) \\ \frac{d}{dr}(g_2^x) \\ F_2 \\ \frac{d}{dr}(F_2) \end{bmatrix} dr \tag{117}$$

GENERALIZED CENTRIFUGAL STIFFNESS COEFFICIENTS

The subscripts of T_{ij} are $i = 1$ and $j = 2$, as for the ${}^{G}M_{12}$ and G_{12} mass properties developed above in Eq. (112) through (117).

$$T_{ij} = T_{12} = \int_0^R \left[\left(\frac{\partial x_p}{\partial q_1}\right)_0 \left(\frac{\partial x_p}{\partial q_2}\right)_0 + \left(\frac{\partial y_p}{\partial q_1}\right)_0 \left(\frac{\partial y_p}{\partial q_2}\right)_0 + (x_p)_0 \left(\frac{\partial^2 x_p}{\partial q_1 \partial q_2}\right)_0 + (y_p)_0 \left(\frac{\partial^2 y_p}{\partial q_1 \partial q_2}\right)_0 \right] dm \tag{118}$$

$$\begin{aligned} T_{ij} = T_{12} = \int_0^R \Big\langle & g_1^x g_2^x \, m + \left[\left\{ \left(\frac{dg_1^z}{dr}\right) F_2 + \left(\frac{dg_2^z}{dr}\right) F_1 \right\} r - (\epsilon + a_{EA} b) F_1 F_2 \right] m\bar{x} \\ & + \left[(g_1^x F_2 + g_2^x F_1) - \left\{ \left(\frac{dg_1^x}{dr}\right) F_2 + \left(\frac{dg_2^x}{dr}\right) F_1 \right\} r \right] m\bar{z} + \left\{ \left(\frac{dg_1^x}{dr}\right)\left(\frac{dg_2^x}{dr}\right) - F_1 F_2 \right\} I_{zz} \\ & + \left\{ \left(\frac{dg_1^x}{dr}\right)\left(\frac{dg_2^z}{dr}\right) + \left(\frac{dg_2^x}{dr}\right)\left(\frac{dg_1^z}{dr}\right) \right\} I_{xz} + \left\{ \left(\frac{dg_1^z}{dr}\right)\left(\frac{dg_2^z}{dr}\right) + F_1 F_2 \right\} I_{xx} \\ & - mr \int_0^r \left\{ \left(\frac{dg_1^x}{du}\right)\left(\frac{dg^x}{du}\right) \; \left(\frac{dg_2^z}{du}\right)\left(\frac{dg_1^z}{du}\right) \right\} du \Big\rangle \, dr \end{aligned} \tag{119}$$

It will be seen that the mode shapes $\left(\frac{dg_1^x}{dr}\right)$ and $\left(\frac{dg_2^x}{dr}\right)$ occur inside an integral with variable upper limit. This complicates numerical calculations, and so the mode shapes are brought outside the integral by changing the order of integration as follows:

$$\int_0^R \theta(v) \left[\int_0^r \phi(u) du \right] dv = \int_0^R \phi(u) \left[\int_r^R \theta(v) dv \right] du \tag{120}$$

so that

$$\int_0^R m(r)\, r \left[\int_0^r \left\{ \left(\frac{dg_1^x}{du}\right)\left(\frac{dg_2^x}{du}\right) + \left(\frac{dg_2^z}{du}\right)\left(\frac{dg_1^z}{du}\right) \right\} du \right] dr$$

$$= \int_0^R \left[\left(\frac{dg_1^x}{du}\right)\left(\frac{dg_2^x}{du}\right) + \left(\frac{dg_2^z}{du}\right)\left(\frac{dg_1^z}{du}\right) \right] \mathcal{M}\, du \tag{121}$$

$$\mathcal{M} = \int_r^R m\, r\, dr \tag{122}$$

Hence,

$$\begin{aligned} T_{12} = \int_0^R \Big[& g_1^x g_2^x m + \left\{ \left(\frac{dg_1^z}{dr}\right) F_2 + \left(\frac{dg_2^z}{dr}\right) F_1 \right\} r\, m\bar{x} - (\epsilon + a_{EA} b) F_1 F_2\, m\bar{x} \\ & + (g_1^x F_2 + g_2^x F_1)\, m\bar{z} - \left\{ \left(\frac{dg_1^x}{dr}\right) F_2 + \left(\frac{dg_2^x}{dr}\right) F_1 \right\} r\, m\bar{z} + \left\{ \left(\frac{dg_1^x}{dr}\right)\left(\frac{dg_2^x}{dr}\right) - F_1 F_2 \right\} I_{zz} \\ & + \left\{ \left(\frac{dg_1^x}{dr}\right)\left(\frac{dg_2^z}{dr}\right) + \left(\frac{dg_2^x}{dr}\right)\left(\frac{dg_1^z}{dr}\right) \right\} I_{xz} + \left\{ \left(\frac{dg_1^z}{dr}\right)\left(\frac{dg_2^z}{dr}\right) + F_1 F_2 \right\} I_{xx} \\ & - \left\{ \left(\frac{dg_1^x}{dr}\right)\left(\frac{dg_2^x}{dr}\right) + \left(\frac{dg_2^z}{dr}\right)\left(\frac{dg_1^z}{dr}\right) \right\} \mathcal{M} \Big]\, dr \end{aligned} \tag{123}$$

$$T_{12} = \int_0^R \left[g_1^z\; g_1^x\; \frac{dg_1^z}{dr}\; \frac{dg_1^x}{dr}\; F_1\; \frac{dF_1}{dr} \right] \begin{bmatrix} 0 & 0 & 0 & 0 & 0 & 0 \\ 0 & m & 0 & 0 & m\bar{z} & 0 \\ 0 & 0 & I_{xx}-\mathcal{M} & I_{xz} & rm\bar{x} & 0 \\ 0 & 0 & I_{xz} & I_{zz}-\mathcal{M} & -rm\bar{z} & 0 \\ 0 & m\bar{z} & rm\bar{x} & -rm\bar{z} & \left[I_{xx} - I_{zz} - (\epsilon + a_{EA} b) m\bar{x} \right] & 0 \\ 0 & 0 & 0 & 0 & 0 & 0 \end{bmatrix} \begin{bmatrix} g_2^z \\ g_2^x \\ \frac{d}{dr}(g_2^z) \\ \frac{d}{dr}(g_2^x) \\ F_2 \\ \frac{d}{dr}(F_2) \end{bmatrix} dr \tag{124}$$

ARTICULATED RIGID BLADE NATURAL FREQUENCIES

Before proceeding any further, it is of interest to obtain the frequencies of the rigid body flapping, lagging, and pitching modes due to the centrifugal force field. The equation of motion for a single degree of freedom q_1 is given by

$$M_{11}\,\ddot{q}_1 - \Omega^2 T_{11}\, q_1 = 0 \tag{125}$$

and for simple harmonic motion $\ddot{q}_1 = -\omega^2 q_1$ so that

$$\frac{\omega}{\Omega} = \sqrt{\frac{-T_{11}}{M_{11}}} \tag{126}$$

where

$$\begin{aligned} T_{11} = \int_0^R \Big[& (g_1^x)^2 m + 2\left(\frac{dg_1^z}{dr}\right) F_1\, r\, m\bar{x} - (\epsilon + a_{EA} b) F_1^2\, m\bar{x} \\ & + 2 g_1^x F_1\, m\bar{z} - 2\left(\frac{dg^x}{dr}\right) F_1\, r\, m\bar{z} + \left\{\left(\frac{dg_1^x}{dr}\right)^2 - F_1^2\right\} I_{zz} \\ & + 2\left(\frac{dg_1^x}{dr}\right)\left(\frac{dg_1^z}{dr}\right) I_{xz} + \left\{\left(\frac{dg_1^z}{dr}\right)^2 + F_1^2\right\} I_{xx} - \left\{\left(\frac{dg_1^x}{dr}\right)^2 + \left(\frac{dg_1^z}{dr}\right)^2\right\} \mathcal{M} \Big]\, dr \end{aligned} \tag{127}$$

$$\mathcal{M} = \int_r^R m\, r\, dr \tag{128}$$

$$\begin{aligned} {}^{G}M_{11} = \int_0^R \Big[& \left\{(g_1^x)^2 + (g_1^z)^2\right\} m - 2 g_1^z F_1\, m\bar{x} + 2 g_1^x F_1\, m\bar{z} \\ & + \left(\frac{dg_1^z}{dr}\right)^2 I_{xx} + 2\left(\frac{dg_1^x}{dr}\right)\left(\frac{dg_1^z}{dr}\right) I_{xz} + \left(\frac{dg_1^x}{dr}\right)^2 I_{zz} + F_1^2 I_{yy} \Big]\, dr \end{aligned} \tag{129}$$

Rigid Blade Flapping Frequency

For a flapping mode

$$g_1^z = 0 \qquad 0 \le r \le e \tag{130}$$

$$g_1^z = \frac{r-e}{R-e} \qquad e \le r \le R \tag{131}$$

$$\frac{dg_1^z}{dr} = 0 \qquad 0 \le r \le e \tag{132}$$

$$\frac{dg_1^z}{dr} = \frac{1}{R-e} \qquad e \le r \le R \tag{133}$$

$$g_1^x = \frac{dg_1^x}{dr} = F_1 = 0 \tag{134}$$

where the flapping hinge is at r = e. In addition, $I_{xx} = 0$.

Then,

$$-T_{11} = \frac{1}{(R-e)^2}\left[I_\beta + e\,S_\beta\right] \tag{135}$$

$$^{G}M_{11} = \frac{1}{(R-e)^2}\, I_\beta \tag{136}$$

$$\frac{\omega}{\Omega} = \sqrt{1 + e\frac{S_\beta}{I_\beta}} \tag{137}$$

where

$$I_\beta = \int_e^R m(r-e)^2\,dr \tag{138}$$

$$S_\beta = \int_e^R m(r-e)\,dr \tag{139}$$

Rigid Blade Lagging Frequency

For a lagging mode,

$$g_1^x = 0 \qquad 0 \le r \le e \tag{140}$$

$$g_1^x = \frac{r-e}{R-e} \qquad e \le r \le R \tag{141}$$

$$\frac{dg_1^x}{dr} = 0 \qquad 0 \le r \le e \tag{142}$$

$$\frac{dg_1^x}{dr} = \frac{1}{R-e} \qquad e \le r \le R \tag{143}$$

$$g_1^z = \frac{dg_1^z}{dr} = F_1 = 0 \tag{144}$$

where the lagging hinge is at $r = e$. In addition, $I_{zz} = 0$. Then,

$$-T_{11} = \frac{e}{(R-e)^2} S_\theta \tag{145}$$

$$^{G}M_{11} = \frac{I_\theta}{(R-e)^2} \tag{146}$$

$$\frac{\omega}{\Omega} = \sqrt{e \frac{S_\theta}{I_\theta}} \tag{147}$$

where

$$I_\theta = \int_e^R m(r-e)^2 dr \tag{148}$$

$$S_\theta = \int_e^R m(r-e) dr \tag{149}$$

Rigid Blade Pitching Frequency

For a pitch mode $F_1 = 1$

$$g_1^z = \frac{dg_1^z}{dr} = g_1^x = \frac{dg_1^x}{dr} = 0 \tag{150}$$

In addition, it is assumed either that the center of gravity is coincident with the elastic axis (i.e., $\bar{x} = 0$) or that the elastic axis is coincident with the OY axis, (i.e., $\epsilon + a_{EA}b = 0$). Then,

$$-T_{11} = I_{zz} - I_{xx} \tag{151}$$

$$^{G}M_{11} = I_{zz} + I_{xx} \tag{152}$$

$$\frac{\omega}{\Omega} = \sqrt{\frac{1-\left(\frac{I_{xx}}{I_{zz}}\right)}{1+\left(\frac{I_{xx}}{I_{zz}}\right)}} \tag{153}$$

where

$$I_{xx} = \int_0^R I_{xx}\,dr \tag{154}$$

$$I_{zz} = \int_0^R I_{zz}\,dr \tag{155}$$

for a plane lamina, I_{xx} is zero, therefore $\omega/\Omega = 1$.

DISSIPATION FUNCTION

In order to avoid the use of complex coefficients in the equations of motion, energy dissipation is assumed to occur due to viscous structural damping, which is the usual assumption made when using the decay-rate method. For the small amount of structural damping present in metal blades ($g = 0.03$ approximately) it makes little difference if into the equations of motion one puts hysteretic structural damping with $g = 0.03$ or viscous structural damping with $C/C_c = 0.015$. Hence, the generalized structural damping force acting in the rth generalized coordinated can be represented in the form

$$\Delta Q_r = -D_{grr}\dot{q}_r \tag{156}$$

It is convenient to obtain D_{grr} from the single-degree-of-freedom relation

$$D_{grr} = g_r \sqrt{{}^{G}M_{rr}\,\omega_r^2\,{}^{G}M_{rr}} = g_r\,\omega_r\,{}^{G}M_{rr} \tag{157}$$

where ${}^{G}M_{rr}$ = generalized inertia of the mode used as the rth generalized coordinate

ω_r = natural frequency of the rth mode

g_r = structural damping coefficient of the rth mode

ELASTIC STIFFNESS

The elastic energy due to small bending and torsional deflections of a blade can be expressed as

$$U = \frac{1}{2}\int_0^R \left[EI_z\left(\frac{d^2h_z}{dr^2}\right)^2 + EI_x\left(\frac{d^2h_x}{dr^2}\right)^2 + GJ\left(\frac{d\alpha}{dr}\right)^2 + K_A^2\left(\frac{d\alpha}{dr}\right)^2 \int_r^R \Omega^2\, m\, r\, dr \right] dr \tag{158}$$

Note that the units of EI_x , EI_z , and GJ must be consistent with those of the deflections. The last term on the right arises from the initial tension stresses in the blade. k_A is the polar radius of gyration of the tensile cross section. The generalized elastic stiffness can be expressed as a part independent of the rotational speed Ω and a part dependent on Ω . These are, respectively,

$$K_{ij} = \frac{\partial^2}{\partial q_i \partial q_j}\left\{\frac{1}{2}\int_0^R \left[EI_z\left(\frac{d^2h_z}{dr^2}\right)^2 + EI_x\left(\frac{d^2h_x}{dr^2}\right)^2 + GJ\left(\frac{d\alpha}{dr}\right)^2\right] dr\right\} \tag{159}$$

$$\Omega^2 L_{ij} = \frac{\partial^2}{\partial q_i \partial q_j}\left\{\left[\frac{1}{2}\int_0^R K_A^2\left(\frac{d\alpha}{dr}\right)^2 \int_r^R \Omega^2\, m\, r\, dr\right] dr\right\} \tag{160}$$

A generalized elastic tension stiffness coefficient L_{12} is determined from the potential energy Eq. (162) by expressing the torsional deflections in the modal form of Eq. (80) and then differentiating as indicated in Eq. (160).

$$U = \frac{1}{2}\int_0^R K_A^2 \left(\frac{d\alpha}{dr}\right)^2 \left\{\int_r^R \Omega^2 m r\, dr\right\} dr \tag{161}$$

$$= \frac{1}{2}\Omega^2 \int_0^R K_A^2 \left[\frac{dF_1}{dr} q_1 + \frac{dF_2}{dr} q_2\right]^2 \left\{\int_r^R m r\, dr\right\} dr \tag{162}$$

Hence

$$\Omega^2 L_{12} = \Omega^2 L_{21} = \frac{\partial^2 U}{\partial q_1 \partial q_2} = \Omega^2 \int_0^R K_A^2 \mathcal{M}\left(\frac{dF_1}{dr}\right)\left(\frac{dF_2}{dr}\right) dr \tag{163}$$

$$= \Omega^2 \int_0^R \left[g_1^z\ g_1^x\ \frac{dg_1^z}{dr}\ \frac{dg_1^x}{dr}\ F_1\ \frac{dF_1}{dr}\right] \begin{bmatrix} 0 & 0 & 0 & 0 & 0 & 0 \\ 0 & 0 & 0 & 0 & 0 & 0 \\ 0 & 0 & 0 & 0 & 0 & 0 \\ 0 & 0 & 0 & 0 & 0 & 0 \\ 0 & 0 & 0 & 0 & 0 & 0 \\ 0 & 0 & 0 & 0 & 0 & K_A^2 \mathcal{M} \end{bmatrix} \begin{bmatrix} g_2^z \\ g_2^x \\ \frac{d}{dr}(g_2^z) \\ \frac{d}{dr}(g_2^x) \\ F_2 \\ \frac{d}{dr}(F_2) \end{bmatrix} dr \tag{164}$$

TOTAL STRUCTURAL STIFFNESS

It will be assumed that the generalized modal inertia and natural frequency of each of the modes are known for the blade rotating in a vacuum at a particular rotor speed Ω_R. Then the integration implied in Eq. (159) for the formulation of the k_{ij} elements can be avoided.

In general, the mode shapes used as generalized coordinates will be considered to be semirigid, a term used in fixed-wing flutter to mean that the same mode shapes are used for all forward speeds. Irrespective of whether the generalized coordinates are arbitrary modes or orthogonal modes at zero forward speed, they will be arbitrary modes to some extent for non-zero forward speeds. However, if a sufficient number of generalized

coordinates are used in the solution, then for any forward speed these arbitrary modes will give the correct coupled mode shapes. The question is: Just what comprises a sufficient number? Fortunately, the effect of forward speed on the mode shapes is small, so that quite often two generalized coordinates are capable of giving a good approximation to the flutter speed. In addition to the effect of forward velocity, it is necessary also to consider variations in the mode shapes due to changes in any other parameter which affects the mode shapes. Here the assumption of semirigidity is not always so satisfactory, as it may require the use of an excessive number of generalized coordinates. In such cases, it is better to use a reduced number of modes and to assume the modes to be semirigid over only a limited range of variation of the parameter and to use new mode shapes for the generalized coordinates as necessary.

The concept of semirigidity can be applied also to rotating blade flutter where rotor speed enters as one of the parameters affecting mode shapes. In this case, it is desirable to be able to assume semirigidity with respect to both forward speed and rotor speed. This is facilitated if each mode involves displacements in 1 degree of freedom only; that is, if each mode is a pure mode. It has been found in practice that modes involving only pure flatwise bending, or pure edgewise bending, or pure torsion have shapes which vary little over a wide range of forward velocity and rotor speed.

Considering the mode shapes to be semirigid, the total structural stiffness acting in a generalized coordinate is composed of an elastic stiffness which is constant and an elastic tension stiffness and centrifugal stiffness which are both proportional to Ω^2. Suppose that the modes are calculated for rotational velocity Ω_R. Let ω_{R_i} be the natural frequency of the ith mode and M_{ii} the corresponding generalized inertia. Then the generalized total structural stiffness at the angular velocity Ω_R is given by

$$\left[C_S\right]_R = \left[{}^{G}M_{ii}\,\omega_{R_i}^2\right] = \left[K\right] + \Omega_R^2\left[L\right] - \Omega_R^2\left[T\right] \qquad (165)$$

where

$\left[{}^{G}M_{ii}\,\omega_{R_i}^2\right]$ is a diagonal matrix of generalized masses multiplied by the corresponding natural frequencies squared, appropriate to the rotational speed Ω_R.

$\left[K\right]$ is the generalized elastic bending and torsion stiffness matrix

$\Omega_R^2\left[L\right]$ is the generalized elastic tension stiffness matrix

$\Omega_R^2\left[T\right]$ is the generalized centrifugal stiffness matrix

coordinates are used in the solution, then for any forward speed these arbitrary modes will give the correct coupled mode shapes. The question is: Just what comprises a sufficient number? Fortunately, the effect of forward speed on the mode shapes is small, so that quite often two generalized coordinates are capable of giving a good approximation to the flutter speed. In addition to the effect of forward velocity, it is necessary also to consider variations in the mode shapes due to changes in any other parameter which affects the mode shapes. Here the assumption of semirigidity is not always so satisfactory, as it may require the use of an excessive number of generalized coordinates. In such cases, it is better to use a reduced number of modes and to assume the modes to be semirigid over only a limited range of variation of the parameter and to use new mode shapes for the generalized coordinates as necessary.

The concept of semirigidity can be applied also to rotating blade flutter where rotor speed enters as one of the parameters affecting mode shapes. In this case, it is desirable to be able to assume semirigidity with respect to both forward speed and rotor speed. This is facilitated if each mode involves displacements in 1 degree of freedom only; that is, if each mode is a pure mode. It has been found in practice that modes involving only pure flatwise bending, or pure edgewise bending, or pure torsion have shapes which vary little over a wide range of forward velocity and rotor speed.

Considering the mode shapes to be semirigid, the total structural stiffness acting in a generalized coordinate is composed of an elastic stiffness which is constant and an elastic tension stiffness and centrifugal stiffness which are both proportional to Ω^2. Suppose that the modes are calculated for rotational velocity Ω_R. Let ω_{R_i} be the natural frequency of the ith mode and M_{ii} the corresponding generalized inertia. Then the generalized total structural stiffness at the angular velocity Ω_R is given by

$$\left[C_s\right]_R = \left[{}^{G}M_{ii}\,\omega_{R_i}^2\right] = \left[K\right] + \Omega_R^2\left[L\right] - \Omega_R^2\left[T\right] \qquad (165)$$

where

$\left[{}^{G}M_{ii}\,\omega_{R_i}^2\right]$ is a diagonal matrix of generalized masses multiplied by the corresponding natural frequencies squared, appropriate to the rotational speed Ω_R.

$\left[K\right]$ is the generalized elastic bending and torsion stiffness matrix

$\Omega_R^2\left[L\right]$ is the generalized elastic tension stiffness matrix

$\Omega_R^2\left[T\right]$ is the generalized centrifugal stiffness matrix

AERODYNAMIC GENERALIZED FORCES

The velocity of the airstream relative to the axis X, Y, Z fixed in the helicopter is specified by the two components, as shown in Figure 9.

v_H is the velocity in the direction of the $\bar{X}$ axis

v_D is the velocity in the direction of the (-Z) axis

The velocity of the airflow relative to the blade is given in terms of the triad of unit vectors $\vec{e}_1$, $\vec{e}_2$, $\vec{e}_3$ fixed in the blade, where

$\vec{e}_1$ lies along the blade radial axis

$\vec{e}_3$ is in the plane of the shaft axis OZ and the rotating axis OX

$\vec{e}_2$ completes the right-handed triad

Then, with reference to Figure 9, the velocity of the airstream relative to the blade is given by

$$\vec{v} = (v_H \cos\beta_s \cos\psi - v_D \sin\beta_s)\vec{e}_1 - \left[v_H \sin\psi + \Omega(e + \bar{r}\cos\beta_s)\right]\vec{e}_2 - \left[v_H \sin\beta_s \cos\psi + v_D \cos\beta_s\right]\vec{e}_3 \qquad (170)$$

The air velocity component in the e_1 direction represents radial flow along the blades; for the aerodynamic model being considered, it does not produce any aerodynamic force. Hence, it is neglected. The magnitude of the air velocity normal to the blade is therefore given by

$$V = \sqrt{\left[v_H \sin\psi + \Omega(e + \bar{r}\cos\beta_s)\right]^2 + \left[v_H \sin\beta_s \cos\psi + v_D \cos\beta_s\right]^2} \qquad (171)$$

The coning angle β_s is included in the derivation of the aerodynamic coefficients. After these coefficients had been programmed, it was realized that the inclusion of the coning angle β_s would complicate unnecessarily the derivation of the structural coefficients, and so it was deleted. Hence, there is the inconsistency in that the coning angle is included in the aerodynamic coefficients but not in the structural. This inconsistency is removed by always specifying $\beta_s = 0$.

With Reference to Figure 10, the virtual work done by the lift L and the moment $M_{c/4}$ acting on an airfoil section of width d_r due to a virtual displacement is given by

$$\delta W = -L\delta h + M_{c/4}\,\delta\alpha \qquad (172)$$

$$\delta W = b\left[-L\,\delta\left(\frac{h}{c}\right) + \frac{M_{c/4}}{b}\,\delta\alpha\right] \tag{173}$$

$$\delta W = Q_h\,\delta\left(\frac{h}{b}\right) + Q_\alpha\,\delta\alpha \tag{174}$$

where Q_h and Q_α are the generalized aerodynamic forces due to vertical displacement and pitch respectively.

Hence,

$$\begin{bmatrix} Q_h \\ Q_\alpha \end{bmatrix} = b\begin{bmatrix} -L \\ \frac{M_{c/4}}{b} \end{bmatrix} \tag{175}$$

The aerodynamic coefficients were previously defined by the equation

$$\begin{bmatrix} -L \\ \frac{M_{c/4}}{b} \end{bmatrix} = -2\pi\rho b^3\,dr\left\{\left(\frac{V}{b}\right)\left[\dot{D}\right]\left\{\dot{\delta}\right\} + \left(\frac{V}{b}\right)^2\left[D\right]\left\{\delta\right\}\right\} \tag{176}$$

where

$$\left[\dot{D}\right] = \begin{bmatrix} \ell_{\dot{h}} & \ell_{\dot{\alpha}} \\ -m_{\dot{h}} & -m_{\dot{\alpha}} \end{bmatrix} \tag{177}$$

$$\left[D\right] = \begin{bmatrix} \ell_h & \ell_\alpha \\ -m_h & -m_\alpha \end{bmatrix} \tag{178}$$

$$\left\{\delta\right\} = \begin{bmatrix} \frac{h}{b} \\ \alpha \end{bmatrix}_{c/4} \tag{179}$$

Also, by definition,

$$h_{EA} = b_R \sum_j f_j(r)\,q_j(t) \tag{180}$$

$$\alpha = \sum_j F_j(r)\,q_j(t) \tag{181}$$

where

$$b_R\,f_i(r) = -g_i^z(r) \tag{182}$$

Therefore,

$$\begin{bmatrix} \frac{h}{b} \\ \alpha \end{bmatrix}_{EA} = \left(\frac{b_R}{b}\right) \begin{bmatrix} 1 & 0 \\ 0 & \frac{b}{b_R} \end{bmatrix} \begin{bmatrix} f_1 & \cdots & f_{ND} \\ F_1 & \cdots & F_{ND} \end{bmatrix} \begin{bmatrix} q_1 \\ \vdots \\ q_{ND} \end{bmatrix} \tag{183}$$

The displacements at the 25% chord and at the elastic axis are related by

$$h_{C/4} = h_{EA} - \left(\frac{1}{2} + a_{EA}\right) b\alpha \tag{184}$$

$$\alpha_{C/4} = \alpha_{EA} \tag{185}$$

That is

$$\{\delta\} = \begin{bmatrix} \frac{h}{b} \\ \alpha \end{bmatrix}_{C/4} = \begin{bmatrix} 1 & -\left(\frac{1}{2} + a_{EA}\right) \\ 0 & 1 \end{bmatrix} \begin{bmatrix} \frac{h}{b} \\ \alpha \end{bmatrix}_{EA} \tag{186}$$

$$= \left(\frac{b_R}{b}\right) \begin{bmatrix} 1 & -\left(\frac{1}{2} + a_{EA}\right) \\ 0 & 1 \end{bmatrix} \begin{bmatrix} 1 & 0 \\ 0 & \left(\frac{b}{b_R}\right) \end{bmatrix} \begin{bmatrix} f_1 & \cdots & f_{ND} \\ F_1 & \cdots & F_{ND} \end{bmatrix} \begin{bmatrix} q_1 \\ \vdots \\ q_{ND} \end{bmatrix} \tag{187}$$

$$= \left(\frac{b_R}{b}\right) [H][B_C][G_M] \{q\} \tag{188}$$

where

$$[H] = \begin{bmatrix} 1 & -\left(\frac{1}{2} + a_{EA}\right) \\ 0 & 1 \end{bmatrix} \tag{189}$$

$$[B_C] = \begin{bmatrix} 1 & 0 \\ 0 & \frac{b}{b_R} \end{bmatrix} \tag{190}$$

$$[G_M] = \begin{bmatrix} f_1 & \cdots & f_{ND} \\ F_1 & \cdots & F_{ND} \end{bmatrix} \tag{191}$$

$$\{q\} = \begin{bmatrix} q_1 \\ q_{ND} \end{bmatrix} \tag{192}$$

Similarly,

$$\{Q_q\} = \left[\left(\frac{b_R}{b}\right)[H][B_c][G_M]\right]' \{Q_\delta\} \tag{193}$$

$$= \left(\frac{b_R}{b}\right)[G_M]'[B_c][H]' \begin{bmatrix} Q_h \\ Q_\alpha \end{bmatrix} \tag{194}$$

Combining equations (175), (176), (188), and (194) gives

$$\{Q_q\} = -2\pi\rho\left(\frac{b_R}{b}\right)^2 b^4\, dr\, [G_M]'[B_c][H]' \begin{bmatrix} \left(\frac{V}{b}\right)[\dot{D}][H][B_c][G_M]\{\dot{q}\} \\ + \left(\frac{V}{b}\right)[D][H][B_c][G_M]\{q\} \end{bmatrix} \tag{195}$$

When the following substitutions are introduced

$$\sigma = \frac{\rho}{\rho_{SL}} \tag{196}$$

$$dr = \ell\, d\eta \tag{197}$$

$$[x_1] = \sigma \frac{b}{b_R}[G_M]'[B_c][H]'[\dot{D}][H][B_c][G_M] \tag{198}$$

$$[x_2] = \sigma[G_M]'[B_c][H]'[D][H][B_c][G_M] \tag{199}$$

$$[B]_{AERO} = \int_{\eta_I}^{\eta_O}\left(\frac{V}{V_R}\right)[x_1]\, d\eta \tag{200}$$

$$[C]_{AERO} = \int_{\eta_I}^{\eta_O}\left(\frac{V}{V_R}\right)^2[x_2]\, d\eta \tag{201}$$

and when integrated to find the generalized force due to the whole blade, the equations become

$$\{Q_q\} = -2\pi\rho_{SL} b_R^2 V_R^2\, \ell \left\{\left(\frac{b_R}{V_R}\right)[B]_{AERO}\{\dot{q}\} + [C]_{AERO}\{q\}\right\} \tag{202}$$

PROVISION FOR MASS BALANCE

Mass balance, which is distributed radially along the blade, is considered separately from the mass of the basic blade structure. When this is done, the following expressions for the structural coefficients are obtained in matrix notation:

$$\left[{}^{G}M\right] = \int_0^R \left[\Phi\right]' \left\{ {}^{\delta}\left[M\right]_{\phi} + t_n {}^{\delta}\left[{}^{G}M\right]_b \right\} \left[\Phi\right] dr \tag{203}$$

$$\left[G\right] = \int_0^R \left[\Phi\right]' \left\{ {}^{\delta}\left[G\right]_{\phi} + t_n {}^{\delta}\left[G\right]_b \right\} \left[\Phi\right] dr \tag{204}$$

$$\left[L\right] = \int_0^R \left[\Phi\right]' \left\{ {}^{\delta}\left[L\right]_{\phi} + t_n {}^{\delta}\left[L\right]_b \right\} \left[\Phi\right] dr \tag{205}$$

$$\left[T\right] = \int_0^R \left[\Phi\right]' \left\{ {}^{\delta}\left[T\right]_{\phi} + t_n {}^{\delta}\left[T\right]_b \right\} \left[\Phi\right] dr \tag{206}$$

where subscript ϕ refers to the basic blade structure, subscript b refers to the mass balance weight, and t_n is a nondimensional parameter to vary the amount of blade mass balance. For $t_n = 0$ mass balance effects become zero. The form of $\left[{}^{G}M_{\phi}\right]$ - - - - - $\left[T_b\right]$ can be obtained by inspection of the expressions for $\left[{}^{G}M\right]$, $\left[G\right]$, $\left[L\right]$, and $\left[T\right]$ obtained previously.

The matrix $\Delta\left[{}^{G}M_{\phi}\right]$ and the other matrices on the right hand sides of Eq. (203) through (206) are determined by using expressions which are completely analogous to those found previously without consideration of separate mass balance.

PROVISION FOR VARIATIONS IN BLADE PARAMETERS

The provision to vary the following parameters is now incorporated into the expressions for the coefficients:

1. Frequencies of the modes used as generalized coordinates.
2. Blade chordwise center-of-gravity position.
3. Blade chordwise elastic axis position.
4. Blade chordwise aerodynamic center position.

Variation of Blade Modal Frequencies

The generalized structural stiffness at the rotor speed Ω_R is given by $\left[C_s\right]_R = \left[{}^{G}M_{ii}\,\omega_{Ri}^2\right]$. The modal frequency ω_{Ri} is considered increased by the amount $y_r\,\omega_{vi}$ where ω_{vi} is specified for each

mode and y_r is an overall variation factor. The new structural stiffness is then given by

$$\left[C_S\right]_R = \left[{}^{G}M_{ii}(\omega_{R_i} + y_v\omega_{v_i})^2 \right] \tag{207}$$

Variation of Blade Chordwise Center of Gravity and Elastic Axis Position

The structural model to be used when changing the center of gravity and elastic axis positions is as follows:

The chordwise center-of-gravity position changes due to a mass balance weight which is moved chordwise. The total mass of the blade remains unchanged, as do the mass and inertial properties of the fixed portion of the blade. The fixed or basic part of the blade and the balance weight are entered into the structural coefficients as separate components, with the magnitude of the balance mass made variable through use of the coefficient t_n .

The input mode shapes, frequencies, and generalized inertias remain unchanged. The effect of an elastic axis shift is to:

1. Change the mass moment and inertia about the elastic axis, but not the mass moment and inertia about the center of gravity. This effect will be taken into account when blade inertias are calculated.

2. Change the aerodynamic-center-to-elastic-axis distance. This is taken into account by changing the value of a_{EA} when the aerodynamic coefficients are calculated.

With reference to Figure 11,

$t_b \Delta\bar{x}$ is the distance the center of gravity of the mass balance weight is shifted aft.

$t_e b \Delta a_{EA}$ is the distance the elastic axis is shifted aft.

Then, for the balance weight,

$$\bar{x}_b = \bar{x}_b' + t_b\Delta\bar{x} - t_e\, b\Delta a_{EA} \tag{208}$$

and for the basic blade,

$$\bar{x}_\phi = \bar{x}_\phi' - t_e b\Delta a_{EA} \tag{209}$$

The elastic axis distance aft of the mid-chord is given by

$$a_{EA} = a'_{EA} + t_e \, \Delta a_{EA} \tag{210}$$

First, the changes in the blade inertias referring to the new position of the elastic axis are calculated.

The mass moment per unit span of the balance weight prior to the application of the coefficient t_n is

$$m_b \bar{x}_b = m_b \bar{x}'_b + m_b (t_b \Delta\bar{x} - t_e \, b \Delta a_{EA}) \tag{211}$$

The same quantity for the basic blade is

$$m_\phi \bar{x}_\phi = m_\phi \bar{x}'_\phi - m_\phi t_e \, b \Delta a_{EA} \tag{212}$$

The balance weight edgewise mass moment of inertia per unit span is

$$I_{zz_b} = I_{zz_{b_{CG}}} + m_b (\bar{x}'_b)^2 + 2(t_b \Delta\bar{x} - t_e b \Delta a_{EA}) m_b \bar{x}'_b + m_b (t_b \Delta\bar{x} - t_e b \Delta a_{EA})^2 \tag{213}$$

$$I_{zz_b} = I'_{zz_b} + 2(t_b \Delta\bar{x} - t_e b \Delta a_{EA}) m_b \bar{x}'_b + m_b (t_b \Delta\bar{x} - t_e b \Delta a_{EA})^2 \tag{214}$$

The corresponding quantity for the basic blade is

$$I_{zz_\phi} = I'_{zz_\phi} - 2 t_e b \Delta a_{EA} m_\phi \bar{x}'_\phi + m_\phi (t_e b \Delta a_{EA})^2 \tag{215}$$

The balance weight product of inertia per unit span is

$$I_{xz_b} = I_{xz_{b_{CG}}} + m_b \left[\bar{x}'_b + (t_b \Delta\bar{x} - t_e b \Delta a_{EA}) \right] \bar{z}_b \tag{216}$$

$$I_{xz_b} = I'_{xz_b} + m_b (t_b \Delta\bar{x} - t_e b \Delta a_{EA}) \bar{z}_b \tag{217}$$

The corresponding quantity for the basic blade is

$$I_{xz_\phi} = I'_{xz_\phi} - t_e b \Delta a_{EA} m_\phi \bar{z}_\phi \tag{218}$$

The inertial properties $m_b \bar{z}_b$ and I_{xx_b} for the balance weight and $m\bar{z}$ and I_{xx} for the basic blade are not changed. The changes in the aerodynamic coefficients due to shifting the elastic axis are now calculated. This is done by changing the value of a_{EA} used in the calculation of the $[H]$ matrix, which is thereby redefined as

$$[H] = \begin{bmatrix} 1 & -\left(\frac{1}{2} + a'_{EA} + t_e \Delta a_{EA}\right) \\ 0 & 1 \end{bmatrix} \tag{219}$$

Variation of Blade Chordwise Aerodynamic Center Position

In addition to arbitrary variation of the position of the aerodynamic center there is also a shift in the aerodynamic center due to reverse flow. These effects will be considered separately. Consider first an arbitrary variation in the position of the aerodynamic center. Suppose the aerodynamic center shifted aft a distance $t_a b \delta_{AC}$, as shown in Figure 12.

In classical flutter, changes in lift and moment due to very small motions of the blade are considered. For steady flow, the aerodynamic center is not coincident with the center of pressure except for airfoils with a zero steady moment at zero lift. However, when considering incremental changes, the aerodynamic center and the center of pressure become coincident. In flutter, the two terms are used interchangeably and usually refer to the point through which the incremental lift force acts, for nonoscillatory motion. This definition of the aerodynamic center means that for oscillatory motions there will in general be an oscillatory moment acting at the aerodynamic center (center of pressure). A shift in the aerodynamic center is defined to be such that the forces and moments acting at the old position of the aerodynamic center are transferred unchanged to the new position of the aerodynamic center.

That is,

$$\begin{bmatrix} -\tilde{L} \\ \frac{\tilde{M}}{b} \end{bmatrix}^N = \begin{bmatrix} -L \\ \frac{M}{b} \end{bmatrix}^O \tag{220}$$

where the quantities on the right hand side are applied at a distance Δb aft of the 25% chord and the quantities at the left hand side are applied at a distance $(\Delta b + t_a b \delta_{AC})$ aft of the 25% chord, as shown on Figure 12. The position of the aerodynamic center will be denoted henceforth by using the superscript notation above.

If the relation between forces and moments at the 25% chord and at the aerodynamic center is considered, we have, for the two aerodynamic center positions,

$$\begin{bmatrix} -L_{c/4} \\ \frac{M_{c/4}}{b} \end{bmatrix}^{O} = \begin{bmatrix} 1 & 0 \\ \Delta & 1 \end{bmatrix} \begin{bmatrix} -L \\ \frac{M}{b} \end{bmatrix}^{O} \tag{221}$$

and

$$\begin{bmatrix} -L_{c/4} \\ \frac{M_{c/4}}{b} \end{bmatrix}^{N} = \begin{bmatrix} 1 & 0 \\ (\Delta + t_a \delta) & 1 \end{bmatrix} \begin{bmatrix} -\tilde{L} \\ \frac{\tilde{M}}{b} \end{bmatrix}^{N} \tag{222}$$

Combining Eqs. (220), (221), and (222), after some algebraic manipulation, gives

$$\begin{bmatrix} -L_{c/4} \\ \frac{M_{c/4}}{b} \end{bmatrix}^{N} = \begin{bmatrix} 1 & 0 \\ t_a \delta & 1 \end{bmatrix} \begin{bmatrix} -L_{c/4} \\ \frac{M_{c/4}}{b} \end{bmatrix}^{O} \tag{223}$$

Previously, the aerodynamic coefficients were defined in terms of the lift and moment about the 25% chord as follows:

$$\begin{bmatrix} -L_{c/4} \\ \frac{M_{c/4}}{b} \end{bmatrix}^{O} = -2\pi\rho b^3 dr \left\{ \left(\frac{V}{b}\right) \left[\dot{D}\right] \left\{\dot{\delta}\right\} + \left(\frac{V}{b}\right)^2 \left[D\right] \left\{\delta\right\} \right\} \tag{224}$$

The aerodynamic coefficients consistent with the new aerodynamic center position are defined to be

$$\begin{bmatrix} -L_{c/4} \\ \frac{M_{c/4}}{b} \end{bmatrix}^{N} = -2\pi\rho b^3 dr \left\{ \left(\frac{V}{b}\right) \left[\dot{D}\right]^{N} \left\{\dot{\delta}\right\} + \left(\frac{V}{b}\right)^2 \left[D\right]^{N} \left\{\delta\right\} \right\} \tag{225}$$

Substituting Eqs. (224) and (225) into (223) and setting the respective coefficients of $\{\dot{\delta}\}$ and $\{\delta\}$ equal, gives

$$[\dot{D}]^N = [\Delta][\dot{D}] \tag{226}$$

$$[D]^N = [\Delta][D] \tag{227}$$

where

$$[\Delta] = \begin{bmatrix} 1 & 0 \\ t_a\delta & 1 \end{bmatrix} \tag{228}$$

Consider now the effect of reverse flow. Only those quantities that affect the aerodynamic coefficients are involved, since the structural coefficients are the same for forward and reverse flow. Inspection of Figure 13 shows the following relations between forward and reverse flow:

$$\left(a'_{EA} + t_e \Delta a_{EA}\right)^R = -\left(a'_{EA} + t_e \Delta a_{EA}\right)^F \tag{229}$$

$$\left(h_{EA}\right)^R = \left(h_{EA}\right)^F \tag{230}$$

$$\left(\alpha\right)^R = -\left(\alpha\right)^F \tag{231}$$

where superscript F refers to forward flow and superscript R refers to reverse flow .

The change in sign of the pitch angle α shows up as a change in sign of the torsion mode shape F_j through the equation

$$\alpha = \sum_j F_j q_j \tag{232}$$

Reverse flow is said to occur when the component of the air velocity in the $(-\vec{e}_2)$ direction, as previously defined, is negative. That is,

$$v_x = \sin\psi\, v_H + \Omega\left(e + \bar{r}\cos\beta_s\right) < 0 \tag{233}$$

Hence, when $V_x < 0$, reverse flow is allowed for in the following way:

1. Change the sign of $(a'_{EA} + t_e \Delta a_{EA})$ in the matrix $[H]$ so that it becomes

$$[H] = \begin{bmatrix} 1 & -\left[\frac{1}{2} - (a'_{EA} + t_e \Delta a_{EA})\right] \\ 0 & 1 \end{bmatrix} \tag{234}$$

2. Change the sign of F_1 in the second row of the matrix $[G_M]$ so that it becomes

$$[G_M] = \begin{bmatrix} f_1 - - - - - - f_{ND} \\ (-F_1) - - - - - (-F_{ND}) \end{bmatrix} \tag{235}$$

Similar changes are also made in $[H]'$ and $[G_M]'$.

SPANWISE INTEGRATION OF THE COEFFICIENTS

So far, the generalized forces acting in a mode have been expressed in terms of integrations across the blade span. The same procedure has been followed in the definition of the generalized mass and stiffness coefficients. In practice, the integrations are replaced by finite summations, using the trapezoidal rule. The blade is divided into segments or strips, each of which extends from the blade leading edge to the trailing edge, and whose radial or spanwise dimension is a suitable fraction of the blade radius. The segments are labeled $k = 1$ to $k = N_S$ from root to tip, respectively. Considering the structural coefficients and, for convenience, using the form of the coefficients written in matrix notation gives

$$\int_0^R [\Phi]^t \, {}^{\Delta}[a] \, [\Phi] \, dr = \sum_{k=1}^{N_S} [\Phi]_K^t \, {}^{\Delta}[a]_K \, [\Phi]_K \, \Delta r_K \tag{236}$$

The matrix ${}^{\Delta}[a]$ represents any of the structural coefficient matrices. In addition,

$$M(r) = \int_r^R m r dr \tag{237}$$

is replaced by

$$M_K = \frac{1}{2} m \quad (r_K + \frac{1}{4}\Delta r_K)\Delta r_K + \sum_{n=K+1}^{N_S} m \; r_n \Delta r_n \tag{238}$$

The values of m in Eq. (238) are expressed in mass per unit span and are appropriate to each finite segment. When the integrals are replaced by finite summations, it is convenient to change the definitions of the mass terms m, $m\bar{x}$ etc., from "per unit span" to "per segment". The definition of M_k is not changed, since it refers not only to a local part of the blade, but also to a summation involving all parts of the blade outboard of a particular segment. Because of this, the value of M_K cannot be given easily as input data on the basis of a contribution from each segment, and its value at each segment is computed by the program. Let m, $m\bar{x}$ etc., be the inertias per unit span when integrating. Let m_k, $m_k\bar{x}$ etc., be the inertias per blade segment when a finite summation is used. Let $[a]$ be per unit span. Let $[\bar{a}]$ be per blade segment. Then, the above equations become

$$\int_0^R [\Phi]'^{\Delta}[a][\Phi]\,dr \simeq \sum_{k=1}^{N_S} [\Phi]'_K{}^{\Delta}[a][\Phi]_K \Delta r_K = \sum_{k=1}^{N_S} [\Phi]'_K{}^{\Delta}[\bar{a}]_K[\Phi]_K \tag{239}$$

$$M_K = \frac{1}{2} m_K (r_K + \frac{1}{4}\Delta r_K) + \sum_{n=K+1}^{N_S} m_n r_n \tag{240}$$

and any element of $[\bar{a}]_k$ containing M_k is multiplied by Δr_k. When the aerodynamic coefficients are considered,

$$[B]_{aero} = \int_{\eta_I}^{\eta_O} \left(\frac{V}{V_R}\right)[X_1]\,d\eta \simeq \sum_{K=1}^{N_S} \left(\frac{V_K}{V_R}\right)[X_1]_K \tag{241}$$

$$[C]_{aero} = \int_{\eta_I}^{\eta_O} \left(\frac{V}{V_R}\right)^2 [X_2]\,d\eta \simeq \sum_{K=1}^{N_S} \left(\frac{V_K}{V_R}\right)^2 [X_2]_K \tag{242}$$

where

$$[X_1]_k = \sigma\Delta\eta_k\left(\frac{b_k}{b_R}\right)[G_M]'_k\,[B_C]_k[H]'_k[\Delta]_k[\dot{D}]_k[H]_k[B_C]_k[G_M]_k \tag{243}$$

$$[X_2]_k = \sigma\Delta\eta_k[G_M]'_k[B_C]_k[H]'_k[\Delta]_k[D]_k[H]_k[B_C]_k[G_M]_k \tag{244}$$

NONDIMENSIONALIZING THE EQUATIONS OF MOTION

The equations of motion as developed so far can be put in the form

$$\left[A_s\right]\left\{\frac{d^2q}{dt^2}\right\} + \left[B_s\right]\left\{\frac{dq}{dt}\right\} + \left[C_s\right]\left\{q\right\}$$

$$= -2\pi\rho_{SL}b_R^2 V_R^2 \ell \left\{\left(\frac{b_R}{V_R}\right)\left[B\right]_{aero}\left\{\frac{dq}{dt}\right\} + \left[C\right]_{aero}\left\{q\right\}\right\} \qquad (245)$$

where $\left[A_s\right]$ $\left[B_s\right]$ and $\left[C_s\right]$ are the total structural coefficients.

The equations are now multiplied by $\frac{1}{2\pi\rho_{SL}b_R^4\ell}\left(\frac{b_R}{V_R}\right)^2$ and the nondimensional time τ is introduced by the relation

$$\tau = \left(\frac{V_R}{b_R}\right)t \qquad (246)$$

so that

$$\frac{d}{dt} = \left(\frac{V_R}{b_R}\right)\frac{d}{d\tau} \qquad \frac{d^2}{dt^2} = \left(\frac{V_R}{b_R}\right)^2\frac{d^2}{d\tau^2} \qquad (247)$$

After some rearranging, the equations become

$$\left[\frac{A_s}{2\pi\rho_{SL}b_R^4\ell}\right]\left\{\frac{d^2q}{d\tau^2}\right\} + \left\{\left(\frac{b_R}{V_R}\right)\left[\frac{B_s}{2\pi\rho_{SL}b_R^4\ell}\right] + \left[B\right]_{aero}\right\}\left\{\frac{dq}{d\tau}\right\}$$

$$+ \left\{\left(\frac{b_R}{V_R}\right)^2\left[\frac{C_s}{2\pi\rho_{SL}b_R^4\ell}\right] + \left[C\right]_{aero}\right\}\left\{q\right\} = \left\{0\right\} \qquad (248)$$

FINAL FORM OF THE EQUATIONS OF MOTION

The final form of the equations of motion can now be stated, as follows:

$$\left[A\right]_T\left\{\frac{d^2q}{d\tau^2}\right\} + \left[B\right]_T\left\{\frac{dq}{d\tau}\right\} + \left[C\right]_T\left\{q\right\} = \left\{0\right\} \qquad (249)$$

where

$\{q\}$ is a column matrix of generalized coordinates $q_1 \cdots\cdots q_{NO}$

$$\tau = \left(\frac{V_R}{b_R}\right) t \tag{250}$$

$$[B]_T = [D] - 2\Omega\,[G] + [B]_{AERO} \tag{251}$$

$$[C]_T = {}^{Q}[C_S]_R + (\Omega^2 - \Omega_R^2)\left\{{}^{Q}[L] - {}^{Q}[T]\right\} + [C]_{AERO} \tag{252}$$

$$[A]_T = \frac{1}{2\pi\rho_{SL} b_R^4 \ell} \sum_{K=1}^{N_S} \left\{ {}^{\Delta}[{}^{G}M]_{\phi k} + t_n\, {}^{\Delta}[{}^{G}M]_{bk} \right\} \tag{253}$$

$$[D_g] = \frac{1}{2\pi\rho_{SL} b_R^4 \ell} \left(\frac{b_R}{V_R}\right) \left[g_i\,(\omega_{R_i} + y_V \omega_{V_i})\, {}^{G}M_{ii} \right] \tag{254}$$

$${}^{Q}[G] = \frac{1}{2\pi\rho_{SL} b_R^4 \ell} \left(\frac{b_R}{V_R}\right) \sum_{K=1}^{N_S} \left\{ {}^{\Delta}[G]_{\phi k} + t_n\, {}^{\Delta}[G]_{bk} \right\} \tag{255}$$

$$[B]_{AERO} = \sum_{K=1}^{N_S} \left(\frac{V_K}{V_R}\right) [X_1]_K \tag{256}$$

$${}^{Q}[C_S]_R = \frac{1}{2\pi\rho_{SL} b_R^4 \ell} \left(\frac{b_R}{V_R}\right)^2 \left[(\omega_i + y_0 \omega_{V_i})^2\, {}^{G}M_{ii} \right] \tag{257}$$

$${}^{Q}[L] = \frac{1}{2\pi\rho_{SL} b_R^4 \ell} \left(\frac{b_R}{V_R}\right)^2 \sum_{K=1}^{N_S} \left\{ {}^{\Delta}[L]_{\phi k} + t_n\, {}^{\Delta}[L]_{bk} \right\} \tag{258}$$

$${}^{Q}[T] = \frac{1}{2\pi\rho_{SL} b_R^4 \ell} \left(\frac{b_R}{V_R}\right)^2 \sum_{K=1}^{N_S} \left\{ {}^{\Delta}[T]_{\phi k} + t_n\, {}^{\Delta}[T]_{bk} \right\} \tag{259}$$

$$[C]_{AERO} = \sum_{K=1}^{N_S} \left(\frac{V_K}{V_R}\right)^2 [X_2]_K \tag{260}$$

$$
\begin{aligned}
(\Delta M_{\phi k})_{ij} = {} & (g^x_{ki} g^x_{kj} + g^z_{ki} g^z_{kj})\, m_{\phi k} - (g^z_{ki} F_{kj} + g^z_{kj} F_{ki})\, m_{\phi k} \bar{x}_{\phi k} \\
& + (g^x_{ki} F_{kj} + g^x_{kj} F_{ki})\, m_{\phi k} \bar{z}_{\phi k} + \left(\frac{dg^z_{ki}}{dr} \frac{dg^z_{kj}}{dr}\right)(I_{xx})_{\phi k} \\
& + \left(\frac{dg^x_{ki}}{dr} \frac{dg^z_{kj}}{dr} + \frac{dg^x_{kj}}{dr} \frac{dg^z_{ki}}{dr}\right)(I_{xz})_{\phi k} \\
& + \left(\frac{dg^x_{ki}}{dr} \frac{dg^x_{kj}}{dr}\right)(I_{zz})_{\phi k} + (F_{ki} F_{kj})(I_{yy})_{\phi k}
\end{aligned}
\tag{261}
$$

$$
{}^{\Delta}[M]_{\phi k} = [\Phi]'_k \, {}^{\delta}[M]_{\phi k} \, [\Phi]_k \tag{262}
$$

$$
[\Phi]_k = \begin{bmatrix}
g^z_{k1} & g^z_{k2} & - & - & - & - & - & g^z_{kN_D} \\
g^x_{k1} & g^x_{k2} & & & & & & g^x_{kN_D} \\
\frac{d}{dr}(g^z_{k1}) & \frac{d}{dr}(g^z_{k2}) & & & & & & \frac{d}{dr}(g^z_{kN_D}) \\
\frac{d}{dr}(g^x_{k1}) & \frac{d}{dr}(g^x_{k2}) & & & & & & \frac{d}{dr}(g^x_{kN_D}) \\
F_{k1} & F_{k2} & & & & & & F_{kN_D} \\
\frac{d}{dr}(F_{k1}) & \frac{d}{dr}(F_{k2}) & & & & & & \frac{d}{dr}(F_{kN_D})
\end{bmatrix}
\tag{263}
$$

$$
{}^{\delta}[M]_{\phi k} = \begin{bmatrix}
m_{\phi k} & 0 & 0 & 0 & (-m\bar{x})_{\phi k} & 0 \\
0 & m_{\phi k} & 0 & 0 & (m\bar{z})_{\phi k} & 0 \\
0 & 0 & (I_{xx})_{\phi k} & (I_{xz})_{\phi k} & 0 & 0 \\
0 & 0 & (I_{xz})_{\phi k} & (I_{zz})_{\phi k} & 0 & 0 \\
-(m\bar{x})_{\phi k} & (m\bar{z})_{\phi k} & 0 & 0 & (I_{yy})_{\phi k} & 0 \\
0 & 0 & 0 & 0 & 0 & 0
\end{bmatrix}
\tag{264}
$$

$$
\begin{aligned}
(\Delta G_{\phi k})_{ij} = {} & \left(\frac{dg^x_{ki}}{dr} g^x_{kj} - \frac{dg^x_{kj}}{dr} g^x_{ki}\right) m_{\phi k} \bar{x}_{\phi k} \\
& + \left(\frac{dg^z_{ki}}{dr} g^x_{kj} - \frac{dg^z_{kj}}{dr} g^x_{ki}\right) m_{\phi k} \bar{z}_{\phi k} \\
& + \left(\frac{dg^z_{ki}}{dr} F_{kj} - \frac{dg^z_{kj}}{dr} F_{ki}\right) (I_{xx})_{\phi k} \\
& + \left(\frac{dg^x_{ki}}{dr} F_{kj} - \frac{dg^x_{kj}}{dr} F_{ki}\right) (I_{xz})_{\phi k}
\end{aligned} \tag{265}
$$

$$
{}^{\Delta}[G]_{\phi k} = [\Phi]_k^{\prime}\, {}^{\delta}[G]_{\phi k}\, [\Phi]_k \tag{266}
$$

$$
{}^{\delta}[G]_{\phi k} = \begin{bmatrix}
0 & 0 & 0 & 0 & 0 & 0 \\
0 & 0 & -(m\bar{z})_{\phi k} & -(m\bar{x})_{\phi k} & 0 & 0 \\
0 & (m\bar{z})_{\phi k} & 0 & 0 & (I_{xx})_{\phi k} & 0 \\
0 & (m\bar{x})_{\phi k} & 0 & 0 & (I_{xz})_{\phi k} & 0 \\
0 & 0 & -(I_{xx})_{\phi k} & -(I_{xz})_{\phi k} & 0 & 0 \\
0 & 0 & 0 & 0 & 0 & 0
\end{bmatrix} \tag{267}
$$

$$
(L_{\phi k})_{ij} = \frac{dF_{ki}}{dr} \frac{dF_{kj}}{dr} (k a_k)^2 \mathcal{M}_{\phi k} \Delta r_k \tag{268}
$$

$$
{}^{\delta}[L]_{\phi k} = [\Phi]_k^{\prime}\, {}^{\delta}[L]_{\phi k}\, [\Phi]_k \tag{269}
$$

$$
{}^{\delta}[L]_{\phi k} = \begin{bmatrix}
0 & 0 & 0 & 0 & 0 & 0 \\
0 & 0 & 0 & 0 & 0 & 0 \\
0 & 0 & 0 & 0 & 0 & 0 \\
0 & 0 & 0 & 0 & 0 & 0 \\
0 & 0 & 0 & 0 & 0 & 0 \\
0 & 0 & 0 & 0 & 0 & k^2_{ak} \mathcal{M}_{\phi k} \Delta r_k
\end{bmatrix} \tag{270}
$$

$$
\begin{aligned}
\left({}^{\Delta}T_{\phi k}\right)_{ij} = \; & \left(g^{x}_{ki}\, g^{x}_{kj}\right) m_{\phi k} + \left(g^{x}_{ki} F_{kj} + g^{x}_{kj} F_{ki}\right) m_{\phi k} \bar{z}_{\phi k} \\
& - \left(\frac{dg^{x}_{ki}}{dr} F_{kj} + \frac{dg^{x}_{kj}}{dr} F_{ki}\right) r_{\phi k}\, m_{\phi k} \bar{z}_{\phi k} \\
& + \left(\frac{dg^{z}_{ki}}{dr} F_{kj} + \frac{dg^{z}_{kj}}{dr} F_{ki}\right) r_{\phi k}\, m_{\phi k} \bar{x}_{\phi k} \\
& + \left(\frac{dg^{z}_{ki}}{dr} \frac{dg^{z}_{kj}}{dr}\right) \left[(I_{xx})_{\phi k} - \mathcal{M}_{\phi k} \Delta r_k\right] \\
& + \left(\frac{dg^{x}_{ki}}{dr} \frac{dg^{x}_{kj}}{dr}\right) \left[(I_{zz})_{\phi k} - \mathcal{M}_{\phi k} \Delta r_k\right] \\
& + \left(\frac{dg^{x}_{ki}}{dr} \frac{dg^{z}_{kj}}{dr} + \frac{dg^{x}_{kj}}{dr} \frac{dg^{z}_{ki}}{dr}\right) (I_{xz})_{\phi k} \\
& + F_{ki} F_{kj} \left[(I_{xx})_{\phi k} - (I_{zz})_{\phi k} - (\epsilon + a_{EA} b)\, m_{\phi k} \bar{x}_{\phi k}\right]
\end{aligned}
\tag{271}
$$

$$
{}^{\Delta}[T]_{\phi k} = [\Phi]_k' \; {}^{\delta}[T]_{\phi k} \; [\Phi]_k \tag{272}
$$

$$
{}^{\delta}[T]_{\phi k} = \begin{bmatrix}
0 & 0 & 0 & 0 & 0 & 0 \\
0 & m_{\phi k} & 0 & 0 & (m\bar{z})_{\phi k} & 0 \\
0 & 0 & \left[(I_{xx})_{\phi k} - \mathcal{M}_{\phi k} \Delta r_k\right] & (I_{xz})_{\phi k} & (r m \bar{x})_{\phi k} & 0 \\
0 & 0 & (I_{xz})_{\phi k} & \left[(I_{zz})_{\phi k} - \mathcal{M}_{\phi k} \Delta r_k\right] & -(r m \bar{z})_{\phi k} & 0 \\
0 & (m\bar{z})_{\phi k} & (r m \bar{x})_{\phi k} & -(r m \bar{z})_{\phi k} & \left[(I_{xx})_{\phi k} - (I_{zz})_{\phi k} - (\epsilon + a_{EA} b)(m\bar{x})_{\phi k}\right] & 0 \\
0 & 0 & 0 & 0 & 0 & 0
\end{bmatrix}
\tag{273}
$$

The expressions for the mass balance coefficients are identical to the expressions given above except that subscript ϕ is replaced by b.

$$[X_1]_k = \sigma\Delta\eta_k\left(\frac{b_k}{b_R}\right)[G_M]'_k[B_c]_k[H]'_k[\Delta]_k[\dot{D}]_k[H]_k[B_c]_k[G_M]_k \tag{274}$$

$$[X_2]_k = \sigma\Delta\eta_k[G_M]'_k[B_c]_k[H]'_k[\Delta]_k[D]_k[H]_k[B_c]_k[G_M]_k \tag{275}$$

$$[\dot{D}]_k = \begin{bmatrix} l_{\dot{h}} & l_{\dot{\alpha}} \\ -m_{\dot{h}} & -m_{\dot{\alpha}} \end{bmatrix}_k \tag{276}$$

$$[D]_k = \begin{bmatrix} l_h & l_\alpha \\ -m_h & -m_\alpha \end{bmatrix}_k \tag{277}$$

$$[\Delta]_k = \begin{bmatrix} 1 & 0 \\ t_a\delta_K & 1 \end{bmatrix} \tag{278}$$

$$[H]_k = \begin{bmatrix} 1 & -\left[\frac{1}{2} \pm (a'_{EA_k} + t_e\Delta a_{EA_k})\right] \\ 0 & 1 \end{bmatrix} \tag{279}$$

$$[B_c]_k = \begin{bmatrix} 1 & 0 \\ 0 & \left(\frac{b_k}{b_R}\right) \end{bmatrix} \tag{280}$$

$$[G_M]_k = \begin{bmatrix} f_{K1} & - - - - - - & f_{KND} \\ \pm F_{K1} & - - - - - & \pm F_{KND} \end{bmatrix} \tag{281}$$

Reverse flow:

If $$V_{xk} = \sin\psi\, v_H + \Omega\left(e + \bar{r}_K \cos\beta_s\right) < 0 \qquad (282)$$

Then use the negative signs in the expressions for $[H]_k$ and $[G_M]_k$.

Examples of the application of the reverse flow relations are given in Table 1.

The cases listed, except those at $M_N = 0.8$, show satisfactory agreement between the coefficients from different references, and the reverse-flow relations are satisfied. At $M_N = 0.8$, Reference 7 satisfied the reverse flow relation for calculating ζ_h but not the relation for calculating $\dot{\zeta}_h$. For this case, the greatest discrepancy was in the coefficient $(-m_{\dot{\alpha}})$, a few values of which are given in Table II.

A large proportion of the tabulated coefficients come from Reference 7, and it is unfortunate that these coefficients in many cases satisfy only partially the reverse-flow relations.

When first published (Reference 5), they were criticized for not satisfying these relations. Subsequently, an amended tabulation appeared (Reference 6), and it was claimed that this deficiency had been corrected.

About the same time, Reference 7 appeared; it gave a much more complete table of coefficients, but without claiming that they satisfied the reverse-flow relations. It was assumed that they did; indeed, comparison between the coefficients tabulated in Reference 7 and the revised coefficients in Reference 6 show them to agree exactly or with differences confined to the last decimal place. The matter was not pursued any further, though it would certainly be of interest to do so.

With the reverse-flow relations, it was possible to sort out the coefficients satisfactorily, and a table of coefficients was prepared. These coefficients are given in Table XII. It will be noticed that the coefficients for $M_N = 1.05$ exhibit small oscillations with respect to k.

AERODYNAMIC COEFFICIENTS

GENERAL DISCUSSION OF AERODYNAMIC COEFFICIENTS

The aerodynamic forces acting on a rotor blade appear in the equations of motion in the form of the matrices $[\dot{D}]$ and $[D]$ where

$$[\dot{D}]_k = \begin{bmatrix} \ell_{\dot{h}} & \ell_{\dot{\alpha}} \\ -m_{\dot{h}} & -m_{\dot{\alpha}} \end{bmatrix}_k \tag{283}$$

$$[D]_k = \begin{bmatrix} \ell_h & \ell_\alpha \\ -m_h & -m_\alpha \end{bmatrix}_k \tag{284}$$

That is, at each blade station, eight aerodynamic coefficients are required to specify the aerodynamic forces acting on the blade segment. Each of these coefficients is in general a function of the reduced frequency parameter $k = \omega b/Vy$ and the Mach number. Depending on the forward velocity and the advance ratio, the value of k and M_N at any station will be, in practice, within the range $0 \leq k \leq \infty$ and $0 \leq M_N \leq 1$.

For certain combinations of V_H and μ, k and M_N will have large variations across the blade, so that it is necessary to form a table of aerodynamic coefficients covering a wide range of k and M_N. The values of k and M_N for each segment are calculated, and by interpolation the corresponding value of each of the eight aerodynamic coefficients is obtained.

A search of the literature located tables of incompressible and compressible main surface aerodynamic coefficients in References 2, 3, 4, 5, 6, 7, 8, and 9. The subsonic compressible coefficients were obtained either by direct iteration of Possio's integral equation or by expanding the solution as an infinite series of orthogonal Mathieu functions. Either method of solution has the characteristic that the convergence becomes poorer as k and M_N increase. Because of this, the range of k for which tabulated derivatives are available decreases as M_N increases. This is normally not a restriction, since the range of k values across the blade also decreases as the blade tip Mach number increases. However, the particular method used to interpolate for the coefficients at a blade station requires that the coefficients be tabulated for the same values of k for all Mach numbers. Because of this, full use was made of the available tabulated coefficients for the higher Mach numbers but not for the low Mach numbers. This restriction is most severe for incompressible flow, where the aerodynamic coefficients are available over the interval $0 \leq k \leq \infty$. This semi-infinite interval can be tabulated by transforming it into finite interval $0 \leq \bar{k} \leq 1$ by a transformation such as $\bar{k} = k/k+p$ and by tabulating the coefficients for all Mach numbers versus $\bar{k}$ instead of k. However, for the present study, each of the eight coefficients is tabulated for M_N = 0, .35, .50, .60, .70, .80, .90, .95, 1.0, 1.05 at each of 27

different values of k between k = 0 and k = 0.7.

For reasons which will be discussed below, the last row of the tabulation was repeated twice, giving 29 k values. Thus, the tabulation consists of 2320 values of the coefficients. It was stated previously that the variation of the aerodynamic acceleration coefficients with change in k for compressible flow was one of the reasons for including the acceleration coefficients with the displacement coefficients. If they had been kept separate, it would have been necessary to store 3480 instead of 2320 values of the coefficients in the high-speed store of the computer when, even with 2320 values, space was at a premium.

The value of some of the coefficients approaches infinity as $k \to 0$ or ∞. These limiting cases will be considered for incompressible flow, but the same principles apply for all Mach numbers.

The case k = 0 is considered first. The lift due to pitch rate in this case is given by

$$L = 2\pi\rho_{SL}\, b^3 \Delta r \left(\frac{V}{B}\right) l_{\dot{\alpha}} \cdot \dot{\alpha} \tag{285}$$

where

$$l_{\dot{\alpha}} = \left[\frac{1}{2} + F(k) + \frac{G(k)}{k}\right] \tag{286}$$

For simple harmonic motion, this becomes

$$L = 2\pi\rho_{SL}\, b^3 \Delta r \left\{\left(\frac{V}{b}\right)\left[\frac{1}{2}+F(k)\right]\dot{\alpha} + \left(\frac{V}{b}\right)^2 \left[i\left(\frac{\omega}{\omega_0}\right)G(k)\right]\alpha\right\} \tag{287}$$

where

ω is the solution frequency

ω_0 is the solution frequency assumed when calculating $l_{\dot{\alpha}}$

The case of $k = \omega_0 b / V = 0$, that is, steady-flow aerodynamic is now considered. In practice, steady and oscillatory flows occur with $\omega/\omega_0 = 1$; and considering the fact that $0.5 \leq F(k) \leq 1$ and $-0.188 \leq G(k) \leq 0$ the above equations show that the theory predicts finite airloads for all values of k. It is the artifice of using $\omega/\omega_0 \neq 1$ in particular $\omega_0 = 0$, for the aerodynamic associated with vibration modes $\omega \neq 0$ that leads to apparently infinite airloads. If $\omega/\omega_0 = 1$ and since $F(k) = 1$, $G(k) = 0$, and $\dot{\alpha} = 0$ for $\omega = \omega_0 = 0$ the above equation gives $L = 0$ at $k = 0$, so that the contribution to the steady-state loading due to $l_{\dot{\alpha}}$ is zero. This same result can be ob-

tained with $\omega/\omega_\alpha \neq 1$ if $\left[l_{\dot{\alpha}}\right]_{k=0} = -\infty$ is replaced by $\left[l_{\dot{\alpha}}\right]_{k=0} = 0$. That is, it is quite valid to tabulate $l_{\dot{\alpha}} = 0$ at k = 0, and this was done in the table of aerodynamic coefficients.

The difficulty that occurs in the case $k = \infty$ has been discussed before and is due to lumping the acceleration coefficients with the displacement coefficients. If the components due to inertia were neglected then the displacement coefficients such as $-m_\alpha$ would remain finite as $k \to \infty$ because

$$-m_\alpha = -k^2\left(\frac{3}{16}\right) \tag{288}$$

is due solely to the inertia coefficient $m_{\ddot{\alpha}} = 3/16$. The effect of aerodynamic inertia is generally considered to be of secondary importance, and the contribution of the aerodynamic inertias will be progressively reduced to zero by making all coefficients constant above $M_N = 0.7$. This avoids the uncertainty of extrapolating curves from k = 0.7 to = 3, say, when the curve at k = 0.7 is almost vertical. To keep the coefficients constant, the tabulated values of the coefficients at k = 0.7 are repeated twice and labeled k = 0.8 and k = 0.9 respectively. This causes the linear extrapolation routine to calculate values for the coefficients which are the same as those at k = 0.7. The effect of progressively neglecting the aerodynamic inertias above k = 0.7 is further reduced by noting the following from the relation $V = \omega b / k$: as k increases, V decreases, so that the region $k > 0.7$ is fortunately associated with very low dynamic pressures, which cause the coefficients for $k > 0.7$ to make only a very small contribution to the equations of motion.

Two dimensional theory gives infinite airloads for steady flow at $M_N = 1$. This singularity disappears for oscillatory flow ($k \neq 0$) or with the inclusion of finite span effects. The choice has to be made between tabulating coefficients at $M_N = 1$, $k = 0$ for a particular aspect ratio or simply making all coefficients zero. For simplicity, the latter was decided upon so that the tabulated coefficients cannot be used for steady flow at $M_N = 1$.

NOTATION

It is necessary to transform the tabulated coefficients available in the previously stated references so that they conform to the notation for this study. These transformations are now reviewed.

Each reference, in general, uses different symbols when defining the coefficients, so for convenience the defining equations will be stated in terms of the notations already adopted for lift, pitching moment, semichord, etc.

The coefficients from Reference 2 will be converted first and are defined by

$$\frac{-1}{\rho\, 2\, b V^2 \Delta r}\begin{bmatrix} -L \\ \frac{M}{2b} \end{bmatrix}_{LE} = \begin{bmatrix} (l_z' + i\, l_z'') & (l_\alpha' + i\, l_\alpha'') \\ -(m_z' + i\, m_z'') & -(m_\alpha' + i\, m_\alpha'') \end{bmatrix}\begin{bmatrix} \frac{h}{2b} \\ \alpha \end{bmatrix}_{LE} \tag{289}$$

with the relations

$$2\rho b V^2 \Delta r = (2\pi\rho b^3 \Delta r)\left[\left(\frac{V}{b}\right)\frac{1}{\pi k}\right]\omega \tag{290}$$

$$2\rho b V^2 \Delta r = (2\pi\rho b^3 \Delta r)\left[\left(\frac{V}{b}\right)^2 \frac{1}{\pi}\right] \tag{291}$$

and for simple harmonic motion,

$$i\omega\left(\frac{h}{b}\right) = \frac{\dot{h}}{b} \tag{292}$$

$$i\omega\alpha = \dot{\alpha} \tag{293}$$

also

$$\begin{bmatrix} -L \\ \frac{M}{b} \end{bmatrix}_{C/4} = \begin{bmatrix} 1 & 0 \\ -\frac{1}{2} & 2 \end{bmatrix}\begin{bmatrix} -L \\ \frac{M}{2b} \end{bmatrix}_{LE} \tag{294}$$

$$\begin{bmatrix} \frac{h}{2b} \\ \alpha \end{bmatrix}_{LE} = \frac{1}{2}\begin{bmatrix} 1 & -\frac{1}{2} \\ 0 & 2 \end{bmatrix}\begin{bmatrix} \frac{h}{b} \\ \alpha \end{bmatrix}_{C/4} \tag{295}$$

Then the equations become

$$\frac{-1}{2\pi\rho\, b^3 \Delta r}\begin{bmatrix} -L \\ \frac{M}{b} \end{bmatrix}_{C/4} = \left(\frac{V}{b}\right)\frac{1}{2\pi k}\begin{bmatrix} 1 & 0 \\ -\frac{1}{2} & 2 \end{bmatrix}\begin{bmatrix} l_z'' & l_\alpha'' \\ -m_z'' & -m_\alpha'' \end{bmatrix}\begin{bmatrix} 1 & -\frac{1}{2} \\ 0 & 2 \end{bmatrix}\begin{bmatrix} \frac{\dot{h}}{b} \\ \dot{\alpha} \end{bmatrix}_{C/4}$$

$$+\left(\frac{V}{b}\right)^2 \cdot \frac{1}{2\pi}\begin{bmatrix} 1 & 0 \\ -\frac{1}{2} & 2 \end{bmatrix}\begin{bmatrix} l_z' & l_\alpha' \\ -m_z' & -m_\alpha' \end{bmatrix}\begin{bmatrix} 1 & -\frac{1}{2} \\ 0 & 2 \end{bmatrix}\begin{bmatrix} \frac{h}{b} \\ \alpha \end{bmatrix}_{C/4} \tag{296}$$

If this is compared with the defining equation,

$$\frac{-1}{2\pi\rho b^3\Delta r}\begin{bmatrix}-L\\ \frac{M}{b}\end{bmatrix}_{C/4} = \frac{V}{b}\begin{bmatrix}l_{\dot{h}} & l_{\dot{\alpha}}\\ -m_{\dot{h}} & -m_{\dot{\alpha}}\end{bmatrix}\begin{bmatrix}\frac{\dot{h}}{b}\\ \dot{\alpha}\end{bmatrix}_{C/4} + \left(\frac{V}{b}\right)^2\begin{bmatrix}l_h & l_\alpha\\ -m_h & -m_\alpha\end{bmatrix}\begin{bmatrix}\frac{h}{b}\\ \alpha\end{bmatrix}_{C/4} \tag{297}$$

the following relations between the coefficients are obtained:

The damping coefficients are:

$$\begin{bmatrix}l_{\dot{h}} & l_{\dot{\alpha}}\\ -m_{\dot{h}} & -m_{\dot{\alpha}}\end{bmatrix} = \frac{1}{2\pi k}\begin{bmatrix}1 & 0\\ -\frac{1}{2} & 2\end{bmatrix}\begin{bmatrix}l_z'' & l_\alpha''\\ -m_z'' & -m_\alpha''\end{bmatrix}\begin{bmatrix}1 & -\frac{1}{2}\\ 0 & 2\end{bmatrix} \tag{298}$$

$$l_{\dot{h}} = \frac{l_z''}{2\pi k} \tag{299}$$

$$l_{\dot{\alpha}} = \frac{1}{\pi k}\left(l_\alpha'' - \frac{l_z''}{4}\right) \tag{300}$$

$$-m_{\dot{h}} = \frac{1}{\pi k}\left[(-m_z)'' - \frac{l_z''}{4}\right] \tag{301}$$

$$-m_{\dot{\alpha}} = \frac{1}{\pi k}\left[2(-m_\alpha'') - \frac{1}{2}\left\{l_\alpha'' + (-m_z'')\right\} + \frac{l_z''}{8}\right] \tag{302}$$

The stiffness coefficients are

$$\begin{bmatrix}l_h & l_\alpha\\ -m_h & -m_\alpha\end{bmatrix} = \frac{1}{2\pi}\begin{bmatrix}1 & 0\\ -\frac{1}{2} & 2\end{bmatrix}\begin{bmatrix}l_z' & l_\alpha'\\ -m_z' & -m_\alpha'\end{bmatrix}\begin{bmatrix}1 & -\frac{1}{2}\\ 0 & 2\end{bmatrix} \tag{303}$$

$$l_h = \frac{l_z'}{2\pi} \tag{304}$$

$$l_\alpha = \frac{1}{\pi}\left(l_\alpha' - \frac{l_z'}{4}\right) \tag{305}$$

$$-m_h = \frac{1}{\pi}\left[\left(-m_z'\right) - \frac{\ell_z'}{4}\right] \tag{306}$$

$$-m_\alpha = \frac{1}{\pi}\left\{2\left(-m_2'\right) - \frac{1}{2}\left[\ell_\alpha' + \left(-m_z'\right) + \frac{\ell_z'}{8}\right]\right\} \tag{307}$$

The coefficients ℓ_z'', ℓ_α'', $-m_z''$, $-m_\alpha''$, ℓ_z', ℓ_α', $-m_z'$, and $-m_\alpha'$ are tabulated in Tables 2 through 2d, pages 34 through 41 of Reference 2.

The coefficients in Reference 3 are defined by

$$\frac{-1}{4\rho b V^2 k^2 \Delta r}\begin{bmatrix} -L \\ \frac{M}{b} \end{bmatrix}_{EA} = \begin{bmatrix} (L_1 + i L_2) & (L_3 + i L_4) \\ (M_1 + i M_2) & (M_3 + i M_4) \end{bmatrix}\begin{bmatrix} \frac{h}{b} \\ \alpha \end{bmatrix}_{EA} \tag{308}$$

and

$$\frac{-1}{4\rho b V^2 k^2 \Delta r}\begin{bmatrix} -L \\ \frac{M}{b} \end{bmatrix}_{LE} = \begin{bmatrix} (L_1' + i L_2') & (L_3' + i L_4') \\ (M_1' + i M_2') & (M_3' + i M_4') \end{bmatrix}\begin{bmatrix} \frac{h}{b} \\ \alpha \end{bmatrix}_{LE} \tag{309}$$

but only the primed derivatives are tabulated.

The following relations are used:

$$4\rho b V^2 k^2 \Delta r = \left(2\pi\rho b^3 \Delta r\right)\left[\left(\frac{V}{b}\right)^2 \cdot \frac{2}{\pi k} \cdot k^2\right]\omega \tag{310}$$

$$4\rho b V^2 k^2 \Delta r = \left(2\pi\rho b^3 \Delta r\right)\left[\left(\frac{V}{b}\right) \cdot \frac{2}{\pi} \cdot k^2\right] \tag{311}$$

For simple harmonic motion,

$$i\omega\left(\frac{h}{b}\right) = \frac{\dot{h}}{b} \tag{312}$$

$$i\omega\alpha = \dot{\alpha} \tag{313}$$

$$\begin{bmatrix} -L \\ \frac{M}{b} \end{bmatrix}_{c/4} = \begin{bmatrix} 1 & 0 \\ -\frac{1}{2} & 1 \end{bmatrix} \begin{bmatrix} -L \\ \frac{M}{b} \end{bmatrix}_{LE} \tag{314}$$

$$\begin{bmatrix} \frac{h}{b} \\ \alpha \end{bmatrix}_{LE} = \begin{bmatrix} 1 & -\frac{1}{2} \\ 0 & 1 \end{bmatrix} \begin{bmatrix} \frac{h}{b} \\ \alpha \end{bmatrix}_{c/4} \tag{315}$$

Then the following relations between the coefficients are obtained:

The damping coefficients are

$$\begin{bmatrix} \ell_{\dot{h}} & \ell_{\dot{\alpha}} \\ -m_{\dot{h}} & -m_{\dot{\alpha}} \end{bmatrix} = \frac{2}{\pi k} \begin{bmatrix} 1 & 0 \\ -\frac{1}{2} & 1 \end{bmatrix} \begin{bmatrix} k^2 L_2' & k^2 L_4' \\ k^2 M_2' & k^2 M_4' \end{bmatrix} \begin{bmatrix} 1 & -\frac{1}{2} \\ 0 & 1 \end{bmatrix} \tag{316}$$

$$\ell_{\dot{h}} = \frac{2}{\pi k} \left(k^2 L_2' \right) \tag{317}$$

$$\ell_{\dot{\alpha}} = \frac{2}{\pi k} \left(k^2 L_4' - \frac{1}{2} k^2 L_2' \right) \tag{318}$$

$$-m_{\dot{h}} = \frac{2}{\pi k} \left(k^2 M_2' - \frac{1}{2} k^2 L_2' \right) \tag{319}$$

$$-m_{\dot{\alpha}} = \frac{2}{\pi k} \left(k^2 M_4' - \frac{1}{2} \left[k^2 M_2' + k^2 L_4' \right] + \frac{1}{4} k^2 L_2' \right) \tag{320}$$

The stiffness coefficients are

$$\begin{bmatrix} \ell_h & \ell_\alpha \\ -m_h & -m_\alpha \end{bmatrix} = \frac{2}{\pi} \begin{bmatrix} 1 & 0 \\ -\frac{1}{2} & 1 \end{bmatrix} \begin{bmatrix} k^2 L_1' & k^2 L_3' \\ k^2 M_1' & k^2 M_3' \end{bmatrix} \begin{bmatrix} 1 & -\frac{1}{2} \\ 0 & 1 \end{bmatrix} \tag{321}$$

$$\ell_h = \frac{2}{\pi}\left(k^2 L_1'\right) \tag{322}$$

$$\ell_\alpha = \frac{2}{\pi}\left(k^2 L_3' - \frac{1}{2} k^2 L_1'\right) \tag{323}$$

$$-m_h = \frac{2}{\pi}\left(k^2 M_1' - \frac{1}{2} k^2 L_1'\right) \tag{324}$$

$$-m_\alpha = \frac{2}{\pi}\left(k^2 M_3' - \frac{1}{2}\left[k^2 M_1' + k^2 L_3'\right] + \frac{1}{4} k^2 L_1'\right) \tag{325}$$

The coefficients $k^2 L_2'$, $k^2 L_4'$, $k^2 M_2'$, $k^2 M_4'$, $k^2 L_1'$, $k^2 L_3'$, $k^2 M_1'$ and $k^2 M_3'$ are tabulated in Table I, page 9 of Reference 3.

The coefficients in References 4 and 9 are defined by

$$\frac{1}{\pi\rho b^3 \omega^2 \Delta r}\begin{bmatrix} -L \\ \frac{M}{b} \end{bmatrix}_{c/4} = \begin{bmatrix} \left(L_{hR} + i L_{hI}\right) & \left(L_{\alpha R} + i L_{\alpha I}\right) \\ \left(M_{hR} + i M_{hI}\right) & \left(M_{\alpha R} + i M_{\alpha I}\right) \end{bmatrix}\begin{bmatrix} \frac{h}{b} \\ \alpha \end{bmatrix}_{c/4} \tag{326}$$

The following relations are used:

$$\pi\rho b^3 \omega^2 \Delta r = -\left(2\pi\rho b^3 \Delta r\right)\left[-\left(\frac{V}{b}\right)\cdot\frac{k}{2}\right]\omega \tag{327}$$

$$\pi\rho b^3 \omega^2 \Delta r = -\left(2\pi\rho b^3 \Delta r\right)\left[-\left(\frac{V}{b}\right)^2\cdot\frac{k^2}{2}\right] \tag{328}$$

For simple harmonic motion,

$$i\omega\left(\frac{h}{b}\right) = \frac{\dot{h}}{b} \tag{329}$$

$$i\omega\alpha = \dot{\alpha} \tag{330}$$

Then, the following relations between the coefficients are obtained:
The damping coefficients are

$$\begin{bmatrix} \ell_{\dot{h}} & \ell_{\dot{\alpha}} \\ -m_{\dot{h}} & -m_{\dot{\alpha}} \end{bmatrix} = -\left(\frac{k}{2}\right)\begin{bmatrix} L_{hI} & L_{\alpha I} \\ M_{hI} & M_{\alpha I} \end{bmatrix} \tag{331}$$

$$\ell_{\dot{h}} = -\left(\frac{k}{2}\right) L_{hI} \tag{332}$$

$$\ell_{\dot{\alpha}} = -\left(\frac{k}{2}\right) L_{\alpha I} \tag{333}$$

$$-m_{\dot{h}} = -\left(\frac{k}{2}\right) M_{hI} \tag{334}$$

$$-m_{\dot{\alpha}} = -\left(\frac{k}{2}\right) M_{\alpha I} \tag{335}$$

The stiffness coefficients are:

$$\begin{bmatrix} \ell_h & \ell_\alpha \\ -m_h & -m_\alpha \end{bmatrix} = -\left(\frac{k^2}{2}\right) \begin{bmatrix} L_{hR} & L_{\alpha R} \\ M_{hR} & M_{\alpha R} \end{bmatrix} \tag{336}$$

$$\ell_h = -\left(\frac{k^2}{2}\right) L_{hR} \tag{337}$$

$$\ell_\alpha = -\left(\frac{k^2}{2}\right) L_{\alpha R} \tag{338}$$

$$-m_h = -\left(\frac{k^2}{2}\right) M_{hR} \tag{339}$$

$$-m_\alpha = -\left(\frac{k^2}{2}\right) M_{\alpha R} \tag{340}$$

The coefficients L_{hI}, $L_{\alpha I}$, M_{hI}, $M_{\alpha I}$, L_{hR}, $L_{\alpha R}$, M_{hR} and $M_{\alpha R}$ are tabulated in Reference 4 and pages 409 through 413 of Reference 9.

The coefficients in References 5, 6, and 7 are defined by

$$\frac{1}{\pi \rho b V^2 \Delta r} \begin{bmatrix} -L \\ \frac{M}{b} \end{bmatrix}_{c/2} = \begin{bmatrix} (k_a' + ik_a'') & (k_b' + ik_b'') \\ (m_a' + im_a'') & (m_b' + im_b'') \end{bmatrix} \begin{bmatrix} \frac{h}{b} \\ \alpha \end{bmatrix}_{c/2} \tag{341}$$

The following relations are used:

$$\pi\rho b V^2 \Delta r = -\left(2\pi\rho b^3 \Delta r\right)\left[-\left(\frac{V}{b}\right)\frac{1}{2k}\right]\omega \tag{342}$$

$$\pi\rho b V^2 \Delta r = -\left(2\pi\rho b^3 \Delta r\right)\left[-\left(\frac{V}{b}\right)^2 \frac{1}{2}\right] \tag{343}$$

$$\begin{bmatrix} -L \\ \frac{M}{b} \end{bmatrix}_{c/4} = \begin{bmatrix} 1 & 0 \\ \frac{1}{2} & 1 \end{bmatrix} \begin{bmatrix} -L \\ \frac{M}{b} \end{bmatrix}_{c/2} \tag{344}$$

$$\begin{bmatrix} \frac{h}{b} \\ \alpha \end{bmatrix}_{c/2} = \begin{bmatrix} 1 & \frac{1}{2} \\ 0 & 1 \end{bmatrix} \begin{bmatrix} \frac{h}{b} \\ \alpha \end{bmatrix}_{c/4} \tag{345}$$

Then the following relations between the coefficients are obtained:

The damping coefficients are

$$\begin{bmatrix} \ell_{\dot{h}} & \ell_{\dot{\alpha}} \\ -m_{\dot{h}} & -m_{\dot{\alpha}} \end{bmatrix} = -\left(\frac{1}{2k}\right) \begin{bmatrix} 1 & 0 \\ \frac{1}{2} & 1 \end{bmatrix} \begin{bmatrix} k_a'' & k_b'' \\ m_a'' & m_b'' \end{bmatrix} \begin{bmatrix} 1 & \frac{1}{2} \\ 0 & 1 \end{bmatrix} \tag{346}$$

$$\ell_{\dot{h}} = -\left(\frac{1}{2k}\right) k_a'' \tag{347}$$

$$\ell_{\dot{\alpha}} = -\left(\frac{1}{2k}\right)\left(k_b'' + \frac{1}{2}k_a''\right) \tag{348}$$

$$-m_{\dot{h}} = -\left(\frac{1}{2k}\right)\left(m_a'' + \frac{1}{2}k_a''\right) \tag{349}$$

$$-m_{\dot{\alpha}} = -\left(\frac{1}{2k}\right)\left(m_b'' + \frac{1}{2}\left[m_a'' + k_b''\right] + \left(\frac{1}{2}\right)^2 k_a''\right) \tag{350}$$

The stiffness ocefficients are

$$\begin{bmatrix} \ell_h & \ell_\alpha \\ -m_h & -m_\alpha \end{bmatrix} = -\left(\frac{1}{2}\right)\begin{bmatrix} 1 & 0 \\ \frac{1}{2} & 1 \end{bmatrix}\begin{bmatrix} k_a' & k_b' \\ m_a' & m_b' \end{bmatrix}\begin{bmatrix} 1 & \frac{1}{2} \\ 0 & 1 \end{bmatrix} \tag{351}$$

$$\ell_h = -\left(\frac{1}{2}\right) k_a' \tag{352}$$

$$\ell_\alpha = -\left(\frac{1}{2}\right)\left(k_b' + \frac{1}{2}k_a'\right) \tag{353}$$

$$-m_h = -\left(\frac{1}{2}\right)\left(m_a' + \frac{1}{2}k_a'\right) \tag{354}$$

$$-m_\alpha = -\left(\frac{1}{2}\right)\left(m_b' + \frac{1}{2}\left[m_a' + k_b'\right] + \left(\frac{1}{2}\right)^2 k_a'\right) \tag{355}$$

The coefficients in Reference 8 are defined by

$$\frac{-1}{4\rho b V^2 k^2 \Delta r}\begin{bmatrix} -L \\ \frac{M}{b} \end{bmatrix}_{LE} = \begin{bmatrix} (L_1 + iL_2) & (L_3' + iL_4') \\ (M_1' + iM_2') & (M_3' + iM_4') \end{bmatrix}\begin{bmatrix} \frac{h}{b} \\ \alpha \end{bmatrix}_{LE} \tag{356}$$

Note the similarity to the definition used in Reference 3. By use of the same procedure as that for Reference 3, the following relations between the coefficients can be obtained:

The damping coefficients are

$$\begin{bmatrix} \ell_{\dot h} & \ell_{\dot\alpha} \\ -m_{\dot h} & -m_{\dot\alpha} \end{bmatrix} = \left(\frac{2k}{\pi}\right)\begin{bmatrix} 1 & 0 \\ -\frac{1}{2} & 1 \end{bmatrix}\begin{bmatrix} L_2 & L_4' \\ M_2' & M_4' \end{bmatrix}\begin{bmatrix} 1 & -\frac{1}{2} \\ 0 & 1 \end{bmatrix} \tag{357}$$

$$\ell_{\dot h} = \frac{2k}{\pi}\left(L_2\right) \tag{358}$$

$$\ell_{\dot\alpha} = \frac{2k}{\pi}\left(L_4' - \frac{1}{2}L_2\right) \tag{359}$$

$$-m_{\dot{h}} = \frac{2k}{\pi}\left(M_2' - \frac{1}{2}L_2\right) \tag{360}$$

$$-m_{\dot{\alpha}} = \frac{2k}{\pi}\left(M_4' - \frac{1}{2}\left[M_2' + L_4'\right] + \frac{1}{4}L_2\right) \tag{361}$$

The stiffness coefficients are

$$\begin{bmatrix} \ell_h & \ell_\alpha \\ -m_h & -m_\alpha \end{bmatrix} = \left(\frac{2k^2}{\pi}\right)\begin{bmatrix} 1 & 0 \\ -\frac{1}{2} & 1 \end{bmatrix}\begin{bmatrix} L_1 & L_3' \\ M_1' & M_3' \end{bmatrix}\begin{bmatrix} 1 & -\frac{1}{2} \\ 0 & 1 \end{bmatrix} \tag{362}$$

$$\ell_h = \frac{2k^2}{\pi}(L_1) \tag{363}$$

$$\ell_\alpha = \frac{2k^2}{\pi}\left(L_3' - \frac{1}{2}L_1\right) \tag{364}$$

$$-m_h = \frac{2k^2}{\pi}\left(M_1' - \frac{1}{2}L_1\right) \tag{365}$$

$$-m_\alpha = \frac{2k^2}{\pi}\left(M_3' - \frac{1}{2}\left[M_1' + L_3'\right] + \frac{1}{4}L_1\right) \tag{366}$$

Not only are the available tabulated coefficients in differing notations, but they also cover varying ranges of k and M_N. A computer program was written to transform the coefficients into the required notation and to assemble the coefficients in order of k and M_N. There is a degree of overlapping in the resulting tabulation because, for particular combinations of k and M, coefficients are available from more than one source. This overlapping permits a check to be made of the accuracy of the coefficients.

From an inspection of the table, it would be seen that although good agreement was obtained in the majority of cases, a significant minority of cases remained in which discrepancies of various magnitudes existed between the coefficients. In particular, for $M_N = 0.8$, the discrepancies were large and it was not obvious as to which were the correct coefficients. In an attempt to sort out the accurate from the inaccurate coefficients, it was decided to apply reciprocal flow relations to all of the available coefficients.

RECIPROCAL FLOW RELATIONS FOR UNSTEADY, COMPRESSIBLE FLOW

For an airfoil executing small oscillation in a nonstationary compressible inviscid flow, the relationship between the pressure acting on the airfoil in direct flow and the pressure acting on the airfoil when it travels in the reverse direction is given by Reference 10. From Figure 14,

$$\iint_{\text{PLANFORM}} P\,\bar{w}\,ds = \iint_{\text{PLANFORM}} \bar{P}\,w\,ds \tag{367}$$

where

P	is the pressure difference across the airfoil in direct flow
$\bar{P}$	is the pressure difference across the airfoil in reverse flow
w	is the vertical velocity in direct flow of the air in contact with the airfoil
$\bar{w}$	is the vertical velocity in reverse flow of the air in contact with the airfoil

and where Eqs. (368), (370), (372), and (374) define direct-flow quantities and Eqs. (369), (371), (373), and (375) are reverse flow quantities.

$$w = \left(V\frac{\partial}{\partial x} + \frac{\partial}{\partial t}\right) z_s \tag{368}$$

$$\bar{w} = \left(-V\frac{\partial}{\partial x} + \frac{\partial}{\partial t}\right) \bar{z}_s \tag{369}$$

and for simple harmonic motion

$$z_s = z_{sa} e^{i\omega t} \tag{370}$$

$$\bar{z}_s = \bar{z}_{sa} e^{i\omega t} \tag{371}$$

$$w = w_a\, e^{i\omega t} \tag{372}$$

$$\bar{w} = \bar{w}_a\, e^{i\omega t} \tag{373}$$

Hence,

$$w_a = \left(V\frac{\partial}{\partial x} + i\omega\right) z_{sa} \tag{374}$$

$$\bar{w}_a = \left(-V\frac{\partial}{\partial x} + i\omega\right) \bar{z}_{sa} \tag{375}$$

in which case the reciprocal or reverse flow relation becomes

$$\iint_{\text{PLANFORM}} P\,\bar{w}_a\,ds = \iint_{\text{PLANFORM}} \bar{P}\,w_a\,ds \tag{376}$$

The application of this relation to a two-dimensional airfoil is now considered.

Most unsteady aerodynamic theories, in particular those on which the tabulated coefficients are based, neglect airfoil thickness effects and so replace the airfoil by a flat plate of zero thickness. This, of course, gives rise to singularities at the leading and trailing edges, the singularity at the trailing edge being removed in the usual manner by the application of the Kutta condition. With this model, a two-dimensional airfoil presents the same shape to the airstream irrespective of whether it is in direct or reverse flow. Hence, if the airfoil executes the same motion in both direct and reverse flow, the pressure distribution over the airfoil is the same for both flows; that is, $P = \bar{P}$, and the airfoil will experience the same lift and moment.

With Reference to Figure 15, the following Eqs. (377) through (381) are obtained for direct flow.

$$z_s = -(h_{c/4} + x\alpha)e^{i\omega t} \tag{377}$$

Hence

$$z_{s\alpha} = -(h_{c/4} + x\alpha) \tag{378}$$

So that

$$w_a = \left(V\frac{\partial}{\partial x} + i\omega\right) z_{s\alpha} \tag{379}$$

$$w_a = -\left[V\alpha + i\omega(h_{c/4} + x\alpha)\right] \tag{380}$$

since $\frac{\partial h}{\partial x}$ and $\frac{\partial \alpha}{\partial x}$ vanish,

$$w_a = -V\left[\left(\frac{i\omega}{V}\right)h_{c/4} + \left(1 + \frac{i\omega x}{V}\right)\alpha\right] \tag{381}$$

With reference to Figure 15, the following equations (382) through (386) are obtained for reverse flow.

$$\bar{z}_s = -(h_{c/4} - x\alpha)e^{i\omega t} \tag{382}$$

Hence

$$\bar{z}_{s\alpha} = -(h_{c/4} - x\alpha) \tag{383}$$

so that

$$\bar{w}_\alpha = \left(-V\frac{\partial}{\partial x} + i\omega\right)\bar{z}_{s\alpha} \tag{384}$$

$$\bar{w}_\alpha = -\left[V\alpha + i\omega\,(h_{c/4} - x\alpha)\right] \tag{385}$$

$$\bar{w}_\alpha = -V\left[\left(\frac{i\omega}{V}\right)h_{c/4} + \left(1 - \frac{i\omega x}{V}\right)\alpha\right] \tag{386}$$

Eqs. (387) and (388) consider pure translational motion in direct and reverse flow:

$$w_\alpha = -V\left(\frac{i\omega}{V}\right)h_{c/4} \tag{387}$$

$$\bar{w}_\alpha = -V\left(\frac{i\omega}{V}\right)h_{c/4} \tag{388}$$

when the reverse flow theorem for two dimensional flow is applied,

$$\int_{\text{CHORD}} P\bar{w}_\alpha\,dx = \int_{\text{CHORD}} \bar{P}\,w_\alpha\,dx \tag{389}$$

Hence,

$$\int_{CHORD} P\left[-V\left(\frac{i\omega}{V}\right)h_{c/4}\right]dx = \int_{CHORD} \bar{P}\left[-V\left(\frac{i\omega}{V}\right)h_{c/4}\right]dx \tag{390}$$

defining

$$L^{h} = \int_{CHORD} P\,dx \qquad \bar{L}^{h} = \int_{CHORD} \bar{P}\,dx \tag{391}$$

then the equation gives

$$L^{h} = \bar{L}^{h} \tag{392}$$

This states that the lift due to pure translational motion is the same in direct and reverse flow, a result deduced previously from physical considerations.

Pure translational motion in direct flow, and pitching about the 75% chord point in reverse flow are expressed as follows:

$$w_{\alpha} = -V\left(\frac{i\omega}{V}\right)h_{c/4} \tag{393}$$

$$\bar{w}_{\alpha} = -V\left(1 - \frac{i\omega}{V}x\right)\alpha \tag{394}$$

If w_{α} and $\bar{w}_{\alpha}$ are substituted into the reverse flow theorem

$$\int_{CHORD} P\left\{-V\left(1 - \frac{i\omega}{V}x\right)\alpha\right\}dx = \int_{CHORD} \bar{P}\left\{-V\left(\frac{i\omega}{V}\right)h_{c/4}\right\}dx \tag{395}$$

defining

$$L^{h}_{c/4} = \int_{CHORD} P\,dx \tag{396}$$

$$\bar{L}^{-\alpha(3/4)}_{3c/4} = \int_{CHORD} \bar{P}\,dx \tag{397}$$

$$-M^{h}_{C/4} = \int_{CHORD} Px\,dx \tag{398}$$

Then the equation gives

$$\left[L^{h}_{C/4} + ik\frac{M^{h}_{C/4}}{b} \right]\alpha = ik\, L^{-\alpha(3/4)}_{3C/4}\left(\frac{h_{C/4}}{b}\right) \tag{399}$$

where

$L^{h}_{C/4}$ is the lift at 25% chord due to pure translational motion in direct flow

$M^{h}_{C/4}$ is the moment at 25% chord due to pure translational motion in direct flow

$L^{-\alpha(3/4)}_{3C/4}$ is the lift at 75% chord due to pitching motion about 75% chord in reverse flow

As shown previously for a two-dimensional wing,

$$L^{-\alpha(3/4)}_{3C/4} = L^{\alpha(3/4)}_{3C/4} \tag{400}$$

Hence, the reverse-flow relation becomes:

$$\left[L^{h}_{C/4} + ik\frac{M^{h}_{C/4}}{b} \right]\alpha = ik\, L^{\alpha(3/4)}_{3C/4}\left(\frac{h_{C/4}}{b}\right) \tag{401}$$

Expressions can now be obtained for $L^{h}_{C/4}$, $M^{h}_{C/4}$ and $L^{\alpha(3/4)}_{3C/4}$ in terms of the aerodynamic coefficients which were defined by the equation.

$$\frac{-1}{2\pi\rho b^3 \Delta r}\begin{bmatrix} -L \\ \frac{M}{b} \end{bmatrix}_{C/4} = \left(\frac{V}{b}\right)\begin{bmatrix} l_{\dot{h}} & l_{\dot{\alpha}} \\ -m_{\dot{h}} & -m_{\dot{\alpha}} \end{bmatrix}\begin{bmatrix} \left(\frac{\dot{h}}{b}\right) \\ \dot{\alpha} \end{bmatrix}_{C/4} + \left(\frac{V}{b}\right)^2\begin{bmatrix} l_h & l_\alpha \\ -m_h & -m_\alpha \end{bmatrix}\begin{bmatrix} \left(\frac{h}{b}\right) \\ \alpha \end{bmatrix}_{C/4} \tag{402}$$

If the relations for simple harmonic motion are applied, the equation can be put in the form

$$\frac{-1}{2\pi\rho V^2 b \Delta r}\begin{bmatrix} -L \\ \frac{M}{b} \end{bmatrix}_{C/4} = \begin{bmatrix} ik l_{\dot{h}} + l_h & ik l_{\dot{\alpha}} + l_\alpha \\ ik(-m_{\dot{h}}) - m_h & ik(-m_{\dot{\alpha}}) - m_\alpha \end{bmatrix}\begin{bmatrix} \frac{h}{b} \\ \alpha \end{bmatrix}_{C/4} \tag{403}$$

The equation can now be transformed so that it is in terms of forces and displacements at the 75% chord point.

$$\frac{-1}{2\pi\rho V^2 b\Delta r}\begin{bmatrix} L \\ \frac{M}{b}\end{bmatrix}_{3C/4} = \begin{bmatrix} 1 & 0 \\ -1 & 1\end{bmatrix}\begin{bmatrix} ik\ell_{\dot{h}}+\ell_h & ik\ell_{\dot{\alpha}}+\ell_\alpha \\ ik(-m_{\dot{h}})-m_h & ik(-m_{\dot{\alpha}})-m_\alpha\end{bmatrix}\begin{bmatrix} 1 & -1 \\ 0 & 1\end{bmatrix}\begin{bmatrix} \frac{h}{b} \\ \alpha\end{bmatrix}_{3C/4} \tag{404}$$

From these two equations, it can be shown that

$$L^h_{C/4} = 2\pi\rho V^2 b\Delta r\left[ik\ell_{\dot{h}} + \ell_h\right]\left(\frac{h_{C/4}}{b}\right) \tag{405}$$

$$\frac{M^h_{C/4}}{b} = -2\pi\rho V^2 b\Delta r\left[ik(-m_{\dot{h}}) - m_h\right]\left(\frac{h_{C/4}}{b}\right) \tag{406}$$

$$L^{\alpha(3/4)}_{3C/4} = 2\pi\rho V^2 b\Delta r\begin{bmatrix} 1 & 0\end{bmatrix}\begin{bmatrix} ik\ell_{\dot{h}}+\ell_h & ik\ell_{\dot{\alpha}}+\ell_\alpha \\ ik(-m_{\dot{h}})-m_h & ik(-m_{\dot{\alpha}})-m_\alpha\end{bmatrix}\begin{bmatrix} -1 \\ 1\end{bmatrix}\alpha \tag{407}$$

$$L^{\alpha(3/4)}_{3C/4} = 2\pi\rho V^2 b\Delta r\left[ik(\ell_{\dot{\alpha}}-\ell_{\dot{h}}) + (\ell_\alpha-\ell_h)\right]\alpha \tag{408}$$

Substituting into the reverse-flow relation and dividing through by $2\pi\rho V^2 b\Delta r$ gives

$$\left\{(ik\ell_{\dot{h}} + \ell_h) - ik\left[ik(-m_{\dot{h}}) - m_h\right]\right\}\left(\frac{h_{C/4}}{b}\right)\alpha$$
$$= ik\left[ik(\ell_{\dot{\alpha}}-\ell_{\dot{h}}) + (\ell_\alpha-\ell_h)\right]\left(\frac{h_{C/4}}{b}\right)\alpha \tag{409}$$

Separating the equation into real and imaginary parts gives

$$\left\{\ell_h + k^2\left[-\ell_{\dot{h}} + \ell_{\dot{\alpha}} - m_{\dot{h}}\right]\right\}$$
$$+ ik\left\{\ell_{\dot{h}} - \left[-\ell_h + \ell_\alpha - m_h\right]\right\} = 0 \tag{410}$$

Equating the real and imaginary parts to zero gives the reverse-flow relation in terms of the aerodynamic coefficients.

$$\ell_{\dot{h}} = -\ell_h + \ell_\alpha - m_h \tag{411}$$

$$\ell_h = -k^2\left[-\ell_{\dot{h}} + \ell_{\dot{\alpha}} - m_{\dot{h}}\right] \tag{412}$$

It will be noticed that the coefficients $(-m_{\dot{\alpha}})$ and $(-m_{\alpha})$ are missing from the above equations, so that the reverse flow relation provides no check on the tabulated values of these coefficients. Although the reverse flow relation obtained above corresponds to that given in References 11 and 10, it was hoped that by considering additional motions in direct and reverse flow, additional reverse flow relations containing the missing coefficients would be obtained. To this end the following motions were considered, and the corresponding reverse-flow relations were found to be as follows:

Pitching about the 25% chord point in direct flow; pure translational motion in reverse flow.

$$ik\, L_{c/4}^{\alpha(1/4)} \left(\frac{h_{c/4}}{b}\right) = \left[L_{3c/4}^{h} + ik\,\frac{M_{3c/4}^{h}}{b}\right] \alpha \tag{413}$$

Pitching about the 25% chord point in direct flow; pitching about the 75% chord point in reverse flow.

$$\left[L_{c/4}^{\alpha(1/4)} + ik\,\frac{M_{c/4}^{\alpha(1/4)}}{b}\right]\alpha = \left[L_{3c/4}^{\alpha(3/4)} + ik\,\frac{M_{3c/4}^{\alpha(3/4)}}{b}\right]\alpha \tag{414}$$

However, these additional relations gave the same relations between the coefficients as obtained before. The search was not continued beyond this stage but it would be very useful to obtain a reverse-flow relation involving $(-m_{\dot{\alpha}})$ and $(-m_{\alpha})$.

It is possible to state the reverse-flow relations in the notations of the references from which the tabulated coefficients were obtained. For reference, they are listed below:

Reference 2

$$l_z' = -2k\left[-l_z'' + l_\alpha'' - m_z''\right] \tag{415}$$

$$l_z'' = 2\left[-l_z' + l_\alpha' - m_z'\right] \tag{416}$$

Reference 3

$$k^2 L_1' = -k \left[-2k^2 L_2' + k^2 L_4' + k^2 M_2' \right] \tag{417}$$

$$k^2 L_2' = k \left[-2k^2 L_1' + k^2 L_3' + k^2 M_1' \right] \tag{418}$$

Reference 4

Reference 9

$$L_{hR} = -k \left[-L_{hI} + L_{\alpha I} + M_{hI} \right] \tag{419}$$

$$L_{hI} = k \left[-L_{hR} + L_{\alpha R} + M_{hR} \right] \tag{420}$$

Reference 5, 6

Reference 7

$$k_a' = -k \left(k_b'' + m_a'' \right) \tag{421}$$

$$k_a'' = k \left(k_b' + m_a' \right) \tag{422}$$

Reference 8

$$L_1 = -k \left[-2L_2 + L_4' + M_2' \right] \tag{423}$$

$$L_2 = k \left[-2L_1 + L_3' + M_1' \right] \tag{424}$$

GENERAL PROCEDURES FOR OBTAINING FLUTTER SOLUTIONS

The following is a brief summary of the steps involved in obtaining flutter solutions, and it includes an outline of the computer program.

The geometry of the blade is stated, including the spanwise breakdown of the blade into segments, as required for the numerical integration. Then the mass properties of the fixed portion of the blade and of the mass balance weight, if any, are input. The remaining structural data to be stated include such things as the position of the mid-chord of the blade aft of a radial reference axis and the chordwise position of the blade elastic axis and center of gravity in relation to the mid-chord.

Up to 10 generalized coordinates may be chosen to describe the vibration characteristics of the blade. The modes used as generalized coordinates are assumed to have fully coupled flatwise, edgewise, and torsional displacements. These modes can be elastic or rigid-body modes. If modes are chosen which have one or two of these freedoms missing, the flatwise, edgewise, and torsional displacements must still be specified for each mode, with zero displacements being input for the missing freedoms. The natural frequency, structural damping and generalized modal inertia must also be stated for each mode.

All coefficients in the equations of motion are calculated by the program. The structural and aerodynamic forces on each blade segment are calculated and then summed across the blade span to find the generalized force acting in each of the generalized coordinates. The structural coefficients are stored after being calculated and are recalculated only if the mass data or mode shapes are altered. However, the aerodynamic coefficients are recalculated for each eigenvalue solution. To calculate the aerodynamic coefficients, the reduced frequency $k = \omega b/V$ (which is based on an assumed flutter frequency ω) and the Mach number at each station are found. Then, from the table of aerodynamic coefficients contained in the program, the values for the coefficients at each blade station are found by interpolation.

The major variable in the program is helicopter forward speed. Up to 10 velocities may be input at a time. The secondary variables are:

1. Modal frequency.
2. Amount of mass balance.
3. Position of the mass balance weight.
4. Aerodynamic center.
5. Elastic axis position.
6. Assumed flutter frequency.

7. The set of generalized coordinates used for the solution.

Item (7) needs some explanation, since generalized coordinates are not variables in the same sense as mass balance. Suppose a set $Q = (q_1 \quad q_n)$ of generalized coordinates is input, where $n \leq 10$. Then, any subset of Q may be chosen for solution, the generalized coordinates selected being stated as part of the input data. This facility is used when it is desired to find out the contribution that certain generalized coordinates are making to the flutter mechanism. In particular, if uncertainty exists as to how many vibration modes to input to the program, then extra modes may be included. After initial solutions are made to determine the contribution to the flutter mechanism of these extra modes, they may be dropped from all subsequent calculations if their contribution is found to be small.

In addition to the above variables, all or any part of the input data may be changed. However, the process is not as straightforward as changing the secondary variables.

After each eigenvalue solution corresponding to a particular value of forward speed, the results are printed out for each eigenvector in the following form:

Frequency in cycles per minute.

Decay rate C/C_c .

Strength vectors.

If the decay rate C/C_c is positive, then the mode is stable; if negative, then the mode is unstable and is undergoing divergent oscillations. If, as airspeed increases, the frequency of a mode drops to zero, this means that there is a divergent aerodynamic force acting against the elastic and centrifugal restoring forces so that the net restoring force is reduced to zero. For higher airspeeds, the modal frequency will remain at zero but the divergent aerodynamic forces are now predominant and the mode suffers static divergence. The strength vectors, or eigenvectors, give the relative proportion of the generalized coordinates in each coupled mode corresponding to a particular eigenvalue, and also the phase angle between the generalized coordinates. The eigenvectors quite often assist in the interpretation of flutter solutions.

After the eigenvalue solutions have been obtained for the specified set of forward speeds, a digital plot is made of the results. Three plots are made in the following order:

1. Frequency ω versus decay rate C/C_c , as shown in Figure 16.

2. Decay rate C/C_c versus forward velocity V_H as shown in Figure 17.

3. Frequency ω versus forward velocity V_H as shown in Figure 17.

The first plot is used to identify the eigenvalues. The eigenvalues corresponding to the first forward velocity are plotted as 1, those corresponding to the second forward velocity as 2, and so on up to the tenth forward velocity (if input), the corresponding eigenvalues being printed as Q . The first plot is thus a root locus plot with forward velocity as the running parameter. The eigenvalues are identified by their values at the lowest forward velocity, and then the variation of the eigenvalues with increasing forward velocity can be traced. Usually the numbers corresponding to a particular mode will be grouped together as shown and can be identified by inspection. If ambiguity exists, it can often be resolved by noting the variation of the eigenvectors with increasing forward velocity; if this fails, the ambiguity can always be resolved by obtaining further eigenvalue solutions, with sufficiently small increments in the forward velocity. However, a reasonable estimate of the flutter speed can often be obtained in spite of any ambiguity, in which case the ambiguity need not be resolved.

In the second and third digital plots, the eigenvalues are plotted as an asterisk. When the eigenvalues have been identified by using the first plot, the corresponding points in the remaining two plots may be identified. This enables curves to be drawn, which give the variation of decay rate and frequency with changing forward velocity for each mode. Flutter occurs if a curve falls below the axis $C/C_c = 0$. Static divergence occurs if a curve meets the axis $\omega = 0$ and $C/C_c \leq 0$.

Sometimes, two or more eigenvalues have the same value within the accuracy of resolution of the digital plot. In this case, they are plotted as 0.

DOCUMENTATION OF COMPUTER PROGRAM

Items completing the following documentation of the classical flutter computer program are available at the U. S. Army Aviation Materiel Laboratories, Fort Eustis, Virginia.

1. Short description of problem.
2. Description of solution method.
3. Equations used in computer solution are given by reference to this report.
4. Definitions of input symbols in program.
5. Definitions of generated symbols in program.
6. Definitions of output symbols in program.
7. Listing of program source deck, sample input, and sample output.
8. Running instructions for program and estimate of running time.
9. Statement of type and configuration of computer used in the program development, including any special features.
10. Name and level of programming language used in the program.

Copies of the program source deck and a sample input deck are also available at USAAVLABS.

The following basic information is supplied here to permit potential users to evaluate the usefulness of the program for their purposes.

The program determines rotor blade flutter speeds, frequencies, and mode shapes, using classical flutter theory in conjunction with the fixed azimuth assumption.

The generalized structural inertia, gyroscopic coupling, and centrifugal stiffness coefficients are obtained for use in the Lagrange equations of motion, with arbitrary modes being used as degrees of freedom. The generalized aerodynamic coefficients are obtained by using standard classical flutter theory. The resulting equations of motion form an eigenvalue problem, which is solved by Tarnove's method. The eigenvalues are complex, in general, and define flutter frequency and modal damping. The condition that modal damping is zero defines the flutter speeds, and the eigenvectors define the flutter mode shapes.

The program is designated E480 and is intended for use on the UNIVAC 1108. The source program is written in the FORTRAN IV language. It is divided into two parts, E480A and E480B, which can be executed independently. E480A solves the actual flutter equations, while E480B provides punched card aerodynamic coefficient data for E480A. Each separate case of E480B requires 20 seconds of machine time, and E480A requires about .1 second for each eigenvalue solution with a three-degree-of-freedom case.

COMPUTER SOLUTION TEST CASE

A test case was prepared to check the computer solution. It is taken from Reference 12, and involves the pitch-plunge flutter of a two-dimensional airfoil. The equations of motion can be put into the form

$$\begin{bmatrix} \dfrac{m(g_1^2)^2}{2\pi\rho_{SL} b_R^4 \ell} & \dfrac{-m\bar{x}(g_1^2)F_2}{2\pi\rho_{SL} b_R^4 \ell} \\ \dfrac{-m\bar{x}(g_1^2)F_2}{2\pi\rho_{SL} b_R^4 \ell} & \dfrac{I_\alpha F_2^2}{2\pi\rho_{SL} b_R^4 \ell} \end{bmatrix} \begin{bmatrix} \ddot{q}_h \\ \ddot{q}_\alpha \end{bmatrix} + \begin{bmatrix} \dfrac{m\omega_h^2(g_1^2)^2}{2\pi\rho_{SL} b_R^2 V_R^2 \ell} & \dfrac{-mr_\alpha\omega_\alpha^2(g_1^2)F_2 Z}{2\pi\rho_{SL} b_R^2 V_R^2 \ell} \\ 0 & \dfrac{I_\alpha\omega_\alpha^2 F_2^2(1-\gamma Z)}{2\pi\rho_{SL} b_R^2 V_R^2 \ell} \end{bmatrix} \begin{bmatrix} q_h \\ q_\alpha \end{bmatrix} = \begin{bmatrix} 0 \\ 0 \end{bmatrix} \tag{425}$$

where

q_h = generalized coordinate of the mode consisting of pure vertical translation

q_α = generalized coordinate of the mode consisting of pure pitch about the pitch axis

$r_\alpha\gamma$ = distance of the elastic axis aft of the aerodynamic center

r_α = radius of gyration about the pitch axis

ω_h = natural frequency of the q_h generalized coordinate

ω_α = natural frequency of the q_α generalized coordinate

$$I_\alpha = I_{yy} \tag{426}$$

$$Z = 2\left(\frac{C_{L\alpha}}{2\pi}\right)\frac{1}{\mu}\frac{1}{\left(r_\alpha/b\right)}\left(\frac{V}{b\omega_\alpha}\right)^2 \tag{427}$$

$$\mu_m = \frac{m}{\pi\rho b^2} \tag{428}$$

$$b_R = b \tag{429}$$

It will be noticed that there is no structural or aerodynamic damping present in the equations of motion and that the asymmetry of the stiffness matrix is clearly apparent. This asymmetry has the potential to cause the frequencies of the undamped vibration modes to coalesce. Flutter occurs at the airspeed at which the frequencies of the undamped modes become equal. The relationship of the various axes is shown in Figure 18. The airfoil data are listed in Table III.

Substituting these airfoil data into the equations of motion yields

$$\begin{bmatrix} 1.2516 & -1.8774 \\ -1.8774 & 14.125 \end{bmatrix} \begin{bmatrix} \ddot{q}_h \\ \ddot{q}_\alpha \end{bmatrix} + \begin{bmatrix} .57151 \times 10^{-4} & -.47962 \times 10^{-2} Z \\ 0 & .016123(1 - .179Z) \end{bmatrix} \begin{bmatrix} q_h \\ q_\alpha \end{bmatrix} = \begin{bmatrix} 0 \\ 0 \end{bmatrix} \tag{430}$$

where $Z = .03968\ (V/33.8)^2$ with V in knots.

The airfoil data were input to the computer program, and the above coefficients were compared with those calculated by the program for a range of values of V. In all cases, the coefficients were identical within the accuracy of the desk machine calculations.

The eigenvalue solution to the test case is given in Figure 5 of Reference 12. The results were converted into the notation of the computer program output, and the two methods of solution were compared in Figures 19 and 20. Within the accuracy with which solutions could be read from Figure 5 of Reference 12, the two methods of solution give identical results. In particular, the flutter and divergence speeds as quoted in Reference 12 are compared in Table IV with those obtained by the computer program.

To run the test case with the computer program, it was necessary to use a special tabulation of the aerodynamic coefficients. The tabulation consisted of the set of coefficients given in Table V.

This set is the same as would be used for a solution using conventional aerodynamic coefficients at $M_N = 0$, $k = 0$ except that $\ell_{\dot{h}} = 0$ instead of 1. This means that the lift-curve slope of $dC_L/d\alpha = 2\pi$ for a uniform vertical translational velocity is replaced by zero, thus eliminating all aerodynamic damping. It is use of $\ell_{\dot{h}} = 0$ which gives the flutter solutions in Figures 19 and 20 their unusual appearance.

The test case was also run with the tabulated set of 2320 aerodynamic coefficients previously described. This served as a partial check on the use of this table of coefficients in the computer program. The solution was run specifying $M_N = 0$, $k = 0$ and the results are compared in Figures 21 and 22 with the computer solution obtained through simplified aerodynamics. In passing, it may be noted that the simplified theory is not a good approximation for this test case. This is probably due to the fact that the flutter is of the milder type and that the two modal frequencies do not cross.

This was the only test case in which a check was made of the solution frequencies and decay rates. However, many more check cases were run to verify that the coefficients in the equations of motion were being calculated correctly and that the various facilities available in the program were working correctly. The number of generalized coordinates used in these checks varied from 2 to 10, the latter being the maximum number for which the flutter solution was programmed.

CORRELATION OF CLASSICAL FLUTTER CALCULATIONS WITH AVAILABLE EXPERIMENTAL DATA

DISCUSSION OF EXPERIMENTAL DATA AVAILABLE FOR CORRELATION

Correlation with experimental blade flutter data obtained at high Mach numbers and high advance ratios had been intended. However, no such data could be located in the literature on the subject. Instead, the choice lay between results obtained by NASA Langley, Reference 13, for a model rotor in hover ($\mu = 0$) for high Mach numbers, and results obtained by Cornell Aeronautical Laboratory, Reference 16, for a model rotor in essentially incompressible flow at high advance ratios. As the emphasis of the study was on the effect of compressibility, it was decided to use the results obtained by NASA Langley for hover. The Cornell Aeronautical Laboratory results were used for further correlation.

Correlation could be attempted with only part of the NASA Langley data, as a large part of it was obtained with high pitch angle settings, so that the blade was either undergoing stall flutter or at least operating at angles of incidence for which classical flutter theory is not valid.

CORRELATION WITH NASA LANGLEY EXPERIMENTAL RESULTS

The correlation was divided into three parts, each part using a different blade configuration. The blades used were designated NACA 23012 1(R), NACA 23012 2(F) and NACA 23012 2(R). The main rotor and blade characteristics are stated below.

The tests were conducted in the Langley vacuum sphere with a single articulated blade. Thus, the blade operated at the hover condition. The density and speed of sound of the testing medium could be varied. There was no lag hinge and no data were given for edgewise motions; so the blade was assumed to be rigid in the edgewise direction. All blades tested, for which correlation was attempted, had an NACA 23012 airfoil section. The blades were considered to be rigid in flatwise bending and torsion for the inner 8 inches of radius. The remaining 38 inches of radius was considered as a uniform cantilever having the properties given in Table VI.

Difficulty was encountered in getting the calculated nonrotating elastic bending frequencies to correlate with the measured values stated in Table VI. The cantilever torsion frequencies presented no difficulty. Eventually, it was decided to increase the blade EI so as to give a first bending frequency equal to the measured value and to ignore any difference between calculated and measured second bending frequencies. The required values for EI are those stated in the table. This approach was justified in that flutter occurred between the flapping and torsion modes, with very little participation of the elastic bending modes.

Before proceeding with a discussion of the correlation results, mention will be made of the convention used to refer to the coupled blade modes obtained from the eigenvalue solution. The labeling of the coupled modes follows the conventional practice of referring to a mode by the name of the generalized coordinate with which it becomes identical as the airspeed approaches zero.

This assumes, of course, that the generalized coordinates are normal modes. Otherwise, the coupled mode will always be a combination of two or more generalized coordinates. As airspeed increases, the proportion of the generalized coordinates in any coupled mode will vary. Hence, a "torsion" mode will start out as being predominantly torsional; but by the time flutter or static divergence occurs, it may be predominantly flapping. Hence, the statement that torsional divergence occurs is not meant to imply that the mode shape was torsional when the instability occurred but rather that the coupled mode that suffered instability started out at zero airspeed as being a torsion mode.

Correlation Using NACA 23012 1(R)

Flutter occurred at low Mach numbers. This case was run because results were available for very small blade pitch angles. The calculated and experimental results are compared in Figure 23, where both reduced flutter speed $V_{0.8R}/b\omega$ and the ratio of the flutter frequency to blade first natural torsional frequency are plotted as a function of blade pitch angle. The curve of reduced flutter speed separates the stable and unstable regions, with the unstable region lying above the flutter curve. As the blade pitch angle is increased, the reduced flutter speed drops slightly at first and then rapidly as the blade apparently begins to stall. As the pitch angle is further increased, the reduced flutter speed decreases until some minimum value is reached. Further increases in pitch angle result in a rather sharp rise in the reduced flutter speed. The curve of frequency ratio shows that a reduction in the value of the reduced flutter speed is accompanied by an increase in flutter frequency.

The portion of the flutter curve corresponding to low pitch angles defines the region of classical flutter, whereas the portion of the curve corresponding to high pitch angles defines the region of stall flutter. As shown by the frequency ratio curve, classical flutter occurred at a frequency lying between the flapping and torsion mode frequencies corresponding to the fact that the classical flutter resulted from coupling of the flapping and torsion modes. On the other hand, stall flutter occurred at a frequency very nearly equal to the first torsional natural frequency corresponding to the fact that stall flutter is a predominantly torsional oscillation.

The calculated values are valid for small pitch angles only, and the results were plotted for $(\theta_{0.8R})_s = 0°$. It can be seen that reasonable correlation of flutter speed was obtained but that the flutter frequency was considerably lower than the experimental values. This discrepancy will be considered again later.

Correlation Using NACA 23012 2(R)

Figure 24 presents the comparison of the experimental and calculated results. The reduced flutter speed now includes the ratio $\sqrt{\rho/\rho_0}$ which was introduced to reduce the scatter of the experimental results obtained at different densities of the testing medium. The reduction in scatter occurs because the experimental flutter speeds occurred at approximately constant dynamic pressure, that is at constant equivalent airspeed. The reduced flutter speed is plotted against the blade tip Mach number, variations in tip Mach number being obtained by varying the speed of sound in the testing medium from approximately 500 fps to 1000 fps. The calculated results show the reduced flutter speed decreasing slowly at first, then more rapidly as the tip

Mach number increases from $M_t = 0.2$ to $M_t = 0.7$. Then the reduced flutter speed decreases more slowly until a minimum occurs at $M_t = .9$, after which it begins to increase rapidly. This beneficial effect of increasing Mach number is due to the rearward shift in aerodynamic center as the Mach number increases and can be explained as follows. The negative aerodynamic spring acting in the torsion mode is composed of two parts. The first is a function of the aerodynamic center-to-elastic-axis spacing and is the usual negative aerodynamic spring encountered in fixed-wing flutter. The second part is proportional to the square of the rotor RPM and is a function of the aerodynamic-center-to-center-of-gravity spacing (Reference 1, pp 153 through 156). With the 2(R) blade, the elastic axis is at 26.5% chord; for low Mach numbers, the aerodynamic center is at 25% chord so that the negative aerodynamic spring due to the aerodynamic-center-to-elastic-axis spacing is negligible. Hence, the only negative aerodynamic spring in the torsion mode is due to the aerodynamic-center-to-center-of-gravity spacing. This is large since the center of gravity is 10.8% chord aft of the 25% chord. Hence, as rotor RPM is increased, the frequency of the torsion mode decreases as can be seen in Figure 25. The torsion mode becomes coincident in frequency with, first, the second flatwise mode; then, the first flatwise mode; and, finally, the flapping mode. As the torsion mode frequency crosses a bending mode frequency, it has the opportunity to couple with that mode to produce flutter. Whether it does or not is a function, among other things, of the dynamic coupling between the bending and torsion modes and the amount of damping in each of the modes. For the case under consideration, flutter occurred only when the torsion mode frequency crossed the flapping mode frequency, as can be seen in Figure 26.

At transonic Mach numbers, the aerodynamic center moves aft, thereby decreasing the aerodynamic-center-to-center-of-gravity spacing, and hence reducing the negative aerodynamic spring in the torsion mode. Thus the frequency of the torsion mode decreases more slowly as a function of rotor RPM as the aerodynamic center shifts aft. This delays to higher values of rotor RPM the point at which frequency coincidence and, hence, flutter occur. As long as the center of gravity is not too far aft, a Mach number will eventually be reached where the torsion mode frequency no longer decreases with increasing rotor RPM and may even begin to increase. In either case, if the torsion mode frequency has not come close to the flapping mode frequency, then flutter is eliminated. From Figure 24, it can be seen that the beneficial effect of high Mach numbers was much more pronounced with the experimental results than with the calculated values; this indicates that perhaps the aerodynamic center moved aft faster on the test blade than was implied by the theoretical aerodynamic coefficients.

In passing, it can be stated that the above mechanism by which coupled bending-torsion flutter occurs with a rotating blade is quite general. The mechanism can be described in the following way. A negative aerodynamic spring must exist in the torsion mode to cause its frequency to decrease with increasing rotor RPM. A negative aerodynamic spring will result when the elastic axis, or the center of gravity, or both, are aft of the aerodynamic center. As the torsion mode frequency decreases, it will cross the bending modes from the highest to the lowest frequencies. With each cross-

ing, there is the possibility that flutter will occur; and with each successive crossing, this possibility increases because the potential to flutter is greatest with the low-frequency bending modes. Also, there is quite a chance that after the torsion mode has crossed the lowest bending (or flapping) mode, its frequency will drop to zero, at which point static divergence occurs, as shown in Figure 25. Thus, if flutter occurs, there is a good chance that static divergence will occur at a slightly higher rotor RPM. In fact, if flutter does not occur until after frequency coincidence has occurred, as is sometimes the case, then static divergence may occur before flutter.

Returning to Figure 24, it can be seen that reasonable correlation of flutter speed occurred for the lower blade pitch angle (namely, $(\theta_{0.8R})_s = 7.2^\circ$) but that the calculated flutter speed is unconservative when compared with the experimental results for the larger pitch angle (namely, $(\theta_{0.8R})_s = 11.2^\circ$). The drop in the measured flutter speed at the higher pitch angles is consistent with the results given in Figure 23 and would indicate that the flutter mechanism is changing from classical flutter to stall flutter. The frequency curve in Figure 24 shows that for both values of blade pitch angle, the flutter frequency was approximately equal to the nonrotating blade torsion frequency, which indicates that perhaps the flutter mechanism for the instability at the lower pitch angle was also more in the nature of stall flutter.

Correlation Using NACA 23012 2(F)

Blade 2(F) is very similar to blade 2(R) considered in the previous section. The main difference is that the center of gravity has been moved forward so that it is 2.5% chord aft of the elastic axis instead of 10.8% chord. The comparison of experimental and calculated flutter speeds is given in Figure 27. Comparing the results for blade 2(F) with those for blade 2(R) given in Figure 24 shows that decreasing the center-of-gravity offset has caused the reduced flutter velocity for the experimental results to increase slightly, but that the reduced flutter velocity for the calculated results has almost doubled. Again, the measured flutter frequencies are considerably higher than the calculated values. The most disturbing aspect of the lack of correlation is that the predicted flutter speed is considerably higher than the measured values, that is, the predicted flutter speed is unconservative. The discrepancies between the measured and calculated values as outlined above could be attributed to the model blade's experiencing stall flutter, since the transition from classical to stall flutter is marked by the following characteristics:

1. The sensitivity of flutter speed to center-of-gravity offset decreases and practically disappears.

2. The flutter frequency increases considerably.

3. The flutter speed decreases considerably.

Items 2. and 3. can be seen in Figure 23.

Satisfactory correlation of reduced flutter speed was obtained for blades 1(R) and 2(R), both of which had a large center-of-gravity offset. The lack of correlation of the flutter frequency for blades 2(R) and 2(F) and the unconservative reduced flutter speed calculated for blade 2(F) could be explained by assuming that the flutter mechanism was stall flutter rather than classical flutter. Such an explanation, however, cannot be used to explain the lack of correlation of flutter frequency when considering blade 1(R). Hence, it was decided to attempt to correlate with the experimental flutter results stated in Reference 14.

CORRELATION WITH CORNELL AERONAUTICAL LABORATORY EXPERIMENTAL RESULTS

The test equipment consisted of a single-blade hydraulically driven rotor mounted above a test trailer which was towed along an airport taxistrip. Blade chordwise center-of-gravity position was adjusted by means of lead weights housed in a cylindrical pod at the blade tip. Two features of the blade were somewhat unusual. One was the location of the blade elastic axis at 41% chord. This gives a large negative aerodynamic spring in the torsion mode due to the large aerodynamic-center-to-elastic-axis spacing. In this respect, the blade is more akin to a fixed wing. The other feature was the very low frequency of the rigid body pitch mode. This frequency was varied during the testing. Otherwise, the Cornell model blade was similar to the NASA Langley model blade. The blade was untwisted and articulated in flapping with a zero offset flapping hinge. There was no lag hinge and since no data were given in the edgewise direction, the blade was assumed to be rigid for edgewise deformations. With respect to flatwise bending and torsion, the blade was also assumed to be rigid out to a blade radius of 7 inches. The characteristic blade parameters are given in Table VII.

From the blade characteristics it appears that the blade had small center-of-gravity offset, as the center of gravity was only 1.5% chord aft of elastic axis. However, the pitch frequency was much lower than the cantilever torsion frequency, so that flutter occurred as a result of coupling between the flapping and rigid-body pitch modes. Hence, for the unbalanced blade, with the feathering axis at 25% chord, the center-of-gravity offset was 16% chord, which, in combination with the low pitch frequency and the large negative aerodynamic spring in the pitch mode, resulted in flutter at low forward speeds and rotor RPM. Because of the very low rotor rotational speeds employed, flutter was obtained up to $\mu = 0.7$ at relatively low forward velocities, with a blade tip Mach number always less than 0.3.

Correlation was attempted with the results given in Figures 10(a), 10(b), and 10(c) of Reference 16. The structural parameters varied were blade pitch frequency and blade chordwise center-of-gravity location, the latter being varied by means of balance weights added to a pod at the blade tip. A diagram of the pod and the balance weight positions is given in Reference 14. The parameters corresponding to the correlation cases are given in Table VIII.

where

$\bar{\omega}_{\phi_1}$ is the nonrotating first flatwise bending frequency

$\bar{\omega}_{\theta_0}$ is the nonrotating rigid-body pitch frequency

$\bar{x}_b^*$ is the distance of the balance weights ahead of the 25% chord

$\frac{\bar{x}_E}{c}$ is the equivalent center-of-gravity location. It is defined in Reference 14 as the chordwise center of gravity location of a rectangular blade having a uniform mass distribution such that the ratio of the pitching-flapping product of inertia to the flapping inertia is the same as that of the nonuniform blade being studied.

$\frac{a_{\beta\theta_0}}{\sqrt{a_{\beta\beta}\, a_{\theta_0\theta_0}}}$ is an alternative measure of the inertial coupling between the flapping and pitch modes, defined in Reference 14.

$$\frac{\bar{x}_E}{c} = -\frac{1}{3b}\frac{a_{\beta\theta_0}}{a_{\beta\beta}} = -.1905\frac{a_{\beta\theta_0}}{a_{\beta\beta}} \tag{431}$$

The experimental data of Figure 10(c) in Reference 16 is for the case of no added weights, and represents flutter of the uniform unbalanced blade.

The results given in Figure 28 pertain to data for the flatwise to torsion frequency ratio $\bar{\omega}_{\phi_1}/\bar{\omega}_{\theta_0} = .63$, with $\bar{\omega}_{\theta_0} = 132.5$ radians/sec. The rotor speed at which flutter occurred is denoted by Ω, and $\bar{\omega}_{\theta_0}$ is the nonrotating rigid-body pitch frequency. Hence, raising the flutter speed Ω corresponds to decreasing the value of $\bar{\omega}_{\theta_0}/\Omega$. Nondimensionalizing the flutter speed Ω with respect to the pitch frequency $\bar{\omega}_{\theta_0}$ allows experimental results obtained at different values of $\bar{\omega}_{\theta_0}$ to be plotted together, as the flutter speed is roughly proportional to $\bar{\omega}_{\theta_0}$. It can be seen that the predicted flutter speeds agree very well with the measured values. The calculated flutter speed corresponding to a particular value of μ was obtained by simultaneously increasing forward speed and rotor speed so as to keep μ constant. For example, the results corresponding to $\mu = 0$ are given in Figures 29 and 30. Figure 29 is a plot of the coupled modal frequencies versus Ω, and Figure 30 is a plot of the corresponding modal decay rates. The decay rate of the flapping mode changes at $\Omega = 345$ RPM from being convergent to divergent, giving a flutter speed of 345 RPM. The results are of particular interest, as, from the frequency and damping curves, it would appear that the flutter occurs between the flapping and first bending modes. This was the only case in which this occurred, and it was also the only case for which the pitch frequency was above the first flatwise bending frequency. A detailed

investigation was made of this case, from which it was deduced that:

1. The only modes to couple together to give flutter were flapping and rigid-body pitch. The resulting flutter frequency and decay rate were a good approximation to the five mode solution.

2. The addition of first flatwise bending to the flapping-pitch binary gave a solution almost identical to the five mode solution.

3. The second flatwise bending mode and cantilever torsion modes made a negligible contribution to the flutter mechanism and could have been deleted from the analysis.

Thus, flutter was due to coupling of the flapping and rigid-body pitch modes as was to be expected, and this was found to be the flutter mechanism for all of the cases that were studied.

The results given in Figure 31 pertain to data for the lower pitch frequency; they can be compared directly with Figure 10(c) of Reference 16. The pitch frequency of the blade has been reduced from 132.5 rad/sec to 64.5 rad/sec so that the nonrotating pitching frequency is now lower than the nonrotating first flatwise bending frequency, with the $\bar{\omega}_{\phi_1}/\bar{\omega}_{\theta_0} = 1.31$. The variations of the coupled modal frequencies and decay rates with increasing airspeed and Ω for $\mu = 0.5$ are given in Figures 32 and 33 respectively. These variations are typical of the variations in coupled modal frequency and decay rate that were obtained in all the remaining cases. It can be seen that, due to the large negative aerodynamic spring in the pitch mode, the pitch mode frequency decreases rapidly with increasing airspeed or Ω. Flutter occurs near the airspeed at which the pitch mode frequency crosses the flapping mode frequency. It can be seen that the flutter is extremely violent, the decay rate of the flapping mode changing from $C/C_c = 0.30$ (stable) to $C/C_c = 0.0$ (flutter) with an increase in rotor speed of only 13 RPM. This is to be expected with pitch-flap flutter, especially with the large aerodynamic-center-to-center-of-gravity and pitch-axis-to-center-of-gravity offsets. After frequency coalescence of the pitch and flapping modes, the frequency of the pitch mode continues to decrease until flapping divergence occurs. In some of the other cases, the frequency of the pitch and flapping modes remained almost equal after flutter occurred, and static divergence did not take place.

In Figure 31, it will be noted that the calculated results are now somewhat conservative; that is, the calculated flutter speed is lower than the experimental flutter speed. Also plotted is the flutter speed calculated in Reference 16. It can be seen that the calculated flutter speed of the present study lies between the measured value and the value calculated in Reference 16.

The experimental data of Figure 10(b) in Reference 16 is for the partially balanced case, with the results shown in Figure 34. The calculated flutter

speed is now lower than both the measured value and the value calculated by Cornell. For high advance ratios, both calculated values are extremely conservative with respect to the measured flutter speed. For example, at $\mu = 0.5$, the rotational flutter speed calculated in Reference 14 is .50 times the measured rotational flutter speed. The calculations of the present study give a rotational flutter speed 139 times the measured rotational flutter speed

The Reference 16 results were obtained by using an analogue solution, and the stability of the rotating blade was considered; whereas the present study uses the stopped-rotor approach, the solutions being obtained with the rotor stopped at an azimuth angle of $\psi = 90^\circ$, which is considered to be the most unstable azimuth angle with respect to classical flutter. Hence, there is an inherent degree of conservatism in the stopped rotor approach; ideally, solutions should be obtained for different positions around the azimuth angle with the resulting maximum and minimum flutter speeds bounding the actual flutter speed. For example, the region of instability may extend over an azimuth angle of 60°. While the blade is passing through this region, its oscillations will be diverging. For the remaining 300° of rotation, they will be dying away. The flutter speed would be obtained by integrating the buildup and decay of the oscillations for one revolution, flutter occurring when the oscillation amplitude at the end of the 360° rotation was equal to the amplitude at the beginning. However, this approach was beyond the scope of the study.

Referring again to Figure 34, one can see that the measured flutter speed occurred at a constant value of rotor speed (for $\overline{\omega}_{b_0}$ constant) independent of the advance ratio. That is, the measured flutter rotor speed did not vary with forward velocity, which is a very surprising result. The coefficients in the flutter equations are obtained by integrating blade structural and aerodynamic properties, including the mode shapes, across the span. With a fixed wing, this integration or averaging process for a simple planform results in a good definition of flutter speed through use of the wing properties at the 75% span. A similar effect would be expected for a rotating blade for which, in addition, the airspeed varies spanwise. The flutter speed of a rotating blade would then be a function of the airspeed at some spanwise station, say 80% span, and would be independent of the combination of rotor speed and forward velocity giving the velocity at the station. Both sets of calculated results behave in this manner. As forward speed increases, the rotor speed at which flutter occurs decreases, so that flutter occurs at the same value of average blade airspeed. However, the measured flutter speeds in Figure 34 seem to indicate that the flutter mechanism depends predominantly on rotor speed and is not influenced by changes in the average airspeed of the blade. This trend of the experimental results certainly deserves to be investigated thoroughly, as it seems to indicate that some aspect of the flutter mechanism is missing from the theoretical flutter calculations.

The results given in Figure 35 pertain to the almost completely balanced blade of Figure 10(a) in Reference 16. The flatwise to torsion frequency ratio is $\overline{\omega}_{\phi_1} / \overline{\omega}_{\theta_0} = 1.03$, and the torsion natural frequency is $\overline{\omega}_{\theta_0} = 65.9$ rad/sec. Again, the test results show that flutter

occurred at constant rotor speed. The digital solutions are so conservative as to bear little relation to the measured results. Flutter still consists of pitch flap coupling, and the question arises as to why flutter occurred between flapping and pitch when the inertia coupling between these modes is almost zero. If one looks at the change in the measured flutter speed with changing mass balance as given in Table IX, it can be seen that the measured flutter speed increased by a factor of 4 from the unbalanced to the fully balanced case, whereas the calculated flutter speeds increased only slightly. It is this insensitivity of the calculated results to changing mass balance that makes the correlation so poor for the fully balanced blade. In Figures 34 and 35 the results have been plotted for the case where the mass balance coefficients were not added to the equations of motion. Again the insensitivity of the calculated flutter speed to changing mass balance is apparent.

The results given in Figure 36 pertain to the balanced blade of Figure 10(a) in Reference 16 with the flatwise to torsion frequency ratio $\overline{\omega}_{\phi_1}/\overline{\omega}_{\theta_0} = 1.44$ and the natural torsion frequency $\overline{\omega}_{\theta_0} = 46.9$ rad/sec. Again the insensitivity of the calculated flutter speed to changing mass balance has caused the calculated flutter speed to be extremely conservative.

SUMMARY OF CORRELATION WITH NASA-LANGLEY AND CORNELL TEST RESULTS

The correlation with Cornell test results was begun because of the poor correlation of flutter frequency that occurred with the NASA-Langley model results. The frequencies at which the Cornell model blade fluttered are not stated, and so a comparison of calculated and measured flutter frequencies cannot be made. However, it was hoped to achieve satisfactory correlation of flutter speed, which is much more important than flutter frequency. From the above review of the correlation with Cornell data, it can be seen that this was not achieved. The overall correlation is certainly encouraging, but in some areas questions remain to be answered. For cases where it is reasonably certain that the model blade was undergoing classical flutter, the calculated flutter speed was in every case either equal to or below the measured flutter speed. This conservative nature of the calculated flutter speed is important. It may cause concern unnecessarily, but it gives assurance that classical flutter will not occur below the calculated speed.

The emphasis of the study was on the effects of compressibility at the high advance ratios at which present-generation helicopters are operating. It was for this purpose that the compressible aerodynamic coefficients were assembled and used in the computer program for obtaining flutter solutions. However, because of the lack of test data, the correlation had to be made with cases involving either high Mach numbers in hover or very low Mach numbers in hover and in forward flight. In fact, quite a few of the cases were for the hover condition involving low tip Mach numbers for which a satisfactory unsteady aerodynamic theory exists (Reference 15). It is expected that use of the Loewy coefficients in these cases would improve the correlation obtained.

It is unfortunate that test results were not available for the high Mach number, high advance ratio flight regime; not only is this the area where a proven method is needed to predict classical flutter speeds, but it is also the area where the compressible aerodynamic coefficients used in the computer solution are considered to be applicable. On the other hand, the validity of these coefficients for the hover case with low tip Mach numbers is questionable.

It is felt that the methods developed during the present study can be used as a design tool in evaluating blade flutter speeds and in determining the sensitivity of the flutter speed to changes in design parameters. It is suggested that the compressible aerodynamic coefficients be replaced by Loewy coefficients for cases involving low tip Mach numbers with low advance ratios.

EFFECTS OF VARIATIONS IN PARAMETERS

DESCRIPTION OF BASIC CONFIGURATION

It was decided to use the NACA 23012 2(F) model blade described in Reference 13 for the parametric variations, with the same variations being considered for the two cases where the blade root is considered fixed and articulated. The rotor speed and chordwise center-of-gravity position were adjusted to give reasonably strong flutter at about $\mu = 0.25$. Otherwise, if flutter is weak, small changes in parameters are likely to have a very stabilizing effect; whereas with violent flutter, large changes in the parameters may have little effect in reducing the flutter. Initial solutions attempted to adjust the speed of sound so that at $\mu = .50$, the Mach number was unity. This is equivalent to testing the model blade in a gas such as Freon, for which the speed of sound is much less than in air. However, varying the speed of sound had a confusing effect on the flutter speed, so this attempt was not pursued and the solutions were run with the speed of sound equal to 1116 ft/sec. Therefore, the blade tip Mach number at which flutter occurred was relatively low. Air density was set at its standard sea level value. All cases studied were for the advancing blade.

The main parameters defining the nominal case for the articulated and hingeless blades are given in Table X.

The blade is considered to be rigid for the first 8 inches out from the rotation axis. For the remaining 38 inches, the blade is uniform and the structural data refer to the uniform part of the blade. The parameter variations that were considered are summarized in Table XI. In the case numbers, A refers to the articulated blade and R to the nonarticulated (rigid) blade. It will be noticed that each parameter is varied individually from the nominal case; simultaneous variations are not considered. The variations for the articulated blade are considered first.

The results are presented in the form of stability boundaries such as those shown in Figure 39. The advance ratio μ at which instability either begins or ends, is plotted versus the parameter under consideration. For a particular curve, the unstable region is always above the curve except for the case where a loop occurs. In this case, the unstable region lies inside the loop so that as advance ratio increases, instability occurs on crossing the lower boundary and stability is regained on crossing the upper boundary. The stable region of interest is the area lying below the flutter curves and is that region in which a practical helicopter blade must operate. The upper boundary of this region is shown shaded in the diagrams. Some of the curves are drawn in as broken lines to indicate that only the form of the variation is known, not the exact shape and position of the curves. The precise location of the curves can always be determined by obtaining additional flutter solutions. This was not attempted, as all information required from the parametric variation is contained in the broken curves.

RESULTS FOR THE ARTICULATED BLADE

For reference, the variation of the solution frequency and decay rate versus rotor speed is given in Figures 37 and 38, respectively, for the nominal blade operating in hover. The blade flutters at 1190 RPM, at which speed the torsional mode and flapping mode frequencies are almost equal.

Cases 1.A1 and 1.A2 of Table XI consider two elastic axis positions in addition to the nominal position; the results are shown in Figure 39. Figure 39 also shows a number of additional results, which were obtained to permit better definition of the instability boundaries. With the elastic axis at 25% chord, the major contribution to the negative aerodynamic stiffness is the aerodynamic-center-to-center-of-gravity spacing, and this contribution is unchanged as the elastic axis is shifted aft. However, moving the elastic axis toward the blade trailing edge increases the aerodynamic-center-to-elastic-axis spacing, which begins to make a sizeable contribution to the negative aerodynamic stiffness, thereby causing a reduction in the torsional divergence speed. The reduction in the elastic-axis-to-center-of-gravity spacing from 13% to 3% chord and finally to -7% chord (center of gravity ahead of the elastic axis) has eliminated flutter of the first flatwise mode, raised the flutter speed of the flapping mode, and eliminated flutter below the torsional divergence speed.

As the elastic axis moves from 37.1% chord to 37.2% chord, the roles played by the flapping and torsional modes are interchanged, but there is no discontinuity in the curves as a result of this switch. On the root locus plots generated by the program, the flapping and torsional modes approach each other when the advance ratio increases, and for some special value of elastic axis position between 37.1% and 37.2% chord, they will meet tangentially from opposite directions. At this point the flapping and torsional modes have identical frequency, damping, and motion. Further increases in the advance ratio cause the root locus paths to leave the point of intersection at right angles to the incident paths. It is then arbitrary as to which of the retreating paths is termed the flapping or torsional mode. As the advance ratio is increased, one of the modes reaches a divergent instability and then the other reaches a flutter instability. The onset of these instabilities provides the points on the boundaries in Figure 39 where the flutter instability and the divergence instability modes interchange. With the elastic axis forward or aft of this special position, the flapping and torsional branches each break away without reaching a point of intersection. In this case, the modes can, as usual, retain the designations assigned for $\mu = 0$. For forward positions of the elastic axis it is the torsional mode which meets the $\omega = 0$ axis and therefore suffers static divergence, whereas for aft positions it is the flapping mode which meets the $\omega = 0$ axis.

The switch in the stability of the torsional and flapping modes is a result of the change in the modal coupling that occurs as the elastic axis is shifted aft. This effect is examined in Figures 40 and 41, in which the amplitude ratio q_h / q_α and the phase angle are plotted versus advance ratio, for both the flapping and the torsional modes. Figure 40 considers the elastic axis at 25% chord, and it can be seen that in hover, the fla-

ping mode begins as a predominantly flapping motion $q_h/q_\alpha = 16$ while the torsional mode beings as a predominantly torsional motion $q_h/q_\alpha = 0.6$. As advance ratio increases, the amount of torsional motion in the flapping mode increases, and, simultaneously the amount of flapping motion in the torsional mode increases so that the modal ratios of the two modes approach each other. At $\mu = .35$, the two ratios become almost identical. A similar effect occurs with the elastic axis at 45% chord, Figure 41; however, in this case the amount of flapping displacement in the torsional mode is greater in hover than with the elastic axis at 25% chord. It can be seen that the mode with the smaller phase angle at hover is the one which suffers static divergence.

The effect of moving the elastic axis aft may be summarized by saying that the effect is to increase the flutter speed but to cause a decrease in the static divergence speed. An optimum location for this blade occurred with the elastic axis in the range 32% to 40% chord.

Cases 2.A1, 2.A2, 2.A3, and 2.A4 of Table XI consider four center-of-gravity positions in addition to the nominal position; the results are shown in Figure 42.

As the center of gravity moves aft the static divergence speed decreases uniformly, corresponding to the fact that increasing the aerodynamic-center-to-center-of-gravity spacing causes a corresponding increase in the negative aerodynamic stiffness acting in the torsion mode.

A threshold value for the center-of-gravity offset occurs, below which flutter will not occur. Once the threshold value is reached, the flutter speed decreases steadily as the center of gravity moves aft. However, the sensitivity to center-of-gravity offset decreases at the same time so that the flutter curve flattens out.

Cases 3.A1 and 3.A2 of Table XI consider two torsional stiffnesses in addition to the nominal value, the results are shown in Figure 43.

Increasing GJ raises the torsional divergence speed as expected. It also has the effect of raising the flutter speed until finally the flapping mode appears to flutter above the static divergence speed. In fact, increasing GJ may have eliminated flapping flutter because for $GJ/(GJ)_{NOM} = 1.328$, frequency coalescence of the torsional and flapping modes occurs at $\mu = .366$ yet flutter has not occurred by the time static divergence sets in at $\mu = .45$. Sometimes, however, flutter does not begin until after frequency coincidence has occurred. For example, at $GJ/(GJ)_{NOM} = 1.$, frequency coincidence of the torsional and flapping modes occurs at $\mu = .235$, but coupled flapping-torsion flutter does not begin until $\mu = .27$. Also, the difference in rotor speed at which frequency coincidence and static divergence occur decreases with increasing GJ, as can be seen from Figure 44. Hence, it is more likely that the flutter sets in after torsional divergence has occurred rather than that flutter has been eliminated.

Cases 4.A1 and 4.A2 of Table XI consider two blade flatwise bending stiffnesses in addition to the nominal value; the results are shown in Figure 45.

Increasing EI has eliminated the flutter involving the first flatwise bending and torsional modes. However, the other flutter mode involving mainly the rigid-body flapping and torsional modes shows little change with increasing EI, as is to be expected. Hence, increasing the flatwise bending stiffness will raise the flutter speed and perhaps will eliminate flutter modes involving elastic flatwise bending; however, it cannot help toward increasing the flutter speed of flutter modes in which flatwise motion is due principally to rigid-body flapping.

Cases 5.A1 and 5.A2 of Table XI consider two blade mass variations in addition to the nominal; the results are shown in Figure 46.

Changing the blade mass has comparatively little effect on the static divergence speed. The main effect is to cause a change in the flutter mode. For a blade mass distribution half the nominal value, the flutter mode involves first flatwise bending, while for a blade mass distribution twice the nominal value, the flutter mode involves rigid body flapping. Based on the results obtained in cases 5.A1 and 5.A2, it is expected that the flutter speed of the light blade (half the nominal mass) could be raised substantially by increasing the blade bending stiffness. By comparison, the heavy blade should be relatively insensitive to changes in the flatwise bending stiffness.

Cases 6.A1 and 6.A2, of Table XI consider two variations in blade pitching inertia, in addition to the nominal value; the results are shown in Figure 47.

Increasing or decreasing I_α from its nominal value reduces the stable operating range of the rotor. In fact for $I_\alpha/(I_\alpha)_{NOM} < 0.4$ and $I_\alpha/(I_\alpha)_{NOM} > 2$, the rotor suffers flapping flutter for $\mu \geq 0$, so that there is no stable operating region.

RESULTS FOR THE NONARTICULATED BLADE

For reference, the variation of the solution frequency and decay rate versus rotor speed is given in Figures 48 and 49, respectively, for the nominal blade operating in hover. The blade flutters at 1160 RPM, followed by static divergence at 1400 RPM. Also shown in Figure 50 is the variation of the critical advance ratio versus rotor speed. As expected, the higher the rotor speed, the lower the advance ratio at which instability occurs, until finally the blade flutters in the hover condition for $\Omega = 1160$ RPM. This is in contrast to the Cornell experimental flutter data in which instability occurred at approximately constant rotor speed irrespective of the advance ratio.

Cases 1.R1 and 1.R2 of Table XI consider two elastic axis positions in addition to the nominal position; the results are shown in Figure 51. The results are similar to those of the articulated case, and the comments made for that case apply also to the hingeless blade. However, because the hingeless blade does not have a flapping mode, the following equivalence of modes exists:

Articulated Rotor	Hingeless Rotor
Flapping	First Flatwise
First Flatwise	Second Flatwise
Second Flatwise	Third Flatwise

Thus, for example, the behavior of the nonarticulated blade's second flatwise bending mode should be compared to the first flatwise bending mode of the articulated blade, since the mode shapes and frequencies will tend to be approximately the same. It should be noted that the results shown in Figures 39 and 51 are applicable to the blades considered, and it should not be concluded that the results are typical for all practical ranges of the various blade parameters.

Cases 2.R1, 2.R2, 2.R3, and 2.R4 of Table XI consider four center-of-gravity positions in addition to the nominal position; the results are shown in Figure 52. Again, the results are very similar to those of the articulated case, and the comments made for the articulated blade apply also to the hingeless blade. Only one static divergence speed is shown (namely, at 13% center-of-gravity offset) because, for all other center-of-gravity offsets, the highest value of μ for which solutions were obtained was below the divergence speed. If solutions had been obtained for higher values of μ, then static divergence would have occurred in every case. It should be noted that no flutter instability was found, for the range of μ considered, in the case of the 2.5% center-of-gravity offset. Therefore only the solutions for the remaining 4 cases appear in Figure 52.

Cases 3.R1 and 3.R2 of Table XI consider two torsional stiffnesses in addition to the nominal value; the results are shown in Figure 53. The results are similar to the corresponding results for the articulated blade. The difference may be attributed to the fact that the torsional frequency does not decrease as rapidly with increase in μ for the hingeless blade as it does for the articulated blade. This result applies to the particular configuration treated, and should not be applied to blades of conventional stiffness.

Cases 4.R1 and 4.R2 of Table XI consider two blade flatwise bending stiffnesses in addition to the nominal value; the results are shown in Figure 54. Increasing the EI raises the frequency of the first flatwise mode bringing it closer in frequency to the torsional mode. As a result, frequency coincidence of these two modes occurs at increasingly lower values of μ as EI increases, which causes a reduction in the flutter speed. There is probably no simple explanation for the increase in the torsional divergence speed with increase in EI, since torsional divergence occurs well above the flutter speed. Hence, by the time it occurs, the first flatwise and torsional modes are so strongly coupled that one cannot interpret changes in torsional divergence speed in terms of single-degree-of-freedom results for a torsional mode.

Cases 5.R1 and 5.R2 of Table XI consider two blade mass variations in addition to the nominal; the results are shown in Figure 55. Changing blade mass again causes an indicated switch in the stability of modes. The results are considerably different in detail from the corresponding results for the articulated blade. However, the practical result is the same; namely, that changing blade mass does not significantly alter the stable operating range of the blade.

Cases 6.R1 and 6.R2 of Table XI consider two variations in blade pitching inertia in addition to the nominal value; the results are shown in Figure 56. The results are almost identical to the corresponding results for the articulated case except that, as noted before, the second flatwise mode does not flutter in the hingeless case.

SIGNIFICANCE OF CLASSICAL FLUTTER ANALYSIS AND RESULTS

The method of solution developed for this study has proved to be versatile and well suited to design use. A number of assumptions and approximations were made when deriving the equations of motion. It was considered that the resulting simplified equations should still be able to predict flutter speeds with acceptable accuracy. It was initially intended to check these simplified equations by comparing the solutions with experimental flutter data obtained from blades operating at high tip Mach numbers and advance ratios. As explained previously this was not possible. The correlation that was attempted proved encouraging, but many questions remain to be answered. What is still needed is to be able to correlate with a large body of accurate experimental test data at high advance ratios and tip Mach numbers. The estimated accuracy of experimentally determined rotating blade flutter speeds is rarely stated, if ever. Thus, in a correlation study, the experimental results have to be assumed to be accurate. Yet, the possibility of inaccuracies existing in the experimental results is considerable. Examples have occurred in the past where, for the simpler case of two-dimensional airfoils oscillating in incompressible flow, discrepancies between measured and calculated flutter speeds were removed by improvements in the experimental technique. In addition, there is the possibility that a measured flutter speed may not be due to classical flutter. It would be more satisfactory if the solution to the simplified equations and the experimental determination of flutter speeds could be made part of one test program.

The limited correlation that was attempted showed that the calculated flutter speed was always conservative for those cases in which it was reasonably certain that the flutter mechanism was classical flutter. At times, the results were so conservative as to be of little use in predicting flutter speeds. It may be pointed out that a considerable difference exists between attempting to predict accurate flutter speeds and a parametric study in which the effect on the flutter speed due to changing parameters is investigated. In the latter case, which is usually the major portion of a flutter investigation, the accuracy of the solutions is of secondary importance. The main interest is the detection and approximate location of any regions of instability. The accurate evaluation of their extent is of secondary importance. The major requirement for parametric variations is that the equations of motion always give conservative flutter solutions. Then the method is capable of locating all regions of instability, with the calculated boundaries enclosing the true boundaries, the difference between the two being a function of the degree of conservatism of the flutter solution. The possibility of missing an instability is then confined to incorrect choice of the parameters. From past experience and with an understanding of the flutter mechanism, a great deal of information can be obtained from such investigations, and it can be applied toward obtaining a flutter clearance. This use of indirect methods was widespread before the introduction of electronic computation aids; it will have to be relied on at present for helicopter blade flutter in the high-speed flight condition until either a more satisfactory aerodynamic theory is developed or existing approximate theories can be checked experimentally over a wide

range of flight conditions. Until these improvements become available, it is considered that the simplified equations of motion developed in this study represent an acceptable method for investigating the flutter characteristics of a helicopter blade in high-speed flight; it is believed that this method is suited for design use where speed of solution is essential.

The parametric study should be used with caution, as it has limited applicability. In this respect, it may be noted that the equations of motion have many types of coupling terms, and any one may contribute critically. For a particular class of blade or a particular flight condition, certain coupling terms will predominate; if variations are made within this class, the variations will have a characteristic form. However, for a different class of blade or flight condition, other coupling terms will predominate and cause the parameter variations to take on an entirely different form. It appears that the center-of-gravity offset is one of the few parameters that are important for most classes of blades. The same situation applies to fixed-wing flutter. Parameter variations have been published considering straight, high-aspect-ratio wings with no lumped masses, traveling at low subsonic speeds. However, these results do not apply if the wing is traveling at high subsonic Mach numbers or if a flexibly mounted store is added to the outboard portion of the wing. These limitations do not decrease the usefulness of parameter variations in general, but they do mean that a new set of curves has to be generated when investigating a new class of blade or flight condition.

EXTENDED NORMAL MODE TRANSIENT ANALYSIS CALCULATIONS CORRESPONDING TO CLASSICAL FLUTTER INVESTIGATIONS

PURPOSES AND METHODS

The extended Normal Mode Transient Analysis was employed to perform blade response calculations corresponding to blade configurations and flight conditions for which classical flutter was calculated.

The purpose of these calculations was to provide comparative results and to obtain time histories of blade response over a complete rotor revolution, part of which was unstable from the standpoint of the fixed azimuth classical flutter calculation.

It should be noted that the fixed azimuth classical flutter calculation and the extended Normal Mode Transient Analysis are quite different in their basic assumptions. As pointed out in the introduction of this volume, these fixed-azimuth classical flutter calculations consider pertinent inertial and elastic blade structural effects, together with unsteady, compressible aerodynamic loadings. These aerodynamic loadings include phase lag effects which arise because of blade motions in an assumed steady velocity field appropriate to a particular azimuth position. This assumption permits solution of the flutter stability equations in a manner which is mathematically similar to the usual fixed-wing flutter problem, since the coefficients of the equations are constant in time. The extended Normal Mode Transient Analysis, in contrast, integrates the blade differential equations of motion in a step-by-step fashion, considering pertinent inertial and structural effects, as well as the time history of instantaneous aerodynamic loadings, including stall and compressibility effects. These loadings, however, are so-called quasi-steady loadings. This refers to the determination of aerodynamic loadings by steady-state airfoil data and by the instantaneous relative velocity vector at the 75% chord point of each blade strip. This excludes phase lag effects between motion and aerodynamic loading, which are usually included in flutter calculations. As pointed out earlier, this precludes prediction of classical flutter in some cases. However, the type of classical flutter arising because of aft center-of-gravity location on a fixed wing can be predicted with quasi-steady aerodynamic effects. Hence, it could be expected that the extended Normal Mode Transient Analysis results would reflect classical flutter-type instabilities due to aft blade center-of-gravity position.

Therefore, the blade configuration chosen was that used for the classical flutter parameter study. This blade had a flapping hinge only for the articulated case, and was assumed to be, rigidly built in for the nonarticulated case. Edgewise motions were suppressed in both cases. In the articulated case, rigid-body flapping, two flatwise bending modes, and one torsional mode were considered. The natural frequencies of these modes were 1.11, 2.69, 4.81, and 5.62 cycles per revolution, respectively. In the nonarticulated case, three flatwise bending modes and one torsional mode were considered. The natural frequencies of these modes were 1.43, 4.12, 8.48, and 6.14 cycles per revolution, respectively. In order to

make the results comparable to those for the classical flutter calculations, the rotor was assumed to be very lightly loaded, with a collective pitch setting of 1°. A small loading of this magnitude was used to insure that some blade excitation was present, which would make any tendency toward instability more apparent. The shaft angle of attack for the rotor was effectively zero. In common with the classical flutter calculation, no cyclic pitch input was considered. The normal full-scale Reynolds number aerodynamic data were used, appropriate to an NACA 0012 airfoil. Since blade angles of attack remained low, the blade response results of interest were assumed to be unaffected by Reynolds number and airfoil camber.

The extended Normal Mode Transient Analysis was started with the blade at the zero azimuth position. Starting values for articulated blade flapping were estimated to be steady flapping angles in each case. The first flatwise bending amplitude was used in the same way for the nonarticulated blade. Starting values for all other elastic modal velocities and displacements were zero.

After starting in the above manner, the numerical integration of the blade equations of motion was allowed to proceed for a maximum of 10 rotor revolutions. In many cases, the blade motions became cyclic with respect to rotor azimuth prior to 10 revolutions after starting. In these cases, the computer program automatically terminated the solution, since each of the subsequent revolutions would have been identical if they had been calculated.

CONFIGURATIONS AND FLIGHT CONDITIONS STUDIED

The method described above was employed for each of the configuration flight-condition combinations shown in Table XIII. Pertinent characteristics of the blade were otherwise identical to the nominal blade configuration used in the classical flutter parameter studies.

PRESENTATION AND DESCRIPTION OF NORMAL MODE TRANSIENT ANALYSIS RESULTS

Time histories of flapping and torsion modal displacements are shown in Figures 57 and 58. Results are shown for various center-of-gravity positions at each of the two advance ratios. The solutions for $\bar{x}/c_b = 0$, $-.065$, and $-.0975$ became cyclic within a few revolutions, as shown in Figure 57 for $\bar{x}/c_b = -.0975$. All these solutions were similar, with somewhat smaller flapping and torsional amplitudes for the smaller center-of-gravity offsets. The solution for $\bar{x}/c_b = -.130$, shown in Figure 57, did not become cyclic, even after 10 revolutions. A slowly decaying one-half-per-revolution component can be seen in the torsion modal time history, with every other revolution being similar. It appears that the motions would not grow significantly larger if the solution were allowed to continue. Note, however, that torsional motions are very much larger than for the $\bar{x}/c_b = -.0975$ case. Higher frequency components of approximately four per revolution are visible. Figure 58 is similar to Figure 57, at an even lower advance ratio. Note that the $\bar{x}/c_b = -.130$ case converges rapidly at the lower advance ratio. Setting the center-of-gravity position further

aft, to $\bar{x}/c_b = -.165$ and $-.20$, results in progressively more violent oscillations of a complicated nature. These apparently grow with time until blade destruction occurs.

The nonarticulated blade cases were found to converge rapidly, even with $\bar{x}/c_b = -.130$. The first flatwise response was 46% of the articulated blade flapping response, although the amplitudes of the nonarticulated blade also increased rapidly as the center of gravity was moved aft.

Figure 59 shows blade tip deflections during the last revolution of the various solutions for the articulated blade at advance ratio $\mu = .30$. Comparison with Figure 57 shows that most of the vertical tip deflection is the result of rigid-blade flapping motion. Note that moving the center of gravity aft results in higher average blade twist, which acts like an increase in collective pitch.

In order to present the total elastic blade deformations, Figure 60 was drawn for the articulated blade with advance ratio $\mu = .30$. Note that the elastic blade deflections are essentially cyclic, with a large component of twice rotor frequency. These deformations are the maximum value occurring on the blade and are proportional to bending and twisting stresses and moments at that section of the blade.

Figure 61 is a similar plot for the articulated blade with advance ratio $\mu = .15$ and center-of-gravity positions further aft. Note that for $\bar{x}/c_b = -.165$ and $-.20$, the elastic deformations are noncyclic with azimuth angle and that a predominate frequency of slightly less than three times rotational frequency is present. Note that an enormous increase in the amplitudes of the elastic deformations takes place as the center of gravity is moved aft. It is probable that the deformations would continue to grow if the solution were continued beyond 10 revolutions.

In Figure 62, the total elastic blade deformations are shown for the nonarticulated blade. This blade was stiff enough in flatwise bending to make its behavior distinctly different from the similar articulated blade. The bending deformation d^2w/dx^2 consists almost entirely of one-per-revolution bending. The blade has maximum torsional deflection at the advancing blade position. Note that this deflection could be considered an incipient torsional divergence due to the aft center-of-gravity position.

In Figures 63 and 64, the one-half peak-to-peak nondimensional blade deformations, which are proportional to stress or elastic moments, are plotted against center-of-gravity position for the articulated blade. Figure 65 is a similar plot for the nonarticulated blade. Note that a rapid rise in peak-to-peak deformations occurs for the articulated configurations as the center of gravity is moved aft past certain limits. The corresponding rise for the nonarticulated blade is similar but much less pronounced.

DISCUSSION OF NORMAL MODE TRANSIENT ANALYSIS RESULTS CORRESPONDING TO CLASSICAL FLUTTER INVESTIGATIONS

In this subsection, appropriate comparisons will be made of the extended Normal Mode Transient Analysis results and the corresponding fixed-azimuth classical flutter results.

As pointed out previously, the Normal Mode Transient Analysis and the fixed-azimuth flutter calculation are quite different in their basic intent and analytical approach. In spite of this, some comparisons of the two sets of results should be made. The aft center-of-gravity practical operating boundaries predicted for the limited number of cases considered here do show encouraging agreement between the two methods.

The most important direct comparison is thus of Figures 42, 63 and 64 for the articulated blade, and of Figures 52 and 65 for the nonarticulated blade. As is shown on Figure 42, flatwise-bending-torsion flutter occurs at an advance μ = .30 for a center-of-gravity offset of 11%, followed by flapping-torsion flutter at a center-of-gravity offset of about 12.2%. Figure 63 shows that the flatwise and torsion stresses increase rapidly as the center of gravity is located aft of these two positions. Reference to Figures 57, 58, and 59, however, shows that the flapping motion of the blades increases comparatively little. Inspection of Figure 60 shows frequency components of the order expected for the flatwise-torsion flutter. Thus, some manifestations of the flatwise-torsion flutter predicted for the idealized fixed-azimuth system appear in the Normal Mode Transient Analysis. No particular evidence of a flapping-torsion flutter can be discerned. It would be expected that the fixed-azimuth assumption would be more valid for the higher frequency flutter modes. Similar observations can be made for an advance ratio of μ = .15, for which flatwise-torsion flutter is predicted at a center-of-gravity offset of 15% and flapping-torsion flutter at an offset of 17.5%. The flutter boundary for the nonarticulated blade shown in Figure 52 corresponds to first flatwise-torsion flutter, which corresponds to flapwise-torsion flutter for the articulated blade. The onset of this comparatively low frequency flutter for the fixed-azimuth system is reflected in a fairly gentle rise in stress as center-of-gravity offset increases.

On the basis of the above information, it can be expected that the fixed-azimuth flutter calculations will be most accurate for classical flutter frequencies greater than two times rotor frequency when the advance ratio is greater than μ = .15. When flutter frequencies are smaller, the predictions of flutter speed are expected to be increasingly conservative.

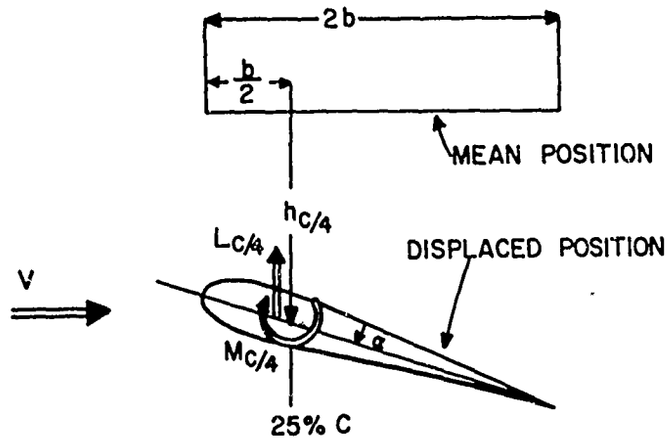

Figure 1. Notation for Forces and Displacements.

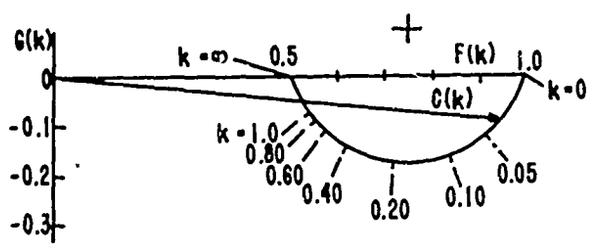

Figure 2. A Complex Polar Plot of C(k) = F(k) + iG(k).

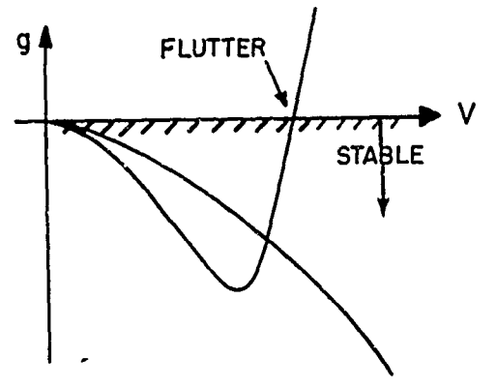

Figure 3. A Typical V-g Plot.

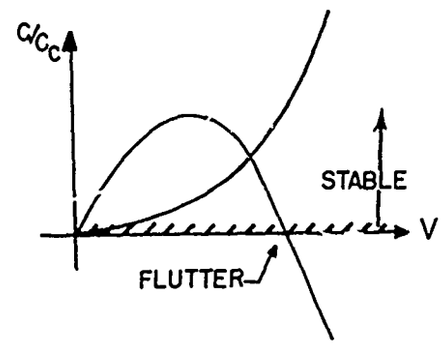

Figure 4. A Typical Variation of Decay Rate C/C_c .

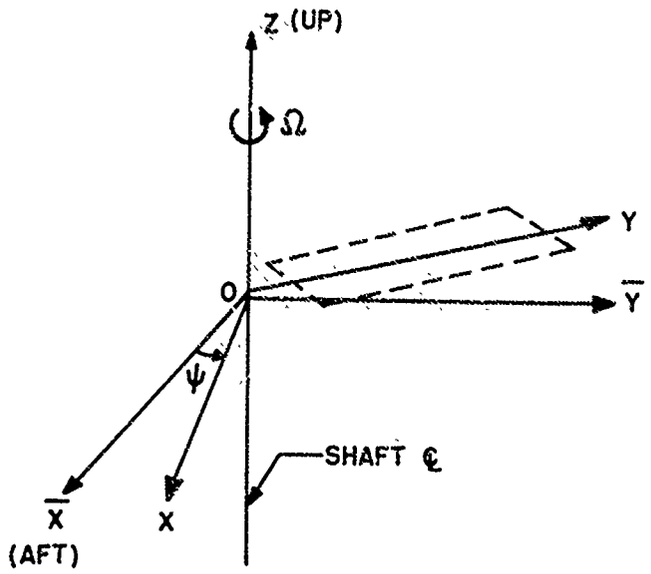

Figure 5. Notation for the Blade Axes.

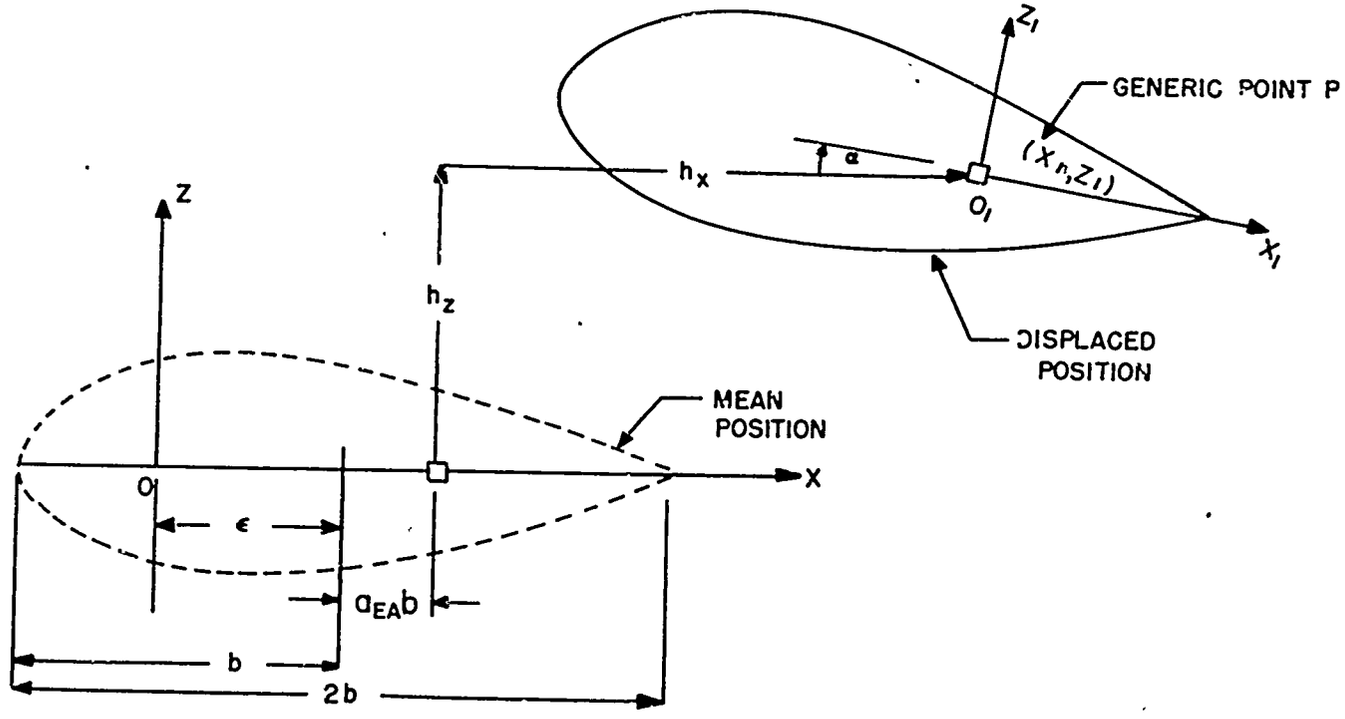

Figure 6. Notation for Blade Displacements.

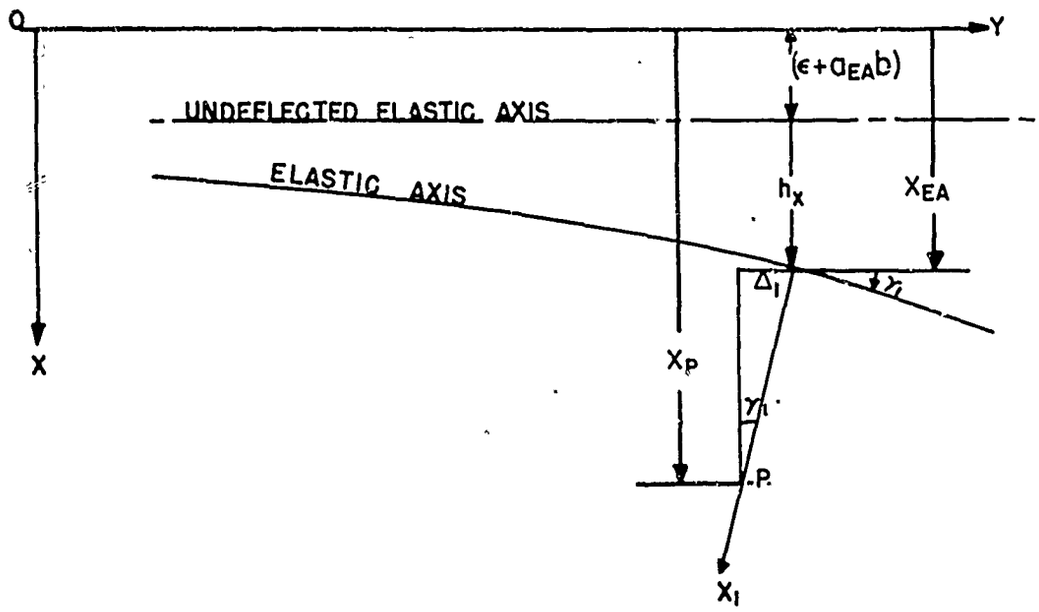

Figure 7. Radial Displacements Resulting From Edgewise Bending.

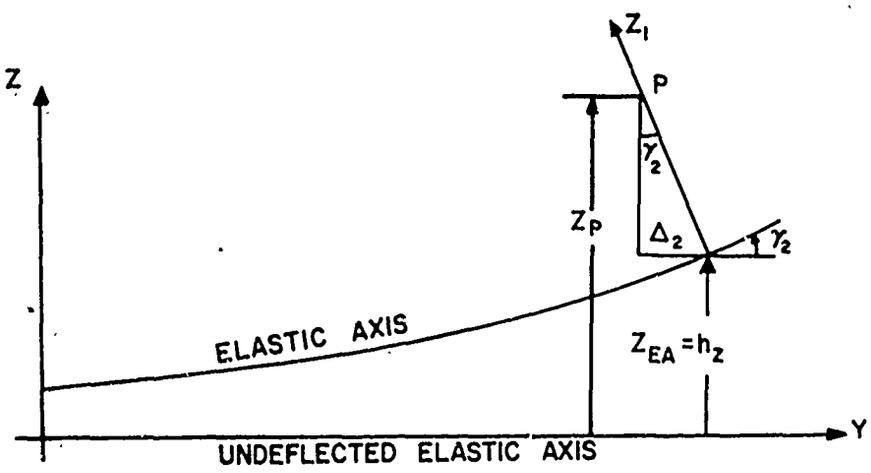

Figure 8. Radial Displacements Resulting from Flatwise Bending.

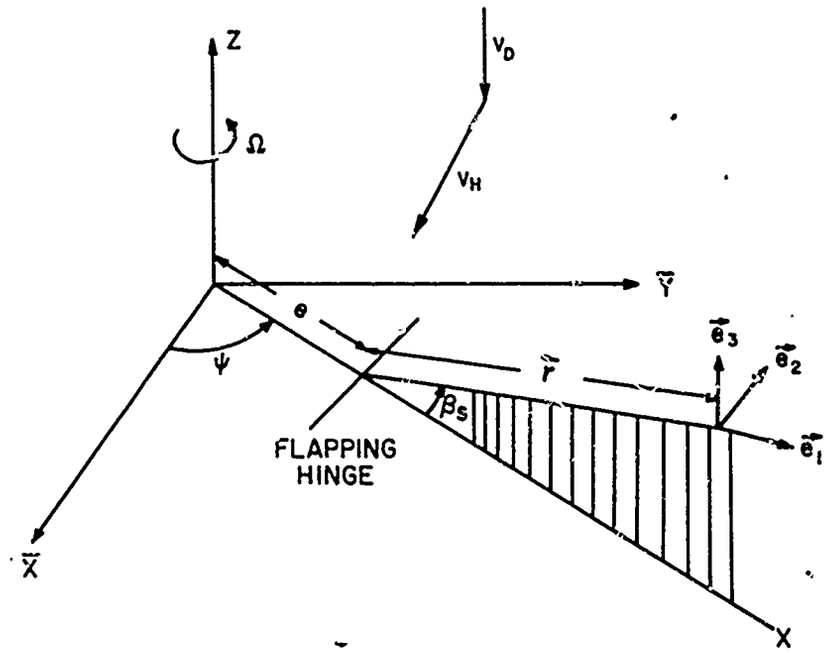

Figure 9. Air Velocity Relative to the Blade.

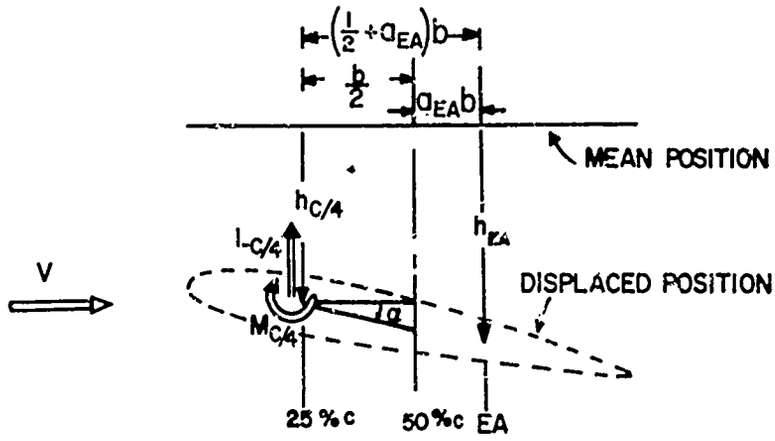

Figure 10. Relation Between the Displacement at 25% Chord and at the Elastic Axis.

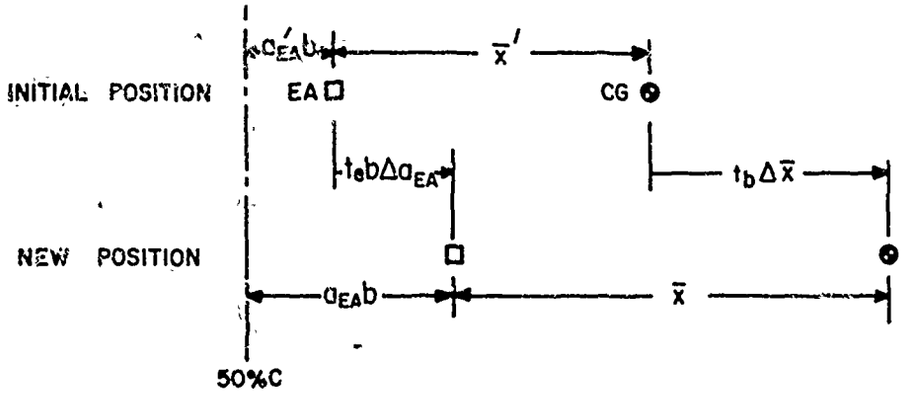

Figure 11. Arbitrary Chordwise Displacement of the Mass Balance Center of Gravity and the Elastic Axis.

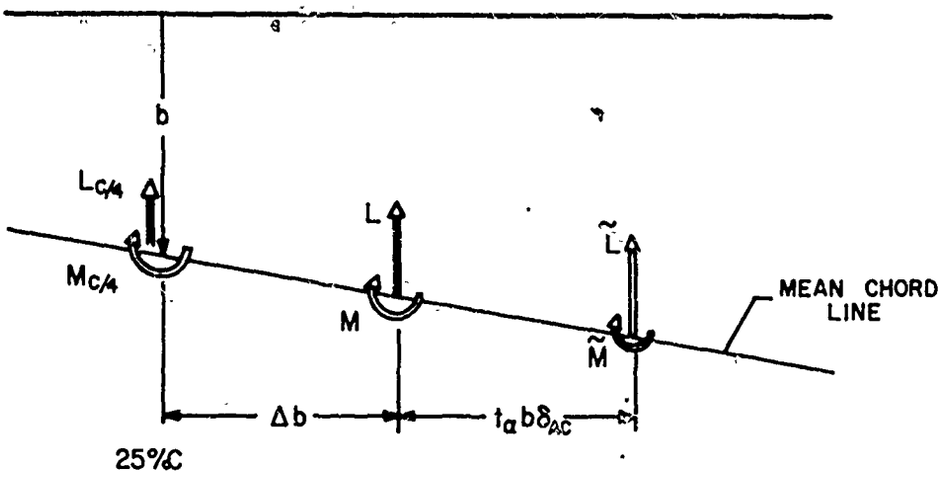

Figure 12. Arbitrary Chordwise Displacement of the Aerodynamic Center.

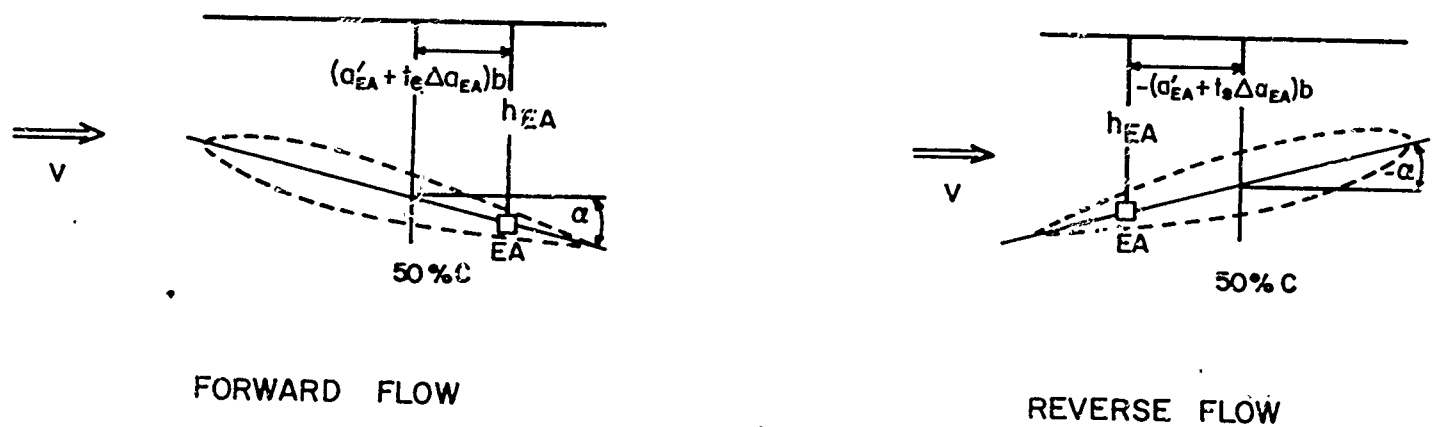

Figure 13. Geometric and Kinematic Relationship Between an Airfoil in Forward and Reverse Flow.

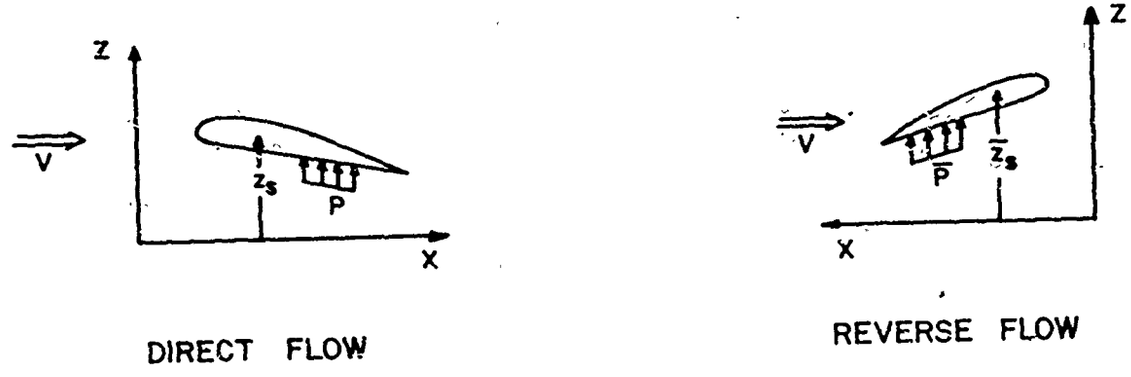

Figure 14. Notation Used for an Airfoil in Either Direct Flow or Reverse Flow.

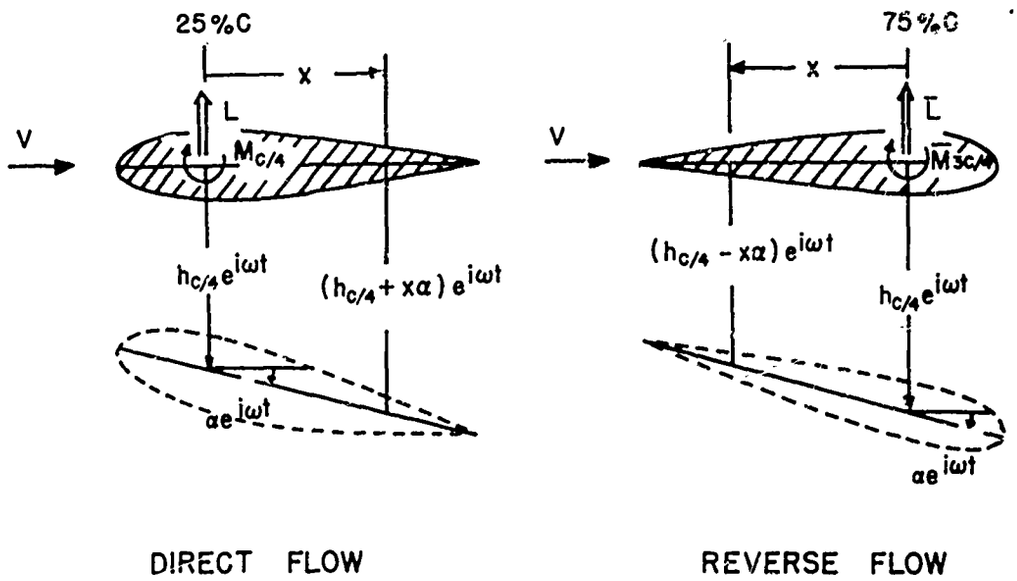

Figure 15. Notation Used for a Two-Dimensional Chordwise Rigid Airfoil in Direct Flow and Reverse Flow.

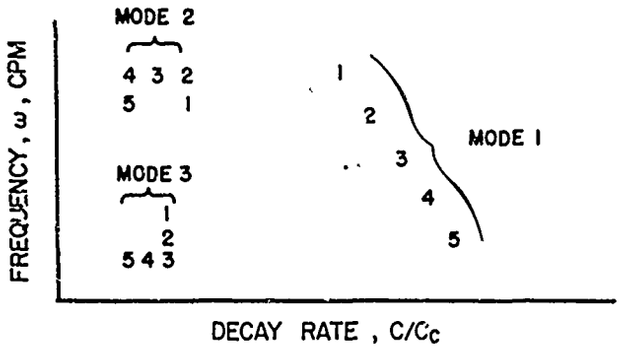

Figure 16. Example of the Use of the Frequency Versus Decay-Rate Digital Plot.

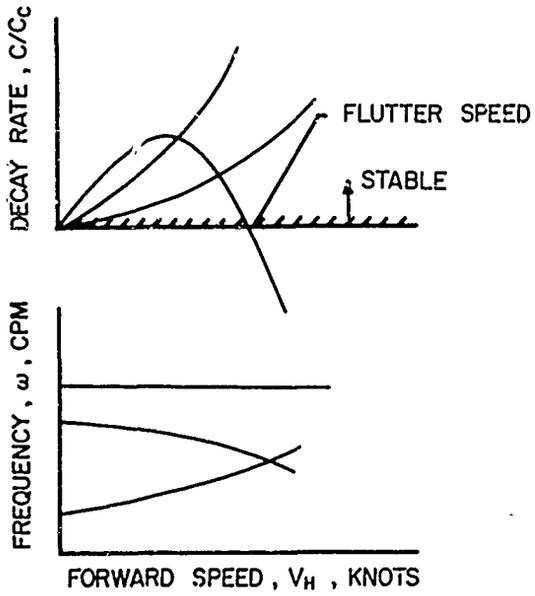

Figure 17. Example of the Digital Plot of Decay Rate and Frequency Versus Forward Velocity.

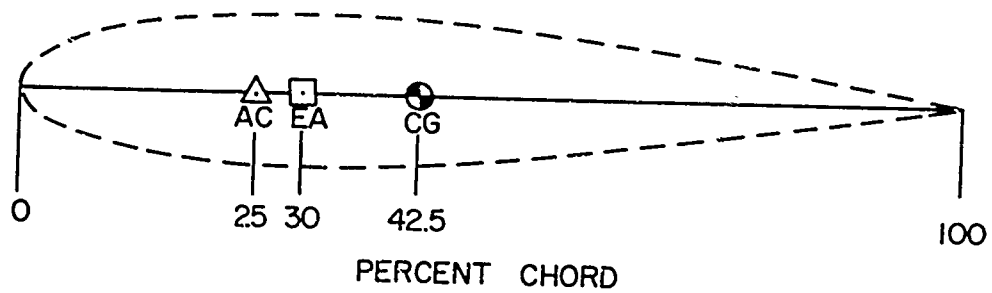

Figure 18. Position of the Aerodynamic Center, Elastic Axis, and Center of Gravity for the Computer Solution Test Case.

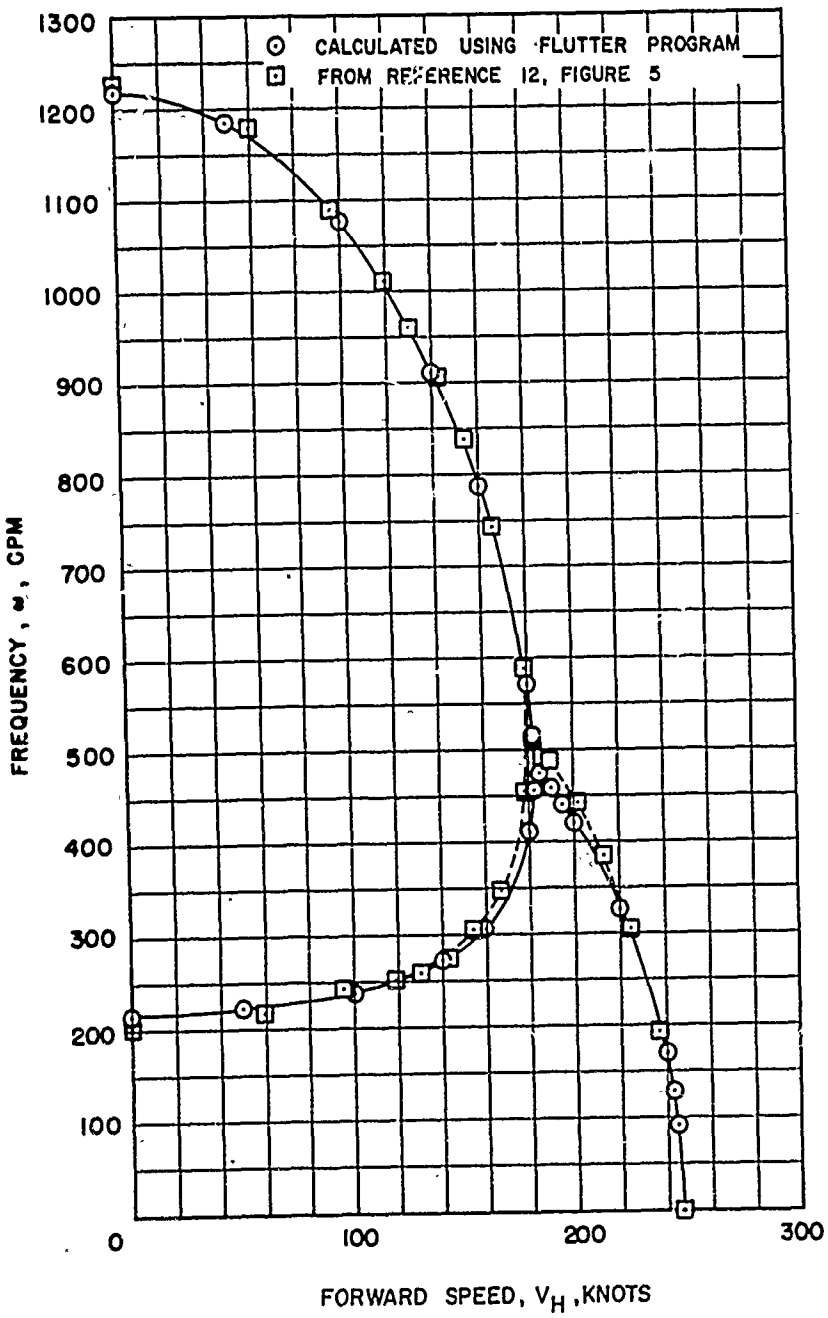

Figure 19. Comparison of Sikorsky Flutter Analysis Results for Flutter Frequency with the Solution of Reference 12.

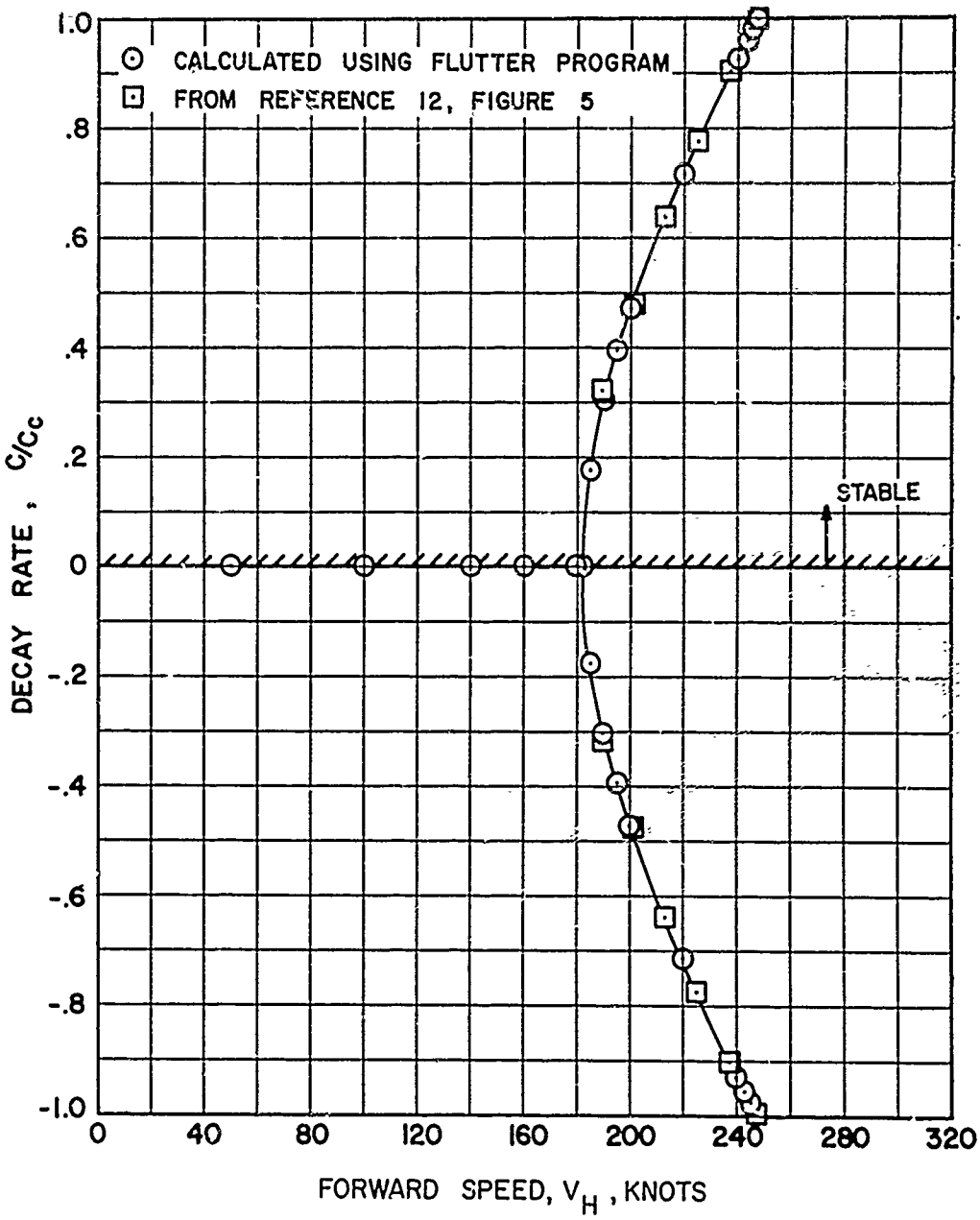

Figure 20. Comparison of Sikorsky Flutter Analysis Results for Decay Rate With the Solution of Reference 12.

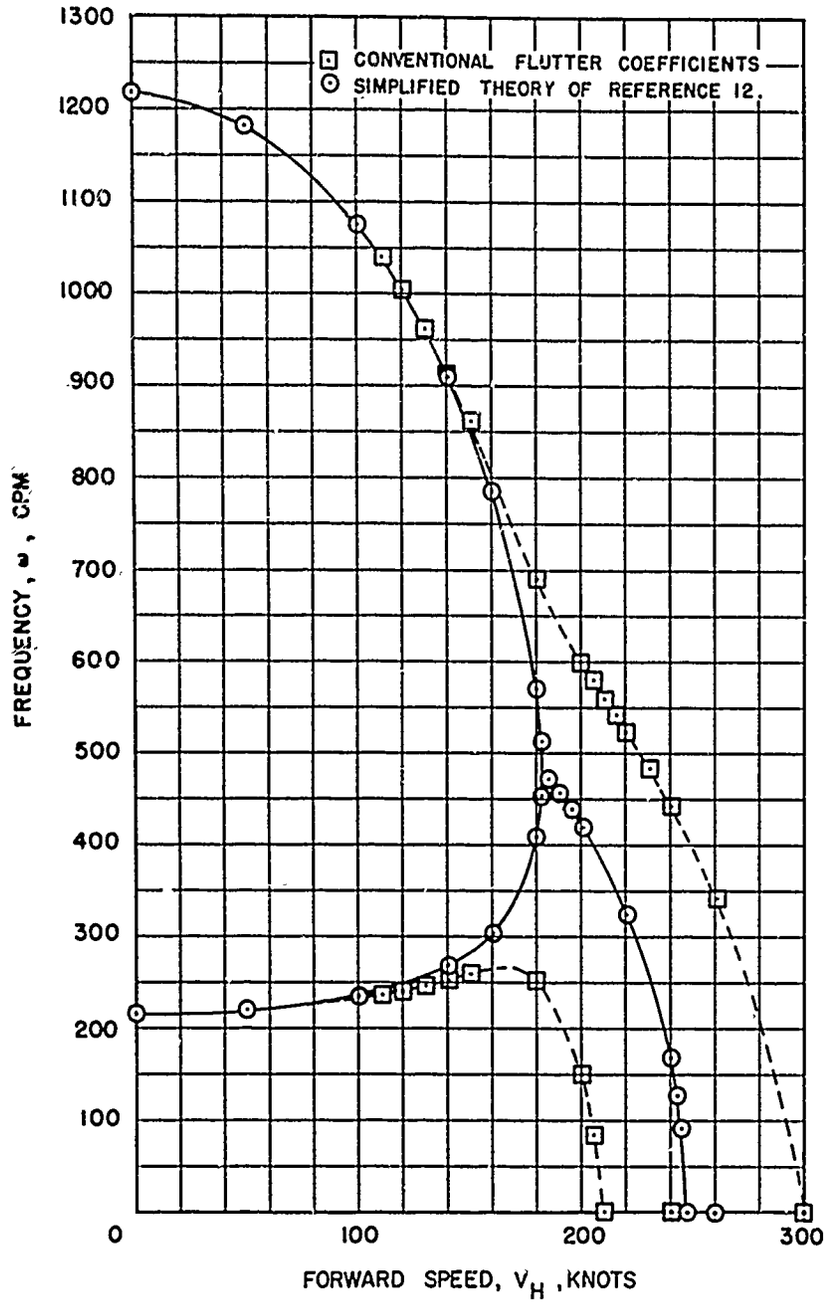

Figure 21. Comparison of the Sikorsky Flutter Analysis Results for Flutter Frequency with the Solution of Reference 12 Using Simplified Aerodynamics.

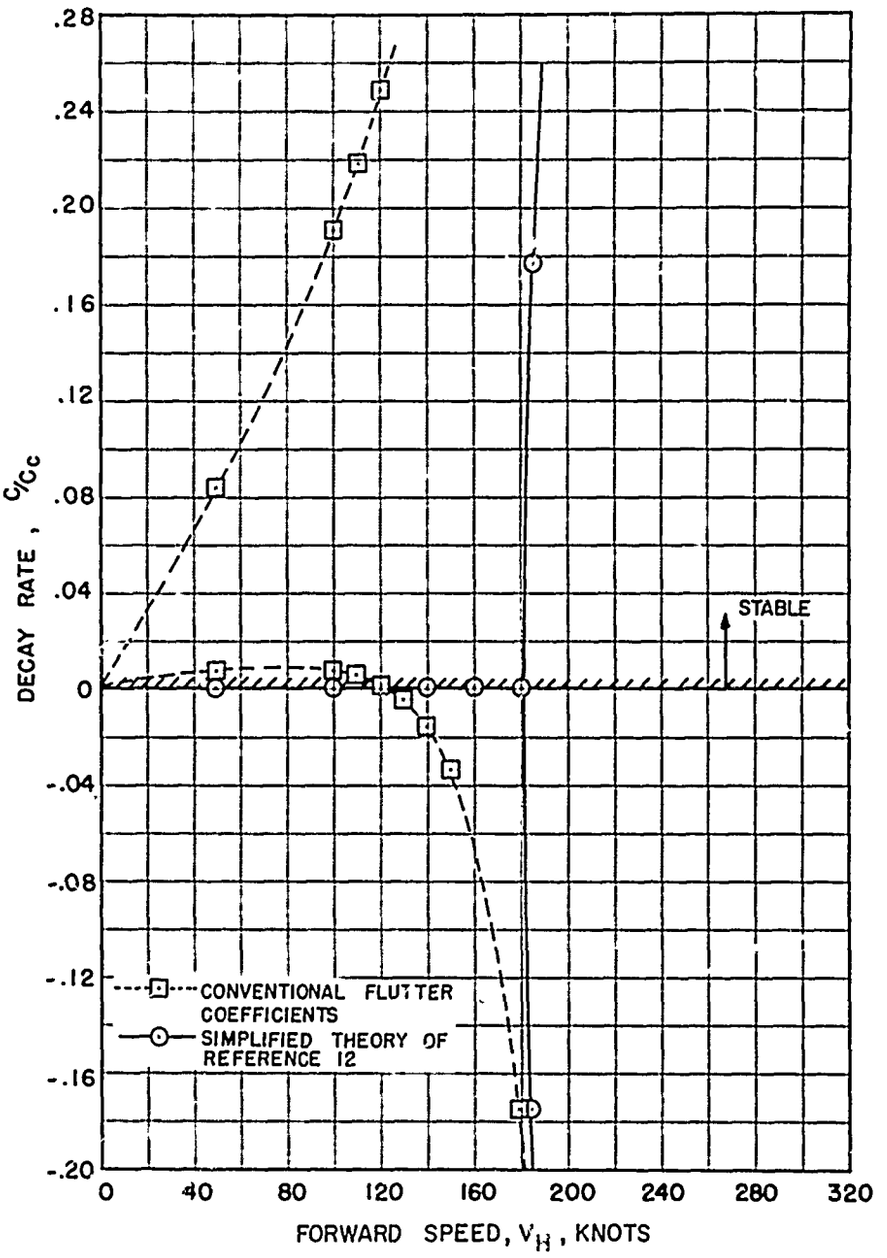

Figure 22. Comparison of the Sikorsky Flutter Analysis Results for Decay Rate with the Solution of Reference 12 Using Simplified Aerodynamics.

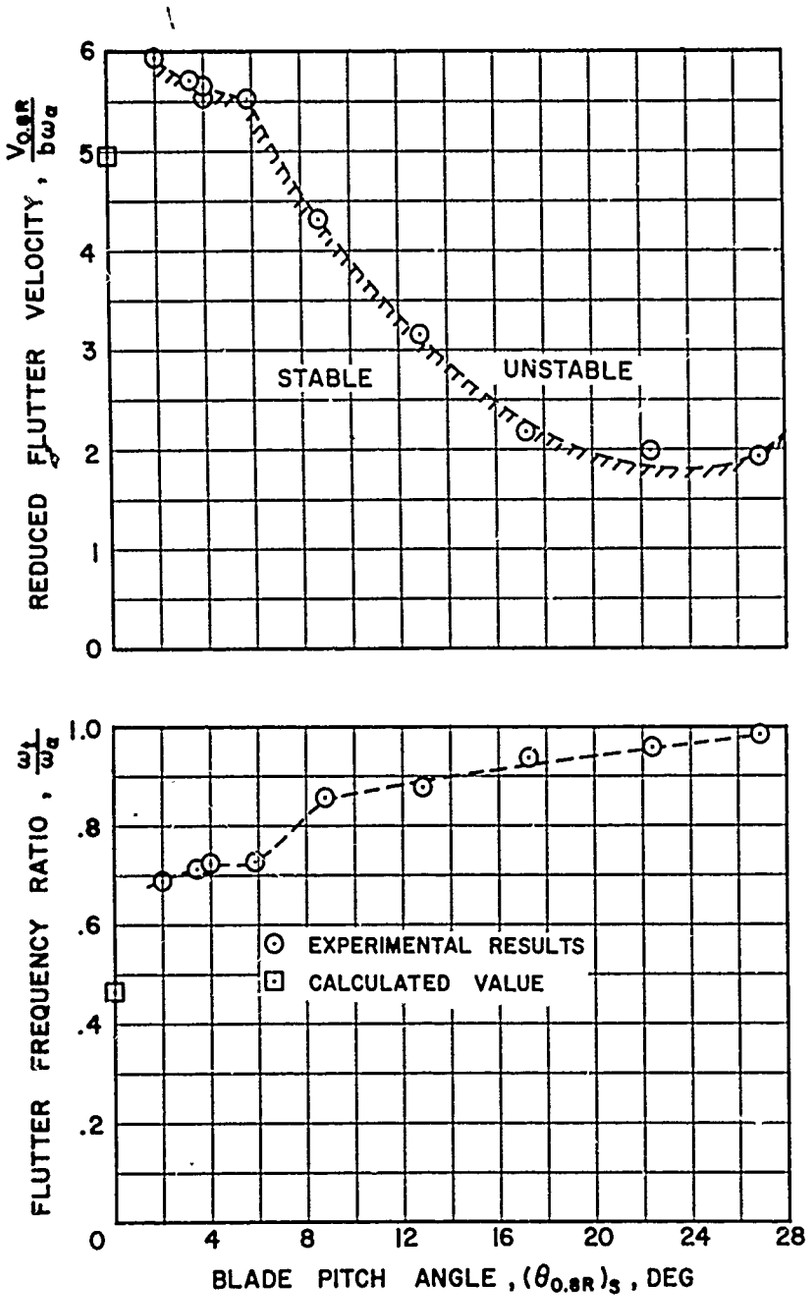

Figure 23. Comparison of Calculated and Measured Flutter Speeds for the Model Helicopter Blade NACA 23012 1(R).

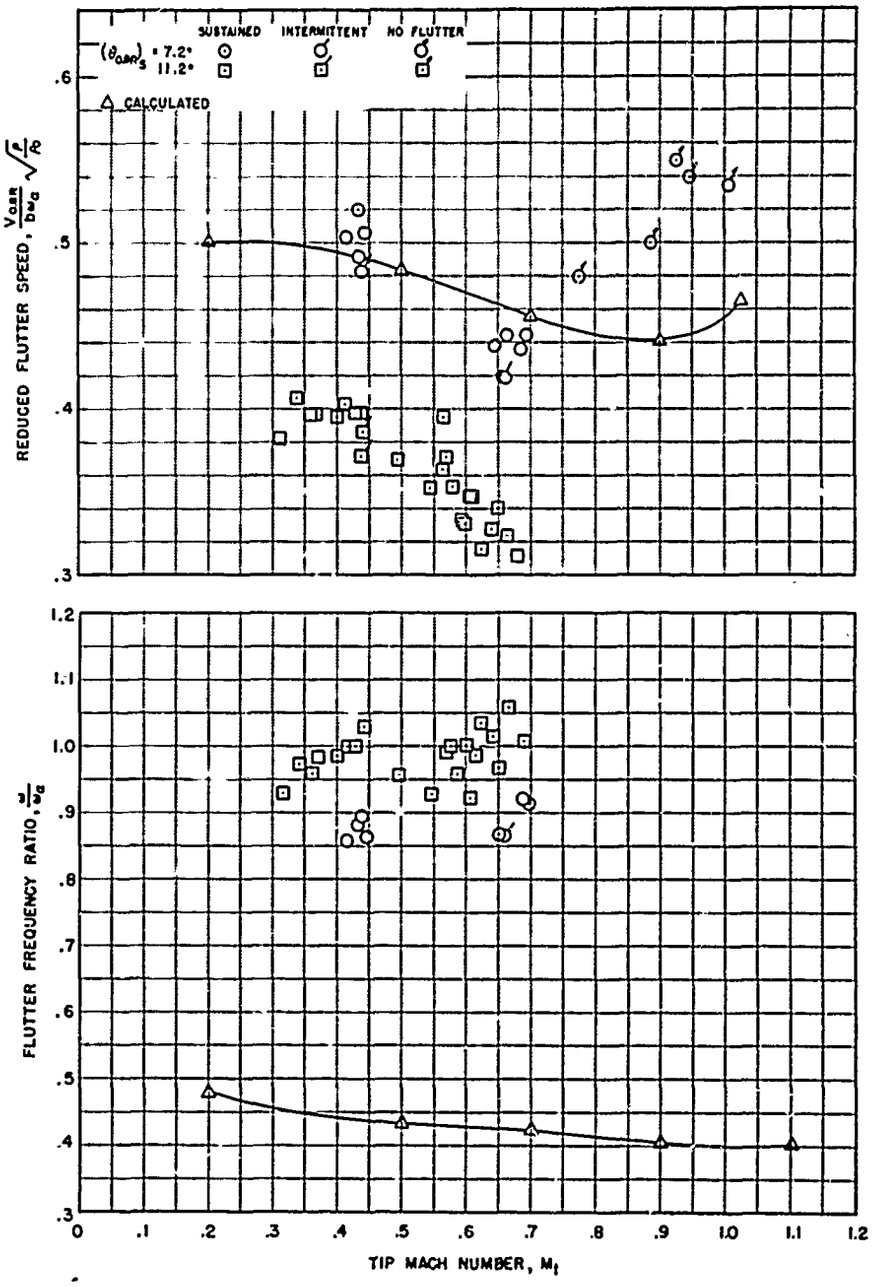

Figure 24. Comparison of Calculated and Measured Flutter Speeds for the Model Blade NACA 23012 2(R).

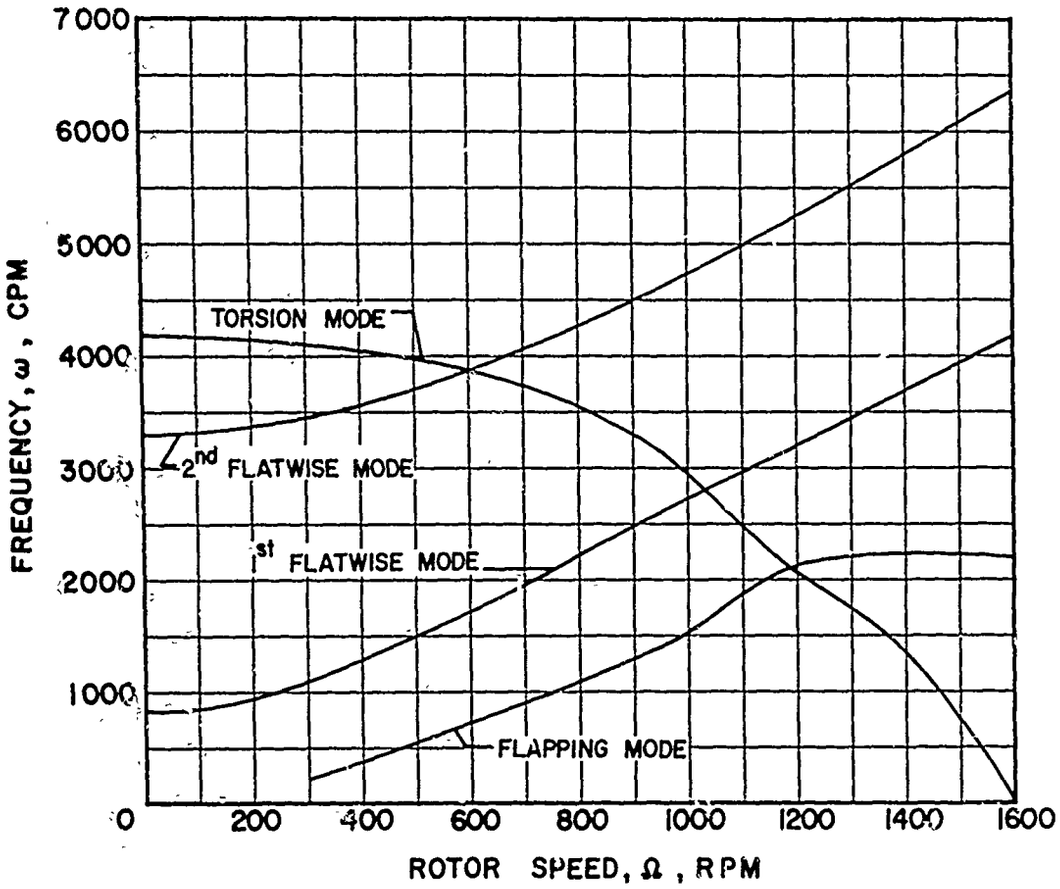

Figure 25. Variation of Solution Frequency With Change in Rotor Speed for the Model Blade NACA 23012 2(R); Tip Mach Number < 0.2.

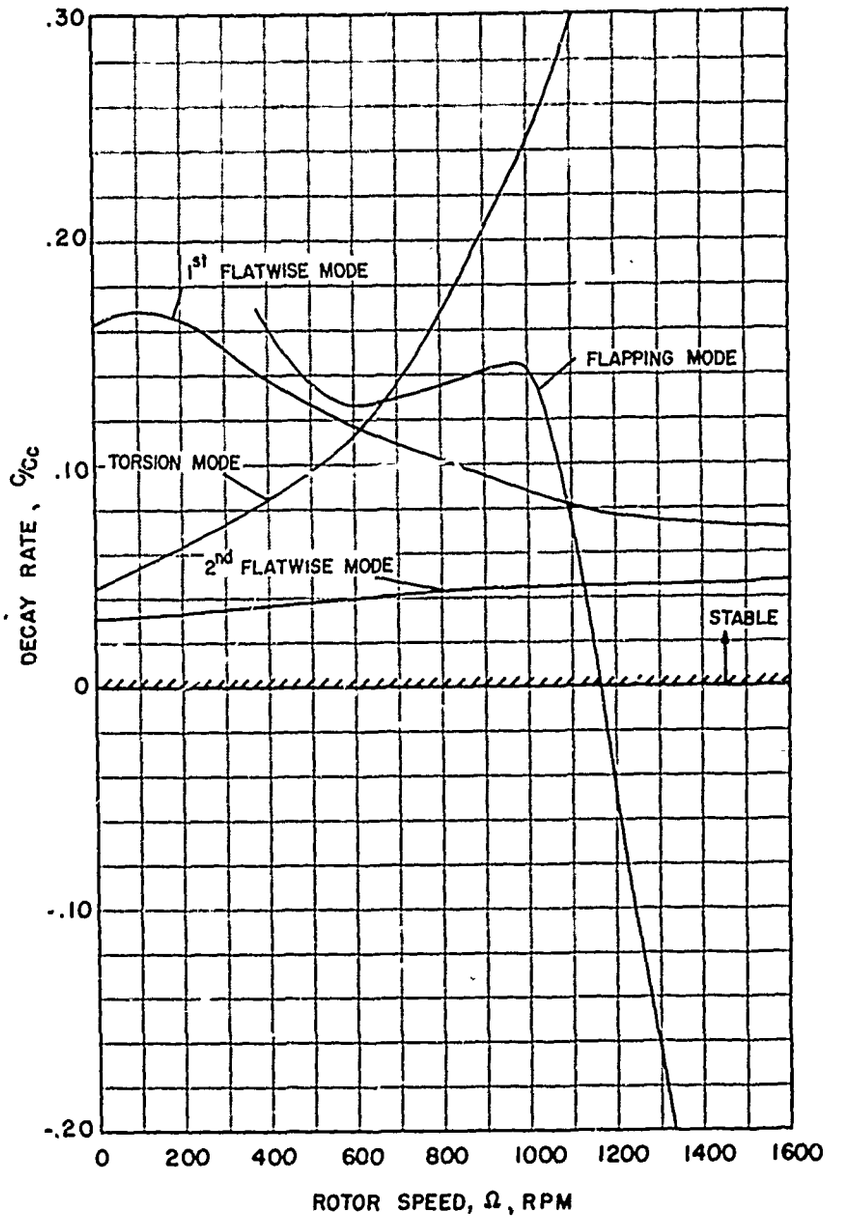

Figure 26. Variation of Solution Decay Rate With Change in Rotor Speed for the Model Blade NACA 23012 2(R); Tip Mach Number < 0.2.

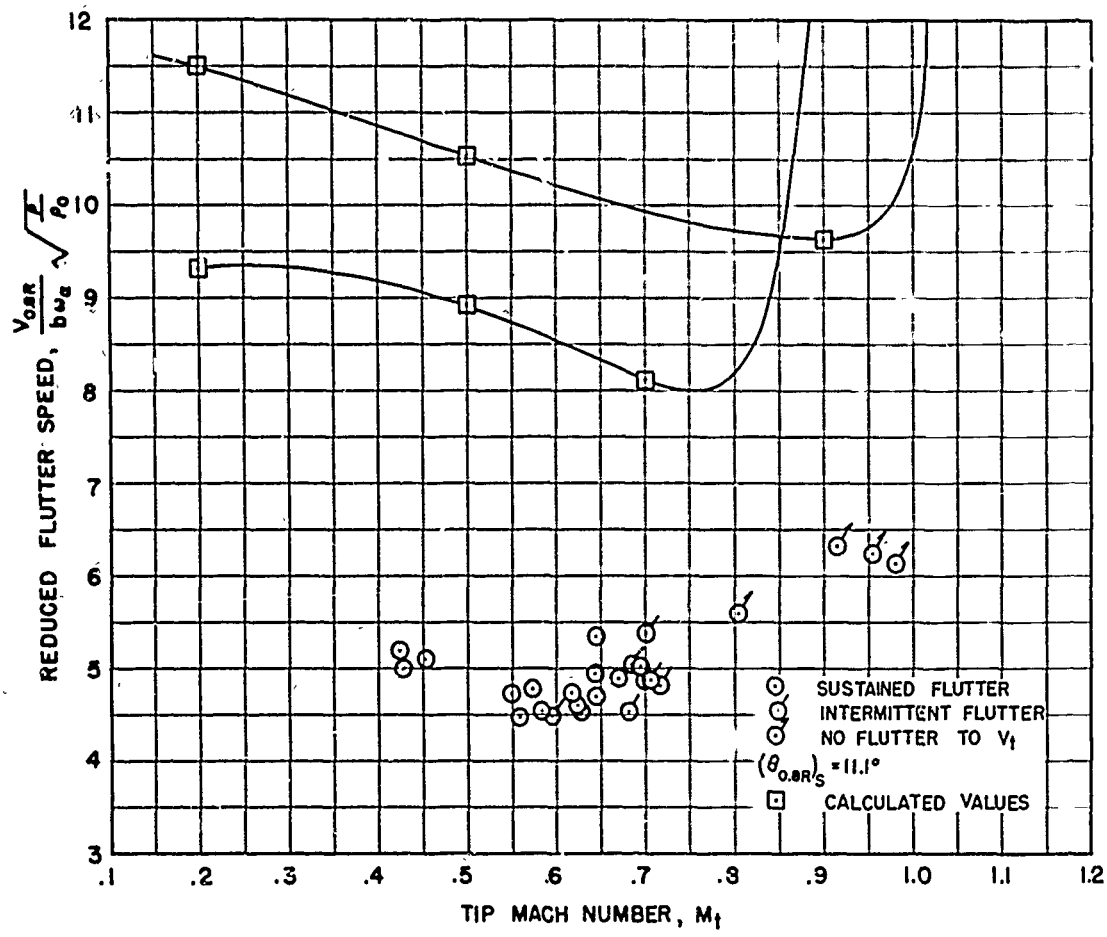

Figure 27. Comparison of Calculated and Measured Flutter Speeds for the Model Blade NACA 23012 2(F).

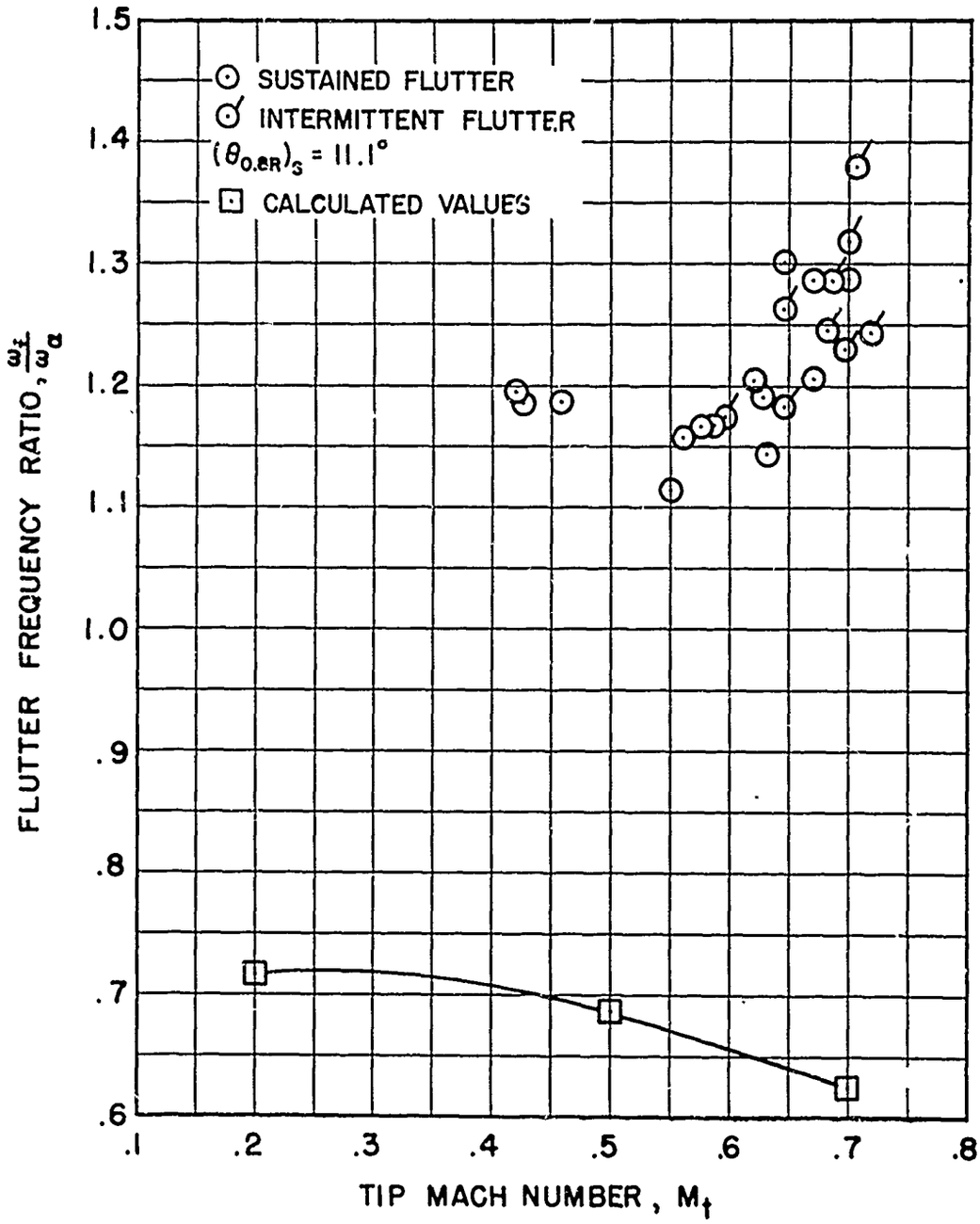

Figure 27. Concluded.

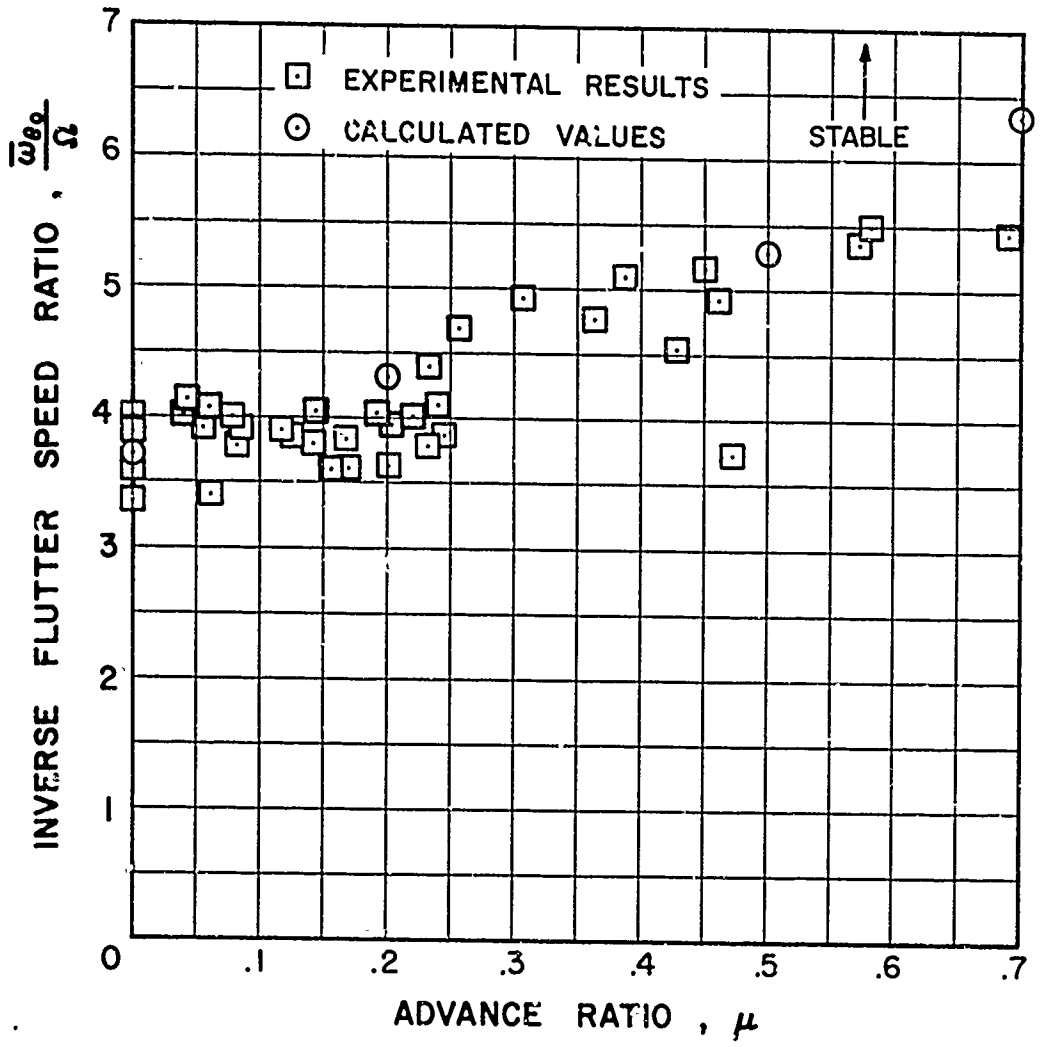

Figure 28. Comparison of Calculated and Measured Flutter Speeds for the CAL Blade Model 4; $\bar{X}_E/C = .139$, $\bar{\omega}_{\phi_1}/\bar{\omega}_{\theta_0} = .63$.

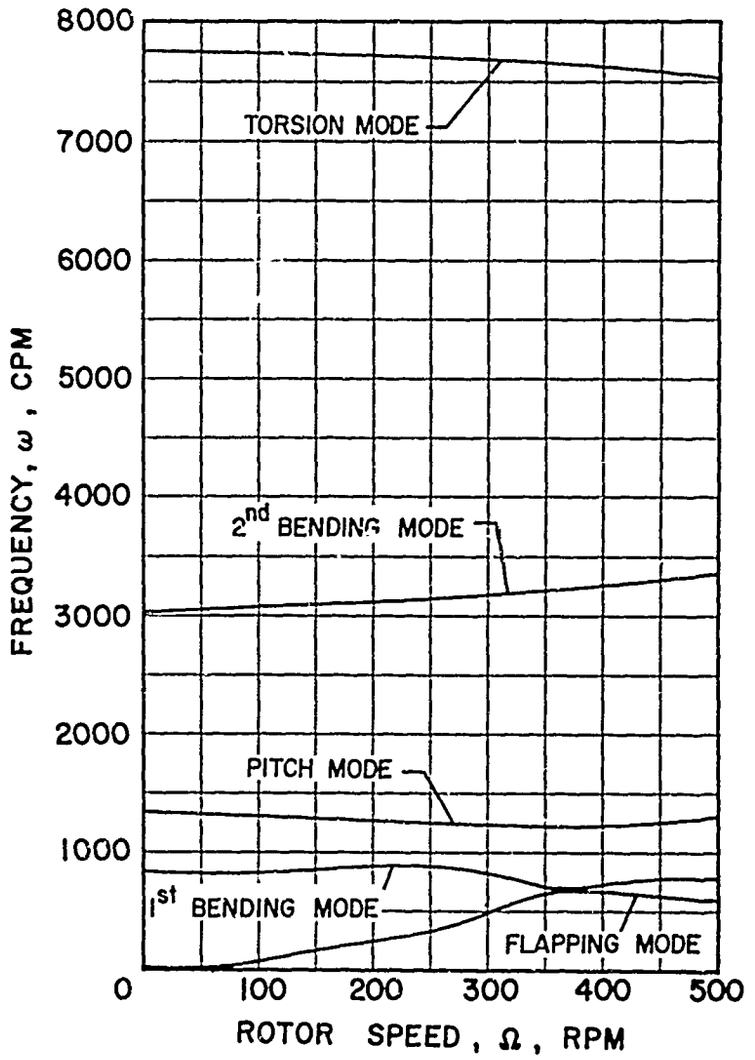

Figure 29. Variation of Solution Frequency With Change in Rotor Speed for the CAL Blade Model 4; $\bar{X}_E/C = .139$, $\bar{\omega}_{\phi_1}/\bar{\omega}_{\theta_0} = .63$, $\mu = 0$.

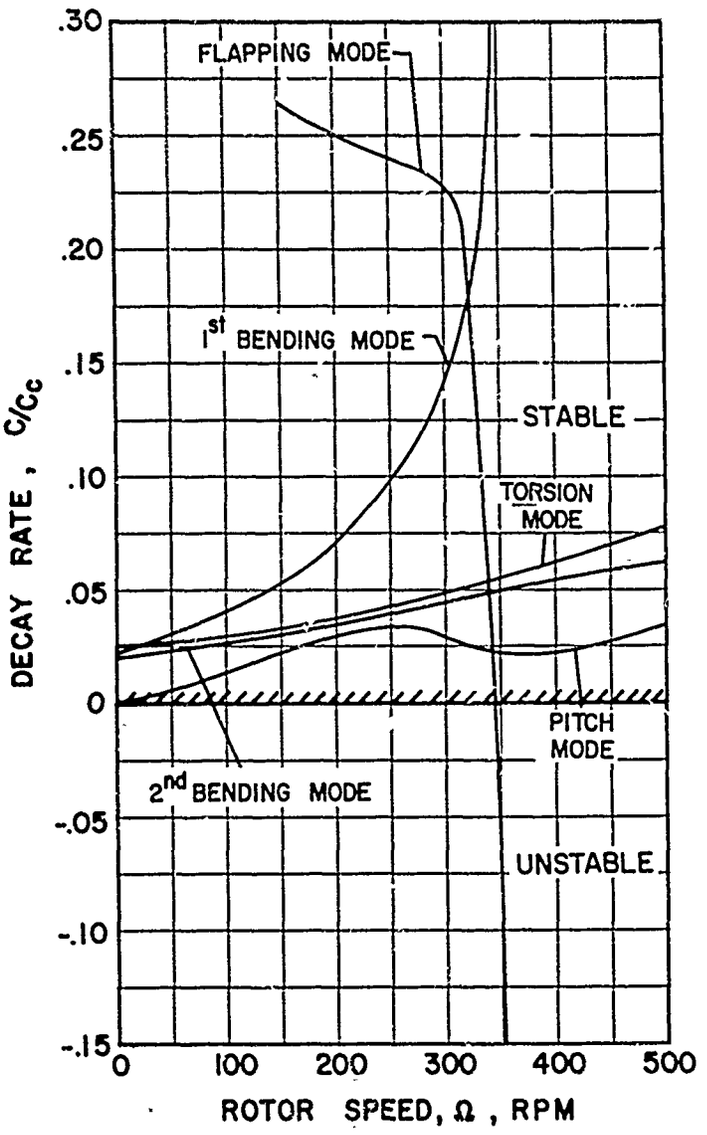

Figure 30. Variation of Solution Decay Rate With Change in Rotor Speed for the CAL Blade Model 4; $\bar{X}_E/C = .139$, $\bar{\omega}_{\phi_1}/\bar{\omega}_{\theta_0} = .63$, $\mu = 0$.

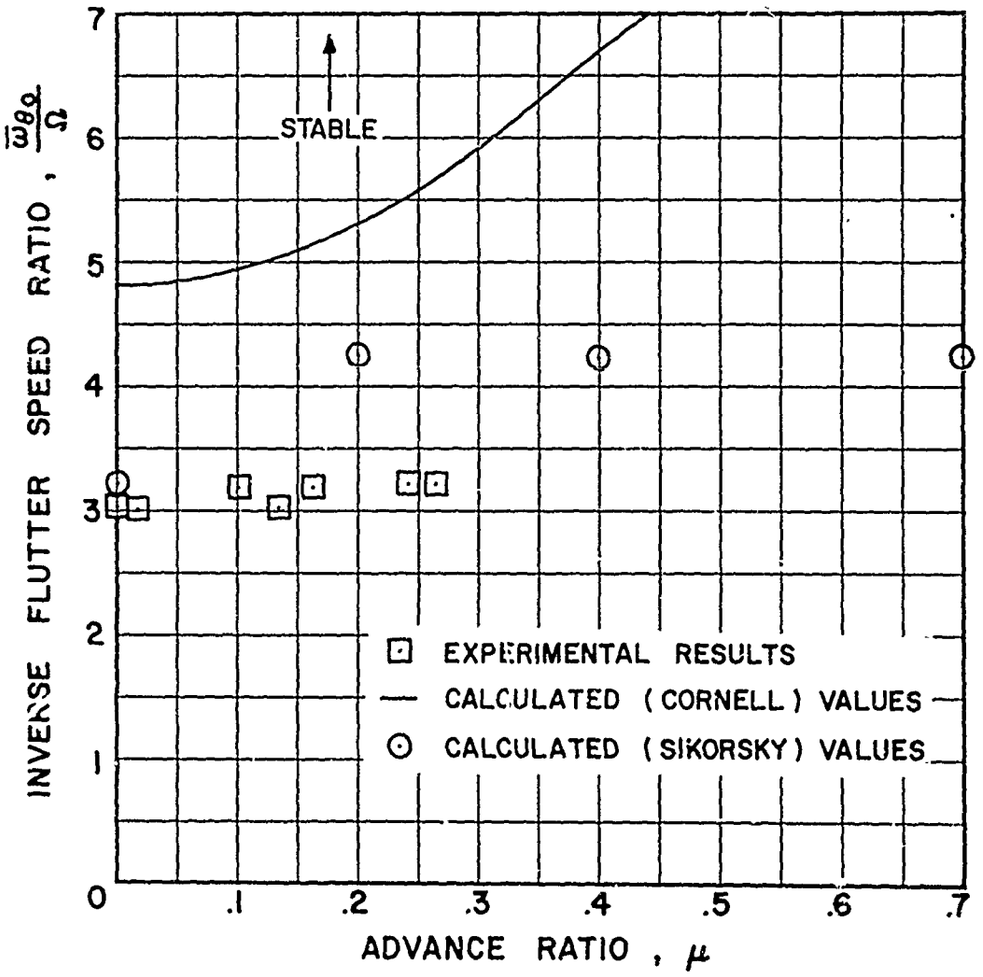

Figure 31. Comparison of Calculated and Measured Flutter Speeds for the CAL Blade Model 4; $\bar{x}_E/C = .139$, $\bar{\omega}_{\phi_1}/\bar{\omega}_{\theta_0} = 1.31$.

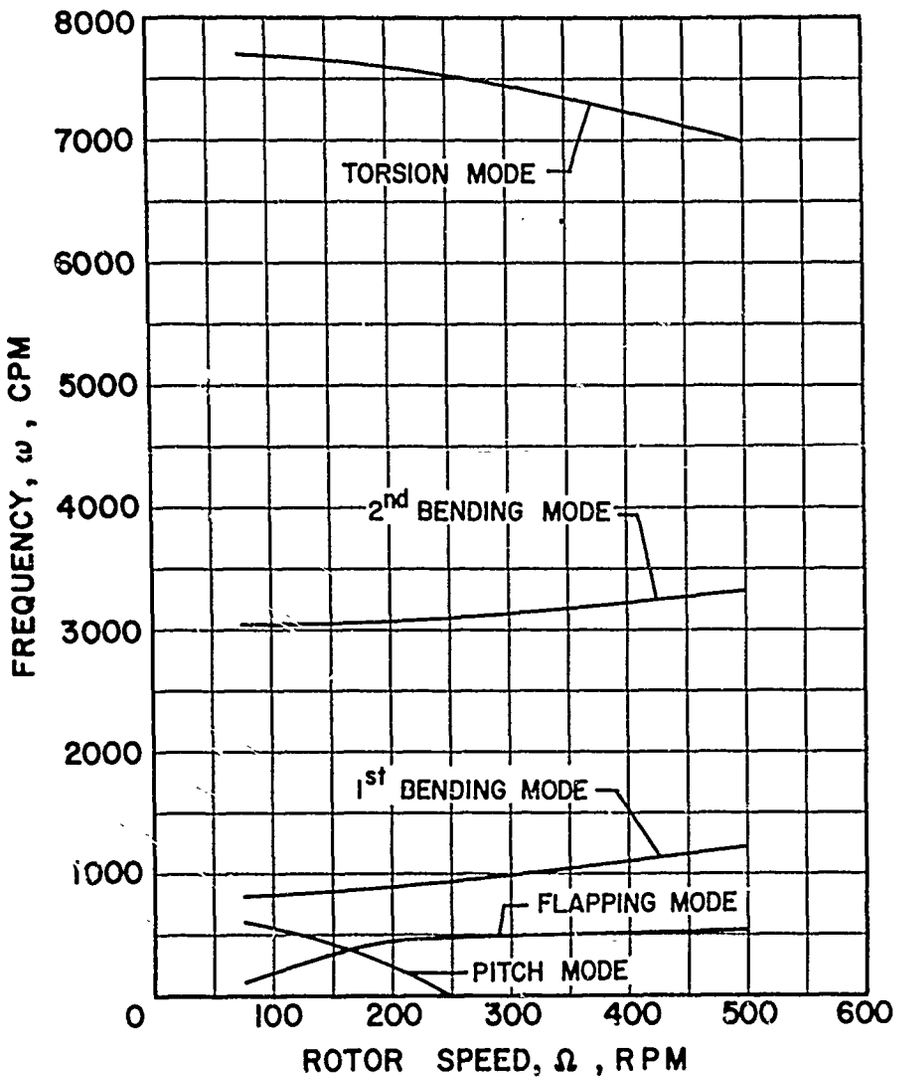

Figure 32. Variation of Solution Frequency With Change in Rotor Speed for the CAL Blade Model 4; $\bar{x}_E/C = .139$, $\bar{\omega}_{\phi_1}/\bar{\omega}_{\theta_0} = .63$, $\mu = .5$.

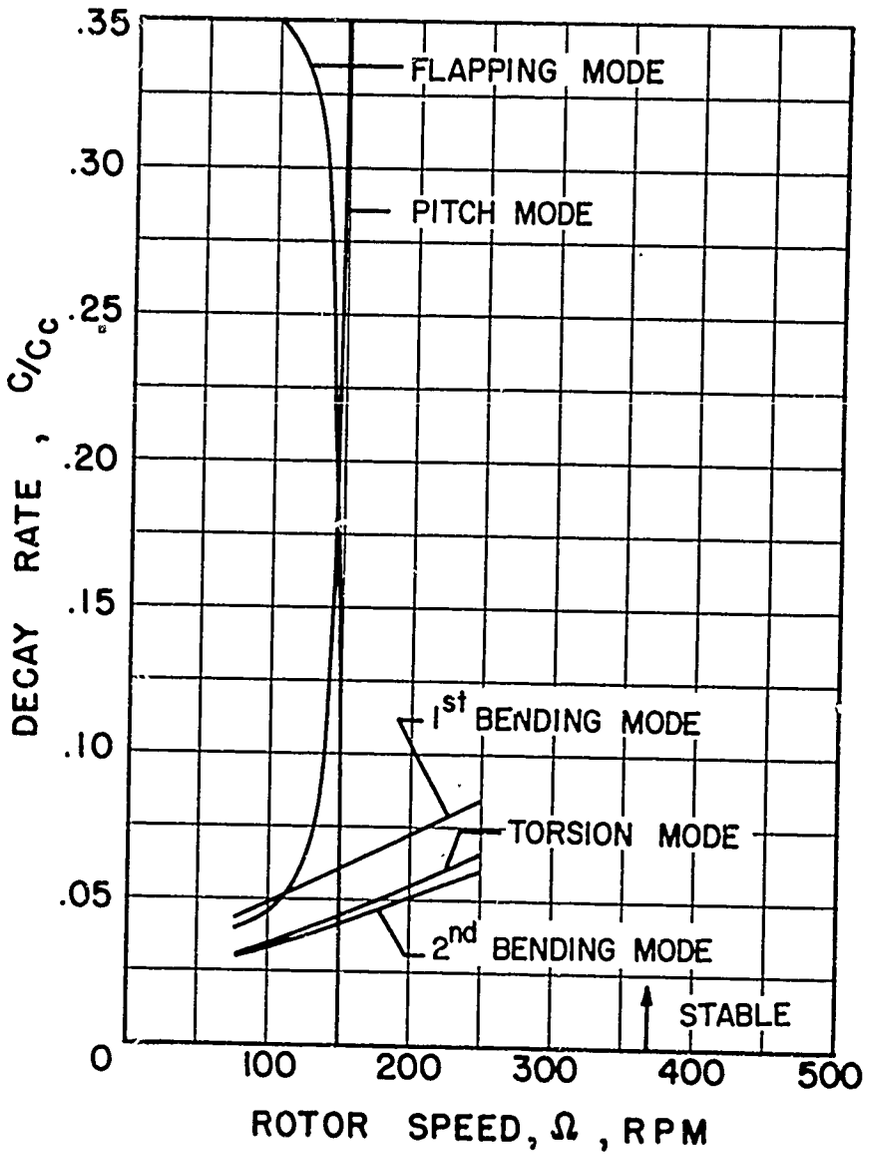

Figure 33. Variation of Solution Decay Rate With Change in Rotor Speed for the CAL Blade Model 4; $\bar{x}_E/C = .139$, $\bar{\omega}_{\phi_1}/\bar{\omega}_{\theta_0} = .63$, $\mu = .5$.

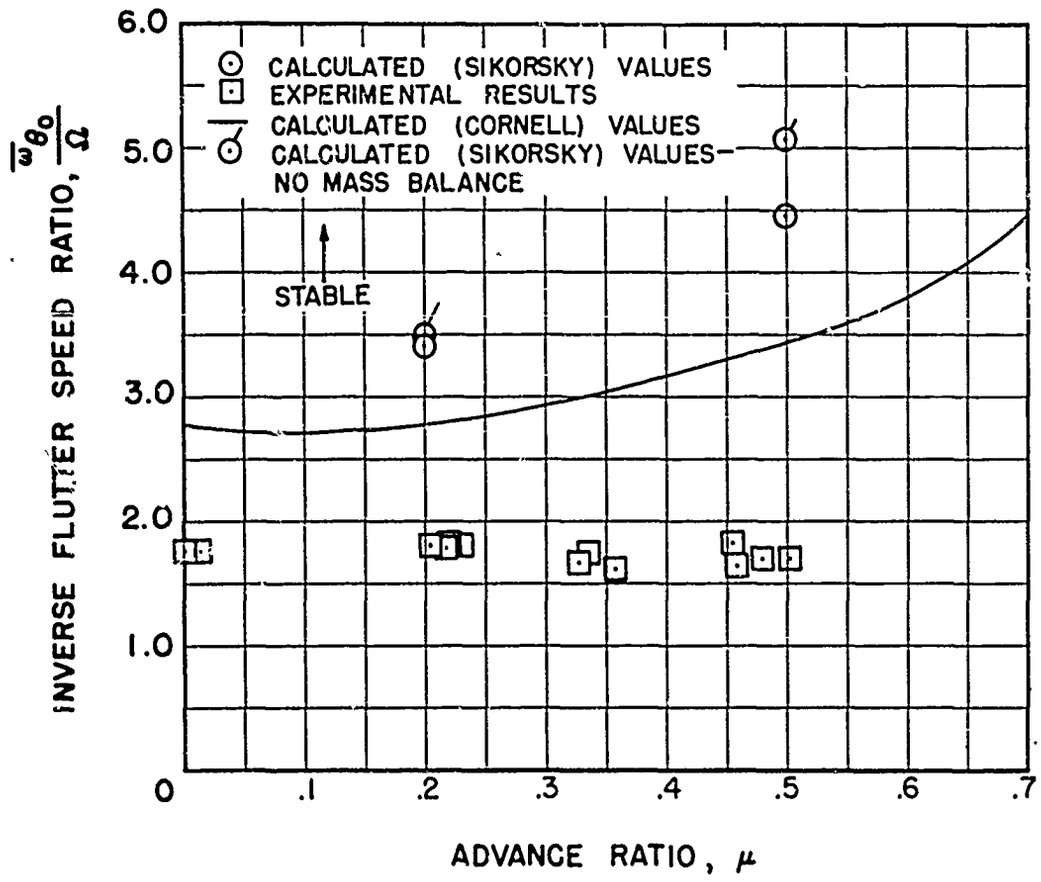

Figure 34. Comparison of Calculated and Measured Flutter Speeds for the CAL Blade Model 4; $\overline{X}_E/C = .044$, $\overline{\omega}_{\phi_1}/\overline{\omega}_{\theta_0} = 1.05$

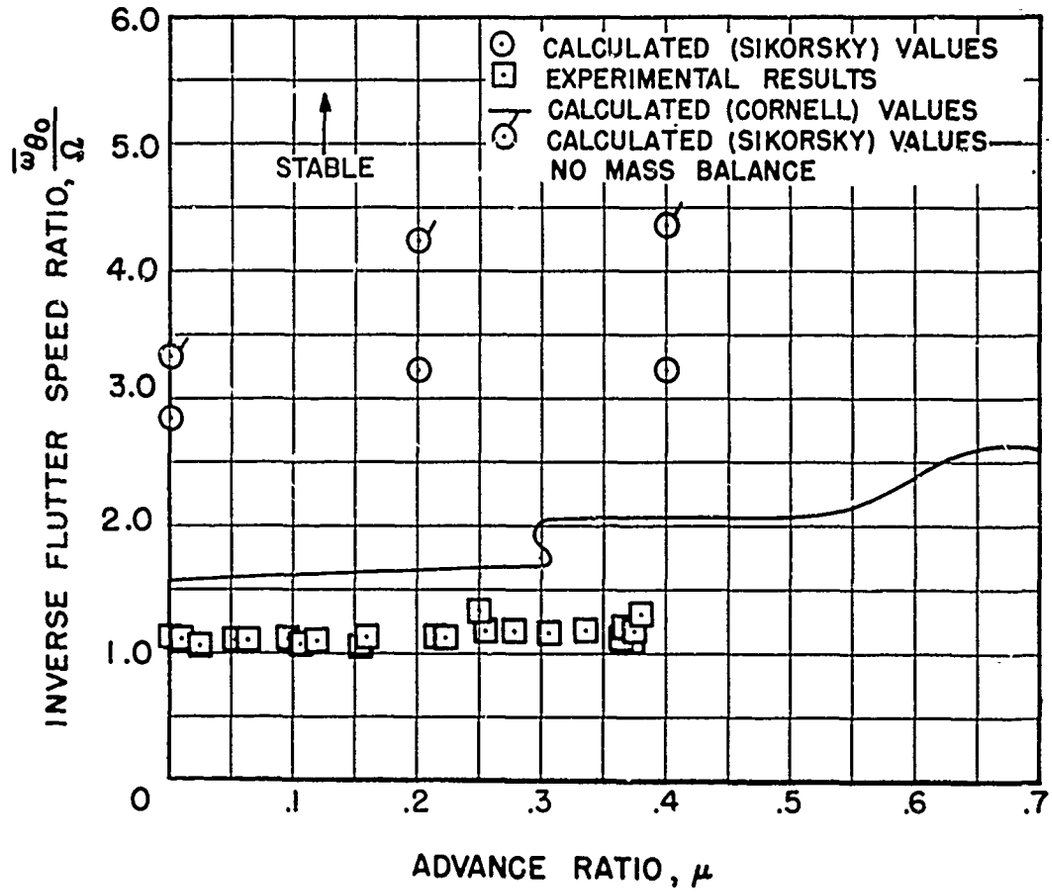

Figure 35. Comparison of Calculated and Measured Flutter Speeds for the CAL Blade Model 4; $\bar{x}_E/C = .0036$, $\bar{\omega}_{\phi_1}/\bar{\omega}_{\theta_0} = 1.03$.

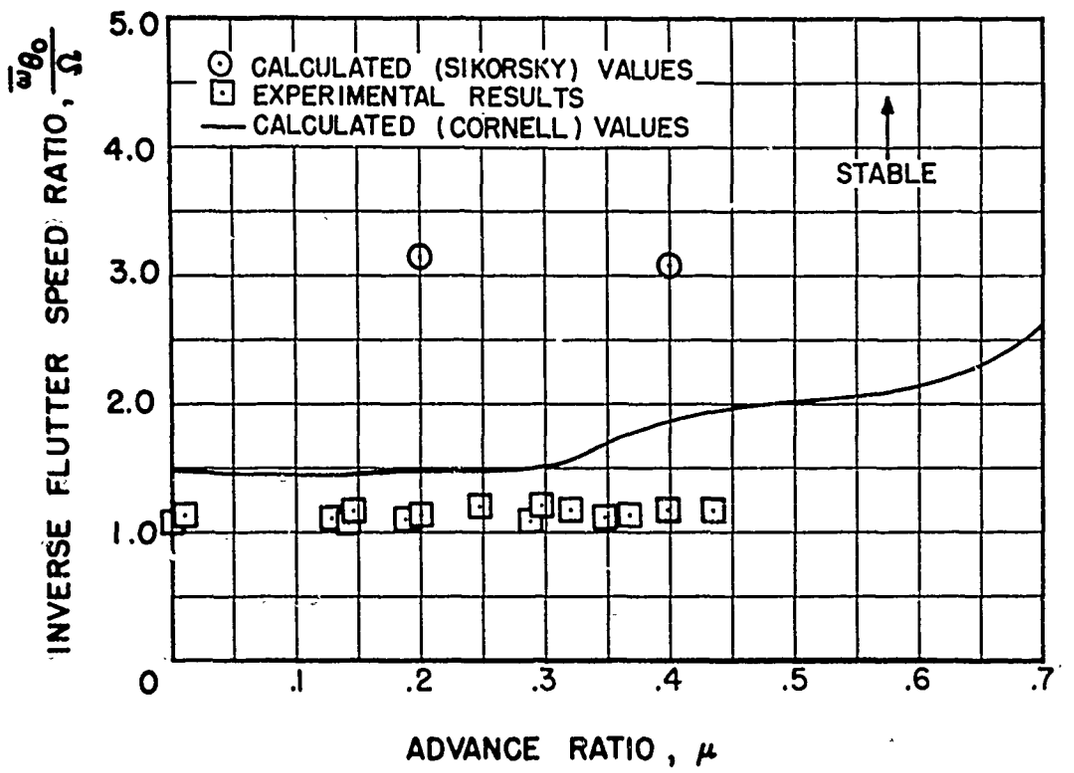

Figure 36. Comparison of Calculated and Measured Flutter Speeds for the CAL Blade Model 4; $\bar{X}_E/C = .0036$, $\bar{\omega}_{\phi_1}/\bar{\omega}_{\theta_0} = 1.44$.

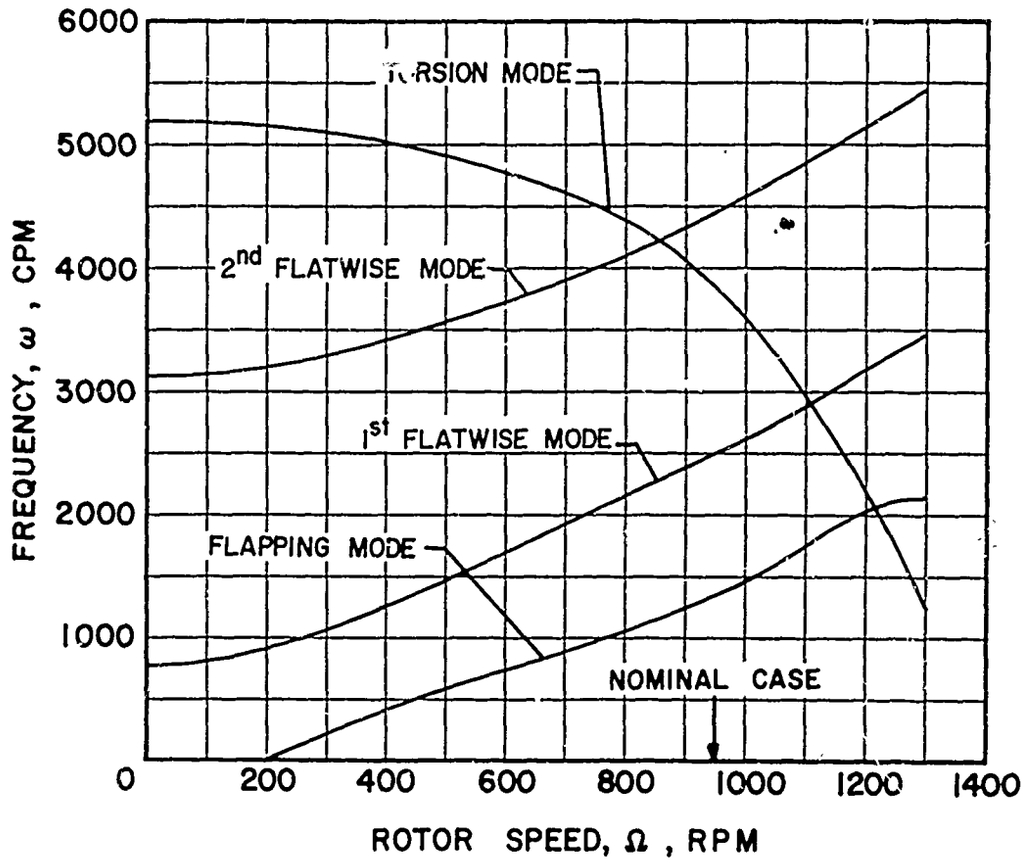

Figure 37. Variation of Solution Frequency With Change in Rotor Speed for the Nominal Articulated Blade; $\mu = 0$.

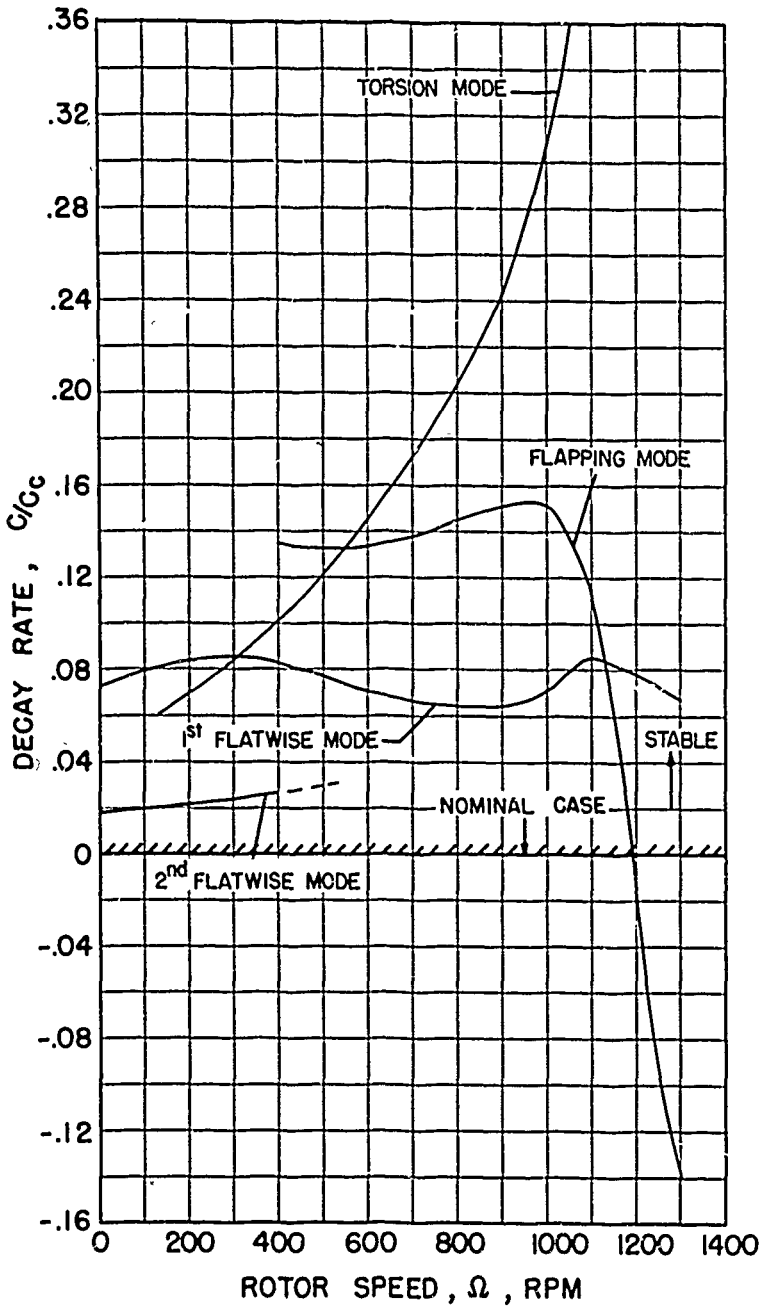

Figure 38. Variation of Solution Decay Rate With Change in Rotor Speed for the Nominal Articulated Blade; $\mu = 0$.

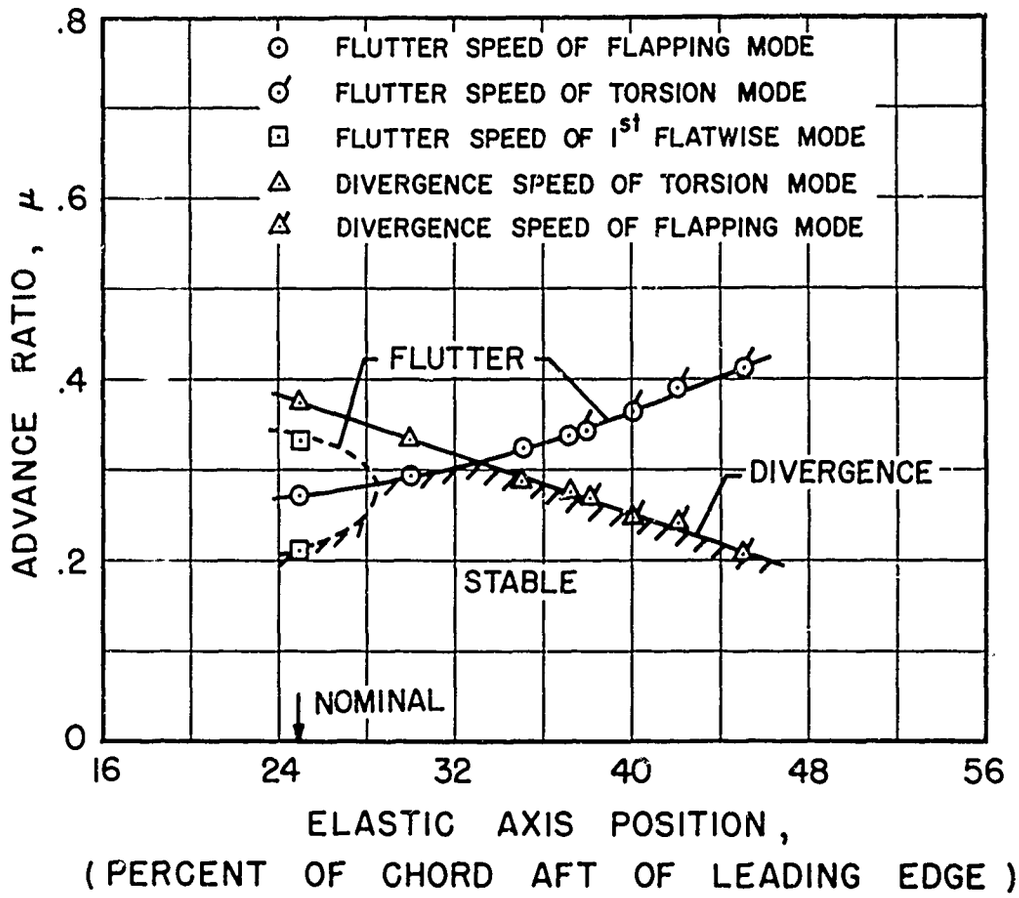

Figure 39. Varying the Chordwise Position of the Elastic Axis for an Articulated Blade.

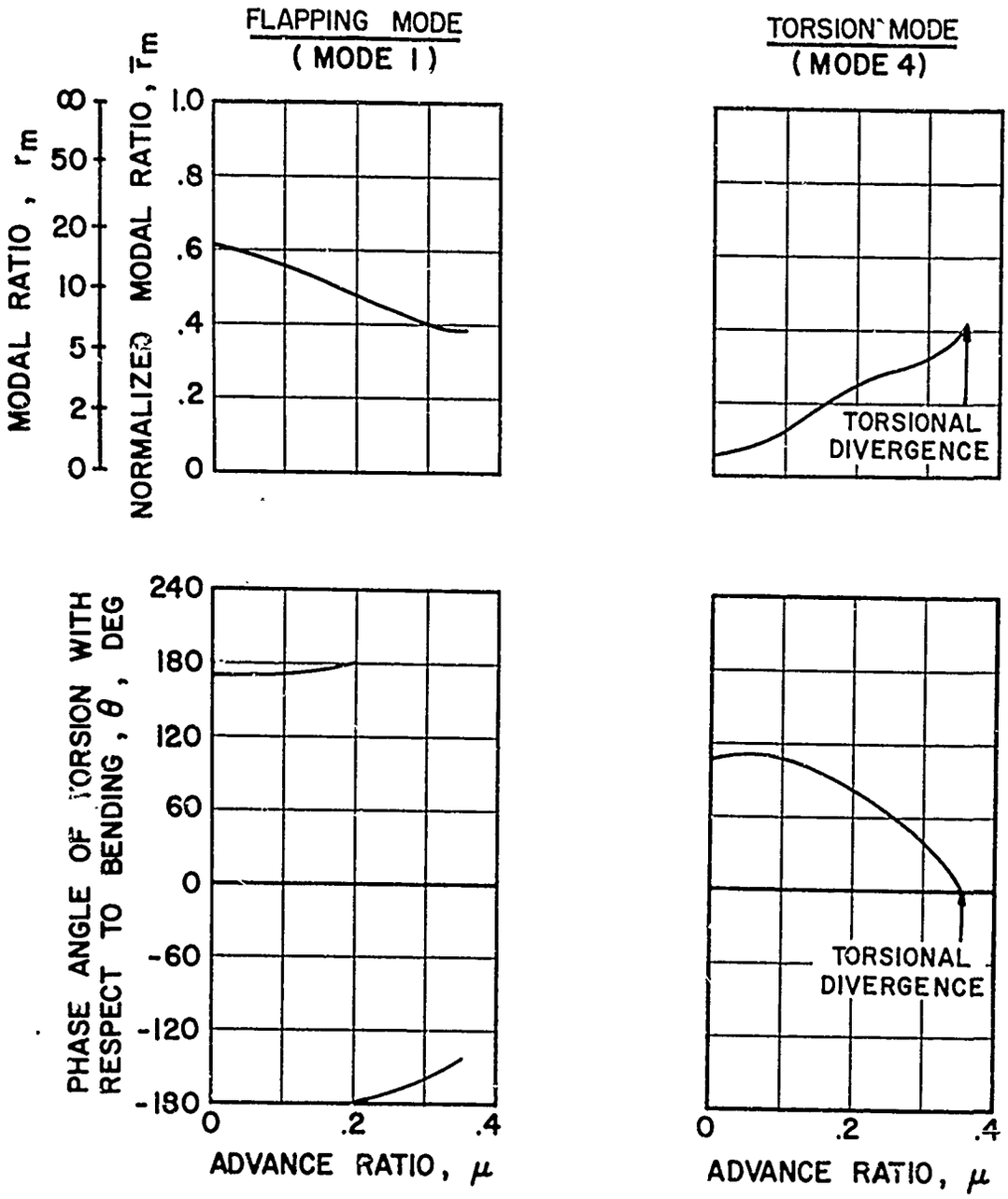

Figure 40. Variation of Modal Amplitude Ratio and Phase Angle With Change in Advance Ratio for the Nominal Articulated Blade.

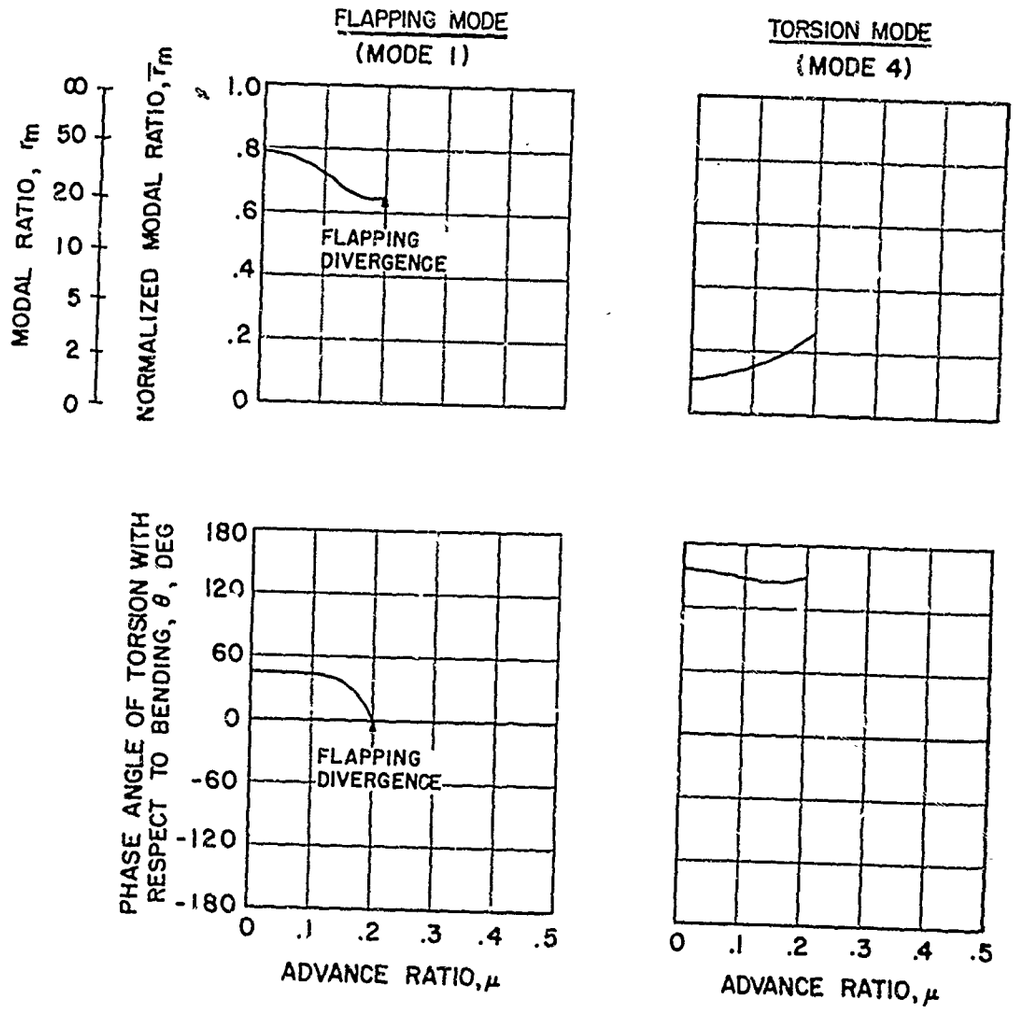

Figure 41. Variation of Modal Amplitude Ratio and Phase Angle With Change in Advance Ratio for the Articulated Blade, Case 1.A2.

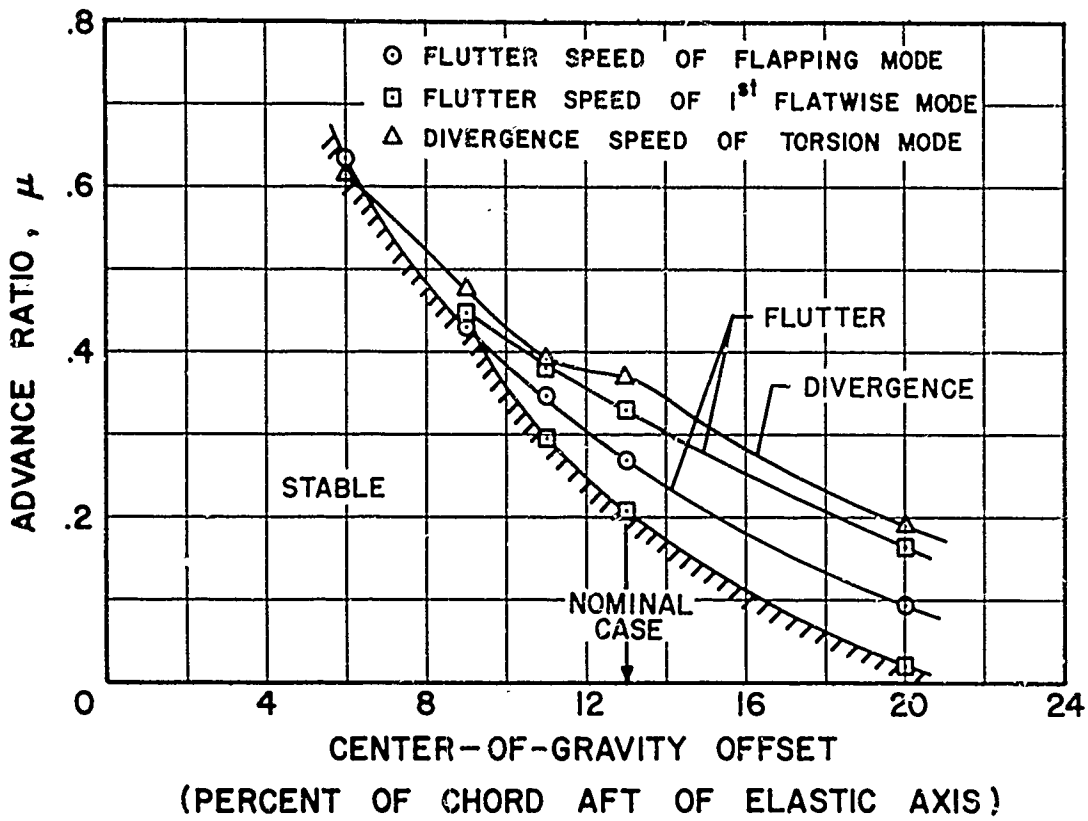

Figure 42. Varying the Chordwise Position of the Center of Gravity for an Articulated Blade.

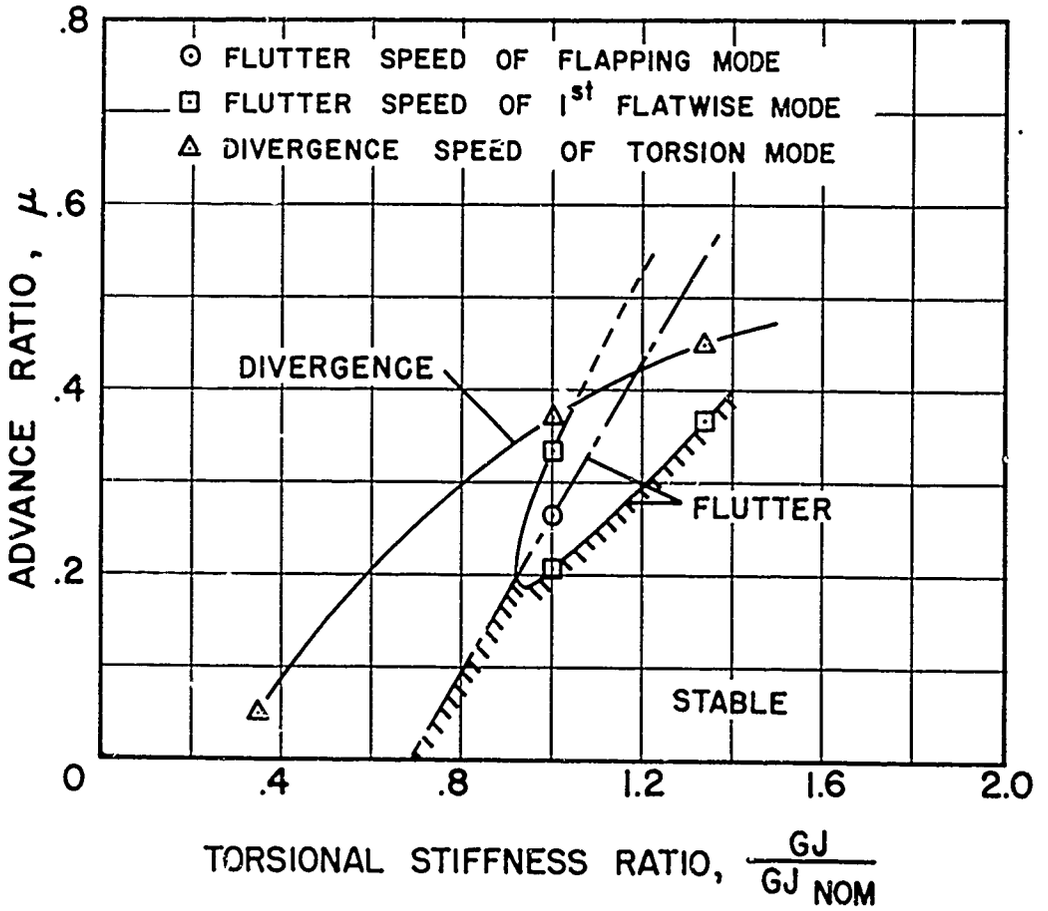

Figure 43. Varying the Blade Torsional Stiffness for an Articulated Blade; GJ_{NOM} = 12,436 Lb-In^2.

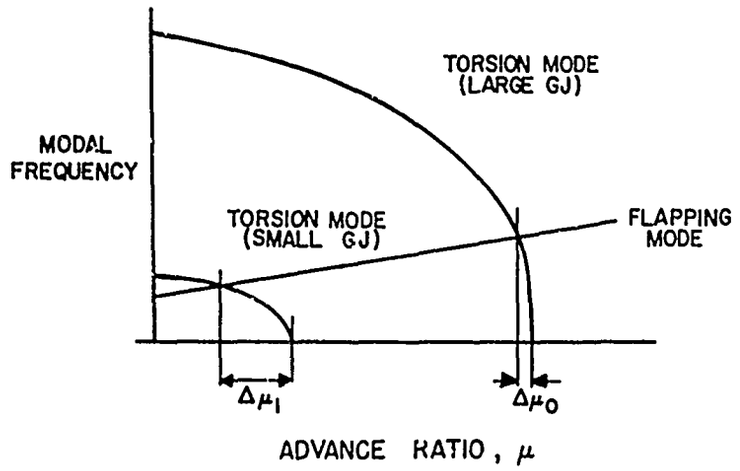

Figure 44. Typical Variation of Torsion Frequency With Change in Advance Ratio for Large Center-of-Gravity Offset.

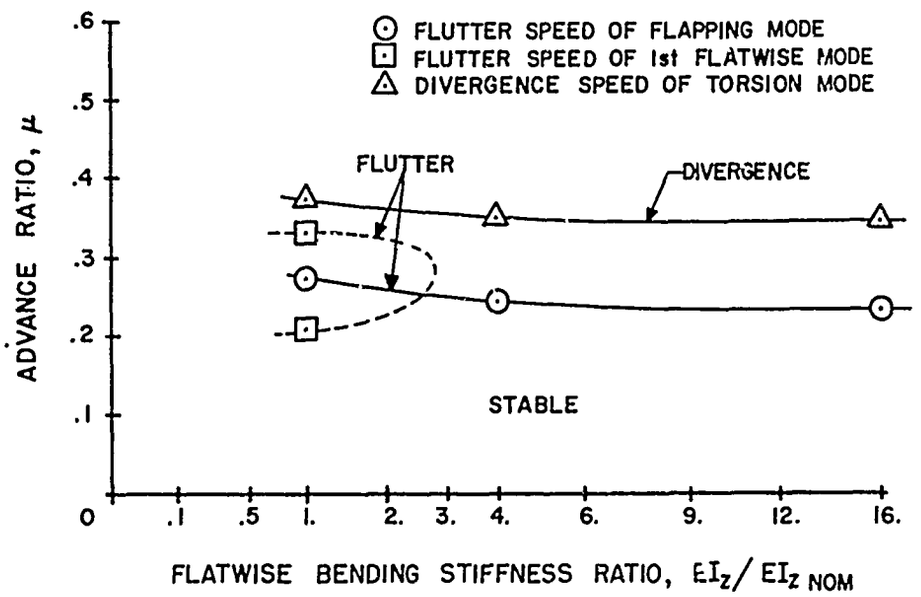

Figure 45. Varying the Blade Flatwise Bending Stiffness for an Articulated Blade; $EI_{z_{NOM}}$ = 29,500 Lb-In.^{2}.

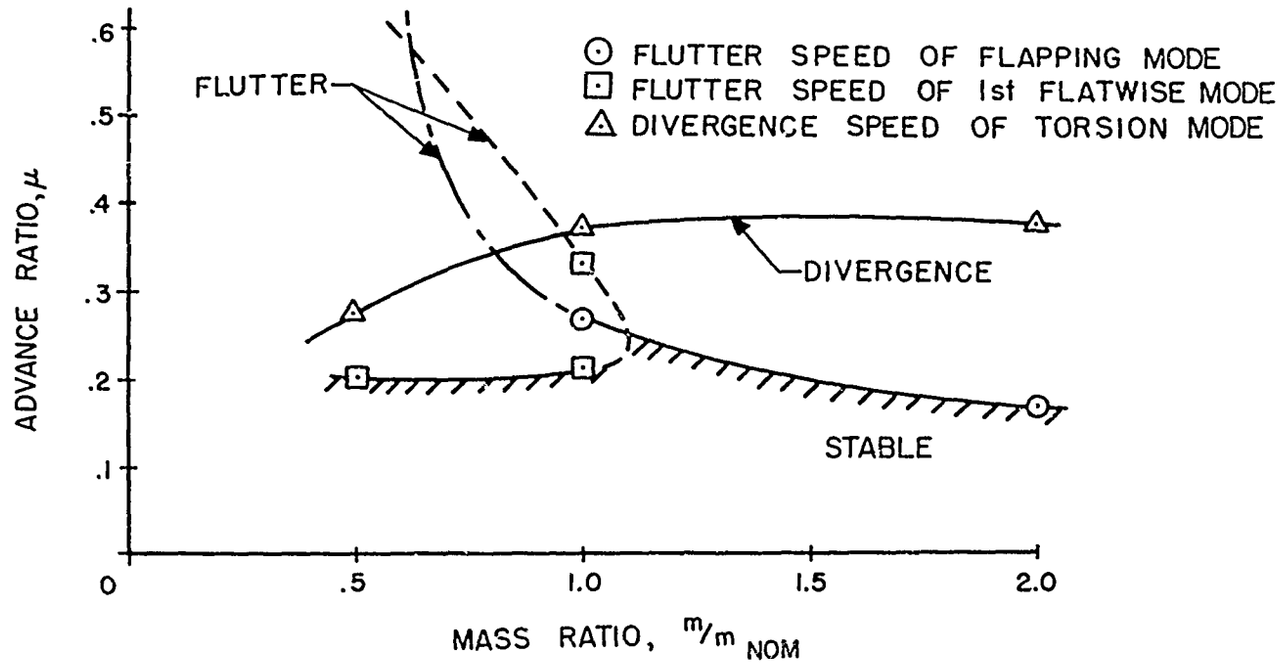

Figure 46. Varying the Blade Mass for an Articulated Blade; m_{NOM} = .0162 Slug/Ft.

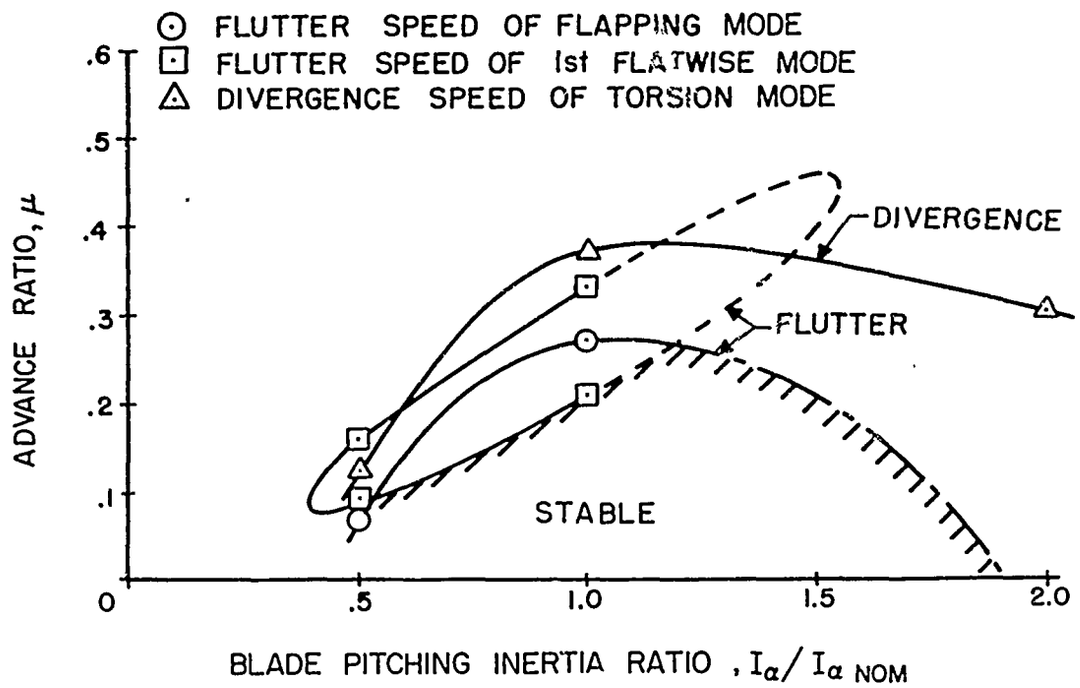

Figure 47. Varying the Blade Pitching Inertia for an Articulated Blade; $I_{\alpha NOM}$ = .742 x 10^{-4} Slug-Ft^2/Ft.

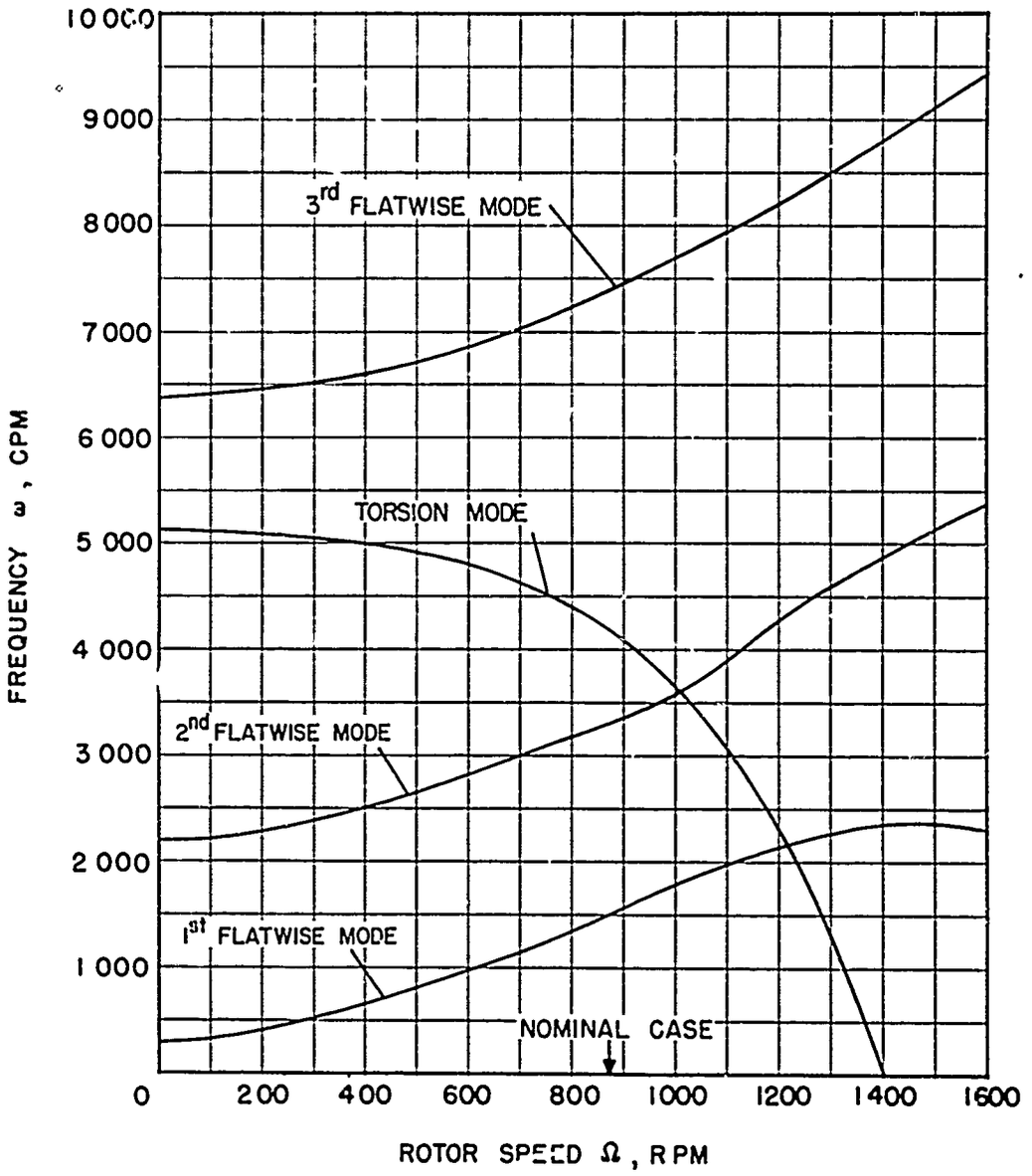

Figure 48. Variation of Solution Frequency With Change in Rotor Speed for the Nominal Nonarticulated Blade; $\mu = 0$.

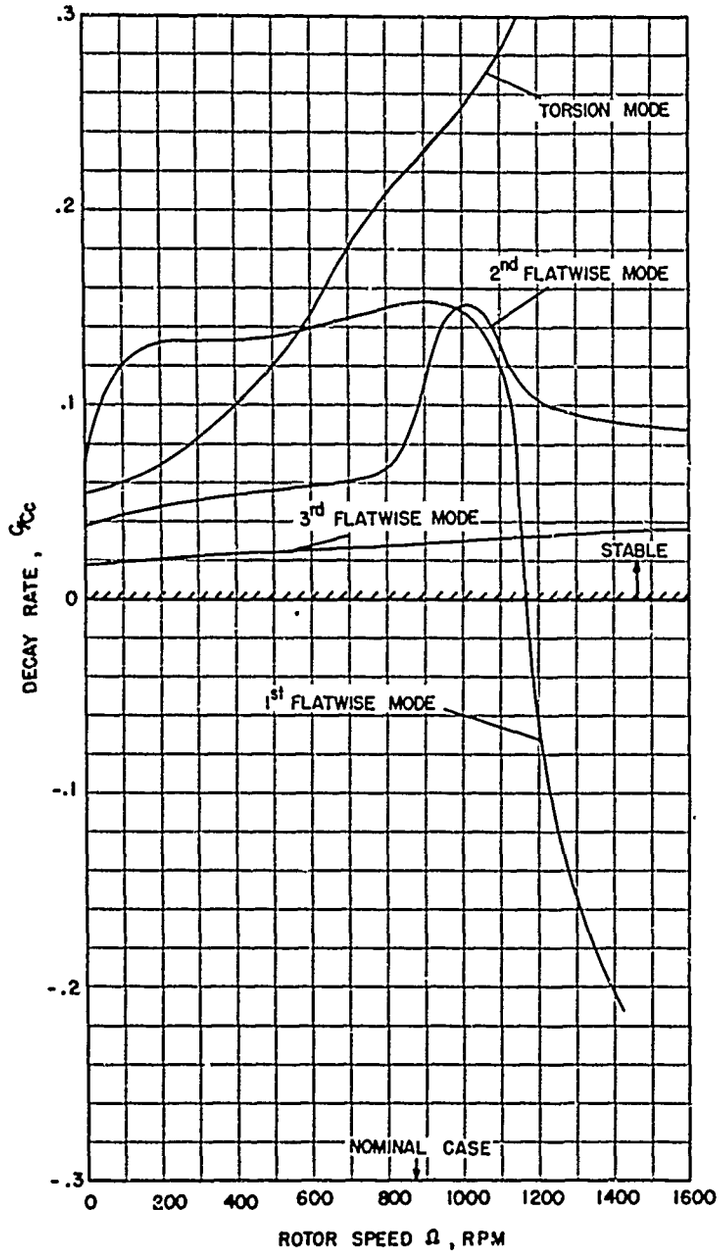

Figure 49. Variation of Solution Decay Rate With Change in Rotor Speed for the Nominal Nonarticulated Blade; $\mu = 0$.

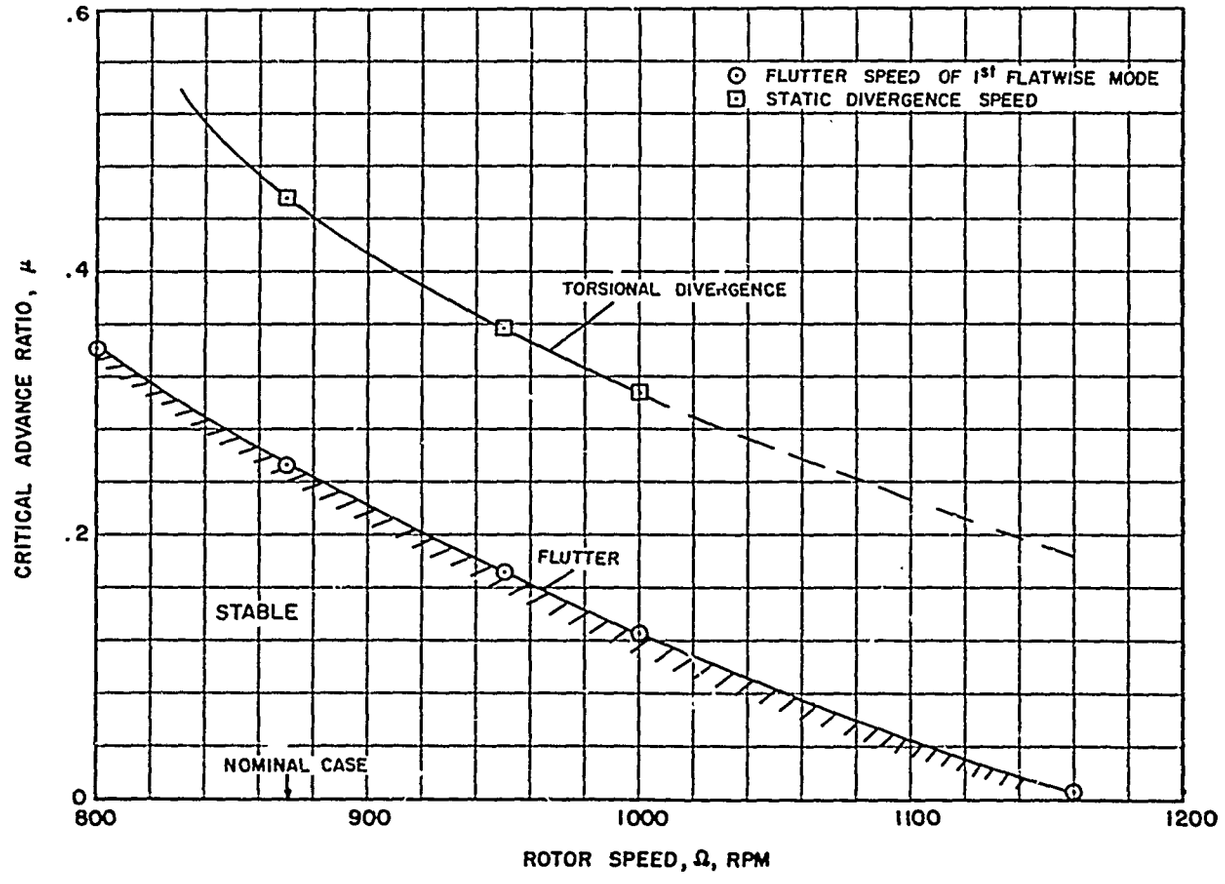

Figure 50. Variation of Critical Advance Ratio With Change in Rotor Speed for the Nominal Nonarticulated Blade.

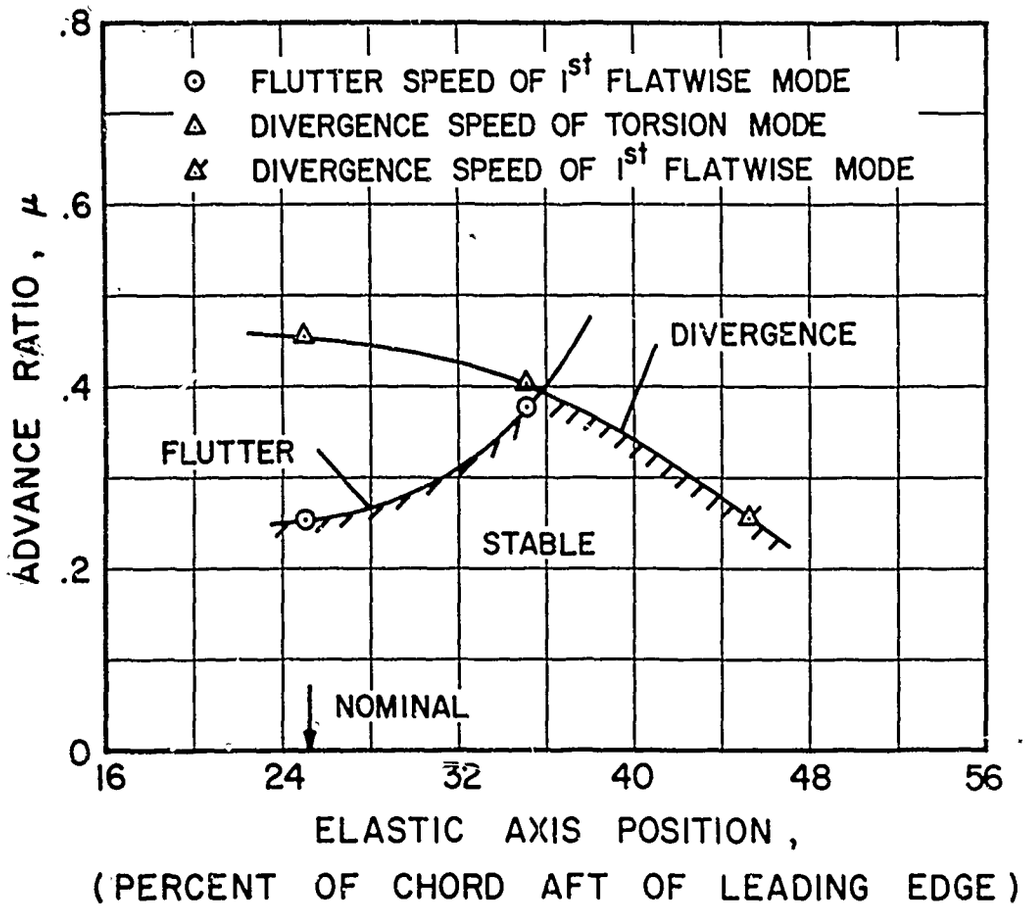

Figure 51. Varying the Chordwise Position of the Elastic Axis for a Nonarticulated Blade.

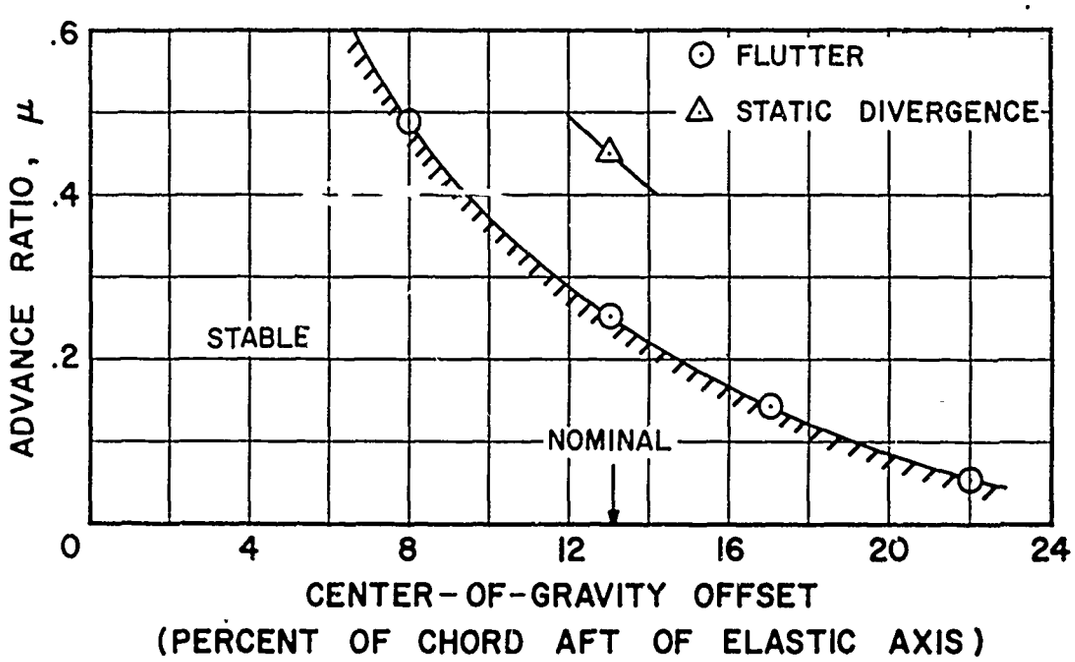

Figure 52. Varying the Chordwise Position of the Center of Gravity for a Nonarticulated Blade.

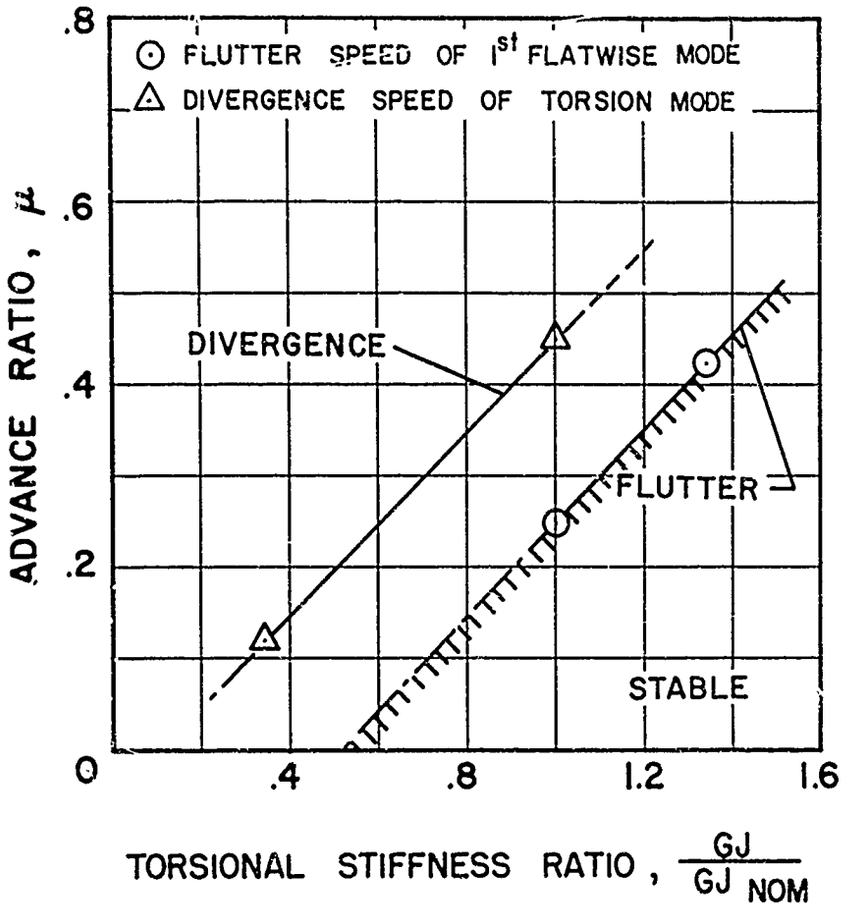

Figure 53. Varying the Blade Torsional Stiffness for a Nonarticulated Blade; GJ_{NOM} = 12, 436 Lb-In^2.

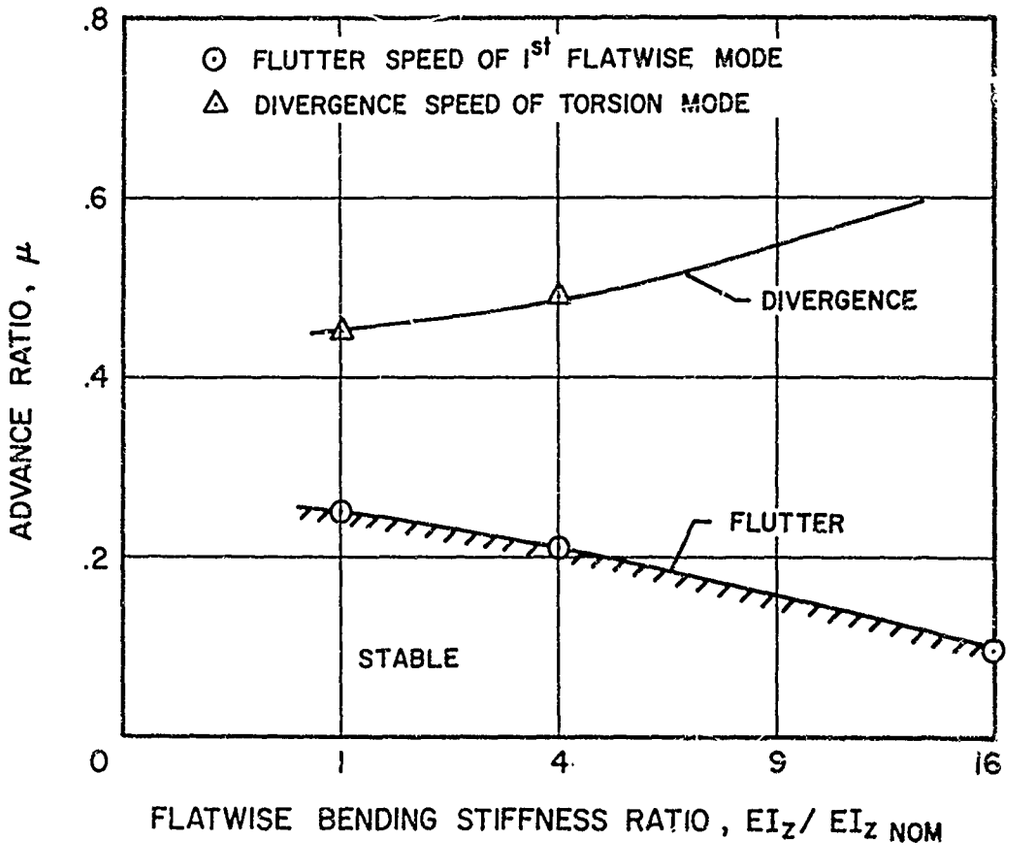

Figure 54. Varying the Blade Flatwise Bending Stiffness for a Nonarticulated Blade: $EI_{Z_{NOM}} = 29,500$ Lb-In.^{2}.

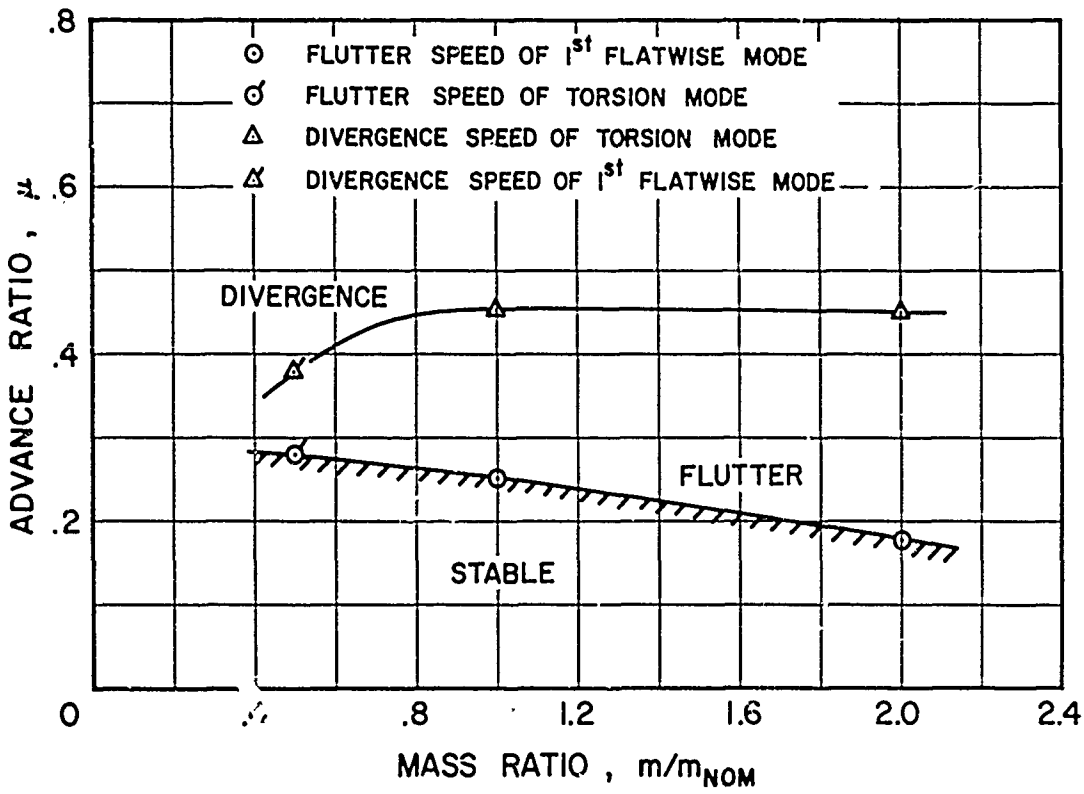

Figure 55. Varying the Blade Mass for a Nonarticulated Blade; m_{NOM} = .0162 Slug/Ft.

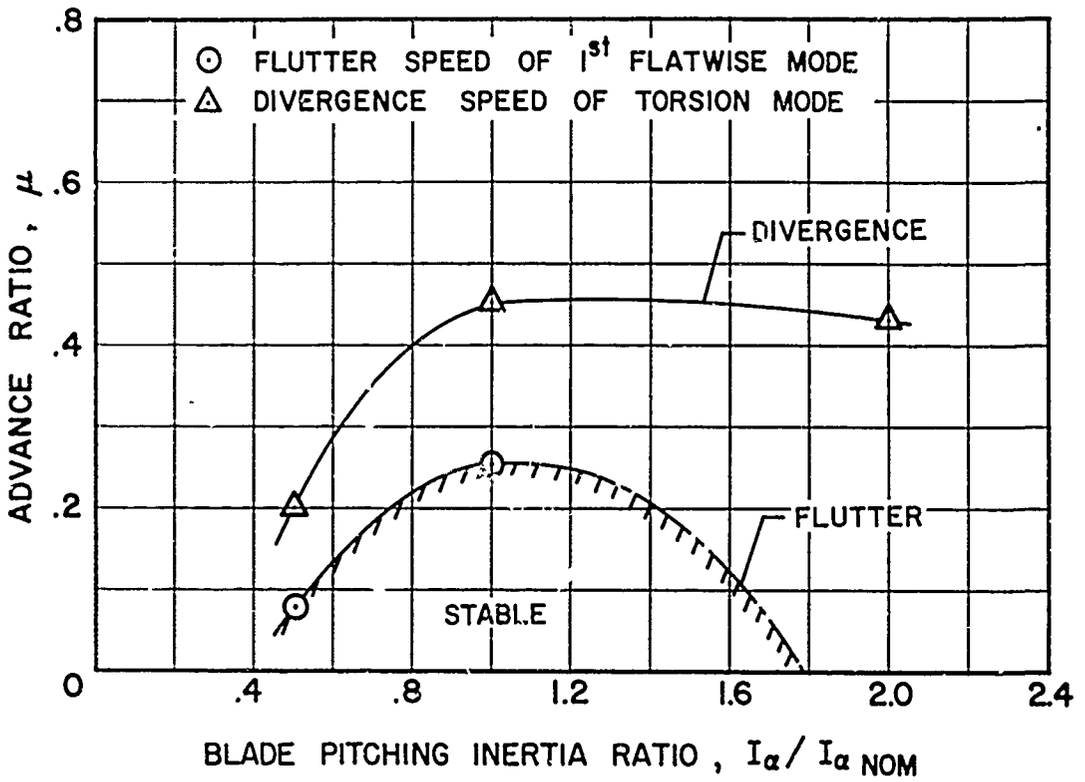

Figure 56. Varying the Blade Pitching Inertia for a Non-articulated Blade; $I_{\alpha\ NOM} = .742 \times 10^{-4}$ Slug-Ft^2/Ft.

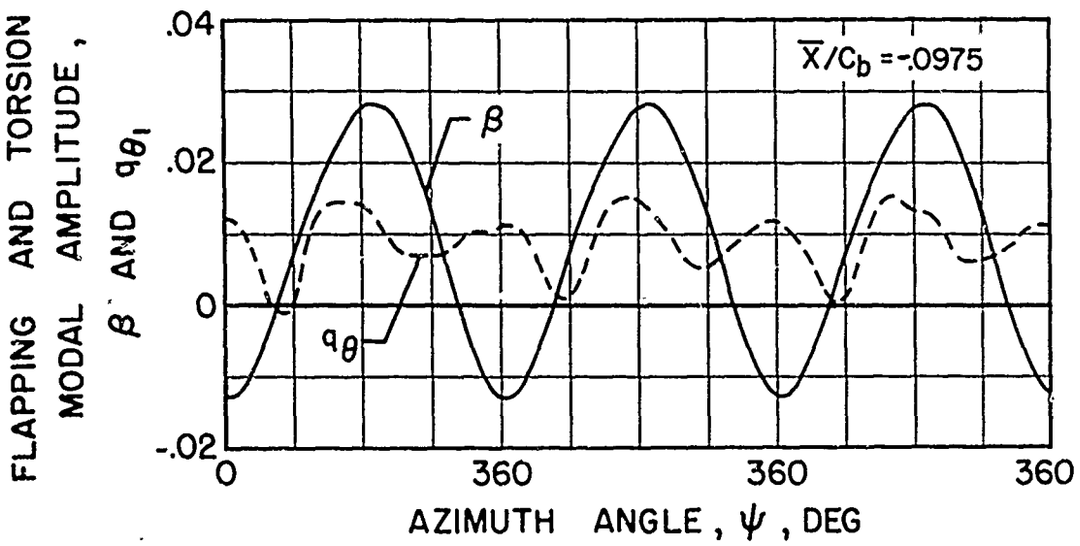

Figure 57. Articulated Blade Flapping and Torsion Modal Time History; $\mu = .30$, $A_{1S} = 0°$, $B_{1S} = 0°$, $\theta_{.75R} = 1.0°$, $\alpha_S \cong 0°$.

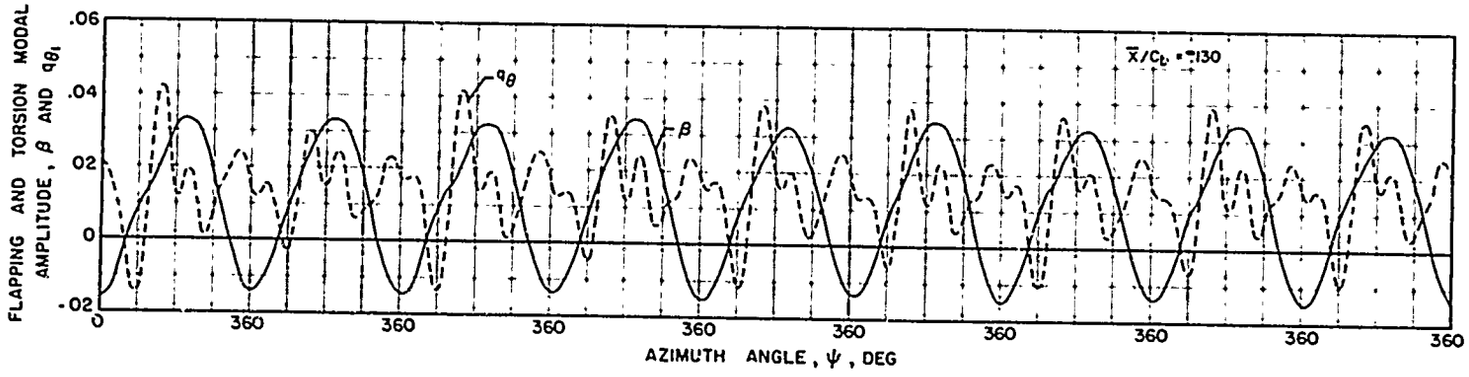

Figure 57. Concluded.

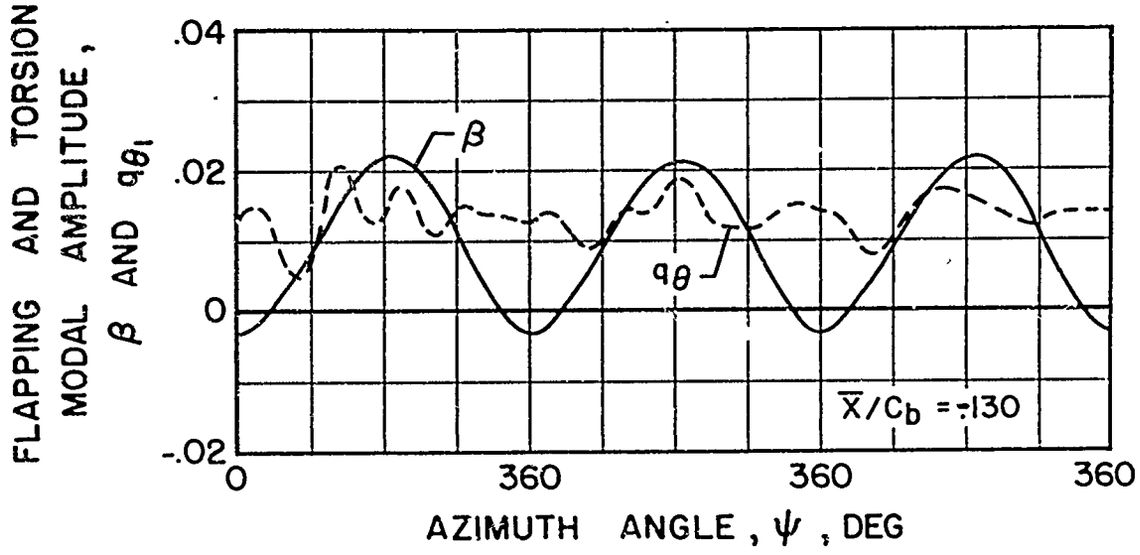

Figure 58. Articulated Blade Flapping and Torsion Modal Time History; $\mu = .15$, $A_{1S} = 0°$, $B_{1S} = 0°$, $\theta_{.75R} = 1.0°$, $\alpha_s \cong 0°$.

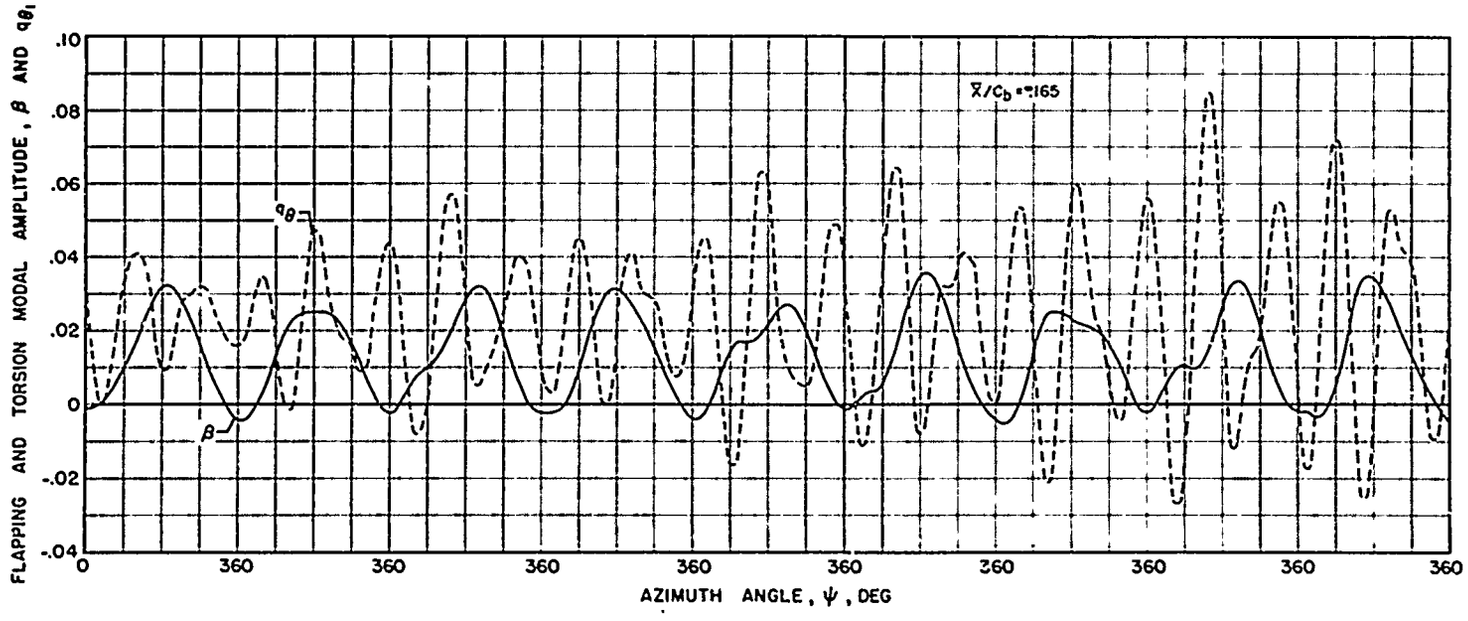

Figure 58. Continued.

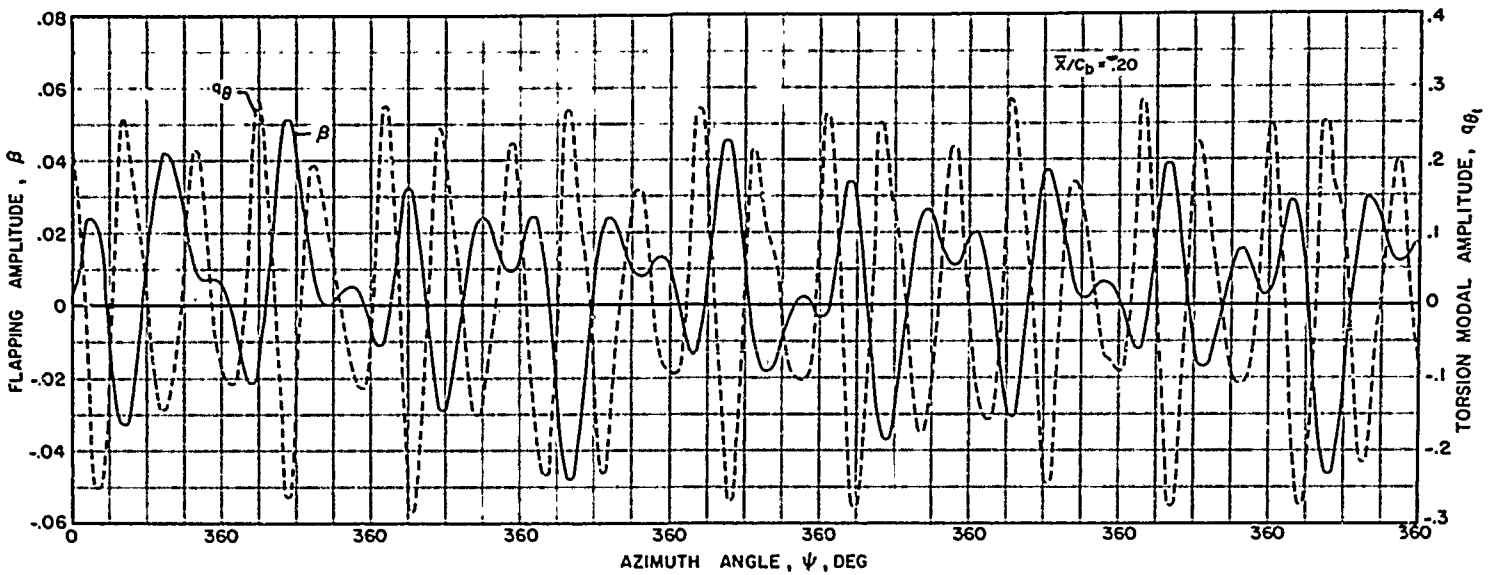

Figure 58. Concluded.

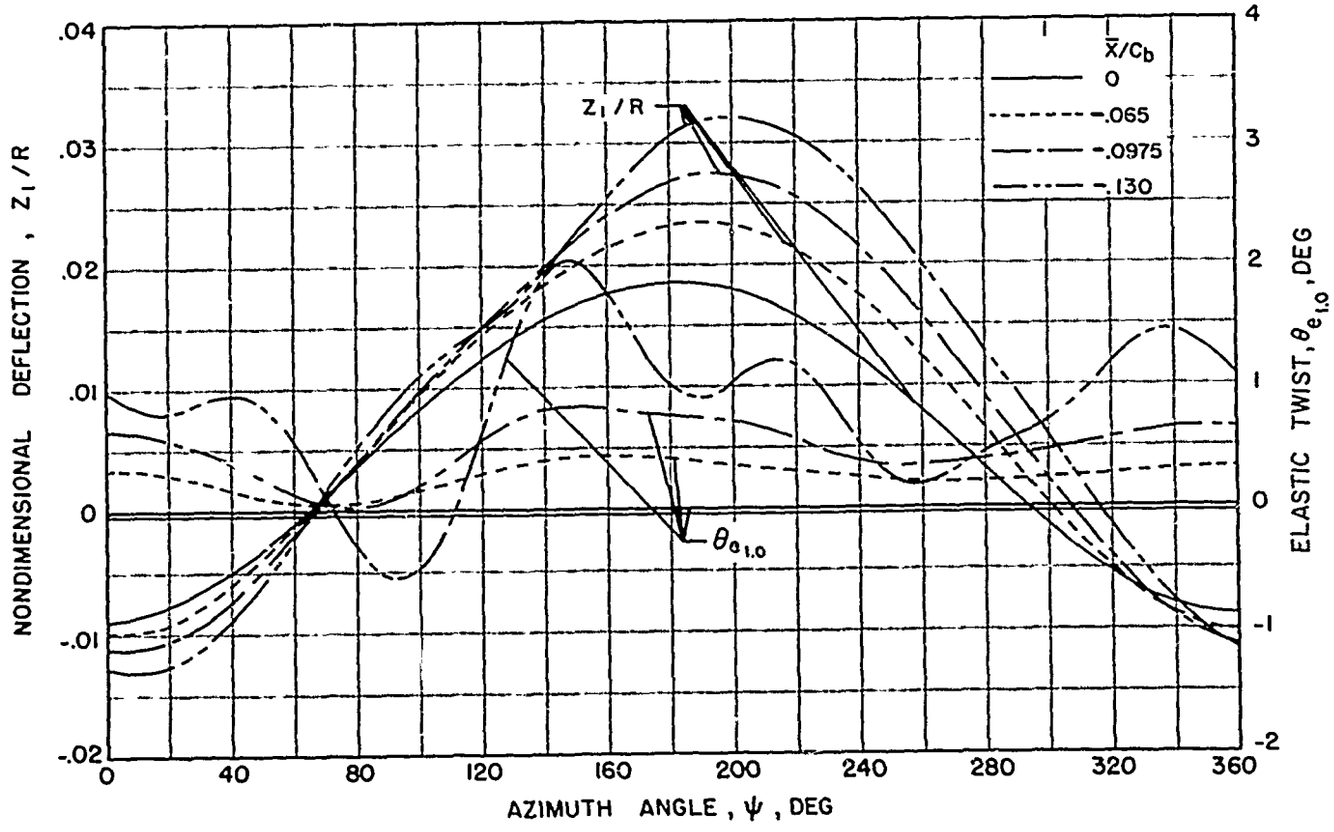

Figure 59. Effect of Aft Center-of-Gravity Position on Articulated Blade Tip Motions Versus Azimuth Angle; $\mu = .30$, $A_{1S} = 0°$, $B_{1S} = 0°$, $\theta_{.75R} = 1.0°$, $\alpha_s \cong 0°$.

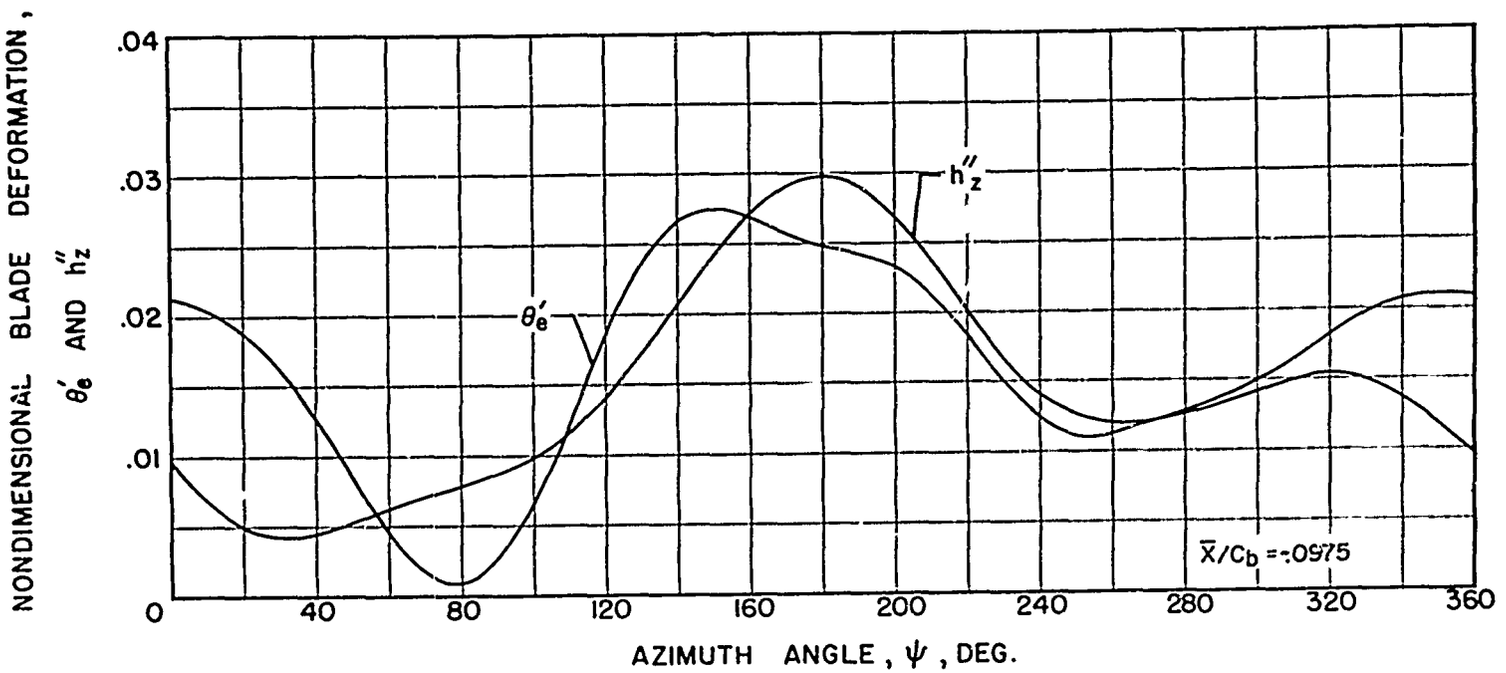

Figure 60. Articulated Blade Elastic Deformations Versus Azimuth Angle With Aft Center-of-Gravity Position; $\mu = .30$, $A_{1S} = 0°$, $B_{1S} = 0°$, $\theta_{.75R} = 1.0°$, $\alpha_S \cong 0°$.

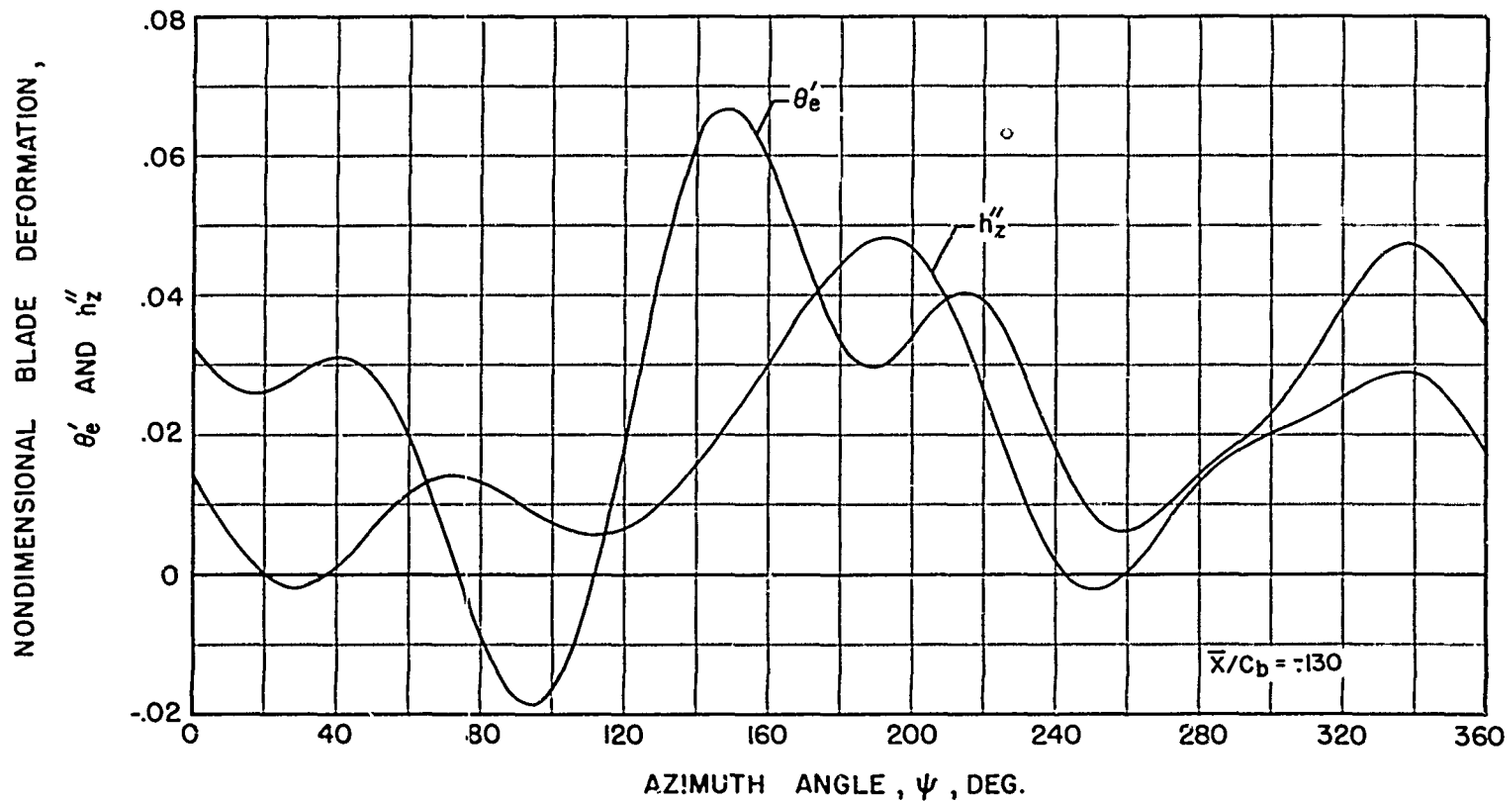

Figure 60. Concluded.

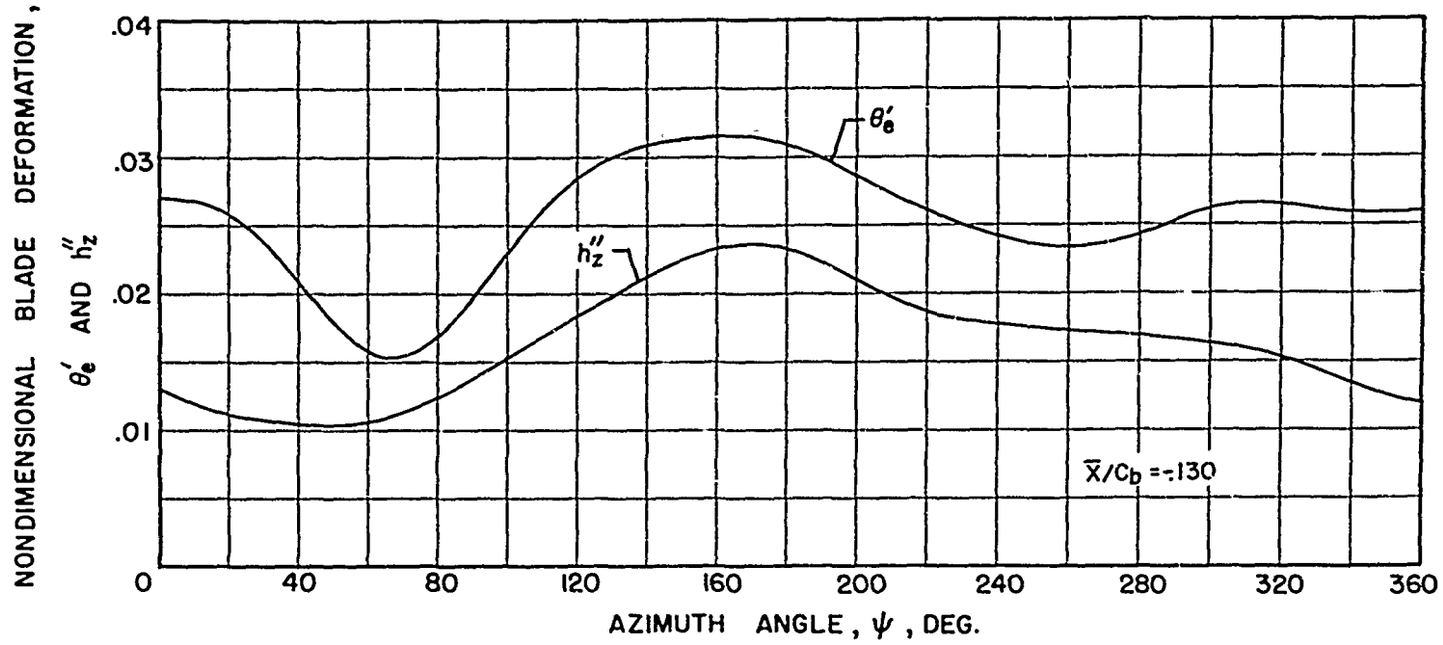

Figure 61. Articulated Blade Elastic Deformations Versus Azimuth Angle With Aft Center-of-Gravity Position; $\mu = .15$, $A_{1S} = 0°$, $B_{1S} = 0°$, $\theta_{.75R} = 1.0°$, $\alpha_S \cong 0°$.

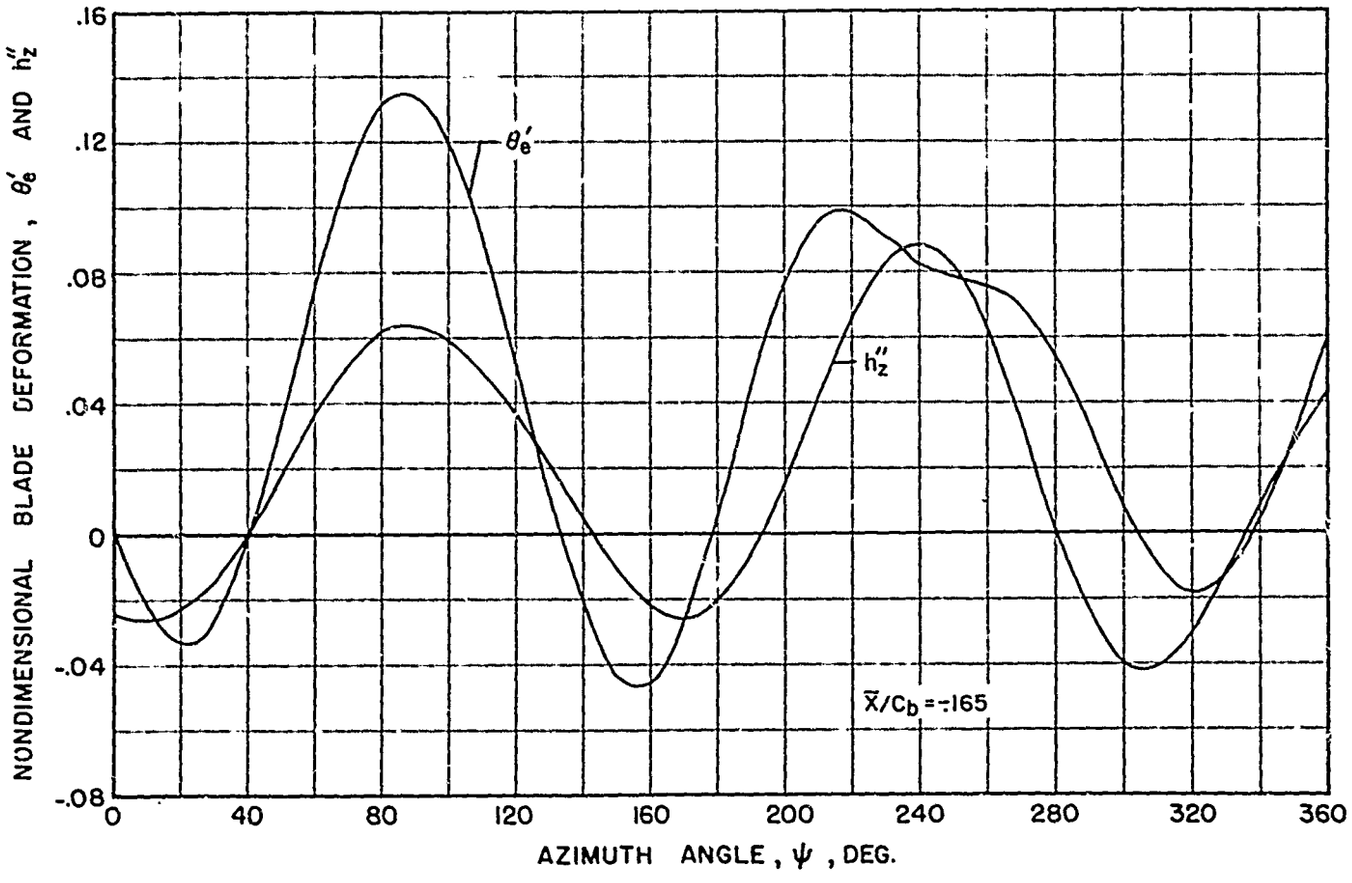

Figure 61. Continued.

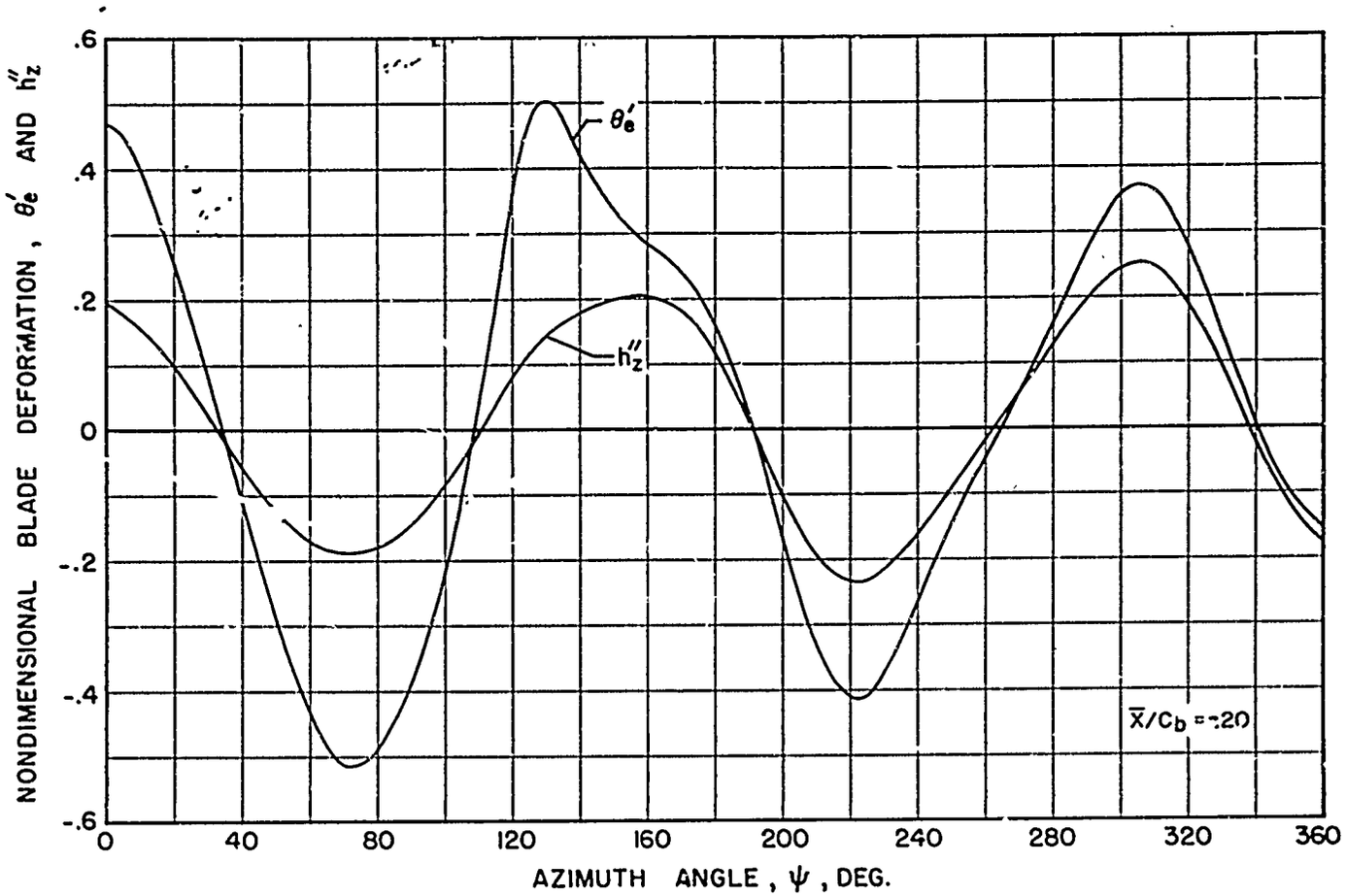

Figure 61. Concluded.

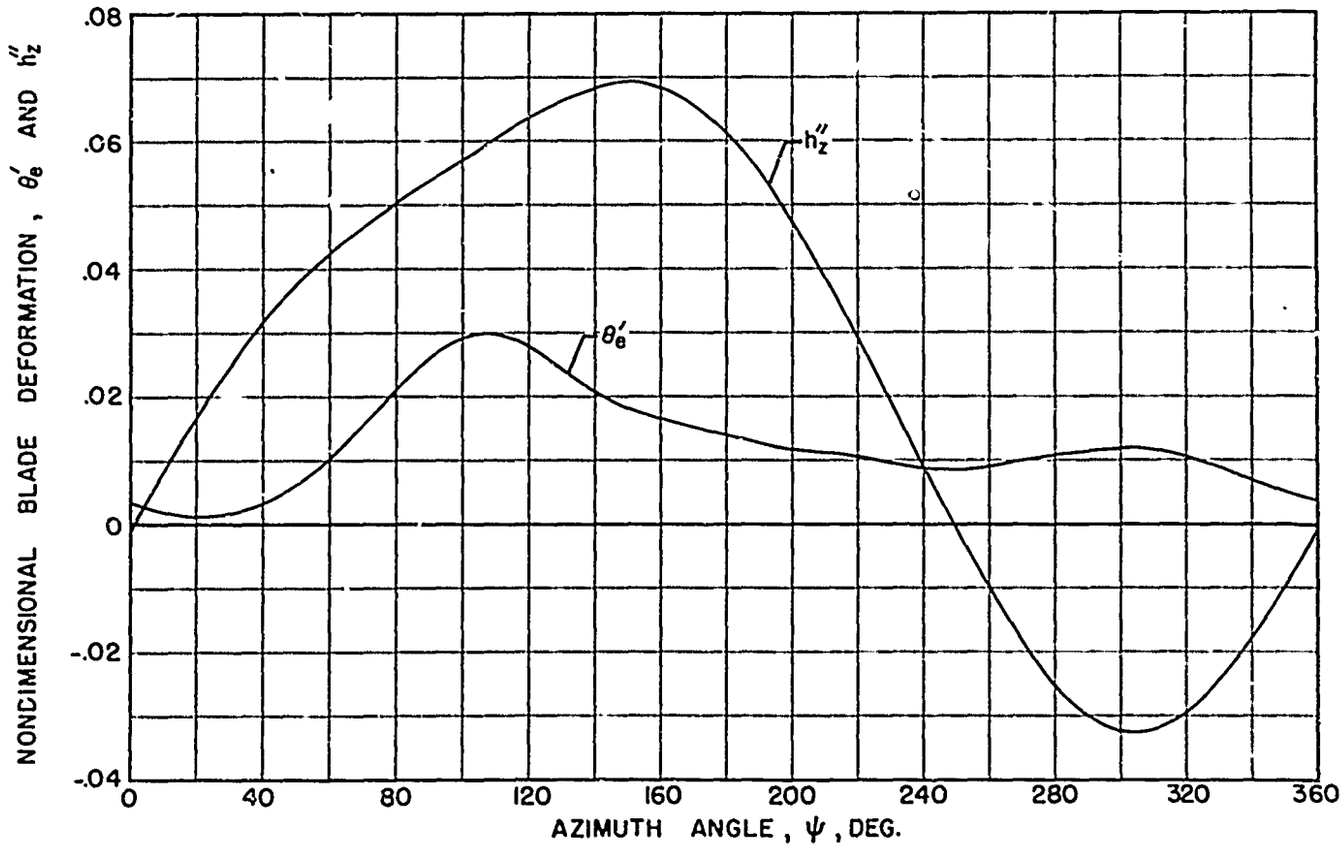

Figure 62. Nonarticulated Blade Deformation Versus Azimuth Angle With Aft Center-of-Gravity Position; $\mu = .30$, $A_{1S} = 0°$, $B_{1S} = 0°$, $\theta_{.75R} = 1.0°$, $\alpha \cong 0°$, $\bar{x}/c_b = -.20$.

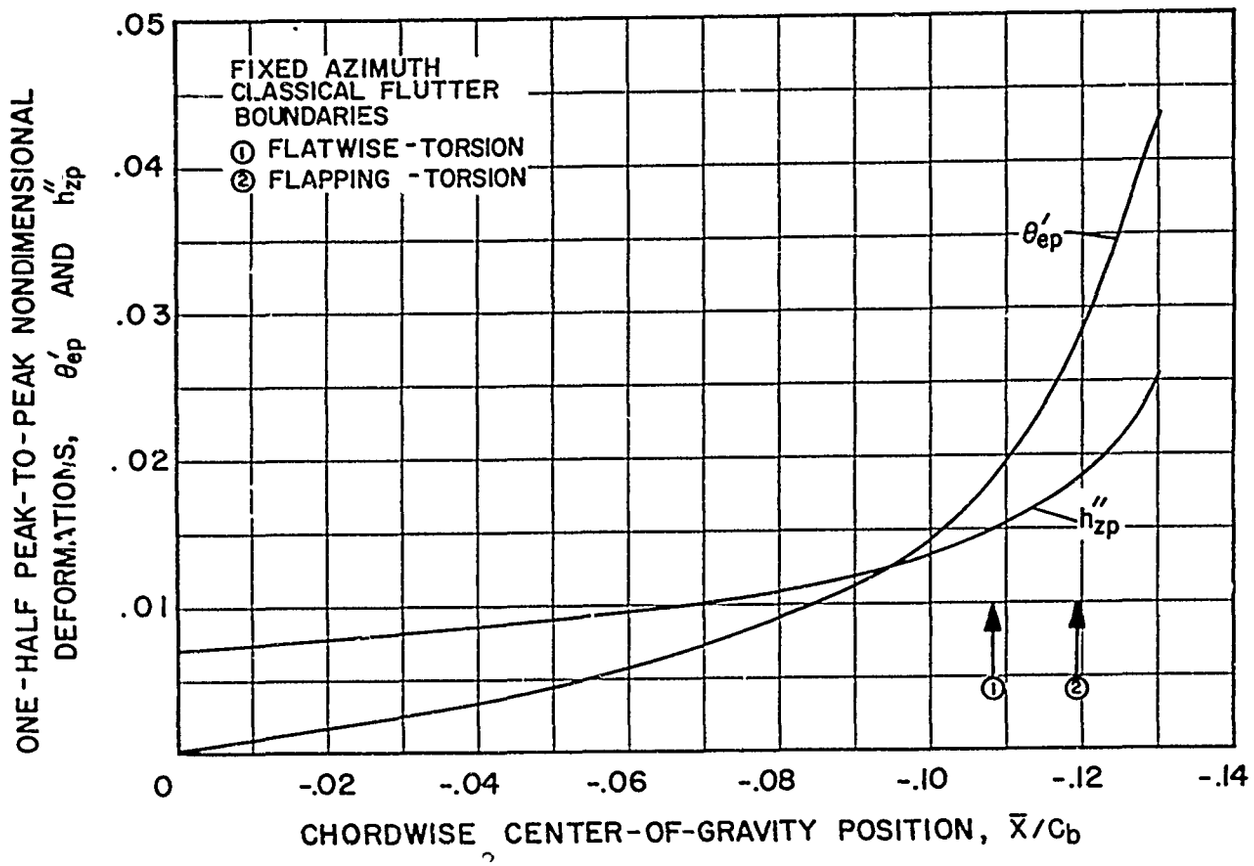

Figure 63. One-Half Peak-to-Peak Articulated Blade Deformations Versus Aft Center-of-Gravity Position; $\mu = .30$, $A_{1S} = 0°$, $B_{1S} = 0°$, $\theta_{.75R} = 1.0°$, $\alpha_S \cong 0°$.

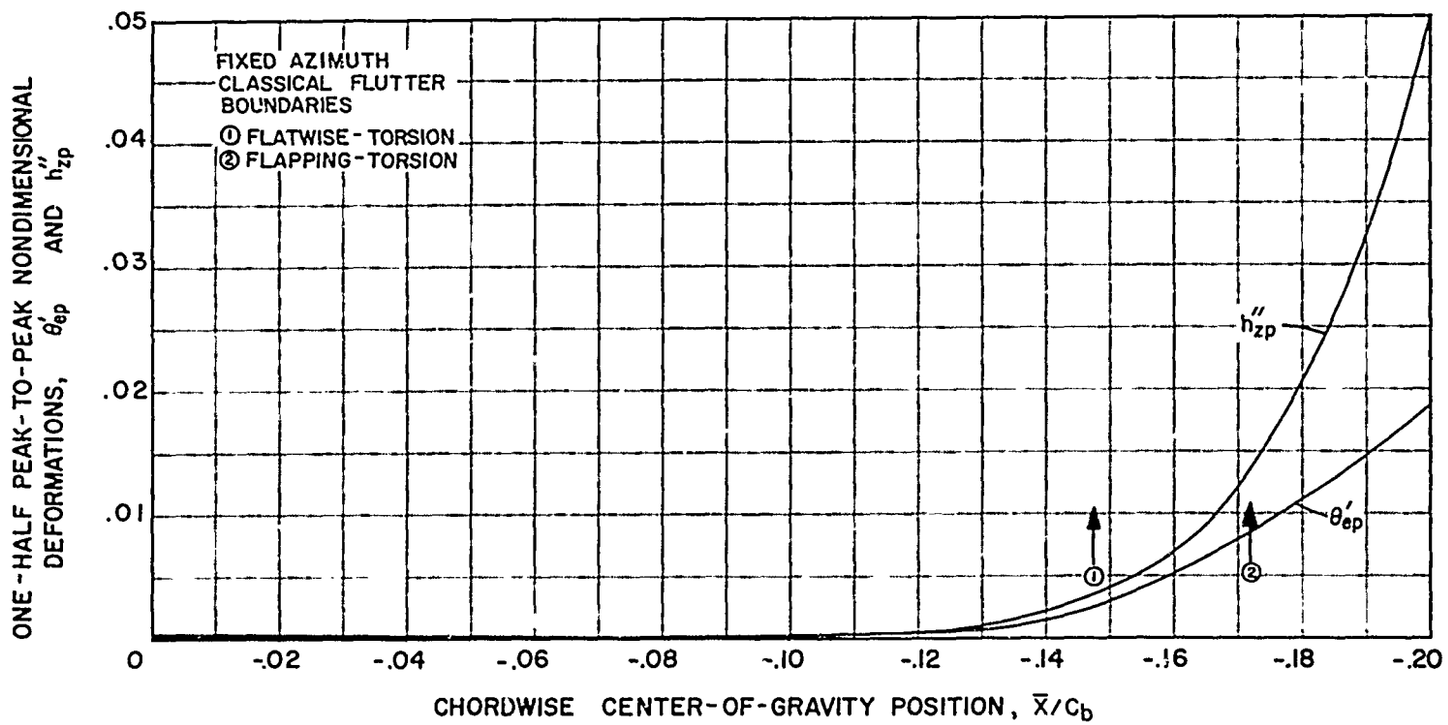

Figure 64. One-Half Peak-to-Peak Articulated Blade Deformations Versus Aft Center-of-Gravity Position; $\mu = .15$, $A_{1S} = 0°$, $B_{1S} = 0°$, $\theta_{.75R} = 1.0°$, $\alpha_S \cong 0°$.

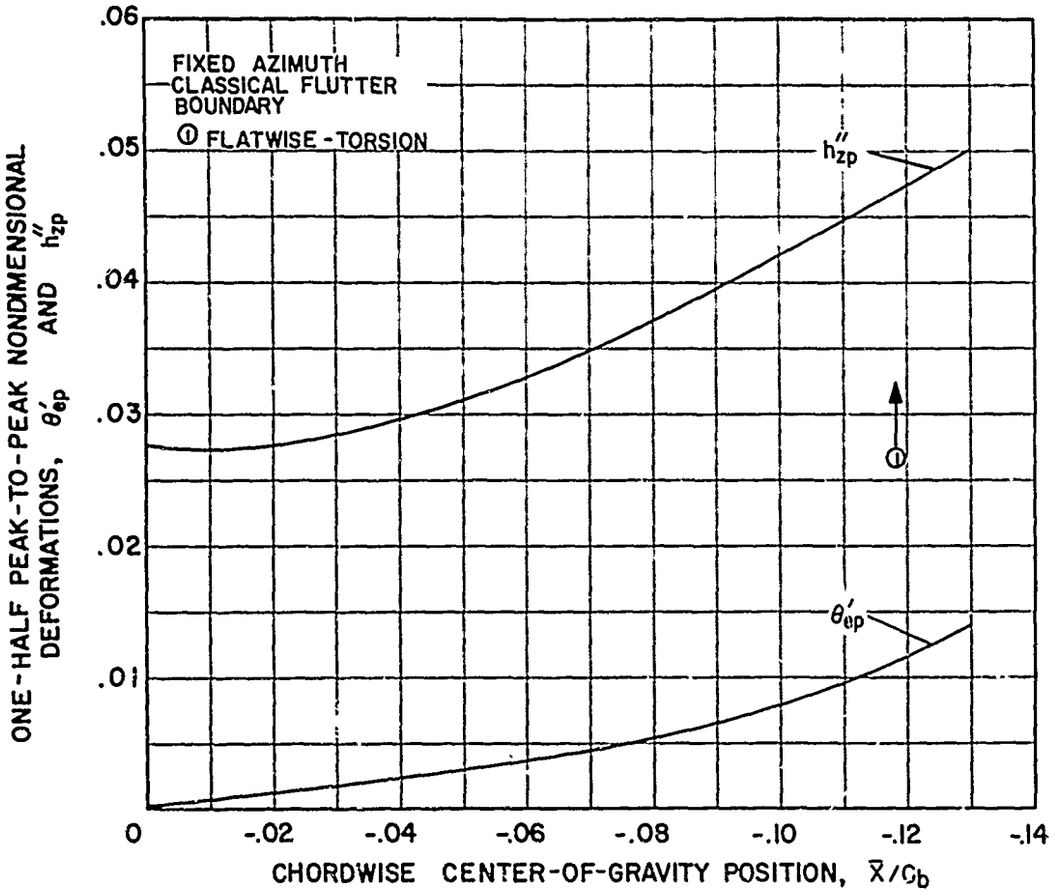

Figure 65. One-Half Peak-to-Peak Nonarticulated Blade Deformations Versus Aft Center-of-Gravity Position; $\mu = .30$, $A_{1S} = 0°$, $B_{1S} = 0°$, $\theta_{.75R} = 1.0°$, $\alpha_S \cong 0°$.

TABLE I. EXAMPLE OF THE APPLICATION OF REVERSE-FLOW RELATIONS

M_N	k	Reference	Tabulated		Calculated Using Reverse-Flow Relations	
			$\dot{l}_h$	l_h	$\dot{l}_h$	l_h
0	0.2	2	.72758	.017730	.72756	.017723
		7	.72750	.017750	.73647	.017720
		9	.72760	.017720	.72760	.017720
0.5	0.2	2	.76426	.030701	.76413	.030723
		4	.76425	.030700	.76429	.030682
		7	.76375	.029850	.77862	.029860
0.8	0.1	2	1.00268	.038675	1.00299	.038706
		7	1.01550	.039200	1.04030	.039720
0.8	0.7	2	.69096	.068596	.69041	.068628
		7	.63607	.059300	.66570	.059325
1.0	0.2	2	.68508	.091657	.68510	.091648
		3	.68513	.091648	.68511	.091650
1.11	0.475	4	.52501	.090162	.52501	.090161
		8	.52501	.090163	.52501	.090162

TABLE II. EXAMPLE OF ERRORS IN THE TABULATED COEFFICIENTS

$M_N = 0.8$

k	$-m_{\dot{\alpha}}$ (REF. 2)	$-m_{\dot{\alpha}}$ (REF. 7)
0.020	——	1.6250
0.025	.58728	——
0.040	——	1.4928
0.050	.94856	——
0.100	.99870	1.16787
0.200	.96130	1.07725

TABLE III. AIRFOIL DATA USED FOR THE TEST CASE

Item	Symbol	Value	Units
Blade Chord	2b	1.0	ft
Blade Mass per Unit Span	m	.16786	slug/ft
Radius of Gyration About Pitch Axis	r_α	.28	ft
Aerodynamic Center Chordwise Position Aft of Leading Edge	AC	25.	% chord
Elastic Axis Chordwise Position Aft of Leading Edge	EA	30.	% chord
Center-of-Gravity Chordwise Position Aft of Leading Edge	CG	42.5	% chord
Vertical Translation Natural Frequency	ω_{h_1}	218.	cpm
Pitching Natural Frequency	ω_{α_1}	1090	cpm
Lift Curve Slope	$C_{L\alpha}$	2π	rad^{-1}
Air Density	ρ	.002378	$slug/ft^3$
Rotational Speed	Ω	0.0	rad/sec
Azimuth Angle	ψ	90.	deg

TABLE IV. COMPARISON OF FLUTTER SPEEDS

SOURCE	FLUTTER SPEED		DIVERGENCE SPEED	
	ft /sec	knots	ft /sec	knots
REF.12	307	181.8	416	246.3
E 480	-	182		247

TABLE V. AERODYNAMIC COEFFICIENTS USED FOR THE TEST CASE

$M_N = 0.0 \quad k = 0.0$

$l_{\dot{h}}$	$l_{\dot{\alpha}}$	$-m_{\dot{h}}$	$-m_{\dot{\alpha}}$	l_h	l_α	$-m_h$	$-m_\alpha$
0.0	0.0	0.0	0.0	0.0	1.0	0.0	0.0

TABLE VI. NACA MODEL BLADE PROPERTIES

Item	Symbol	Values			Unit
Blade Number (Reference 14)		1(R)	2(F)	2(R)	—
Chord	2b	4.0	4.0	4.0	in.
Flapping Hinge Radius	e	2.5	2.5	2.5	in.
Outboard End of Rigid Section		8.0	8.0	8.0	in.
Rotor Radius	R	46	46	46	in.
Center of Gravity Chordwise Position Aft of Leading Edge	CG	37.3	27.5	37.3	% chord
Elastic Axis Chordwise Position Aft of Leading Edge	EA	26.5	25.0	26.5	% chord
Torsional Stiffness	GJ	9,980	8,260	9,210	lb -in.^{2}
Flatwise Bending Stiffness	EI_z	36,700	29,500	32,700	lb -in.^{2}
First Flatwise Bending Frequency	ω_{h_1}	126	113	119	rad/sec

TABLE VI. - Concluded

Item	Symbol	Values			Unit
Second Flatwise Bending Frequency	ω_{h_2}	327	319	331	rad/sec
First Cantilever Torsion Frequency	ω_α	464	439	446	rad/sec
Radius of Gyration About the Pitch Axis	r_α	.9696	.8124	.9696	in.
Blade Mass Density Ratio	μ_M	78	78	78	—
First Flatwise Bending Mode Structural Viscous Damping Coefficient	g_{h_1}	.126	.105	.110	—
Second Flatwise Bending Mode Structural Viscous Damping Coefficient	g_{h_2}	.049	.036	.040	—
First Cantilever Torsion Mode Structural Viscous Damping Coefficient	g_{α_1}	.048	.093	.075	—

TABLE VII. CORNELL AERONAUTICAL LABORATORY MODEL BLADE PROPERTIES

Item	Symbol	Value	Unit
Blade Number (Reference 14)	—	4	—
Chord	2b	3.5	in.
Flapping Hinge Radius	e	0	in.
Outboard End of Rigid Section		7	in.
Rotor Radius	R	48	in.
Shaft Axis Chordwise Position		25	% chord
Feathering Axis Chordwise Position		25	% chord
Center-of-Gravity Chordwise Position Aft of Leading Edge	CG	42.5	% chord
Elastic Axis Position Chordwise Position Aft of Leading Edge	EA	41.0	% chord
First Flatwise Bending Frequency (Calculated)	ω_{h_1}	76.9	rad/sec
Second Flatwise Bending Frequency (Calculated)	ω_{h_2}	924	rad/sec
First Cantilever Torsion Frequency (Calculated)	ω_{α_1}	640	rad/sec

TABLE VII. - Concluded

Item	Symbol	Value	Unit
Rigid Body Pitch Frequency	ω_{θ_0}	46.9-132.5	rad/sec
Blade Mass Density Ratio	μ_M	46.6	
Flapping Mechanical Viscous Damping Coefficient	g_{h_0}	0	
Rigid Body Pitching Mode Structural Viscous Damping Coefficient	g_{α_0}	0	
First Flatwise Bending Mode Structural Viscous Damping Coefficient	g_{h_1}	.04	
Second Flatwise Bending Mode Structural Viscous Damping Coefficient	g_{h_2}	.04	
First Cantilever Torsion Mode Structural Viscous Damping Coefficient	g_{α_1}	.04	

TABLE VIII. CASES USED FOR CORRELATION WITH CORNELL DATA

Reference 16 Figure No.	$\frac{\bar{\omega}_{\phi_1}}{\bar{\omega}_{\theta_0}}$	$\bar{\omega}_{\theta_0}$ RAD/SEC	$\frac{\bar{x}_E}{c_b}$	$\frac{a_{\beta\theta_0}}{\sqrt{a_{\beta\beta}\, a_{\theta_0\theta_0}}}$
10(a)	1.03	65.9	.0036	-.00317
10(a)	1.44	46.9	.0036	-.00317
10(b)	1.05	69.0	.044	-.101
10(c)	.63	132.5	.139	-.338
10(c)	1.31	64.5	.139	-.338

TABLE IX. EFFECT ON FLUTTER SPEED OF VARYING MASS BALANCE

Reference 16 Figure No.	$\frac{a_{\beta\theta_0}}{\sqrt{a_{\beta\beta}\, a_{\theta_0\theta_0}}}$	$\frac{\bar{\omega}_{\phi_1}}{\bar{\omega}_{\theta_0}}$	μ	$\Omega/\bar{\omega}_{\theta_0}$ MEASURED	$\Omega/\bar{\omega}_{\theta_0}$ E 480 SOLUTION
10(c)	-.338	.63	0.0	.25	.27
10(c)	-.338	1.31	0.0	.33	.32
10(b)	-.101	1.05	0.0	.56	-
10(b)	-.101	1.05	0.2	-	.29
10(a)	-.00317	1.03	0.0	1.0	.35
10(a)	-.00317	1.44	0.0	1.0	-
10(a)	-.00317	1.44	0.2	-	.33

TABLE X. BASIC PROPERTIES OF THE BLADE USED FOR THE PARAMETER VARIATION STUDY

Item	Symbol	Value	Unit
Chord	2b	4	in.
Articulated Blade Flapping Hinge Radius	e	2.5	in.
Outboard End of Rigid Section		8	in.
Rotor Radius	R	46	in.
Articulated Blade Rotational Speed	Ω	950	rpm
Nonarticulated Blade Rotational Speed	Ω	870	rpm

TABLE XI. CASES CONSIDERED IN THE VARIATION OF PARAMETERS

Case No.	EA % chord	CG % chord	GJ lb-in.^{2}	EI_z lb-in.^{2}	m slug/ft	I_α x10^4 slug-ft^2/ft
0.A	25	38	12,436	29,500	.01619	.7419
0.R	25	38	12,436	29,500	.01619	.7419
1.A1	35	38	12,436	29,500	.01619	.7419
1.R1	35	38	12,436	29,500	.01619	.7419
1.A2	45	38	12,436	29,500	.01619	.7419
1.R2	45	38	12,436	29,500	.01619	.7419
2.A1	25	31	12,436	29,500	.01619	.7419
2.R1	25	27.5	12,436	29,500	.01619	.7419
2.A2	25	34	12,436	29,500	.01619	.7419
2.R2	25	33	12,436	29,500	.01619	.7419
2.A3	25	36	12,436	29,500	.01619	.7419
2.R3	25	42	12,436	29,500	.01619	.7419
2.A4	25	45	12,436	29,500	.01619	.7419
2.R4	25	47	12,436	29,500	.01619	.7419
3.A1	25	38	4,130	29,500	.01619	.7419
3.R1	25	38	4,130	29,500	.01619	.7419
3.A2	25	38	16,520	29,500	.01619	.7419
3.R2	25	38	16,520	29,500	.01619	.7419

TABLE XI. - Concluded

Case No.	EA % chord	CG % chord	GJ lb-in.^{2}	EI_z lb-in.^{2}	m slug/ft	$I_\alpha \times 10^4$ slug-ft^2/ft
4.A1	25	38	12,436	118,000	.01619	.7419
4.R1	25	38	12,436	118,000	.01619	.7419
4.A2	25	38	12,436	472,000	.01619	.7419
4.R2	25	38	12,436	472,000	.01619	.7419
5.A1	25	38	12,436	29,500	.008093	.7419
5.R1	25	38	12,436	29,500	.008093	.7419
5.A2	25	38	12,436	29,500	.03237	.7419
5.R2	25	38	12,436	29,500	.03237	.7419
6.A1	25	38	12,436	29,500	.01619	.7419
6.R1	25	38	12,436	29,500	.01619	.7419
6.A2	25	38	12,436	29,500	.01619	.7419
6.R2	25	38	12,436	29,500	.01619	.7419

TABLE XII. COMPRESSIBLE FLOW FLUTTER COEFFICIENTS

$M_N = 0.0$

k	$\bar{k}$	$\ell_{\dot{h}}$	$\ell_{\dot{\alpha}}$	$-m_{\dot{h}}$	$-m_{\dot{\alpha}}$	ℓ_h	ℓ_α	$-m_h$	$-m_\alpha$
0	0	1.0000	0.0	0.0	0.0	0.0	1.0	0.0	0.0
.025	.1111	.9543	-2.0216	0.0	.5000	.0019	.9563	-.0002	-.0001
.03	.1305	.9450	-1.7500	0.0	.5000	.0025	.9450	-.0002	-.0002
.04	.1667	.9263	-1.4731	0.0	.5000	.0038	.9250	-.0004	-.0003
.05	.2	.9088	-1.1995	0.0	.5000	.0053	.9130	-.0006	-.0005
.06	.2308	.8920	-.9847	0.0	.5000	.0068	.8997	-.0009	-.0007
.08	.2857	.8605	-.6446	0.0	.5000	.0096	.8717	-.0016	-.0012
.10	.3333	.8320	-.3910	0.0	.5000	.0122	.8467	-.0025	-.0019
.12	.3750	.8063	-.1945	0.0	.5000	.0144	.8243	-.0036	-.0027
.14	.4118	.7832	-.0373	0.0	.5000	.0161	.8000	-.0049	-.0037
.16	.4444	.7628	.0903	0.0	.5000	.0172	.7864	-.0064	-.0048
.18	.4737	.7442	.1960	0.0	.5000	.0178	.7680	-.0081	-.0061
.20	.5	.7276	.2846	0.0	.5000	.0177	.7553	-.0100	-.0075
.22	.5238	.7125	.3592	0.0	.5000	.0171	.7360	-.0121	-.0091
.24	.5455	.6989	.4231	0.0	.5000	.0159	.7292	-.0144	-.0108
.26	.5652	.6865	.4781	0.0	.5000	.0141	.7200	-.0169	-.0127
.28	.5833	.6752	.5258	0.0	.5000	.0117	.7050	-.0196	-.0147
.30	.6	.6650	.5673	0.0	.5000	.0088	.6963	-.0225	-.0169
.34	.6296	.6469	.6357	0.0	.5000	.0013	.6771	-.0289	-.0217
.38	.6552	.6317	.6898	0.0	.5000	-.0084	.6550	-.0361	-.0271
.42	.6774	.6187	.7329	0.0	.5000	-.0201	.6430	-.0441	-.0331
.46	.6970	.6076	.7678	0.0	.5000	-.0339	.6250	-.0529	-.0397
.50	.7143	.5979	.7965	0.0	.5000	-.0496	.6108	-.0625	-.0469
.54	.7297	.5895	.8203	0.0	.5000	-.0673	.5930	-.0729	-.0547
.60	.7500	.5788	.8491	0.0	.5000	-.0973	.5715	-.0900	-.0675
.66	.7674	.5699	.8718	0.0	.5000	-.1315	.5500	-.1089	-.0817
.70	.7778	.5648	.8842	0.0	.5000	-.1565	.5308	-.1225	-.0919

TABLE XII. - Continued

$M_N = 0.35$

k	$\bar{k}$	$l_{\dot{h}}$	$l_{\dot{\alpha}}$	$-m_{\dot{h}}$	$-m_{\dot{\alpha}}$	l_h	l_α	m_h	$-m_\alpha$
0	0.0	1.0675	0.0	0.0	0.0	0.0	1.0675	0.0	-.0003
.025	.1111	1.0075	-2.7200	0.0	.6520	.0025	1.0150	-.0001	-.0010
.03	.1305	.9960	-2.4400	.0	.6380	.0034	1.0060	-.0002	-.0021
.04	.1667	.9975	-2.0488	.0	.6188	.0051	.9851	-.0003	-.0017
.05	.2	.9540	-1.6950	.0	.5960	.0068	.9671	-.0007	-.0010
.06	.2308	.9350	-1.4575	.0008	.5796	.0086	.9491	-.0010	-.0003
.08	.2857	.8969	-1.0141	.0009	.5630	.0122	.9172	-.0018	.0006
.10	.3333	.8635	-.6883	.0013	.5606	.0156	.8896	-.0028	.0006
.12	.3750	.8333	-.4375	.0021	.5615	.0183	.8648	-.0042	-.0003
.14	.4118	.8071	-.2357	.0021	.5636	.0204	.8434	-.0058	-.0014
.16	.4444	.7838	-.0800	.0025	.5622	.0220	.8245	-.0075	-.0025
.18	.4737	.7633	.0456	.0028	.5611	.0232	.8072	-.0094	-.0037
.20	.5	.7450	.1475	.0030	.5590	.0238	.7923	-.0115	-.0045
.22	.5238	.7291	.2327	.0034	.5569	.0239	.7786	-.0138	-.0062
.24	.5455	.7148	.3084	.0041	.5567	.0232	.7658	-.0164	-.0079
.26	.5652	.7017	.3747	.0043	.5568	.0218	.7538	-.0193	-.0098
.28	.5833	.6904	.4316	.0048	.5569	.0199	.7425	-.0223	-.0116
.30	.6	.6802	.4804	.0053	.5570	.0175	.7319	-.0256	-.0135
.34	.6296	.6625	.5599	.0061	.5575	.0112	.7121	-.0328	-.0176
.38	.6552	.6486	.6230	.0069	.5581	.0027	.6934	-.0408	-.0225
.42	.6774	.6373	.6740	.0079	.5590	-.0079	.6753	-.0499	-.0280
.46	.6970	.6283	.7158	.0089	.5603	-.0204	.6575	-.0598	-.0339
.50	.7143	.6213	.7505	.0100	.5618	-.0348	.6397	-.0706	-.0405
.54	.7297	.6158	.7797	.0112	.5634	-.0511	.6217	-.0824	-.0475
.60	.7500	.6103	.8163	.0131	.5663	-.0789	.5940	-.1019	-.0590
.66	.7674	.6075	.8462	.0153	.5694	-.1107	.5651	-.1235	-.0718
.70	.7778	.6068	.8634	.0167	.5717	-.1340	.5450	-.1392	-.0809

TABLE XII. - Continued

$M_N = 0.50$

k	$\bar{k}$	$l_{\dot{h}}$	$l_{\dot{\alpha}}$	$-m_{\dot{h}}$	$-m_{\dot{\alpha}}$	l_h	l_α	$-m_h$	$-m_\alpha$
0	0.0	1.1547	0.0	0.0	0.0	0.0	1.1547	0.0	0.0
.025	.1111	1.0816	-3.6539	.0003	.6651	.0036	1.0849	-.0002	.0003
.03	.1305	1.0650	-3.2500	.0007	.6630	.0040	1.0640	-.0004	.003
.04	.1667	1.038	-2.7595	.0010	.6630	.0061	1.0450	-.0006	.0005
.05	.2	1.0106	-2.3191	.0014	.6566	.0083	1.0185	-.0009	.0006
.06	.2308	.9858	-1.9633	.0018	.6542	.0106	.9975	-.0013	.0008
.08	.2857	.9394	-1.4200	.0026	.6488	.0151	.9566	-.0023	.0009
.10	.3333	.8991	-1.0215	.0034	.6446	.0192	.9215	-.0035	.0010
.12	.3750	.8646	-.7510	.0048	.6400	.0232	.9042	-.0047	.0009
.14	.4118	.8339	-.4938	.0055	.6385	.0259	.8794	-.0066	.0005
.16	.4444	.8069	-.2841	.0059	.6373	.0278	.8573	-.0088	-.0007
.18	.4737	.7836	-.1193	.0068	.6353	.0290	.8385	-.0114	-.0009
.20	.5	.7643	-.0110	.0082	.6333	.0299	.8084	-.0134	-.0013
.22	.5238	.7464	.1102	.0089	.6325	.0304	.7940	-.0166	-.0021
.24	.5455	.7310	.1920	.0097	.6318	.0305	.7850	-.0193	-.0029
.26	.5652	.7177	.2627	.0108	.6315	.0301	.7720	-.0224	-.0039
.28	.5833	.7061	.3263	.0118	.6313	.0289	.7620	-.0257	-.0055
.30	.6	.6958	.3840	.0128	.6316	.0269	.7522	-.0294	-.0073
.34	.6296	.6788	.4790	.0152	.6325	.0214	.7360	-.0377	-.0112
.38	.6552	.6657	.5513	.0173	.6339	.0140	.7250	-.0469	-.0147
.42	.6774	.6562	.6086	.0198	.6361	.0049	.7180	-.0571	-.0182
.46	.6970	.6494	.6553	.0224	.6388	-.0060	.7080	-.0683	-.0228
.50	.7143	.6445	.6950	.0250	.6420	-.0190	.7062	-.0807	-.0279
.54	.7297	.6422	.7274	.0283	.6455	-.0331	.6866	-.0940	-.0327
.60	.7500	.6415	.7674	.0335	.6511	-.0573	.6714	-.1160	-.0407
.66	.7674	.6446	.8009	.0396	.6585	-.0854	.6573	-.1408	-.0493
.70	.7778	.6482	.8196	.0439	.6634	-.1055	.6484	-.1585	-.0551

TABLE XII. - Continued

$M_N = 0.6$

k	$\bar{k}$	$l_{\dot{h}}$	$l_{\dot{\alpha}}$	$-m_{\dot{h}}$	$-m_{\dot{\alpha}}$	l_h	l_α	$-m_h$	$-m_\alpha$
0	0.0	1.2500	0.0	0.0	0.0	0.0	1.2500	0.0	0.0
.025	.1111	1.1561	-4.8027	.0013	.7824	.0038	1.1605	-.0003	.0007
.03	.1305	1.1430	-4.2800	.0016	.7790	.0045	1.1330	-.0004	.0009
.04	.1667	1.1010	-3.6150	.0019	.7709	.0075	1.1093	-.0007	.0014
.05	.2	1.0673	-3.0349	.0024	.7631	.0103	1.0730	-.0011	.0018
.06	.2308	1.0358	-2.5908	.0034	.7587	.0131	1.0503	-.0016	.0023
.08	.2857	.9794	-1.8975	.0050	.7488	.0189	.9957	-.0027	.0031
.10	.3333	.9315	-1.3990	.0066	.7400	.0232	.9592	-.0042	.0037
.12	.3750	.8908	-1.0088	.0079	.7352	.0273	.9378	-.0060	.0042
.14	.4118	.8561	-.7148	.0095	.7297	.0306	.9101	-.0082	.0042
.16	.4444	.8269	-.4959	.0113	.7228	.0336	.8876	-.0104	.0048
.18	.4737	.8019	-.3213	.0132	.7177	.0360	.8685	-.0127	.0054
.20	.5	.7803	-.1725	.0150	.7180	.0376	.8521	-.0155	.0047
.22	.5238	.7616	-.0469	.0165	.7162	.0384	.8378	-.0186	.0043
.24	.5455	.7454	.0590	.0181	.7147	.0385	.8253	-.0220	.0037
.26	.5652	.7315	.1469	.0200	.7142	.0382	.8144	-.0256	.0032
.28	.5833	.7195	.2208	.0217	.7138	.0374	.8050	-.0295	.0030
.30	.6	.7092	.2837	.0237	.7138	.0362	.7969	-.0336	.0025
.34	.6296	.6925	.3886	.0274	.7149	.0320	.7832	-.0427	.0010
.38	.6552	.6805	.4692	.0317	.7173	.0260	.7724	-.0529	-.0005
.42	.6774	.6721	.5324	.0361	.7204	.0183	.7640	-.0643	-.0021
.46	.6970	.6670	.5827	.0410	.7244	.0092	.7575	-.0768	-.0037
.50	.7143	.6646	.6238	.0463	.7291	-.0014	.7528	-.0905	-.0054
.54	.7297	.6643	.6570	.0524	.7339	-.0132	.7496	-.1052	-.0063
.60	.7500	.6678	.6971	.0625	.7435	-.0328	.7476	-.1295	-.0077
.66	.7674	.6745	.7256	.0741	.7512	-.0547	.7484	-.1559	-.0074
.70	.7778	.6808	.7403	.0826	.7572	-.0698	.7510	-.1747	-.0064

TABLE XII. - Continued

$M_N = 0.7$

k	$\bar{k}$	$l_{\dot{h}}$	$l_{\dot{\alpha}}$	$-m_{\dot{h}}$	$-m_{\dot{\alpha}}$	l_h	l_α	$-m_h$	$-m_\alpha$
0	0.0	1.4003	0.0	0.0	0.0	0.0	1.4003	0.0	0.0
.025	.1111	1.2662	-6.7829	.0022	.9882	.0051	1.2714	-.0004	.0017
.03	.1305	1.2330	-6.0500	.0027	.9800	.0065	1.2400	-.0007	.0023
.04	.1667	1.1905	-5.0738	.0039	.9646	.0100	1.2009	-.0010	.0034
.05	.2	1.1400	-4.2580	.0053	.9500	.0125	1.1550	-.0015	.0045
.06	.2308	1.1033	-3.6025	.0071	.9358	.0170	1.1220	-.0021	.0057
.08	.2857	1.0319	-2.6569	.0104	.9138	.0236	1.0581	-.0036	.0079
.10	.3333	.9720	-1.9846	.0135	.8960	.0294	1.0068	-.0053	.0100
.12	.3750	.9238	-1.4840	.0177	.8734	.0344	.9829	-.0075	.0120
.14	.4118	.8832	-1.1048	.0202	.8690	.0386	.9511	-.0099	.0123
.16	.4444	.8497	-.8189	.0230	.8552	.0421	.9251	-.0126	.0147
.18	.4737	.8211	-.5950	.0256	.8489	.0451	.9041	-.0155	.0158
.20	.5	.7970	-.4147	.0289	.8480	.0473	.8868	-.0187	.0180
.22	.5238	.7771	-.2622	.0322	.8471	.0488	.8724	-.0222	.0196
.24	.5455	.7600	-.1375	.0352	.8443	.0497	.8605	-.0261	.0207
.26	.5652	.7452	-.0334	.0382	.8425	.0501	.8506	-.0302	.0218
.28	.5833	.7329	.0541	.0416	.8414	.0500	.8425	-.0347	.0233
.30	.6	.7224	.1251	.0453	.8407	.0497	.8359	-.0394	.0250
.34	.6296	.7060	.2454	.0524	.8408	.0472	.8265	-.0497	.0281
.38	.6552	.6947	.3326	.0607	.8424	.0436	.8212	-.0611	.0324
.42	.6774	.6876	.3987	.0693	.8448	.0388	.8193	-.0735	.0374
.46	.6970	.6836	.4488	.0791	.8478	.0330	.8201	-.0871	.0435
.50	.7143	.6820	.4862	.0897	.8519	.0269	.8235	-.1014	.0499
.54	.7297	.6829	.5140	.1014	.8533	.0197	.8289	-.1165	.0599
.60	.7500	.6868	.5413	.1205	.8556	.0099	.8407	-.1402	.0765
.66	.7674	.6930	.5550	.1415	.8555	-.0015	.8554	-.1647	.0969
.70	.7778	.6979	.5584	.1564	.8536	-.0083	.8664	-.1810	.1125

TABLE XII. - Continued

$M_N = 0.8$

k	$\bar{k}$	$l_{\dot{h}}$	$l_{\dot{\alpha}}$	$-m_{\dot{h}}$	$-m_{\dot{\alpha}}$	l_h	l_α	$-m_h$	$-m_\alpha$
0	0.0	1.6667	0	0.0	0.0	0.0	1.6667	0.0	0.0
.025	.1111	1.4069	-12.5955	.0223	.5873	.0088	1.4115	.0001	.0248
.03	.1305	1.4000	-10.6000	.0230	.7000	.0110	1.3700	-.0003	.0250
.04	.1667	1.2850	-8.2500	.0238	.8550	.0150	1.300	-.0005	.0255
.05	.2	1.2223	-6.6845	.0255	.9486	.0196	1.2456	-.0012	.0261
.06	.2308	1.1925	-5.4871	.0265	.9780	.0238	1.1900	-.0020	.0280
.08	.2857	1.0925	-3.9500	.0300	.9970	.0313	1.1100	-.0030	.0300
.10	.3333	1.0027	-2.9014	.0334	.9987	.0387	1.0473	-.0057	.0342
.12	.3750	.9550	-2.1600	.0375	.9900	.0440	.9950	-.0080	.0370
.14	.4118	.9068	-1.7038	.0410	.9800	.0500	.9550	-.0110	.0400
.16	.4444	.8672	-1.2820	.0450	.9720	.0540	.9250	-.0140	.0435
.18	.4737	.8350	-.8750	.0500	.9650	.0575	.9000	-.0170	.0470
.20	.5	.8021	-.7560	.0557	.9613	.0603	.8834	-.0203	.0506
.22	.5238	.7859	-.5500	.0580	.9500	.0615	.8650	-.0250	.0535
.24	.5455	.7671	-.4000	.0640	.9500	.0638	.8550	-.0290	.0570
.26	.5652	.7512	-.3000	.0700	.9500	.0655	.8500	-.0340	.0610
.28	.5833	.7375	-.2000	.0750	.9500	.0663	.8400	-.0390	.0650
.30	.6	.7258	-.0955	.0796	.9491	.0667	.8347	-.0429	.0694
.34	.6296	.7074	.0400	.0915	.9500	.0665	.8300	-.0550	.0800
.38	.6552	.6934	.1200	.1030	.9500	.0663	.8300	-.0670	.0920
.42	.6774	.6827	.2000	.1150	.9500	.0645	.8350	-.0810	.1050
.46	.6970	.6741	.2400	.1310	.9500	.0625	.8450	-.0940	.1200
.50	.7143	.6891	.2914	.1495	.9518	.0613	.8562	-.1074	.1406
.54	.7297	.6875	.3000	.1600	.9450	.0605	.8700	-.1210	.1600
.60	.7500	.6881	.3196	.1960	.9389	.0619	.8912	-.1405	.1980
.66	.7674	.6890	.3150	.2200	.9220	.0650	.9100	-.1580	.2140
.70	.7778	.6910	.3012	.2498	.9060	.0686	.9283	-.1693	.2794

TABLE XII. - Continued

$M_N = 0.9$

k	$\bar{k}$	$l_{\dot{h}}$	$l_{\dot{\alpha}}$	$-m_{\dot{h}}$	$-m_{\dot{\alpha}}$	l_h	l_α	$-m_h$	$-m_\alpha$
0	0.0	2.2941	0.0	0.0	0.0	0.0	2.2941	0.0	.0002
.025	.1111	1.5470	-27.7916	.1050	-1.7205	.0183	1.5608	.0017	.1112
.03	.1305	1.4700	-21.2500	.0925	-.5650	.0210	1.4800	.0015	.1070
.04	.1667	1.3500	-15.2500	.0835	-.0400	.0260	1.3700	.0013	.1025
.05	.2	1.2637	-11.5244	.0812	.2618	.0315	1.2970	.0011	.0980
.06	.2308	1.1850	-8.7500	.0800	.4750	.0360	1.2100	.0005	.0975
.08	.2857	1.0750	-6.1500	.0810	.7000	.0450	1.1200	-.0010	.0987
.10	.3333	.9915	-4.3378	.0836	.8097	.0525	1.0471	-.0027	.1019
.12	.3750	.9250	-3.2500	.0845	.8500	.0580	1.0000	-.0047	.1050
.14	.4118	.8700	-2.5000	.0875	.8750	.0640	.9500	-.0075	.1080
.16	.4444	.8300	-1.9500	.0900	.8875	.0685	.9150	-.0100	.1125
.18	.4737	.7975	-1.5000	.0950	.8950	.0720	.8850	-.0130	.1160
.20	.5	.7759	-1.2092	.1007	.9046	.0756	.8678	-.0158	.1224
.22	.5238	.7500	-1.0000	.1050	.9055	.0780	.8500	-.0203	.1250
.24	.5455	.7350	-.7500	.1100	.9065	.0805	.8350	-.0235	.1310
.26	.5652	.7200	-.5500	.1150	.9075	.0820	.8200	-.0275	.1375
.28	.5833	.7075	-.4500	.1210	.9085	.0840	.8150	-.0320	.1430
.30	.6	.6987	-.3716	.1260	.9094	.0850	.8135	-.0365	.1480
.34	.6296	.6800	-.1500	.1375	.9075	.0870	.8100	-.0450	.1625
.38	.6552	.6700	-.0500	.1500	.9055	.0880	.8100	-.0550	.1785
.42	.6774	.6625	.0000	.1640	.9035	.0890	.8150	-.0650	.1950
.46	.6970	.6590	.0500	.1780	.9015	.0900	.8200	-.0760	.2125
.50	.7143	.6576	.0896	.1996	.8994	.0917	.8378	-.0875	.2350
.54	.7297	.6500	.1000	.2200	.8750	.0950	.8400	-.0970	.2575
.60	.7500	.6491	.1169	.2479	.8703	.1022	.8663	-.1100	.3050
.66	.7674	.6450	.1500	.2800	.8375	.1130	.8800	-.1225	.3600
.70	.7778	.6423	.0949	.3023	.8186	.1203	.8922	-.1296	.4066

TABLE XII. - Continued

$M_N = 0.95$

k	$\bar{k}$	$l_{\dot{h}}$	$l_{\dot{\alpha}}$	$-m_{\dot{h}}$	$-m_{\dot{\alpha}}$	l_h	l_α	$-m_h$	$-m_\alpha$
0	0.0	3.2025	0.0	0.0	0.0	0.0	3.2025	0.0	-.0002
.025	.1111	1.6043	-41.5331	.1783	-4.2717	.0269	1.6274	.0034	.1984
.03	.1305	1.5050	-32.5000	.1600	-2.4800	.0303	1.5200	.0035	.1870
.04	.1667	1.3650	-21.5000	.1475	-1.1750	.0360	1.3900	.0036	.1750
.05	.2	1.2478	-15.3935	.1401	-.6048	.0411	1.2880	.0037	.1690
.06	.2308	1.1600	-11.7500	.1350	-.2200	.0460	1.2100	.0030	.1655
.08	.2857	1.0425	-7.7500	.1300	.2200	.0540	1.1000	.0025	.1635
.10	.3333	.9549	-5.3253	.1273	.4886	.0616	1.0149	.0014	.1653
.12	.3750	.8900	-4.0000	.1260	.5900	.0670	.9500	.0000	.1660
.14	.4118	.8375	-3.0000	.1270	.6700	.0720	.9100	-.0025	.1690
.16	.4444	.7950	-2.4000	.1285	.7100	.0762	.8750	-.0035	.1725
.18	.4737	.7650	-1.9000	.1305	.7350	.0800	.8500	-.0060	.1775
.20	.5	.7417	-1.4817	.1337	.7433	.0837	.8338	-.0084	.1820
.22	.5238	.7200	-1.2000	.1365	.7550	.0860	.8150	-.0115	.1855
.24	.5455	.7000	-.9000	.1400	.7600	.0880	.8000	-.0140	.1910
.26	.5652	.6850	-.7500	.1435	.7650	.0900	.7900	-.0175	.1960
.28	.5833	.6750	-.6250	.1480	.7655	.0915	.7850	-.0205	.2025
.30	.6	.6647	-.5234	.1525	.7662	.0931	.7811	-.0239	.2081
.34	.6296	.6450	-.3500	.1630	.7600	.0950	.7750	-.0310	.2200
.38	.6552	.6350	-.1250	.1690	.7550	.0960	.7700	-.0395	.2325
.42	.6774	.6250	-.1000	.1725	.7540	.0975	.7700	-.0475	.2460
.46	.6970	.6175	-.0050	.1950	.7530	.0985	.7750	-.0555	.2625
.50	.7143	.6100	.0073	.2091	.7523	.0995	.7811	-.0660	.2861
.54	.7297	.6075	.0250	.2225	.7450	.1010	.7850	-.0710	.3000
.60	.7500	.6025	.0645	.2448	.7240	.1066	.7975	-.0810	.3315
.66	.7674	.6000	.0675	.2700	.6900	.1140	.8050	-.0910	.3650
.70	.7778	.5980	.0712	.2853	.6808	.1183	.8121	-.0957	.3975

TABLE XII. - Continued

$M_N = 1.0$

k	$\bar{k}$	$\ell_{\dot{h}}$	$\ell_{\dot{\alpha}}$	$-m_{\dot{h}}$	$-m_{\dot{\alpha}}$	ℓ_h	ℓ_α	$-m_h$	$-m_\alpha$
0	0.0	0.0	0.0	0.0	0.0	0.0	0.0	0.0	0.0
.025	.1111	1.6466	-61.2997	.2959	-8.2114	.0392	1.6798	.0059	.3297
.03	.1305	1.5105	-46.1823	.2754	-5.8641	.0427	1.5468	.0064	.3122
.04	.1667	1.3210	-29.4134	.2475	-3.2846	.0488	1.3627	.0068	.2899
.05	.2	1.1931	-20.6271	.2295	-2.0116	.0539	1.2396	.0075	.2767
.06	.2308	1.0997	-15.3714	.2169	-1.2584	.0585	1.1504	.0078	.2683
.08	.2857	.9707	-9.5683	.2008	-.4619	.0662	1.0289	.0080	.2597
.10	.3333	.8848	-6.5484	.1913	-.0747	.0724	.9493	.0079	.2564
.12	.3750	.8228	-4.7541	.1854	.1389	.0776	.8931	.0075	.2560
.14	.4118	.7759	-3.5915	.1817	.2665	.0820	.8512	.0068	.2572
.16	.4444	.7392	-2.7911	.1794	.3468	.0858	.8189	.0059	.2594
.18	.4737	.7095	-2.2142	.1781	.3990	.0889	.7935	.0049	.2621
.20	.5	.6851	-1.7836	.1775	.4338	.0917	.7730	.0038	.2652
.22	.5238	.6650	-1.5000	.1777	.4500	.0935	.7550	.0025	.2700
.24	.5455	.6476	-1.1937	.1779	.4729	.0958	.7424	.0010	.2720
.26	.5652	.6325	-.9000	.1785	.4825	.0970	.7350	-.0005	.2750
.28	.5833	.6203	-.8170	.1795	.4899	.0986	.7211	-.0022	.2792
.30	.6	.6093	-.6778	.1807	.4939	.0996	.7129	-.0039	.2828
.34	.6296	.5900	-.5000	.1850	.4950	.1010	.6950	-.0080	.2900
.38	.6552	.5800	-.4000	.1880	.4975	.1012	.6850	-.0120	.2950
.42	.6774	.5700	-.3000	.1910	.4925	.1005	.6770	-.0165	.3025
.46	.6970	.5600	-.2000	.1950	.4825	.0995	.6760	-.0210	.3100
.50	.7143	.5521	-.0375	.1978	.4790	.0979	.6753	-.0253	.3161
.54	.7297	.5450	.0000	.2010	.4725	.0950	.6740	-.0310	.3200
.60	.7500	.5400	.0789	.2070	.4631	.0918	.6730	-.0376	.3300
.66	.7674	.5350	.1100	.2130	.4525	.0860	.6720	-.0475	.3375
.70	.7778	.5369	.1489	.2183	.4479	.0832	.6706	-.0504	.3429

TABLE XII. - Concluded

$M_N = 1.05$

k	$\bar{k}$	$\ell_{\dot{h}}$	$\ell_{\dot{\alpha}}$	$-m_{\dot{h}}$	$-m_{\dot{\alpha}}$	ℓ_h	ℓ_α	$-m_h$	$-m_\alpha$
0	0.0	1.9885	0.0	0.0	0.0	0.0	1.9885	0.0	.9946
.025	.1111	1.8628	-17.3052	.8689	-13.8162	.0115	1.8649	.0094	.8743
.03	.1305	1.8050	-16.5000	.8000	-13.0500	.0165	1.7900	.0133	.8180
.04	.1667	1.6850	-15.3000	.6850	-11.8500	.0265	1.6850	.0205	.6850
.05	.2	1.5438	-14.1282	.5586	-10.4843	.0377	1.5533	.0292	.5757
.06	.2308	1.3350	-12.2500	.4050	-8.5500	.0525	1.3950	.0372	.4150
.08	.2857	1.1000	-9.4500	.1650	-5.9500	.0675	1.0200	.0418	.1500
.10	.3333	.8722	-6.7768	.0096	-3.0860	.0764	.9094	.0388	.0606
.12	.3750	.7500	-4.3500	-.0250	-1.0000	.0775	.7900	.0242	.0450
.14	.4118	.6975	-3.0000	.0150	.1500	.0715	.7500	.0080	.0750
.16	.4444	.7000	-2.1500	.0850	.5000	.0690	.7650	.0025	.1950
.18	.4737	.7100	-1.8000	.1650	.4750	.0708	.7850	.0007	.2500
.20	.5	.7084	-1.5079	.1993	.2541	.0807	.7792	.0090	.2751
.22	.5238	.6750	-1.3000	.1550	.1750	.0920	.7550	.0143	.2500
.24	.5455	.6250	-1.1000	.1350	.1500	.0955	.7200	.0110	.2180
.26	.5652	.6000	-.9750	.1250	.2000	.0945	.6900	.0175	.2110
.28	.5833	.5850	-.7000	.1275	.3500	.0880	.6700	-.0070	.2180
.30	.6	.5700	-.5250	.1300	.5000	.0860	.6600	-.0105	.2250
.34	.6296	.5800	-.4250	.1800	.4500	.0895	.6800	-.0090	.2820
.38	.6552	.5700	-.3000	.1650	.3500	.0963	.6600	.0000	.2620
.42	.6774	.5400	-.1500	.1550	.4000	.0900	.6300	.0010	.2580
.46	.6970	.5275	-.0500	.1650	.5000	.0878	.6250	-.0205	.2750
.50	.7143	.5407	-.0095	.1964	.4418	.0884	.6499	-.0208	.3043
.54	.7297	.5300	.0500	.1925	.4250	.0820	.6450	-.0220	.3100
.60	.7500	.5135	.1074	.1837	.4545	.0801	.6311	-.0375	.2990
.66	.7674	.5130	.1275	.1875	.4250	.0801	.6200	-.0375	.3000
.70	.7778	.5124	.1489	.1998	.4119	.0802	.6301	-.0375	.3107

TABLE XIII. BLADE CONFIGURATIONS AND FLIGHT CONDITIONS FOR EXTENDED NORMAL MODE ANALYSIS CALCULATIONS CORRESPONDING TO CLASSICAL FLUTTER INVESTIGATIONS

Case No.	Articulated or Nonarticulated	μ	$\frac{\bar{x}}{c_b}$
1	Articulated	.30	0.0
2	Articulated	.30	-.065
3	Articulated	.30	-.0975
4	Articulated	.30	-.130
5	Articulated	.15	0.0
6	Articulated	.15	-.130
7	Articulated	.15	-.165
8	Articulated	.15	-.200
9	Nonarticulated	.30	0.0
10	Nonarticulated	.30	-.0975
11	Nonarticulated	.30	-.130

CONCLUSIONS

1. The simplified equations of motion predicted flutter speeds which were conservative when compared with experimental flutter data.

2. Torsional divergence and classical bending-torsion flutter of a rotating blade are closely related, with static divergence occurring usually at a slightly higher speed than flutter.

3. As the blade tip Mach number approaches unity, the rearward shift of the aerodynamic center has a stabilizing effect. The increase in the flutter or divergence speeds was considerably greater with the experimental data than that which occurred with the calculated speeds. This is attributed to the rearward shift of the aerodynamic centers being greater in practice than is implied by the aerodynamic coefficients.

RECOMMENDATIONS

1. The correlation study should be extended to help define in more detail any limitations that exist in the simplified equations of motion.

2. A program should be undertaken which consists of experimental measurement of rotor blade classical flutter speeds at high advance ratios and tip Mach numbers, together with the calculation of the corresponding flutter speeds through the use of the simplified equations of motion.

3. Aerodynamic coefficients taken from Reference 15 should be used in place of the table of compressible aerodynamic coefficients when the blade tip Mach number and advance ratio are low.

4. The effect on the aerodynamic stiffness and damping of bending modes of the spanwise air flow along the blade should be investigated.

5. The effects of blade twist and coning angle should be incorporated into the blade structural coefficients.

6. The conservatism inherent in the fixed azimuth approach should be investigated.

7. As the next step toward developing a more accurate unsteady aerodynamic theory applicable to high Mach numbers and high advance ratios, an attempt should be made to modify the existing two-dimensional fixed-wing unsteady compressible flow theory to include in an approximate fashion the effect of a nonplanar wake, the effect on the circulation of the presence of more than one wake, and the effect of a time-varying dynamic pressure.

8. The experimental occurrence of flutter phenomena, which appear to be a combination of stall flutter and classical flutter has been noted. This type of combined flutter should be studied by analysis and test.

REFERENCES CITED

1. Fung, Y. C., An Introduction to the Theory of Aeroelasticity, John Wiley and Sons, New York, New York, 1955.

2. Jordan, P. F., Aerodynamic Flutter Coefficients for Subsonic, Sonic and Supersonic Flow (Linear Two-Dimensional Theory), Great Britain ARC R&M No. 2932. Aeronautical Research Council, Great Britain, 1953.

3. Nelson, H. C., and Berman, J. H., Calculations on the Forces and Moments for an Oscillating Wing-Aileron Combination in Two-Dimensional Potential Flow at Sonic-Speed, NACA Report 1128 National Advisory Committee on Aeronautics, Langley Aeronautical Laboratory, Langley Field, Virginia, 1953.

4. Luke, Y. L., Tables of Coefficients for Compressible Flutter Calculations, Air Force Technical Report 6200, United States Air Force, Air Materiel Command, Wright Patterson Air Force Base, Dayton, Ohio, 1950.

5. Timman, R., van de Vooren, A. I., and Greidanus, J. H., Aerodynamic Coefficients of an Oscillating Airfoil in Two-Dimensional Subsonic Flow , Journal of the Aeronautical Sciences, Vol. 18, No. 12, December 1951.

6. Timman, R., van de Vooren, A. I., and Greidanus, J. H., Aerodynamic Coefficients of an Oscillating Airfoil in Two-Dimensional Subsonic Flow, Journal of the Aeronautical Sciences, Vol. 21, No. 7, July 1954, Reader's Forum.

7. National Luchtvaartlaboratorium, Tables of Aerodynamic Coefficients for an Oscillating Wing-Flap System in a Subsonic Compressible Flow, N.L.L. Report F 151, National Aeronautical Research Institute, Amsterdam, Holland, May 1954.

8. Garrick, I. E., and Rubinow, S. I., Flutter and Oscillating Air Force Calculations for an Airfoil in a Two-Dimensional Supersonic Flow, NACA Report 846 National Advisory Committee on Aeronautics, Langley Aeronautical Laboratory, Langley Field, Virginia, 1946.

9. Scanlan, Robert H., and Rosenbaum, Robert, Introduction to the Study of Aircraft Vibration and Flutter, The MacMillan Company New York, 1951.

10. Flax, A. H., Reverse-Flow and Variational Theorems for Lifting Surfaces in Nonstationary Compressible Flow, Jounal of the Aeronautical Sciences, Vol. 20, No. 2, February 1953, pp. 120-126.

11. Fettis, H. E., Comments on Aerodynamic Coefficients of an Oscillating Airfoil in Two-Dimensional Subsonic Flow, Journal of the Aeronautical Sciences, Vol. 19, No. 5, May 1952, pp. 353-354.

12. Zimmerman, N. H., Elementary Static Aerodynamics Adds Significance and Scope in Flutter Analysis, Symposium Proceedings on Structural Dynamics of High Speed Flight, Aerospace Industries Association, April 1961, pp. 28-84.

13. Brooks, G. W., and Baker, J. E., An Experimental Investigation of the Effect of Various Parameters Including Tip Mach Number on the Flutter of Some Model Helicopter Rotor Blades, NACA TN 4005, National Advisory Committee on Aeronautics, Langley Aeronautical Laboratory, Langley Field, Virginia, 1958.

14. Du Waldt, F. A., Gates, C. A., and Piziali, R. A., Investigation of Helicopter Rotor Blades Flutter and Flapwise Bending Response in Hovering, WADC TR 59-403, Cornell Aeronautical Laboratory, Buffalo, New York August 1959.

15. Loewy, R. G., A Two-Dimensional Approximation to the Unsteady Aerodynamics of Rotary Wings, CAL Report No. 75, Cornell Aeronautical Laboratory, Buffalo, New York, October 1955.

16. Gates, C. A., and Du Waldt, F. A. , Experimental and Theoretical Investigation of the Flutter Characteristics of a Model Helicopter Rotor Blade in Forward Flight, Aeronautical Systems Division, Technical Report 61-712, Cornell Aeronautical Laboratory, Buffalo, New York, February 1962.

17. Theodorsen, Theodore, General Theory of Aerodynamic Instability and the Mechanism of Flutter, NACA Report 496, National Advisory Committee on Aeronautics, Langley Aeronautical Laboratory, Langley Field, Virginia.

Unclassified
Security Classification

DOCUMENT CONTROL DATA - R & D

(Security classification of title, body of abstract and indexing annotation must be entered when the overall report is classified)

1. ORIGINATING ACTIVITY *(Corporate author)* Sikorsky Aircraft Division of United Aircraft Corporation Stratford, Connecticut	2a. REPORT SECURITY CLASSIFICATION Unclassified 2b. GROUP

3. REPORT TITLE
PREDICTION OF ROTOR INSTABILITY AT HIGH FORWARD SPEEDS
Volume II - Classical Flutter

4. DESCRIPTIVE NOTES *(Type of report and inclusive dates)*
Final Report

5. AUTHOR(S) *(First name, middle initial, last name)*
Clifford J. Astill
Charles F. Niebanck

6. REPORT DATE February 1969	7a. TOTAL NO. OF PAGES 217	7b. NO. OF REFS 17
8a. CONTRACT OR GRANT NO. DA 44-177-AMC-332(T) b. PROJECT NO. 1F125901A13904 c. d.	9a. ORIGINATOR'S REPORT NUMBER(S) USAAVLABS Technical Report 68-18B 9b. OTHER REPORT NO(S) *(Any other numbers that may be assigned this report)* SER-50469	

10. DISTRIBUTION STATEMENT
This document has been approved for public release and sale; its distribution is unlimited.

11. SUPPLEMENTARY NOTES Volume II of a 5-volume report	12. SPONSORING MILITARY ACTIVITY U. S. Army Aviation Materiel Laboratories Fort Eustis, Virginia

13. ABSTRACT

An analytical study was made of the effects of high forward speed on the flutter characteristics of helicopter rotor blades.

Linearized equations of motion were used to represent the dynamics of the rotor blades. The aerodynamic forces were obtained by using a fixed azimuth approach with fixed-wing two-dimensional compressible flow aerodynamic coefficients.

Flutter speeds and flutter frequencies were calculated for two model helicopter blades for which experimental data were available. One blade had been tested in hover at high tip Mach numbers; the other, at high advance ratios with low tip Mach numbers. Agreement between theoretical and experimental data was qualitative.

A parametric study was made of the effect on flutter speed of varying blade chordwise elastic axis and center-of-gravity position, torsional and flatwise bending stiffness, and blade mass ratio and feathering mass moment of inertia.

The extended Normal Mode Transient Analysis was used to perform blade response calculations corresponding to blade configurations and flight conditions for which classical flutter was calculated.

DD FORM 1 NOV 65 1473 REPLACES DD FORM 1473, 1 JAN 64, WHICH IS OBSOLETE FOR ARMY USE.

Unclassified
Security Classification

Unclassified
Security Classification

14. KEY WORDS	LINK A ROLE	LINK A WT	LINK B ROLE	LINK B WT	LINK C ROLE	LINK C WT
Helicopter Rotor Blade Flutter						

Unclassified
Security Classification

1185-69